DESIGN, SYNTHESIS AND POSTSYNTHETIC MODIFICATION OF METAL-ORGANIC MATERIALS FOR HYDROGEN STORAGE AND CHEMOSENSING

DISSERTATION

zur

Erlangung der naturwissenschaftlichen Doktorwürde

(Dr. sc. nat.)

vorgelegt der

Mathematisch-naturwissenschaftlichen Fakultät

der

Universität Zürich

von

Samir Barman

aus

Indien

Promotionskomitee

Prof. Dr. Heinz Berke (Vorsitz und Leitung)

Prof. Dr. Greta R. Patzke

Zürich 2012

LIST OF ABBREVIATIONS

ACRONYM	FULL NAME
Azd	Azulenedicarboxylate
BDC	Benzene-1,4-dicarboxylate
BDP	1,4-benzenedi(4′-pyrazolyl)
BTB	4,4′,4″-benzene-1,3,5-triyltribenzoate
BTT	1,3,5-benzenetristetrazolate
CP	Coordination Polymer
DABCO	1,4-diazabicyclo[2.2.2]octane
DMA	Dimethylamonium
DMF	*N,N'*-Dimethylformamide
EtOH	Ethanol
H_2O	Water
HKUST	Hong Kong University of Science and Technology
HImDC	4,5-Imidazoledicarboxylic acid
INS	Inelastic Neutron Scattering
MBB	Molecular Building Block
MOF	Metal-Organic Framework
IRMOF	Isoreticular Metal-Organic Framework
MOM	Metal-Organic Material
MIL	Material from Institut Lavoisier
MOP	Metal-Organic Polyhedron
NH_2-bdc	2-aminobenzene-1,4-dicarboxylate
NPD	Neutron Powder Diffraction
NU	Northwestern University
PCN	Porous Coordination Network
PSM	Postsynthetic modification
PZDC	Pyrazine-2,3-dicarboxylate

SBU	Secondary Building Unit
SNU	Seoul National University
T^2DC	Thieno[3,2-b]thiophene-2,5-dicarboxylate
TFAA	trifluoroacetic anhydride
TGA	Thermogravimetric analysis
THF	tetrahydrofuran
TPB-3tz	1,3,5-tri-p-(tetrazol-5-yl)phenylbenzene
UV-Vis	Ultraviolet-visible
UMCM	University of Michigan Crystalline Material
XRPD	X-Ray Powder Diffraction
ZMOF	Zeolite-*like* Metal-Organic Framework
ZIF	Zeolitic Imidazolate Framework
δ	chemical shift
μ	descriptor of bridging
ν	frequency
d	doublet
Et	ethyl
Et_2O	ethyl ether
Hz	hertz
iPr	isopropyl
IR	infrared
m	multiplet (NMR)
Me	methyl
NMR	Nuclear Magnetic Resonance
Ph	phenyl
ppm	part per million
quart	quartet
quint	quintet
r.t.	room temperature
s	singlet
t	triplet

Acknowledgements

First and foremost, I would like to express my sincere gratitude to my supervisor Prof. Dr. Heinz Berke for his guidance and encouragement, which he provided throughout my PhD work. I am also highly indebted for his very friendly discussions, help and for giving me the opportunity to work in his group.

I would also like to thank Dr. Koushik Venkatesan for his enormous help and has always been available with lots of enthusiastic ideas.

My special thanks also go to Dr. Hiroyasu Furukawa (UCLA, USA) for his lot of help and scientific discussion throughout my research work.

I would like to thank Dr. Olivier Blacque for so many complicated crystallographic structures he solved for me.

Spring Barbara and Heinz for the elemental microanalysis.

I would like to appreciate Hans-Peter Stalder for his creativity and effectiveness in making mechanical parts related to my research.

I am also grateful to people who helped me in leading my Ph.D. project:

Dr. Thomas Fox for performing innumerable fantastic NMR measurements to establish some part of my chemistry with only NMR studies.

I extend my thanks to some of our collaborators, Dr. Arndt Remhof (EMPA, Switzerland), Dr. Anupam Khutia (University of Düsseldorf) and Ralph Koitz (PCI, University of Zürich) for their kind cooperation and help.

My thanks go to Beatrice Spichtig, Dr. Fredinand Wild, Manfred Jöhri, Susanna Sprokkereef, Nathalie Fichter, Dr. Jae Kuoung Pak and Sabine Stockhause for their support during all these years.

I want to specially thank Dr. Jai Anand Garg and Dr. Sergey Semenov for their huge support, encouragement and lots of help during my work.

I have learnt so much from the group of Prof. Berke, Dr. Venkatesan and Prof. Patzke. Their support and invaluable friendship has helped towards the successful completion of my thesis work in various inexplicable ways. In that respect, I thank all of my friends, Subarata, Michael, Rajesh, Rajkumar, Yanfeng, Carolina, Dybov, Yuzhen, Alex, Gabriel, Anne, Franziska, and Pascal.

I thank the Swiss National Science Foundation, Forschungkredit of University of Zurich and Department of Energy Unites State for financial support.

Everything would not have been possible without the grace of the almighty God equally enough patience and endurance from my parents and lovely wife. Thanks to all of them.

TABLE OF CONTENT

1. METAL-ORGANIC MATERIALS

1.1. Introduction

Metal-Organic Materials (MOMs) encompass discrete as well as extended structures comprised of metal moieties and organic components that are linked *via* coordination bonds to generate zero-, one-, two or three periodic structures (Scheme 1).[1] MOMs has been taking a great deal of industrial and academic research interest because of their fascinating structural diversity and concomitant interminable potential applications.[2] The most intriguing feature of MOMs is that it epitomize the beauty of chemical structures and the power of combining organic and inorganic chemistry, two disciplines often regarded as disparate. Therefore, the hybrid nature of MOMs permits properties of both the organic and the inorganic components. In addition, construction of highly ordered structures could be easily accomplished by taking advantage of the labile nature of the coordination bonds and the reversibility of the interactions, which further allows the materials to be often characterized by X-ray crystallography.

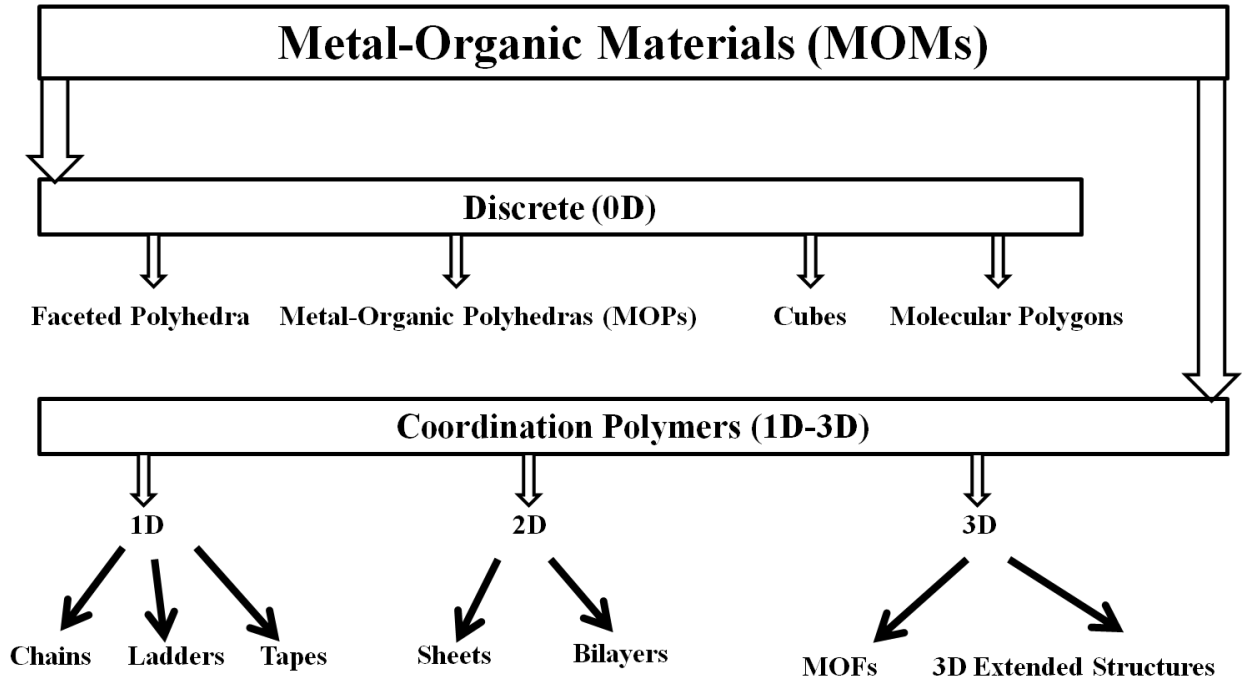

Scheme 1

High order and robust nature of vast majority of MOMs, in conjunction with the propensity of forming regular pores throughout the whole material, allows the optimum properties of MOMs to be easily derived. Moreover, the geometry of coordination and also the pore size, shape and functionality of the final materials is believed to be predicted in some extent through careful selection of metal ions and the organic linkers which are being employed in the reaction mixture.

1.2. Brief Overview of Coordination Chemistry and Coordination Polymers

Although many coordination complexes, for example Prussian blue and copper vitriol were known since the beginning of chemistry; the coordination geometry of the transition metal complexes was first proposed by Alfred Werner and who further developed the basis for modern coordination chemistry. Werner invention brought into existence some of the earliest examples of coordination complexes with a typical chemical formula of MX_2L_4 where M represents the metal in an octahedral geometry (Ni, Co, Fe, Mn, Zn, Cu), X is an anionic ligand (e.g. SCN, CNO, NO_2) and L represents a substituted pyridine or α-alkylarylamine.[3] Other early precedence of coordination complexes was also credited to Karl Andrea Hofmann who discovered the complex of formula $Ni(NH_3)_2Ni(CN)_4.2C_6H_6$ in 1897.[4]

Relatively more recently (1989-1990), the research work by Hoskin and Robson notably made the necessary impetus to the field of coordination polymers. Although, the term 'coordination polymer' existed early since 1960s, and the corresponding research area had been reviewed shortly thereafter.[5,6] Having initiated the *node and spacer* concept, the authors also evidenced some of the preliminary design principles for building functional infinite structures along with some proposed way of constructing novel polymeric materials *via* linking the nodes and rod-like spacer units. Furthermore, the authors also envisaged many possible and attractive applications of the infinite coordination materials for example in catalysis and ion exchange.[5]

1.3. Synthetic Methods

MOMs are often obtained as crystalline products and therefore one need to optimize a suitable crystal growth technique to produce crystals of X-ray diffraction quality. Fortunately, this is perhaps achieved following evaporation, solvent diffusion and hydro or solvothermal synthesis. Brief descriptions of these methods are given in the following section.

Evaporation: Solvent evaporation technique is widely employed for obtaining crystalline material of small molecule compounds. The mechanism of crystal growth in solvent evaporation technique is known to greatly influence by the solvent systems which are being used. Therefore, in order to find the best conditions for crystal growth it is often required to screen a large number of solvents or solvent mixtures. Slower rates of crystal growth can be achieved by decreasing the rate of evaporation of the solvent or by cooling the solution. Formation of only a few rosette-shaped masses is an indication of an insufficient number of nucleation sites. The number of nucleation sites may be increased either by seeding the solution or by scratching the surfaces of the vessel exposed to the solution.

Solvent Diffusion (Layering Technique) and Vapor Diffusion: In a typical crystallization experiment a small amount of concentrated solution containing metal precursor is place in a tube or glass container and the solution of organic ligand is then carefully layered on the top of the solution. The tube is then sealed and left undisturbed. In the passage of time, some crystals may grow by diffusion of the ligand into a metal ion solution. Solvent diffusion can also be adapted by using an H-tube instead of the straight tube type. It should be noted that the mixture of organic ligand solution should be less dense than the metal ion solution and a suitable volume ratio of metal solution/organic solution is typically 1:4 or 1:5.

Although these techniques mentioned above has certain advantages for example the process may require only a very small amount of material for preparing crystals and also it is possible to set up many experiments by varying solvent and experimental conditions at one time. However, the main drawback of these techniques are that the process may take from a few days up to several months to grow suitable crystals due to slow diffusion.[7,8]

Hydro and Solvothermal Synthesis: Metal-organic materials (MOMs) with higher dimensions and high degree of porosities are almost exclusively prepared by hydro or solvothermal techniques, which were firstly introduced for the synthesis of Zeolites. Hydrothermal syntheses are performed using water as the solvent, where as in solvothermal syntheses other solvents except water are used. In a typical synthesis of metal-organic materials under hydro or solvothermal techniques, the precursors mixtures (most often observed to be insoluble in hydrothermal, however reverse are true in case of solvothermal) are loaded in a Teflon-line autoclave or in a closed glass vessel and the reactions are performed in a temperature range between 80-260 °C under autogenous pressure. Apart from pure hydro or solvothermal methods,

mixtures of water and other solvents are also widely employed to prepare myriad of MOM structures. When comparing to the solution preparation of the materials, a hydro or solvothermal techniques plays advanced role to prepare robust and stable MOMs.[9] Furthermore, these techniques permit the solvent temperature beyond its atmospheric pressure boiling point and consequently reduces the viscosity and dielectric constant of the solvent which are found to be beneficial for enhancing the diffusion process and crystal growth.[8,10] Nonetheless, the self-assembly process is largely influenced by many factors such as the structural characteristics of the ligands, coordination nature of metal ions, the solvent system, the template, the pH value of the solution, steric requirement of the counterion, reaction temperature and the ratio of metal to ligand etc. A small variation in one or more of the aforementioned reaction variables is found to have a profound influence on assembly processes thereby on the nature and types of the final products which will be formed. Recent advancement in this research area also evidenced that these techniques can also be successfully used for the preparation of MOMs which undergoes *in situ* precursor ligand synthesis.[11]

1.4. Organic Building Units of MOMs

The organic components in MOMs serve as the metal bridging units; therefore multitopic organic linkers are generally employed during the preparation of polymeric network structures. In this context a large number of multitopic nitrogen and oxygen donor, hetero functional organic ligands or even some other types of ligands have also been investigated. Relative high thermal stability of these classes of linkers also provide materials additional support from the collapse of their structural integrity upon exclusion of solvent guests. The following sections will give a brief overview of the MOMs constructed from various organic building blocks.

1.4.1. Based on Nitrogen-Donor Organic Ligands

Large variety of metal-organic materials has been reported where the nitrogen-donor ligands are used as the metal linking units. Unlike metal-carboxylate bond, the relatively higher labile nature of metal-N coordination bond perhaps permit easy rearrangement during self-assembly process and therefore may exhibit supramolecular isomerism. Figure 1 presents some of the nitrogen donor organic linkers used for synthesizing wide range of coordination polymers

(CPs). For example, Robson and co-workers have reported one of the early material Zn(4,4′-bipyridine)$SiF_6 \cdot 2H_2O$ based on nitrogen-donor, 4,4′-bipyridine, ligand.[12] Several other examples of MOMs comprising nitrogen-donor ligands 4,4′-bipyridine or pyrazine and various transition metal ions for examples Zn, Co, Cd, Cu, etc. have been reported by different groups in early 1990.[13-17]

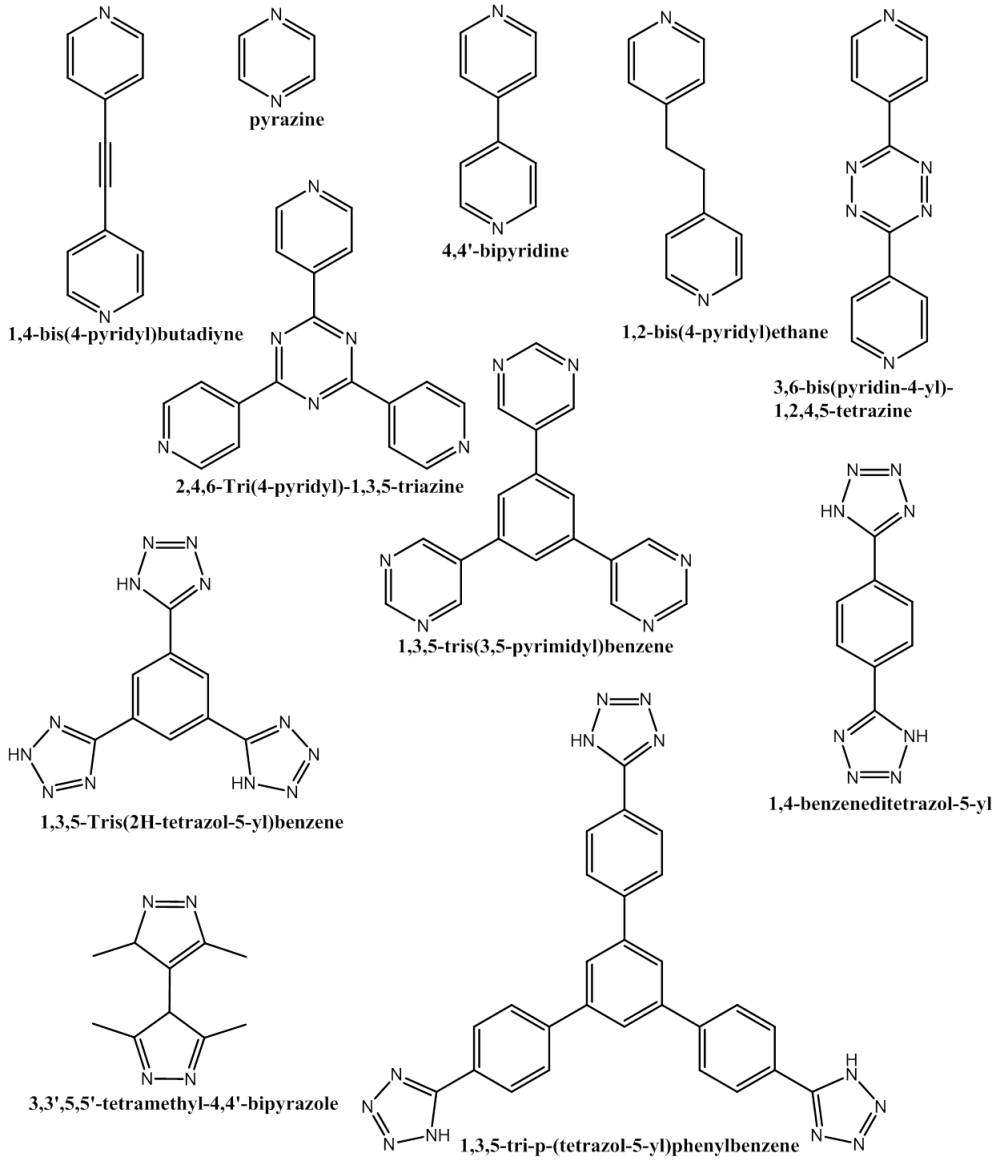

Figure 1. Some examples of nitrogen-donor ligands used for MOMs synthesis.

More recently, a large variety of nitrogen based heterocyclic ligands for instance imidazole, pyrazole, triazole, and tetrazole have been successfully investigated to prepare porous

MOMs. For instance, a new class of 3-dimensional neutral frameworks known as ZIFs (Zeolitic imidazole frameworks) with zeolitic topologies were constructed from various nitrogen based heterocyclic ligands (Figure 2) and tetrahedrally coordinated Zn or Co metal ions.[18,19]

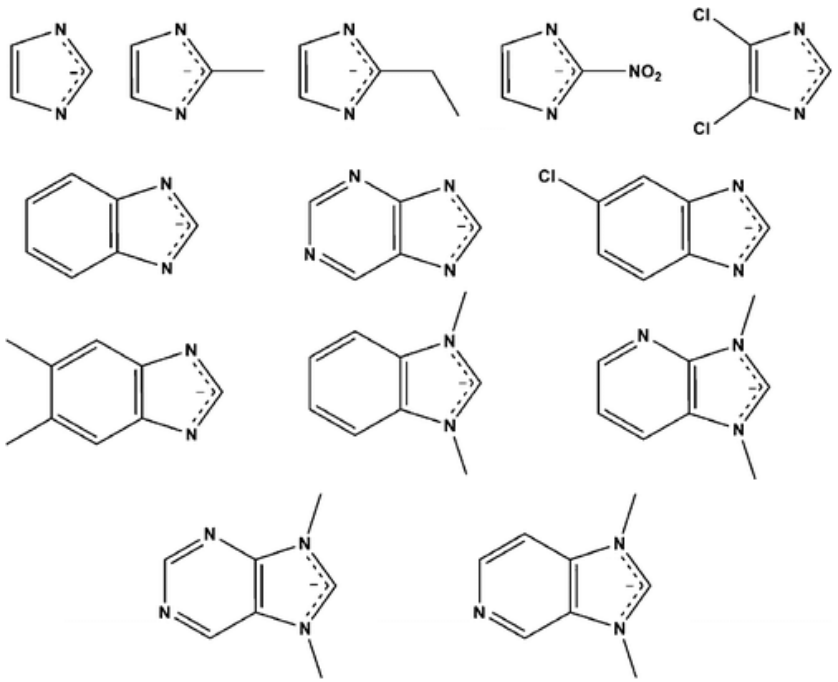

Figure 2. Various ligands used in the synthesis of zeolitic imidazolate frameworks (ZIFs).

Long and co-workers have reported pyrazole based MOF, $Co(BDP)_3 \cdot 2DEF \cdot H_2O$, with a Langmuir surface area of 2670 $m^2\ g^{-1}$ by linking Co^{2+} ions with benzenedi(4′-pyrazolyl) (BDP) where the metal ions are tetrahedrally coordinated by N-atoms from four different BDP^{2-} anions.[20] The group also reported triazolate-bridged framework $H_3[(Cu_4Cl)_3(BTTri)_8]$ comprising of BTTri (BTTri = 1,3,5-tris(1H-1,2,3-triazol-5-yl)benzene) ligand, where the chloride-centered $[Cu_4Cl]^{7+}$ square-planar cluster entities were linked via nitrogen atoms of triangular $BTTri^{3-}$ ligands.[21] Dincă et al. reported interesting tetrazolate-bridged framework $Mn_3[(Mn_4Cl)_3(BTT)_8\ (CH_3OH)_{10}]_2$ by connecting the chloride-centered $[Mn_4Cl]^{7+}$ units with BTT^{3-} anions (BTT^{3-} = 1,3,5-benzenetristetrazolate) which exhibited a total H_2 uptake capacity of 6.9 wt % at 77 K and 90 bar.[22] Later, an isoreticular material based on other tetrazolate ligand H_3TPB-3tz (1,3,5-tri-p-(tetrazol-5-yl)phenylbenzene) was also reported.[23]

1.4.2. Based on Oxygen-Donor Organic Ligands

MOMs constructed from carboxylic acid based ligands are among the most commonly investigated. Wide range of carboxylic acids which includes aromatic (Figure 3), aliphatic mono-, bi- or poly-carboxylic acid have been successfully evaluated. Unlike N-donor molecules, O-donor carboxylic acid ligands have the flexibility to chelate metal ions in different ways for example in monodentate, bis-monodentate, and bi-dentate coordination mode. Especially coordination through bis-monodentate fashion is interesting since it often allows the formation of multinuclear metal carboxylate clusters which enhances the rigidity and the stability of the resulting building block and consequently the final networks. Some of the interesting metal-carboxylate clusters that are employed as building blocks to construct robust 3-dimentional structures are presented in Figure 7 (Section 1.6.). The octahedral shaped $Zn_4O(CO_2)_6$ cluster[24] (Figure 4a) unit was used to produce one of the most popular MOF, namely MOF-5 (or IRMOF-1), based on 1,4-benzenedicarboxylic acid in a cubic framework topology (Figure 4b).[25] Later, the underlying topology of MOF-5 was utilized to accomplished a series of other MOFs known

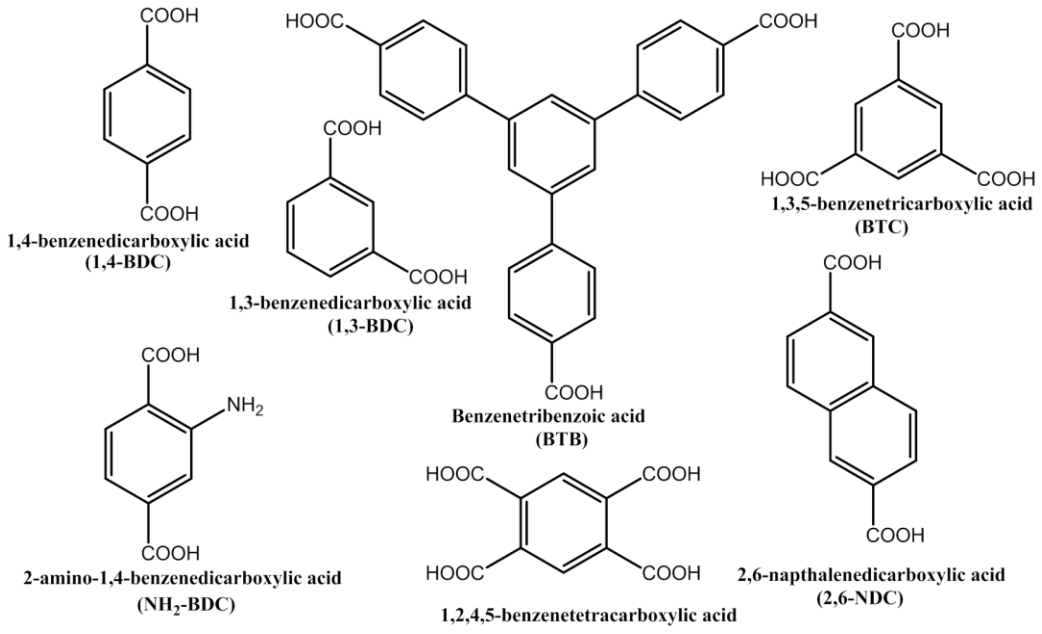

Figure 3. Some examples of aromatic carboxylic acid used for MOMs synthesis.

as IRMOFs (isoreticular metal-organic frameworks) which comprises various carboxylic acids having different functionalities.[26] The well-known MOF-177 was also constructed thereafter by

linking the $Zn_4O(CO_2)_6$ cluster with 4,4′,4″-benzene-1,3,5-triyltribenzoate (BTB) in a 6,3-connected net (Figure 4c), which shows remarkable BET surface area of 4750 m^2 g^{-1} and a pore volume of 1.59 cm^3 g^{-1}.[27]

Other interesting classes of MOFs containing diverse sets of carboxylic acid ligands (Figure 3) and dimetal paddle wheel $[M_2(CO_2)_4]$ (M = Cu, Zn, etc.) cluster units were investigated. For example, HKUST-1 was synthesized from tridentate ligand, 1,3,5-benzenetricarboxylic acid, and $Cu_2(CO_2)_4$ paddlewheel cluster units.[28]

A larger variety of interesting zero periodic structures referred to as nanoballs or metal-organic polyhedras (MOPs), were also synthesized by linking the paddlewheel cluster units with various carboxylate ligands.[29,30]

Férey and co-workers reported a series of materials known as MIL (MIL: Material from Institute Lavoisier) by linking the $Cr_3O(CO_2)_6$ cluster or trimer units with di- or tricarboxylates.[31-33] For instance, porous MOF with giant pores known as MIL-100 was constructed from benzene-1,3,5-tricarboxylic acid and trimeric chromium(III) octahedral cluster units.[31] The highly porous MOF, MIL-101, with a Langmuir surface area of 5500 $m^2g^{-1}$was built from chromium and benzene-1,4-dicarboxylic acid.[32] Other interesting MOFs comprises trimers cluster units based on aluminum or iron and di- or tritopic carboxylate linkers were reported.[34]

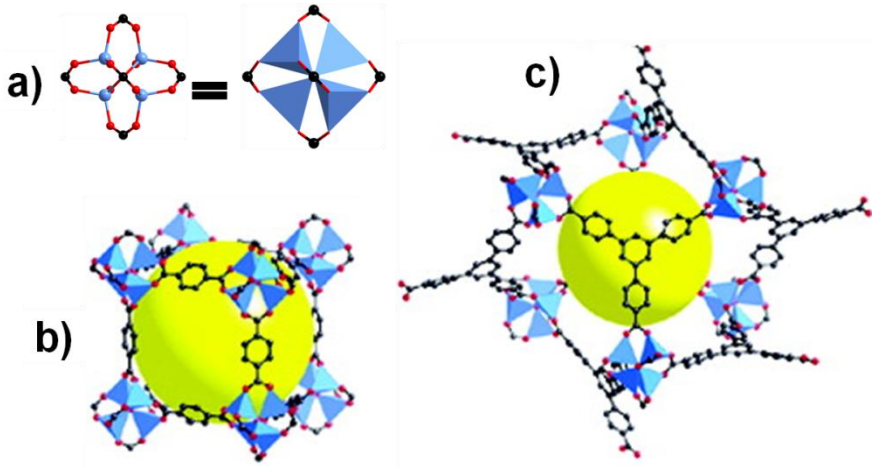

Figure 4. Examples of use of octahedral shaped $Zn_4O(CO_2)_6$ cluster unit (a) to generate MOF-5 (b) using 1,4-benzenedicarboxylic acid (1,4-BDC) and MOF-177 (c) using benzenetribenzoic acid (BTB).[25,27]

1.4.3. Based on Hetero-Functional Ligands

Single organic building block bearing two or more different atoms that can serve as donor in forming coordination bonds are referred to as hetero-functional ligands. In general, this class of ligands contains at least one O- and one N-donor atoms (Figure 5). The presence of multiple donor atoms in single organic building unit leads to the formation of materials with higher diversity and complex structural features. Depending upon the position of the hetero atoms in the ligand, hetero-chelation could be possible and often tend to give an enhanced rigidity to the building block via completing the coordination around the metal atoms whereas precluding the terminal ligands.

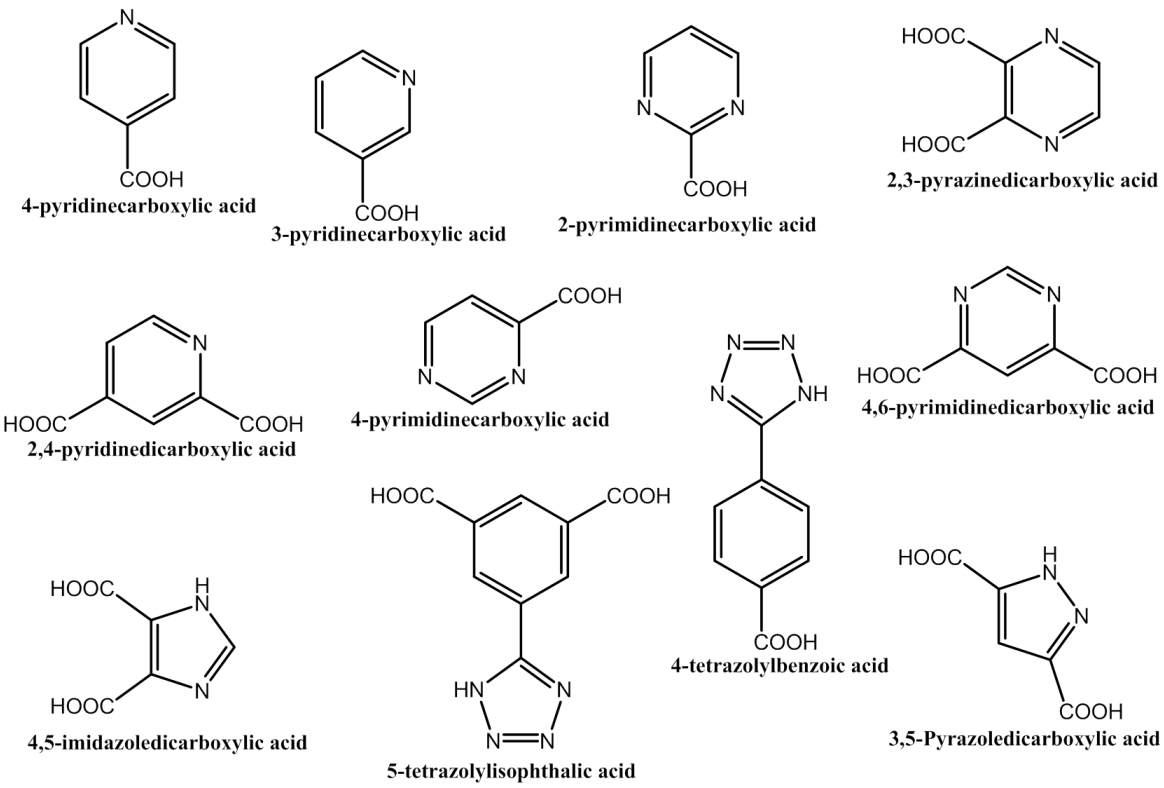

Figure 5. Some examples of aromatic carboxylic acid used for MOMs synthesis.

Early precedence of the use of hetero-functional ligands for example 2,5-pyrazinedicarboxylic includes the construction of MOMs based on hetero-chelating Cu-ligand building block with interesting magnetic properties which was reported by Kitagawa and co-

workers.[35] Other early report evidenced the use of 2,5-pyrazinedicarboxylic in presence of copper or cobalt metal ions to yield chain-like coordination polymers.[36] Taking the advantage of hetero-chelating motifs, Eddaoudi group have recently developed the single-metal-ion-based molecular building block (MBBs) approach for constructing open framework materials.[37-39] In fact, the MBBs approach was successfully employed to produce indium metal ions based zeolite like metal-organic frameworks with **sod** and **rho** topology.[40] The use of 5-tetrazolylisophthalic acid allowed to construct another unique material with 3,24-connected **rht** topology.[41]

1.4.4. Hybrid Organic Ligands

The presence of two types of organic building blocks for example one possessing oxygen-donor atoms (or hetero-functional motifs) while other bearing nitrogen-donor entities in the reaction mixture are shown to be effective in constructing highly open 3D framework materials. The assembly of open 3D structures is presumably to follow two reaction steps. Perhaps in the first step, the metal moieties assemble via bonding through the oxygen-donor building block to generate a two dimensional sheet layers. In the next step, the second ligand connects the 2D sheets in the form of pillaring units to lead to the formation of the final network. If, H-bonding serves as the primary binding motifs to connect between the sheets and the pillaring units, the constructed frameworks may suffer from their structural integrity upon removal of occluded guest solvent molecules. On the other hand, the coordination bonding between the sheets and the pillaring units may provide sufficient robustness to the structures.[42]

Early examples of metal organic materials comprising mixture of ligands were reported by Kondo et al.,[42a] where the 2D sheets layer of $[Cu\{(pzdc)\}_n]$(pzdc = pyrazine-2,3-dicarboxylate) were bridged by different nitrogen donor ligands such as pyrazine (pyz), 4,4′-bipyridine (bpy), 1,2-dipyridylglycol (dpyg), etc via coordination bond to generate a series of highly open framework materials. In 2001, Seki had reported the synthesis of pillared layer (more accurately pillerd-grid) MOMs based on dimetal paddle-wheel units with optimum pore sizes and porosities.[43] Other interesting MOMs constructed from hybrid organic linkers includes $[Zn_2(1,4\text{-bdc})_2dabco]\cdot 4DMF\cdot 0.5H_2O$ and an isoreticular framework, DMOF-1-NH_2.[44,45]

1.4.5. Mixture of Oxygen Donor Ligands

Another interesting approach for constructing MOMs with potentially high porosities deals with the utilization of mixture of organic ligands contains oxygen donor molecular building blocks. The advantage which may associate with this recently adopted approach is that, it permits easy access of different types of pores for examples micro and meso in one material through careful selection of the organic linkers. Indeed, Matzger and co-worker examined this strategy to built two unique MOMs, UMCM-1 ($[Zn_4O(bdc)(btb)_{4/3}]$) (btb = 1,3,5-benzenetribenzoate) and an isoreticular material UMCM-2 ($[Zn_4O(t^2dc)(btb)_{4/3}]$) ($t^2$dc = thieno[3,2-b]thiophene-2,5-dicarboxylate) with extraordinary high Langmuir surface area of 4730 $m^2\ g^{-1}$ and 6060 $m^2\ g^{-1}$ respectively.[46] An isostructural material, UMCM-1-NH_2, was reported by Cohen's group by replacing the bdc linker of UMCM-1with BDC-NH_2.[45] In 2010, Furukawa et al. reported highly open metal-organic materials for example MOF-205 and MOF-210 with remarkable surface areas and pore volume by linking the octahedral shaped $Zn_4O(CO_2)_6$ cluster with a mixture of o-donor carboxylate ligands.[47]

Recently Deng et al. prepared an astounding series of multivariate (MTV) MOF-5 structures that evidenced to posses up to eight distinct functionalities in one phase by employing a mixture of O-donor linkers with varying ratios.[48]

1.5. Postsynthetic Modifications (PSM)

As the synthesis of metal-organic materials are usually performed under solvothermal condition following a ‘‘one pot’’ chemical reaction, there is a lack of opportunity to adjust the functionality and their associated chemical and physical properties. Any alternate approach which would permit the manipulation of the functionality and/or the structural features of the materials after their synthesis will be of great importance. Perhaps, postsynthetic modification is one such method which allows the chemical modification of frameworks by undertaking reactions on the performed MOFs. The idea of postsynthetic modification of coordination solids was suggested in 1990 by Hoskins and Robson.[5b] Recently, the PSM approach has been extensively investigated in order to change the functionality of a wide range of MOFs to achieve the desired properties.[49] The salient feature of PSM is that, it can overcome the limitation of typical harsh solvothermal reaction condition, where many functional groups are found to be

unstable (degrade); and therefore, greatly limit the scope of functional groups which could be incorporated presynthetically.

The postsynthetic modification of the MOFs could be accomplished through non-covalent and covalent interactions, through coordinative interactions or *via* deprotection of the chemical entities (Figure 6).

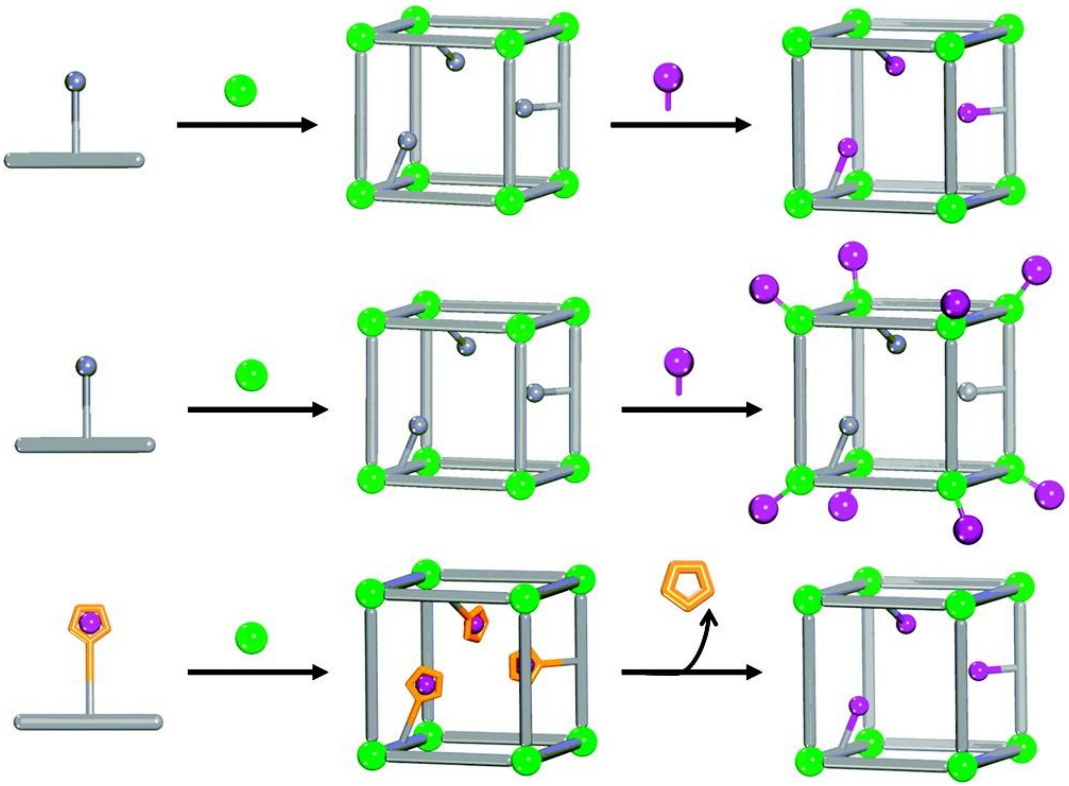

Figure 6. Generic schemes for PSM through covalent interaction at the linkers (top), PSM through coordinative interaction at the SBUs (middle) and PSM though deprotection of the chemical entities (bottom).[49c]

Postsynthetic modification through non-covalent interaction includes removal or exchange of occluded guest solvent molecules and ion exchange of the performed MOFs. However, it should be noted that the ion exchange is largely limited to the charged frameworks while other two types are most frequently seen in MOF chemistry.

Covalent PSM is widely explored over the last few years and is proven to be a powerful and versatile method for introducing a broad range of chemical groups into the MOFs.[49] In general, a suitable reagent is used to modify a component of the MOF under heterogeneous

reaction condition to form a new covalent bond. Mostly, the pendant functional groups of the MOFs which are attached to the organic linkers are derivatized through covalent interaction with different new chemical entities; however, there are some reports where the covalent modification is achieved at the SBUs.[49c] Cohen and co-workers was the first to evidence that the free -NH_2 groups of IRMOF-3 could be readily modified with anhydride in a covalent postsynthetic manner.[50] Recent finding reveals that covalent postsynthetic modification of MOFs could be attained by means of amide coupling, imine condensation, click chemistry, etc.[49,51] Covalent postsynthetic modification at the node, SBUs, of MOFs was first reported by Fischer and co-workers.[52]

PSM through coordinative interactions are generally achieved by adding a suitable ligand to the framework that coordinates to the SBUs of the MOF or by adding a metal source which can bind to the organic linker of the MOF *via* dative bonding. For instance, the open metal sites at the SBU of HKUST-1, which could be generated after removal of the axial aqua ligands, can be rebound by other ligands such as pyridine derivatives through a coordination interaction.[28] Bloch et al. recently reported an interesting examples of dative PSM of the organic linker,[53] in where the open bpy sites of MOF-253 was metallated with Cu(II) and Pd(II) *via* dative bonding.

PSM of MOMs though deprotection of chemical entities involve cleavage of a chemical bonds which can be either covalent, dative or any other type within an intact framework to disclose a chemical functionality and produce materials with different properties. Early example of such type of PSM was reported by Yamada and Kitagawa.[54]

1.6. Secondary Building Units (SBUs)

The bursting research interest in the field of metal-organic materials could be attributed to their potential utilities in a wide variety of technologically important applications. It is therefore significant to have some set of discipline or approaches which may permit the rational design of the suitable materials with desired properties. An emerging approach in the rational designing of extended structure is through the use of secondary building units (SBUs).[55] SBUs are molecular complexes and cluster entities that are linked together by the organic linkers to form extended network structures. The SBUs approach is particularly attractive due to their steric requirements and rigidity which greatly reduces the number of possible underlying network topology that may arise from a given node/spacer (linker) combination.[56] In general a specific

SBU is generated *in situ* under suitable reaction conditions. Mostly, linkers possess carboxylic acid functionality are utilized due to their ability to lock the metal ions into a specific position by chelation through bi-monodentate fashion. Additionally, the use of carboxylate ligands in combination with metal ions leads to the formation of neutral networks. This avoids any requirement for the presence of counter ions that could reduce the porosity of the final solids.

Some of the common SBUs which are used to construct extended structures with high porosity and stability are depicted in Figure 7. In particular, the SBU comprised of bimetallic "paddlewheel" units (Figure 7a) is evidenced to produce a wide variety of MOF structures. The paddle wheel SBUs is generated *in situ* by locking two metal ions (e.g. Cu, Ni, Co, Zn, Fe etc.) with carboxylate linkers under optimized reaction condition. These metal ions on the paddlewheel SBUs can be capped by a solvent molecule or by additional coordinating ligands.[57]

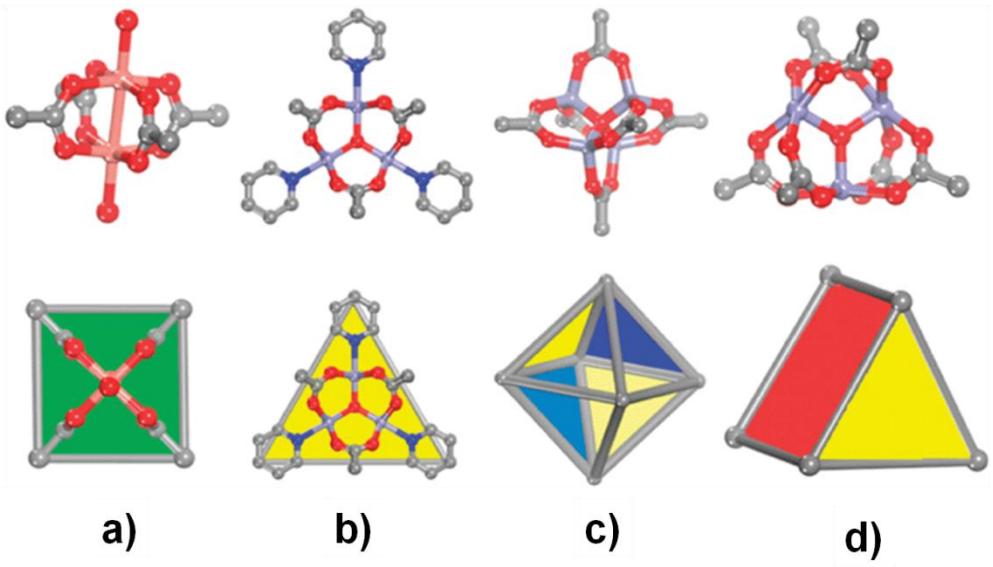

Figure 7. Examples of prototypal secondary building units (SBUs) commonly used in the construction of periodic MOMs. (a) Cupric acetate is a dimetal tetracarboxylate square paddlewheel cluster $[M_2(O_2CR)_4L_2]$ (M = transition metal, L = axial ligand) which mimics a molecular square. Basic chromium(III) acetate, a μ_3-oxo trimetallic hexacarboxylate cluster $[M_3O(O_2CR)_6L_3]$ can be used as either a molecular triangle (b) or a triangular prism (d). (c) Basic zinc acetate is a μ_4-oxo tetrametallic hexacarboxylate cluster, $[M_4O(O_2CR)_6]$, that is prototypal for a molecular octahedron.[1]

Yaghi and co-workers synthesized one of the early investigated framework, known as MOF-2, based on paddle wheel SBUs in which two zinc atoms are linked in a periodic square array.[58] Another unique 3D structure widely known as HKUST-1 was synthesized by William et al. based on paddle wheel SBUs which comprises Cu dimers and each of the Cu ions are further coordinated by one terminal water ligand.[28]

Another interesting SBU which consists of a central tetrahedral oxide ion coordinated to four tetrahedral zinc atoms to form the primary building units, which then further coordinated by carboxylates to form the final secondary building unit $Zn_4O(CO_2)_6$ with octahedral geometry (Figure 7c) is widely investigated. Some of the prototype frameworks for example MOF-5 and IRMOF-3, IRMOF-8 etc were constructed from this SBU.[25,26]

1.7. Reticular Synthesis

Perhaps it remains a challenge for solid state chemists to synthesize materials especially which are extended (i.e. non-molecular) that were designed *a priori* to have structures that would lead to specific functions, although it has been achieved in regular basis in molecular chemistry or even in metal-complex chemistry. This is mainly because of the lack of control over the character of solids produced from one pot chemical reaction, where the starting entities do not maintain their structure during the reaction. Consequently, leads to a poor correlation between the reactants and the products.

Recently, it was proposed by the research group of Yaghi that, new approach for designing of predetermined ordered structures can be realized by starting with well-defined and rigid molecular building blocks which can maintain their structural integrity throughout the construction process.[56,59] In other words, by employing a well-defined reaction condition which may lead to the formation of such molecular building block *in situ* would drive the reaction towards the formation of extended structures *via* assembly of these building units. They defined the approach as reticular designing of porous materials. Indeed, it was successfully examined to prepare a series of extended robust structures popularly known as IRMOFs (isoreticular metal-organic frameworks) which are based on a predetermined SBUs ($Zn_4O(CO_2)_6$) and linear ditopic organic linkers with varied length and functionality as molecular building blocks (Figure 8).[26] There are several other series of isoreticular metal-organic materials which were reported later following the principle of reticular designing of porous materials. For example, Zhou group

synthesized a series of isoreticular MOFs based on $Cu_2(CO_2)_4$ SBUs and tritopic carboxylic acid linkers as molecular building blocks.[60,61]

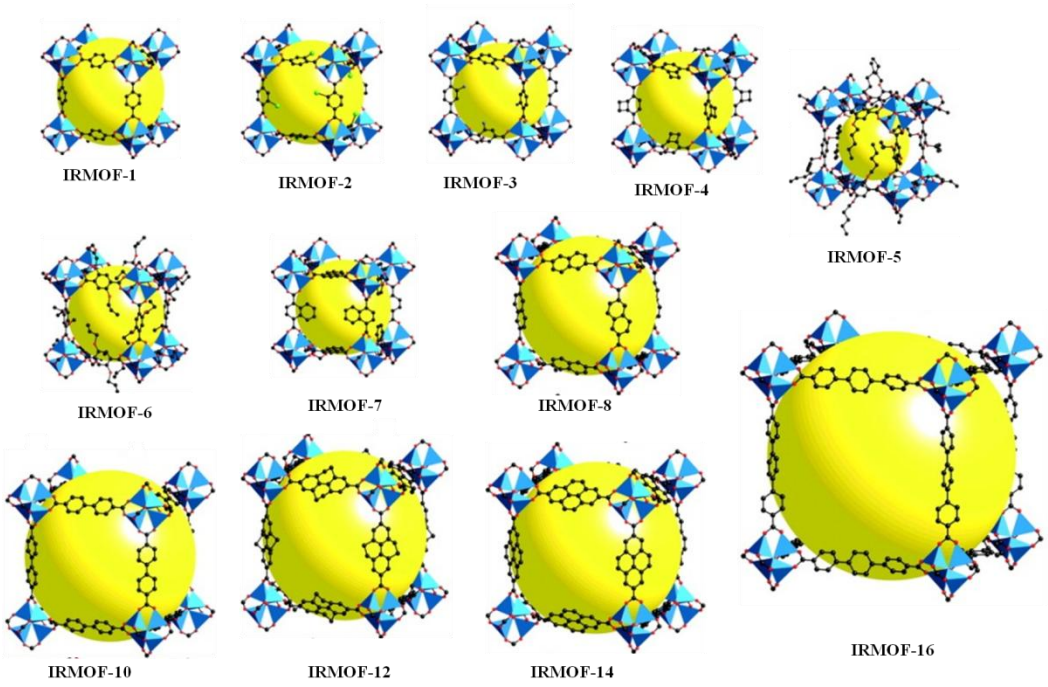

Figure 8. The picture of a series of IRMOFs constructed from liner ditopic O-donar organic linkers with varied length and functionalities in a cubic topology.[26]

Furukawa et al. reported an isoreticular family of MOFs comprising of $Cu_2(CO_2)_4$ SBU and tritopic carboxylic acids.[62a] Recently, Yaghi and co-workers reported a remarkable isoreticular series of materials (termed as IRMOF-74-I to -XI) based on underlying topology of MOF-74.[62b]

1.8. Applications of MOMs

Over the last decades metal-organic materials are attracting immense research attention due to their wide range of potential academic and industrial applications.[2,63] Majority of the application of MOMs are derived based on their unique set of characteristics, such as high surface area, diverse pore structures with tunable pore sizes and geometry, and adjustable internal surface properties. MOMs with high surface area and pore volumes are widely evaluated based on their small molecular storage and separation capacities.[64b,65-67] Other advantages associated with their porosities are also exploited in many applications.[68-70,49c]

For example, heterogeneous catalysis using porous MOMs is widely investigated despite their relatively low thermal and chemical stability when compared to the other porous materials such as zeolite.[68,70] However, MOMs on the other hand offer several unparallel advantages especially high surface area, pore volume and pore sizes as well as possible tunability of the organic link in which functionality can be introduced. In 1994, Fujita and coworkers have reported the catalytic activity of MOF, $\{[Cd(4,4'\text{-bpy})_2](NO_3)_2\}_\infty$ (bpy = bipyridine), for the cyanosilylation of aldehydes.[14] Several other interesting reports appeared thereafter which described the catalytic use of MOMs. Some of these reports dealt with aldol reactions[71], oxidation of olefins[72], acyl transfer reaction,[73] hydroxylation of alkane[74] and other[75]. An interesting study was made by the group of Rosseinsky, where the synthesis of a MOF material containing Brønsted acid sites through postsynthesis protonation of the carboxylate ligands was investigated.[76] Kitagawa and co-workers reported the first example of Knoevenagel condensation reaction catalyzed by a MOF $\{[Cd(4\text{-btapa})_2(NO_3)_2]\cdot 6H_2O\cdot 2DMF\}_n$ (where 4-btapa = 1,3,5-benzenetricarboxylic acid tris[N-(4-pyridyl)amide)].[77] Hwang et al. reported Brønsted basic catalysts.[78] Other interesting reports investigated synthesis of homochiral MOFs[79-85] and enantioselective catalysis using homochiral MOFs.[79,86-91] As already mentioned before, MOFs have been widely exploited for many other applications which includes gas storage and gas separation. Storage of hydrogen, methane, carbon dioxide, carbon monoxide, acetylene, etc. in MOFs is among the mostly investigated. After the pioneering work of Yaghi, a large number of porous MOMs have been investigated for hydrogen storage application.[64] A detailed overview on hydrogen storage in MOFs will be given in Chapter 3. IRMOFs were evaluated based on their methane storage applications by Eddaoudi et al. in 2002.[26] Zhou and co-workers reported a remarkable material PCN-14 with extraordinary high methane uptake capacity.[92] Many other interesting examples directing towards the storage of methane in MOMs have been reported there after.[93] Yaghi's research group exploited the potential utility of MOFs for carbon dioxide storage.[94,95] Other interesting investigations towards the storage of CO_2 in MOFs were also pursued by Férey's[96,97] and Lah's[98] groups. Zhou group demonstrated potential application of MOMs for separation of gas mixture of O_2/N_2, H_2/N_2 and H_2/CO,[99] or H_2/CO, Ar/N_2[100]. The group further reported interesting approach for separation of gas mixture using MAMs (Mesh Adjustable Molecular Sieves).[101] Kitagawa's group investigated application of MOMs towards separation of gases.[77,102,103] Several others reports exploited separation of CO_2/CH_4, CO/N_2,

C_2H_2/CO_2 and CH_4/CO_2 has also appeared.[94,104,105] Separation of H_2/D_2 was reported by Thomas et al.[106] Férey and co-workers investigated control drug release applications of MOFs.[107-109] Another interesting investigation along this direction was made by Lin's group.[110] MOMs were also found to be interesting in the field of sensors,[111,112] magnetism[113,114] and many others[115,116,117,118,119,120].

The following chapters will focus on physical adsorption and hydrogen storage in MOFs by physical adsorption.

1.9. References

1. J. J. Perry IV, J. A. Perman and M. J. Zaworotko, *Chem. Soc. Rev.*, 2009, **38**, 1400–1417.
2. H.-C. Zhou, J. R. Long and O. M. Yaghi, *Chem. Rev.*, 2012, **112**, 673−674.
3. (*a*) J. Lipkowski, *Comprehensive Supramolecular Chemistry* 1996, **6**, 691-714; (*b*) J. Lipkowski, *NATO ASI Series, Series C: Mathematical and Physical Sciences* 1996, **480**, 265-283; (*c*) J. Lipkowski, *Organic Crystal Chemistry* 1991, **4**, 27-35; (*d*) J. Lipkowski, *Inclusion Compounds*, 1984, **1**, 59-103; (*e*) J. Lipkowski, K. Suwinska, G. D. Andreetti and K. Stadnicka, *J. Mol. Struct.*, 1981, **75**, 101-112.
4. K. A. Hofmann and F. Kiispert, *Z. Anorg. Chem.*, 1897, **15**, 204-207.
5. (*a*) B. F. Hoskins and R. Robson, *J. Am. Chem. Soc*., 1989, **111**, 5962-5964; (*b*) B. F. Hoskins, and R. Robson, *J. Am. Chem. Soc*., 1990, **112**, 1546-1954.
6. J. C. Bailar, *Prep. Inorg. React.*, 1964, 1.
7. P. G. Jones, *Chemistry in Britain*, 1981, 222-5.
8. J. Hulliger, *Angew. Chem., Int. Ed.*, 1994, **33**, 143-62.
9. X. X. Zhao, J. P. Ma, Y. B. Dong and R. Q. Huang, *Cryst. Growth Des.,* 2007, **7**, 1058.
10. R. I. Walton, *Chem. Soc. Rev.*, 2002, **31**, 230-8.
11. X. M. Zhang, *Coord. Chem. Rev.*, 2005, **249**, 1201.
12. R. W. Gable, B. F. Hoskins and R. Robson, *J. Chem. Soc., Chem. Commun.,* 1990, **23**, 1677-1678.
13. S. Subramanian, and M. J. Zaworotko, *Angew. Chem., Int. Ed.*, 1995, **34**, 2127-2129.
14. M. Fujita, Y. J. Kwon, S. Washizu and K. Ogura, *J. Am. Chem. Soc.* 1994, **116**, 1151-1152.
15. P. Losier and M. J. Zaworotko, *Angew. Chem., Int. Ed.*, 1997, **35**, 2779-2782.

16. J. Lu, T. Paliwala, S. C. Lim, C. Yu, T. Niu and A. J. Jacobson, *Inorg. Chem.*, 1997, **36**, 923-929.
17. L. R. MacGillivray, S. Subramanian and M. J. Zaworotko, *J. Chem. Soc., Chem. Commun.*, 1994, **11**, 1325-1326.
18. X.-C. Huang, Y.-Y. Lin, J.-P. Zhang and X.-M. Chen, *Angew. Chem., Int. Ed.*, 2006, **45**, 1557-1559.
19. K. S. Park, Z. Ni, A. P. Cote, J. Y. Choi, R. Huang, F. J. Uribe-Romo, H. K. Chae, M. O'Keeffe and O. M. Yaghi, *Proc. Natl. Acad. Sci., U.S.A.* 2006, **103**, 10186-10191.
20. H. J. Choi, M. Dincă and J. R. Long, *J. Am. Chem. Soc.*, 2008, **130**, 7848.
21. A. Demessence, D. M. D'Alessandro, M. L. Foo and J. R. Long, *J. Am. Chem. Soc.*, 2009, **131**, 8784.
22. M. Dincă, A. Dailly, Y. Liu, C. M. Brown, D. A. Neumann and J. R. Long, *J. Am. Chem. Soc.*, 2006, **128**, 16876.
23. M. Dincă, A. Dailly, C. Tsay and J. R. Long, *Inorg. Chem.*, 2008, 47, 11.
24. (*a*) S. Watanabe, *Nature*, 1949, **163**, 225-226; (*b*) H. Koyama and Y. Saito, *Bull. Chem. Soc. Jpn.*, 1954, *27*, 112-114.
25. H. Li, M. Eddaoudi, M. O'Keeffe and O. M. Yaghi, *Nature*, 1999, **402**, 276-279.
26. M. Eddaoudi, J. Kim, N. Rosi, D. Vodak, J. Wachter, M. O'Keeffe and O. M. Yaghi, *Science*, 2002, **295**, 469-472.
27. H. K. Chae, D. Y. Siberio-Pérez, J. Kim, Y. Go, M. Eddaoudi, A. J. Matzger, M. O'Keeffe and O. M. Yaghi, *Nature*, 2004, **427**, 523.
28. S. S. Y. Chui, S. M. F. Lo, J. P. H. Charmant, A. G. Orpen and I. D. Williams, *Science*, 1999, **283**, 1148.
29. B. Moulton, J. Lu, A. Mondal and M. Zaworotko, *Chem. Commun.*, 2001, **9**, 863-864.
30. M. Eddaoudi, J. Kim, J. B. Wachter, H. K. Chae, M. O'Keeffe and O. M. Yaghi, *J. Am. Chem. Soc.*, 2001, **123**, 4368-4369.
31. G. Férey, C. Serre, C. Mellot-Draznieks, F. Millange, S. Surblé, J. Dutour and I. Margiolaki, *Angew. Chem., Int. Ed.*, 2004, **43**, 6296.
32. G. Férey, C. Mellot-Draznieks, C. Serre, F. Millange, J. Dutour, S. Surblé and I. Margiolaki, *Science*, 2005, **309**, 2040.

33. M. Latroche, S. Surblé, C. Serre, C. Mellot-Draznieks, P. L. Llewellyn, J.-H. Lee, J.-S. Chang, S. H. Jhung and G. Férey, *Angew. Chem., Int. Ed.*, 2006, **45**, 8227.

34. (*a*) T. Loiseau, L. Lecroq, C. Volkringer, J. Marrot, G. Férey, M. Haouas, F. Taulelle, S. BourrellyP. L. Llewellyn and M. Latroche, *J. Am. Chem. Soc.*, 2006, **128**, 10223-10230; (*b*) P. Horcajada, S. Surblé, C. Serre, D. Y. Hong, Y. K. Seo, J. S. Chang, J. M. Greneche, I. Margiolaki and G. Férey, *Chem. Commun.*, 2007, **27**, 2820-2822; (*c*) C. Serre, C. Mellot-Draznieks, S. Surblé, N. Audebrand, Y. Filinchuk and G. Férey, *Science*, 2007, **315**, 1828-1831.

35. T. Okubo, M. Kondo and S. Kitagawa, *Synth. Met.*, 1997, **85**, 1661-1662.

36. (*a*) P. Richard, Q. D. Tran and E. F. Bertaut, *Acta Crystallogr. Sect. B*, 1973, **29**, 1111-1115; (*b*) C. J. O'Connor, C. L. Klein, R. J. Majeste and L. M. Trefonas, *Inorg. Chem.*, 1982, **21**, 64-67.

37. (*a*) J. A. Brant, Y. Liu, D. F. Sava, D. Beauchamp and M. Eddaoudi, *J. Mol. Struct.*, 2006, **796**, 160-164; (*b*) M. Eddaoudi and J. F. Eubank, in *Organic Nanostructures*; J.L. Atwood, and J.W. Steed, Eds. WILEY-VCH Verlag GmbH & Co. KGaA: Weinheim, 2008, 251-276.

38. Y. Liu, V. Ch. Kravtsov, R. D. Walsh, P. Poddar, S. Hariharan and M. Eddaoudi, *Chem. Commun.*, 2004, **24**, 2828-2829.

39. Y. Liu, V. Ch. Kravtsov, D. A. Beauchamp, J. F. Eubank and M. Eddaoudi, *J. Am. Chem. Soc.*, 2005, **127**, 7266-7267.

40. (*a*) Y. Liu, V. Ch. Kravtsov, R. Larsen and M. Eddaoudi, *Chem. Commun.*, 2006, 1488-1490; (*b*) M. Eddaoudi, J. F. Eubank, Y. Liu, V. Ch. Kravtsov, R. W. Larsen and J. A. Brant, *Studies in Surface Science and Catalysis* 2007, *170B* (From Zeolites to Porous MOF Materials), 2021-2029.

41. F. Nouar, J. F. Eubank, T. Bousquet, L. Wojtas, M. J. Zaworotko and M. Eddaoudi, *J. Am. Chem. Soc.*, 2008, **130**, 1833-1835.

42. (*a*) M. Kondo, T. Okubo, A. Asami, S. Noro, T. Yoshitomi, S. Kitagawa, T. Ishii, H. Matsuzaka and K. Seki, *Angew. Chem., Int. Ed.*, 1999, **38**, 140-3; (*b*) R. Kitaura, K. Fujimoto, S. Noro, M. Kondo and S. Kitagawa, *Angew. Chem. Int. Ed.*, 2002, **41**, (1), 133-5; (*c*) V. A. Russell, C. C. Evans, W. Li and M. D. Ward, *Science*, 1997, **276**, (5312), 575–9; (*d*) S. C. Zimmerman, *Science*, 1997, **276**, (5312), 543-4.

43. K. Seki, *Chem. Commun.*, 2001, 1496–1497.
44. D. N. Dybtsev, H. Chun and K. Kim, *Angew. Chem., Int. Ed.*, 2004, **43**, 5033.
45. Z. Wang, K. K. Tanabe and S. M. Cohen, *Inorg. Chem.*, 2009, **48**, 296.
46. (a) K. Koh, A. G. Wong-Foy and A. J. Matzger, *Angew. Chem., Int. Ed.*, 2008, **47**, 677–680; (b) K. Koh, A. G. Wong-Foy and A. J. Matzger, *J. Am. Chem. Soc.*, 2009, **131**, 4184-4185.
47. H. Furukawa, N. Ko, Y. B. Go, N. Aratani, S. B. Choi, E. Choi, A. O. Yazaydin, R. Q. Snurr, M. O'Keeffe, J. Kim and O. M. Yaghi, *Science*, 2010, **329**, 424.
48. H. Deng, C. Doonan, H. Furukawa, R. B. Ferreira, J. Towne, C. B. Knobler, B. Wang and O. M. Yaghi, *Science*, 2010, **327**, 846.
49. (*a*) Z. Q. Wang, and S. M. Cohen, *Chem. Soc. Rev.*, 2009, **38**, 1315; (*b*) K. K. Tanabe, and S. M. Cohen, *Chem. Soc. Rev.*, 2011, **40**, 498; (*c*) S. M. Cohen, *Chem. Rev.*, 2012, **112**, 970-1000.
50. Z. Wang and S. M. Cohen, *J. Am. Chem. Soc.*, 2007, **129**, 12368.
51. Y. F. Song and L. Cronin, *Angew. Chem., Int. Ed.*, 2008, **47**, 4635.
52. M. Meilikhov, K. Yusenko and R. A. Fischer, *J. Am. Chem. Soc.*, 2009, **131**, 9644.
53. E. D. Bloch, D. Britt, C. Lee, C. J. Doonan, F. J. Uribe-Romo, H. Furukawa, J. R. Long and O. M. Yaghi, *J. Am. Chem. Soc.*, 2010, **132**, 14382.
54. T. Yamada and H. Kitagawa, *J. Am. Chem. Soc.*, 2009, **131**, 6312.
55. D. J. Tranchemontagne, J. L. Mendoza-Cortés, M. O'Keeffe and O. M. Yaghi, *Chem. Soc. Rev.*, 2009, **38**, 1257.
56. M. Eddaoudi, D. B. Moler, H. L. Li, B. L. Chen, T. M. Reineke, M. O'Keeffe and O. M. Yaghi, *Acc.Chem. Res.*, 2001, **34**, 319.
57. J. L. C. Rowsell and O. M. Yaghi, *Micropor. Mesopor. Mat.*, 2004, **73**, 3.
58. H. Li, M. Eddaoudi, T. L. Groy and O. M. Yaghi, *J. Am .Chem .Soc.*, 1998, **120**, 8571.
59. O. M. Yaghi, H. Li, C. Davis, D. Richardson and T. L. Groy, *Acc. Chem. Res.*, 1998, **31**, 474-484.
60. D. Zhao, D. Yuan, D. Sun and H.-C. Zhou, *J. Am .Chem. Soc.*, 2009, **131**, 9186.
61. D. Yuan, D. Zhao, D. Sun and H.-C. Zhou, *Angew. Chem., Int. Ed.*, 2010, **49**, 5357.
62. (*a*) H. Furukawa, Y. B. Go, N. Ko, Y. K. Park, F. J. Uribe-Romo, J. Kim, M. O'Keeffe and O. M. Yaghi, *Inorg. Chem.*, 2011, **50**, 9147; (*b*) H. Deng, S. Grunder, K. E. Kordova,

C. Valente, H. Furukawa, M. Hmadesh, F. Gandara, A. C. Whalley, Z. Liu, J. F. Stoddart and O. M. Yaghi, *Science*, 2012, **336**, 1018-1023.

63. J. R. Long and O. M. Yaghi, *Chem. Soc. Rev.*, 2009, **38**, 1213.
64. (*a*) N. L. Rosi, J. Eckert, M. Eddaoudi, D. T. Vodak, J. Kim, M. O'Keeffe and O. M. Yaghi, *Science*, 2003, **300**, 1127-1129; (*b*) M. P. Suh, H. J. Park, T. K. Prasad and D.-W. Lim, *Chem. Rev.*, 2012, **112**, 782–835.
65. J.-R. Li, J. Sculley and H.-C. Zhou, *Chem. Rev.*, 2012, **112**, 869-932.
66. H. Wu, Q. Gong, D. H. Olson and J. Li, *Chem. Rev.*, 2012, **112**, 836-868.
67. K. Sumida, D. L. Rogow, J. A. Mason, T. M. McDonald, E. D. Bloch, Z. R. Herm, T.-H. Bae and J. R. Long, *Chem. Rev.*, 2012, **112**, 724-781.
68. A. Corma, H. Garcıa, and F. X. Llabres i Xamena, *Chem. Rev.*, 2010, **110**, 4606-4655.
69. P. Horcajada, R. Gref, T. Baati, P. K. Allan, G. Maurin, P. Couvreur, G. Férey, R. E. Morris and C. Serre, *Chem. Rev.*, 2012, **112**, 1232-1268.
70. M. Yoon, R. Srirambalaji and K. Kim, *Chem. Rev.*, 2012, **112**, 1196-1231.
71. S. Horike, M. Dincă, K. Tamaki and J. R. Long, *J. Am. Chem. Soc.*, 2008, **130**, 5854-5855.
72. Y. Lu, M. Tonigold, B. Bredenkötter, D. Volkmer, J. Hitzbleck and G. Langstein, *Z. Anorg. Allg. Chem.*, 2008, **634**, 2411–2417.
73. A. M. Shultz, O. K. Farha, J. T. Hupp and S. T. Nguyen, *J. Am. Chem. Soc.*, 2009, **131**, 4204-4205.
74. K. S. Suslick, P. Bhyrappa, J. H. Chou, M. E. Kosal, S. Nakagaki, D. W. Smithenry and S. R. Wilson, *Acc. Chem. Res.*, 2005, **38**, 283-291.
75. M. H. Alkordi, Y. Liu, R. W. Larsen, J. F. Eubank and M. Eddaoudi, *J. Am. Chem.Soc.*, 2008, **130**, 12639-12641.
76. M. J. Ingleson, J. P. Barrio, J. Bacsa, C. Dickinson, H. Park and M. J. Rosseinsky, *Chem. Commun.*, 2008, **11**, 1287-1289.
77. S. Hasegawa, S. Horike, R. Matsuda, S. Furukawa, K. Mochizuki, Y. Kinoshita and S. Kitagawa, *J. Am. Chem. Soc.*, 2007, **129**, 2607-2614.
78. Y. K. Hwang, D. Y. Hong, J. S. Chang, S. H. Jhung, Y. K. Seo, J. Kim, A. Vimont, M. Daturi, C. Serre and G. Férey, *Angew. Chem., Int. Ed.*, 2008, **47**, 4144-4148.
79. J. S. Seo, D. Whang, H. Lee, S. I. Jun, J. Oh, Y. J. Jeon and K. Kim, *Nature*, 2000,

404, 982-986.

80. C. J. Kepert, T. J. Prior and M. J. Rosseinsky, *J. Am. Chem. Soc.*, 2000, **122**, 5158-5168.
81. D. Bradshaw, T. J. Prior, E. J. Cussen, J. B. Claridge and M. J. Rosseinsky, *J. Am. Chem. Soc.*, 2004, **126**, 6106-6114.
82. Z. Lin, A. M. Z. Slawin and R. E. Morris, *J. Am. Chem. Soc.*, 2007, **129**, 4880-4881.
83. J. Zhang, S. M. Chen, T. Wu, P. Y. Feng and X. H. Bu, *J. Am. Chem. Soc.*, 2008, **130**, 12882-12883.
84. C. D. Wu and W Lin, *Angew. Chem., Int. Ed.*, 2005, **44**, 1958-1961.
85. L. Ma and W. Lin, *J. Am. Chem. Soc.*, 2008, **130**, 13834-1835.
86. L. Ma, C. Abney and W. Lin, *Chem. Soc. Rev.*, 2009, **38**, 1248-1256.
87. O. R. Evans, H. L. Ngo and W. Lin, *J. Am. Chem. Soc.*, 2001, **123**, 10395-10396.
88. A. Hu, H. L. Ngo and W. Lin, *Angew. Chem., Int. Ed.*, 2003, **42**, 6000-6003.
89. K. Tanaka, S. Oda and M. Shiro, *Chem. Commun.*, 2008, 820-822.
90. R. Vaidhyanathan, D. Bradshaw, J. N. Rebilly, J. P. Barrio, J. A. Gould, N. G. Berry and M. J. Rosseinsky, *Angew. Chem., Int. Ed.*, 2006, **45**, 6495-6499.
91. M. J. Ingleson, J. P. Barrio, J. Bacsa, C. Dickinson, H. Park and M. J. Rosseinsky, *Chem. Commun.*, 2008, **11**, 1287-1289.
92. S. Ma, D. Sun, J. M. Simmons, C. D. Collier, D. Yuan and H.-C. Zhou, *J. Am. Chem. Soc.*, 2008, **130**, 1012-1016.
93. S. Ma and H.-C. Zhou, *Chem. Commun.*, 2010, **46**, 44-53.
94. B. Wang, A. P. Cote, H. Furukawa, M. O'Keeffe and O. M. Yaghi, *Nature*, 2008, **453**, 207-211.
95. A. R. Millward and O. M. Yaghi, *J. Am. Chem. Soc.*, 2005, **127**, 17998-17999.
96. S. Bourrelly, P. L. Llewellyn, C. Serre, F. Millange, T. Loiseau and G. Férey, *J. Am. Chem. Soc.*, 2005, **127**, 13519-13521.
97. P. L. Llewellyn, S. Bourrely, C. Serre, A. Vimont, M. Daturi, L. Hamon, G. D. Weireld, J. S. Chang, D. Y. Hong, Y. K. Hwang, S. H. Jhung and G. Férey, *Langmuir*, 2008, **24**, 7245-7250.
98. M. Park, D. Moon, J. W. Yoon, J. S. Chang and M. S. Lah, *Chem. Commun.*, 2009, **15**, 2026-2028.

99. S. Q. Ma, X. S. Wang, D. Q. Yuan and H.-C. Zhou, *Angew. Chem., Int. Ed.*, 2008, **47**, 4130-4133.

100. B. L. Chen, S. Q. Ma, F. Zapata, F. R. Fronczek, E. B. Lobkovsky and H.C. Zhou, *Inorg. Chem.*, 2007, **46**, 1233-1236.

101. S. Q. Ma, D. Sun, X. S. Wang and H.-C. Zhou, *Angew. Chem.*, 2007, **46**, 2458-2462.

102. R. Matsuda, R. Kitaura, S. Kitagawa, Y. Kubota, R. V. Belosludov, T. C. Kobayashi, H. Sakamoto, T. Chiba, M. Takata, Y. Kawazoe and Y. Mita, *Nature*, 2005, **436**, 238-241.

103. R. Kitaura, K. Seki, G. Akiyama and S. Kitagawa, *Angew. Chem., Int. Ed.*, 2003, **42**, 428-431.

104. B. Chen, C. Liang, J. Yang, D. S. Contreras, Y. L. Clancy, E. B. Lobkovsky, O. M. Yaghi and S. Dai, *Angew. Chem., Int. Ed.*, 2006, **45**, 1390-1393.

105. S. Bourrelly, P. L. Llewellyn, C. Serre, F. Millange, T. Loiseau and G. Férey, *J. Am. Chem. Soc.*, 2005, **127**, 13519-13521.

106. B. Chen, X. Zhao, A. Putkham, K. Hong, E. B. Lobkovsky, E. J. Hurtado, A. J. Fletcher and K. M. Thomas, *J. Am. Chem. Soc.*, 2008, **130**, 6411-6423.

107. P. Horcajada, T. Chalati, C. Serre, B. Gillet, C. Sebrie, T. Baati, J. F. Eubank, D. Heurtaux, P. Clayette, C. Kreuz, J. S. Chang, Y. K. Hwang, V. Marsaud, P. Nhi. Bories, L. Cynober, S. Gil, G. Férey, P. Couvreur and R. Gref, *Nat. Mater.*, 2010, **9**, 172-178.

108. P. Horcajada, C. Serre, M. Vallet-Regi, M. Sebban, F. Taulelle and G. Férey, *Angew. Chem., Int. Ed.*, 2006, **45**, 5974-5978.

109. P. Horcajada, C. Serre, G. Maurin, N. A. Ramsahye, F. Balas, M. Vallet-Regi, M. Sebban, F. Taulelle and G. Férey, *J. Am. Chem. Soc.*, 2008, **130**, 6774-6780.

110. W. J. Rieter, K. M. Pott, K. M. L. Taylor and W. Lin, *J. Am. Chem. Soc.*, 2008, **130**, 11584-11585.

111. M. D. Allendorf, C. A. Bauer, R. K. Bhakta and R. J. T. Houk, *Chem. Soc. Rev.*, 2009, **38**, 1330-1352.

112. L. E. Kreno, K. Leong, O. K. Farha, M. Allendorf, R. P. Van Duyne and J. T. Hupp, *Chem. Rev.*, 2012, **112**, 1105-1125.

113. M. Kurmoo, *Chem. Soc. Rev.,* 2009, **38**, 1353-1379.

114. W. Zhang and R.-G. Xiong, *Chem. Rev.*, 2012, **112**, 1163-1195.

115. Z. Wang and S. M. Cohen, *Chem. Soc. Rev.*, 2009, **38**, 1315-1329.

116. A. M. Spokoyny, D. Kim, A. Sumrein and C. A. Mirkin, *Chem. Soc. Rev.*, 2009, **38**, 1218-1227.
117. T. Uemura, N. Yanai and S. Kitagawa, *Chem. Soc. Rev.*, 2009, **38**, 1328-1336.
118. D. Zacher, O. Shekhah, C. Woell and R. A. Fischer, *Chem. Soc. Rev.*, 2009, **38**,1418-1429.
119. Y. Cui, Y. Yue, G. Qian and B. Chen, *Chem. Rev.*, 2012, **112**, 1126-1162.
120. C. Wang, T. Zhang and W. Lin, *Chem. Rev.*, 2012, **112**, 1084-1104.

2. PHYSICAL ADSORPTION

2.1. Introduction

The nanoporous materials are described to be a subset of porous materials which has porosity greater than 0.4 and pore diameters in the range of 1-100 nm.[1] Nanoporous materials encompasses a regular organic or inorganic or organic-inorganic hybrid framework supporting a regular, porous structure. According to the International Union of Pure and Applied Chemistry (IUPAC),[2] nanoporous materials can be subdivided based on their pores sizes into three main categories; namely, microporous material, mesoporous material and macroporous material. More specifically, materials with pore dimensions smaller than 2 nm are called micropores, where as the materials with pores dimensions between 2 nm and 50 nm are termed mesopores and finally the material with pore dimension greater than 50 nm are called macroporous.

In 1881, Kayser was the first to introduce the term adsorption in literature referring to the condensation of gases on the bare surface.[3,4] To explain the result of adsorption experiments Kayser further introduced the terms isotherm and isotherm curve. Later in 1909, to define the special phenomenon where a precise distinction between the adsorption and absorption could not be made, a new term sorption was proposed by McBain.[5]

Because the gas adsorption method permitted the analysis of wide range of porous materials having the pore size in the range of 0.35 nm to >100 nm, this by far remains one of the most extensively used method, among many others for characterizing nanoporous materials.[6] The enrichment or accumulation of one or more components, whether molecules, atoms or ions, in an interfacial layer between two bulk phases are termed as adsorption.[2,7,8] The solid is referred to the adsorbent, the gas which is adsorbable is adsorptive and the fluid in the adsorbed state is the adsorbate. The adsorption process can be classified in two major categories namely physical adsorption and chemical adsorption. In chemical adsorption the interaction between the adsorbate and adsorbent are comparable in strength to a chemical bond, where as in physical adsorption a weak asorbent and adsorbate interaction is involve.

As the evaluation of surface area is performed based on the number of molecules adsorb on the surface and their cross section area i.e. the effective area covered by each adsorbate on the surface. The distinct feature of physisorption process which involves weak interaction between adsorbent and adsorbate allows the latter to cover the entire surface of the adsorbent and thereby

permits a precise determination of the surface area. In addition, physisorption is a reversible phenomenon, which permits a rapid equilibrium between the adsorption and desorption processes and therefore both the processes could be easily studied.[9]

2.2. Forces of Physical Adsorption

Long range attractive dispersive (or van der Waals) interaction and short range repulsive interaction between adsorbate and the adsorbent are two principal forces that are involved during physisorption process.[10,11] The attractive forces between the adsorbate and adsorbent are induced due to the instantaneous fluctuation of the electrical dipole moments in either atoms or molecules, even though there is no permanent dipole moment in these atoms or molecules. In addition, Debye forces may also involve during the physisorption process if permanent dipole of one molecule induces dipole in other molecule. Furthermore, attractive forces can also involve between a charged adsorbent and a polar adsorbate molecules or between polar molecules and molecules with quadrupoles moment of the molecules (for example CO_2 and N_2). The repulsive force between the adsorbate and adsorbent may arise from the penetration or overlap of the electron cloud between adjacent molecules and the surfaces. At short distances, the repulsion force is significant and increases rapidly.

2.3. Adsorption Isotherms and their Classifications

Adsorption isotherms are defined as the plots of the weight of adsorbate versus the pressure of the adsorbate at a constant temperature.

The quantity of adsorbate taken up by an adsorbent is proportional to the mass of the adsorbent, temperature T, the pressure p of the adsorbate and the nature of adsorbate/adsorbent. Therefore, if the quantity of absorbate is expressed as n, in moles per gram of adsorbent, then n can be expressed using the following equation:

$$n = \mathrm{f}(p,T,\text{adsorbate},\text{adsorbent})$$

This equation can be represented in a more simplified form (below) in cases where a particular adsorbate, adsorbent and at a specific temperature is considered.

$$n = \mathrm{f}(p)_{T,\text{adsorbate},\text{adsorbent}}$$

If pressure p is expressed in terms of relative vapour pressure, i. e. p/p_0, then the above equation can be expressed as:

$$n = f(p/p_0)_{T,\text{adsorbate,adsorbent}}$$

The above equation is often used for the graphical representation of uptake profiles in the form of an adsorption isotherm.

Adsorption isotherms are important in characterizing porous materials either by estimating the surface area/pore volumes, pore size distribution, assessing the surface chemistry of the adsorbents or by determining the fundamentals of the adsorption process. There are six different groups of physisorption isotherms which are classified according to their respective shapes (Figure 1). Among them the first five types were originally proposed by Brunauer, Deming, Deming and Teller (B.D.D.T),[12,13] whereas the last type-VI isotherm was later proposed by Sing et al.[14,15]

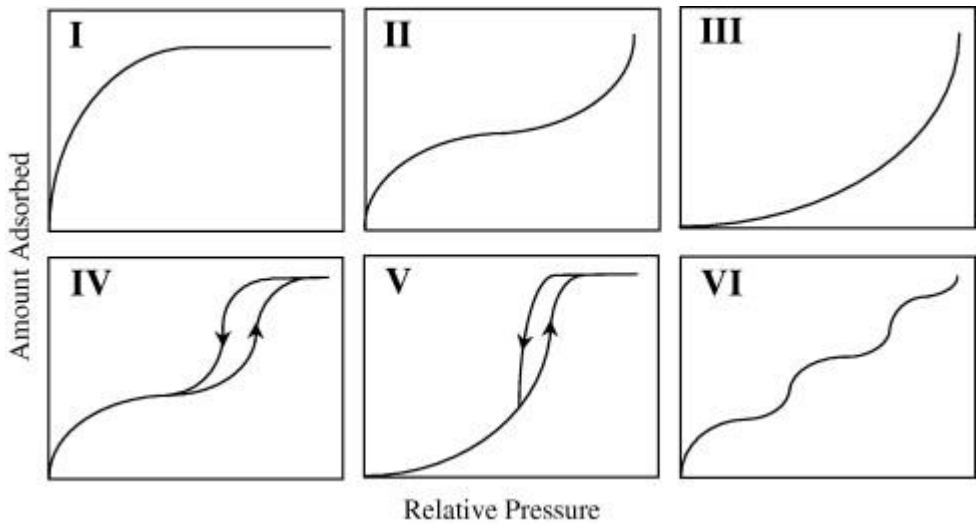

Figure 1. The IUPAC classification for adsorption isotherms (Types I–VI) with the *x*-axis representing the relative pressure (P/P_0) of the fluid and the *y*-axis denoting amount of gas adsorbed.[2]

Type I reversible isotherms which also sometime refers to as Langmuir isotherms are typical of microporous solids and chemisorption isotherms. A distinct feature of type-I isotherm is a rapid increase in the amount of gas adsorbed over the low relative pressure range and then approaches a limiting value as P/P_0 increases to 1. Type I isotherm are mostly restricted to monolayer adsorption. The rapid increase in the amount of gas adsorbed over the low pressure is primarily attributed to the micropore filling of the adsorbent and then a subsequent nearly flat plateau indicates that the micropores are filled. Therefore, the limiting uptake is mainly determined by the accessible micropore volume rather than by internal surface area. Adsorption of nitrogen on carbon materials at 77 K and ammonia on charcoal at 273 K often show type-I isotherm behaviour.[16,17]

Reversible Type II isotherms are obtained for non-porous or macroporous solids and are not restricted to monolayer adsorption rather a multilayer adsorption occurs at higher relative pressure following a monolayer adsorption at relative low pressure.

Reversible *Type III Isotherms* are relatively uncommon and the plots obtained are convex to the relative pressure axis over the entire range. The typical convex feature of type-III isotherms are indicative of weak adsorbate-adsorbent interactions[18] and are mostly associated with non-porous and microporous adsorbents.

Type IV Isotherm has a characteristic hysteresis loop, which is commonly associated with the presence of mesoporosity in the solid. Interestingly, the shape of the isotherms is found to be unique for each adsorbent system. The observed hysteresis loop of type-IV isotherms correspond to the capillary condensation.[2]

Type V Isotherm may associate with micro- as well as mesoporous materials. Type *V* isotherms are also found to have a convex feature with respect to the relative pressure axis and therefore indicative of weak adsorbate-adsorbent interactions.[18]

Type VI Isotherm – are generally obtained for solids which are extremely homogeneous, and contain non-porous surfaces. The unique shape of the isotherm is due to the complete formation of monomolecular layers before progression to a subsequent layer. It was proposed that the isotherms arise from adsorption on where the monolayer capacity corresponds to the step height.[19]

2.4. Surface Area Evaluation form Sorption Isotherms

For evaluating the surface area of the porous materials especially porous MOMs using sorption isotherms, two methods namely, Langmuir method and the BET method are extensively used.

Langmuir Equation (method): Using a kinetic approach Irving Langmuir in 1916 was able to describe the type I isotherm based on the assumption that adsorption is limited to a monolayer of adsorbate.[20] Further assumption which was taken into consideration is that the adsorption energy is uniform over the entire surface of the adsorbent. Therefore the ability of an adsorbate molecule to adsorb at a given site of the adsorbent is independent of the occupation of the neighboring sites. In addition, it is further assumed that the energy of adsorption for the first layer is considerably larger when compared to second and higher layers; therefore, a multilayer adsorption can only take place at much higher pressures.[21] A suitable form of Langmuir equation which could be employed for testing the experimental data is expressed as:

$$p/n = 1/Kn_m + p/n_m,$$

where, p is the pressure, n and n_m are the amount adsorbed at a certain pressure and the amount at completed monolayer adsorption respectively, and K is the adsorption coefficient (depends on the strength of adsorption). Therefore, a plot of p/n versus p should lead to a straight line with $1/Kn_m$ as the intercept and with a slope of $1/n_m$. The surface area (A) can then be calculated using the following relation:

$$A = N_m A x = (n_m N_A A_x)/M_W$$

Where, N_m is the number of molecule of adsorbate in a completed monolayer of unit area, A_x and M_W are the cross section area and the molecular weight of the adsorbate respectively and N_A is the Avogadro number.

BET Theory: The BET theory was proposed by Stephen Brunauer, Paul Hugh Emmett, and Edward Teller in 1938.[22] The concept of the theory is an extension of the Langmuir kinetic theory to multilayer adsorption, therefore enables to determine the surface area of solids where a multilayer adsorption occurs. The theory also enables to estimate the number of molecules required to form a monolayer even if a complete monolayer is never achieved. It is further

thought that under an equilibrium condition the distribution of adsorbate between the different layers is constant and there is no interaction among adsorbed molecules.

The assumption of the BET theory includes the adsorption energy of the adsorbate at any layers is same and therefore formation of new adsorbed layer is possible before another one is finished. The BET equation can be expressed as follows:

$$1/n[(p_0/p) - 1] = 1/n_m C + C - 1/n_m C(p/p_0)$$

Where, p and p_0 are the equilibrium and the saturation pressure of adsorbates at the temperature of adsorption, n is the adsorbed gas quantity (for example, in volume units), and n_m is the monolayer adsorbed gas quantity. Therefore, a plot of $1/((p_0/p) - 1)$ versus p/p_0 results in a straight line with a slope: $s = C - 1/ n_m C$ and an intercept: $I = 1/n_m C$, n_m can then be calculated: $n_m = 1/ s+1$ and as a result the surface area can be evaluated ($A = (n_m N_A A_x)/M_W$).

2.5. Pore Volume and Pore Size Characterization

2.5.1. Estimation of Pore Volume

While estimating the total pore volume it is often assumed that the pores are filled with adsorbate (for example nitrogen or argon) in its liquid state at a relative pressure close to unity. Therefore, adsorbed volume (V_{ads}) can be easily converted to a liquid volume (V_{liq}) using the following relationship: $V_{liq} = (P_a.V_{ads}.V_m)/RT$; Where, P_a and T are the ambient pressure and temperature, respectively, V_m is the molar volume of the liquid adsorbate and R is the roentgen constant.

2.5.2. Pore Size Evaluation

There are several methods, for example Barrett, Joyner and Halenda (BJH) method[23], the Dollimore and Heal (DH) method[24], the t-method of Halsey[25], the de Boer method[26], the Dubinin-radushkevitch (DR) method[27], the Dubinin-astakhov (DA) method[28], the Horvath-kawazoe (HK) method[29], the Saito-foley (SF) method[30]or the density functional theory (DFT) and monte carlo simulation methods[31-33], which has been successfully employed to evaluate the pore size and to assess the pore size distribution with high accuracy. In order to interpret the relation between experimental and simulated isotherms a generalized adsorption isotherm

equation is used. It is assumed that the total isotherm consist of a number of individual single pore isotherms multiplied by their relative distribution over a range of pore sizes.

2.6. Isosteric Heat of Adsorption (Q_{st})

When the adsorbate molecules are adsorbed on the surface of the solid heat is usually released. This is mainly because of the loss of motion of the adsorbate molecules. Alternatively, the reverse may occur during the desorption process. The temperature change of the adsorbent during the adsorption and desorption process is known as the isosteric heat of adsorption and are often denoted as Q_{st}. This is an important parameter which gives an insight into understanding the types and the strength of the interactions which are taking place between the adsorbate and adsorbent as well as to the kinetics of the process and a measure of the adsorption equilibrium.

The isosteric heat (Q_{st}) of H_2 adsorption are calculated from the hydrogen adsorption isotherms measured at two different temperatures, in most of the cases at 77 and 87 K, by fitting the data to virial equation or the Langmuir-Freundlich equation[34]. The calculation is found to be suitable for estimating the coverage dependent heat of H_2 adsorption, although, information about the position and the number of adsorption sites could not be ascertained. The H_2 interaction energy corresponding to the strongest binding site of MOFs is referred to as zero-coverage isosteric heat of H_2 adsorption. For determining the isosteric heat (Q_{st}) of H_2 adsorption two different methods are frequently used.

Method 1: A virial-type expression is used (eq 1), which is composed of parameters a_i and b_i that are independent of temperature.[35] In eq 1, P is the pressure, N is the amount of adsorbed H_2 gas, T is the temperature, and m and n represent the number of coefficients required to adequately describe the isotherms. Adsorption isotherms measured at two different temperatures are fit to the equation by using the statistical programs such as *R* statistical software package.[36]

$$\ln P = \ln N + \frac{1}{T}\sum_{i=0}^{m} a_i N^i + \sum_{i=0}^{n} b_i N^i \qquad (1)$$

To estimate the values of the isosteric heat of H_2 adsorption, eq 2 could be applied, where R is the universal gas constant.

$$Q_{st} = -R\sum_{i=0}^{m} a_i N^i \qquad (2)$$

Method 2: The virial-type equation[37], eq 3, is used to fit the adsorption data at a fixed temperature.

$$\ln(N/P) = A_0 + A_1N + A_2N^2 + A_3N^3 + \cdots \quad (3)$$

In eq 3, P is pressure, N is amount of adsorbed gas, and A_0, A_1, etc. are virial coefficients. A_0 is related to the adsorbate-adsorbent interactions, whereas A_1 describes adsorbate-adsorbate interactions.

Q_{st} for H_2 adsorption is calculated as a function of surface coverage by using Clausius-Clapeyron equation (eq 4), where R is the gas constant.

$$Q_{st} = R \ln (P_1/P_2) \times T_1T_2/(T_2 - T_1) \quad (4)$$

2.7. References

1. G. Q. Lu and X. S. Zhao, *Nanoporous Materials Science and Engineering*, Vol. 4, Imperial College Press, London 2004.
3. H. Kayser, *Wied. Ann.*, 1881, **14**, 450.
2. K. S. W. Sing, D. H. Everett, R. A. W. Haul, L. Moscou, R. A. Pierotti, J. Rouquerol and T. Siemieniewska, *Pure and Appl. Chem.*, 1985, **57**, 603-619.
4. J. Sameshima, *Bull. Chem. Soc. Jpn.*, 1927, **2** (1), 1-10.
5. J. W. McBain, *Phil. Mag.*, 1909, **18**, 916.
6. J. Rouquerol, D. Avnir, C. W. Fairbridge, D. H. Everett, J. H. Haynes, N. Pernicone, J. D. F. Ramsay, K. S. W. Sing and K. K. Unger, *Pure and Appl. Chem.*, 1994, **66**, 1739-1758.
7. D. H. Everett, *Pure and Appl. Chem.*, 1972, **31**, 577-638.
8. R. L. Burwell, *Pure and Appl. Chem.*, 1976, **46**, 71-90.
9. S. Lowell, J. E. Shields, M. A. Thomas and M. Thommes, *Characterization of Porous Solids and Powders: Surface Area, Pore Size and Density*, Kluwer Academic Publishers, Dordrecht **2004**.
10. M. Polanyi, *Trans. Faraday Soc.*, 1932, **28**, 316-33.
11. E. A. Flood, *The solid-gas interface*. Edward Arnold: London, 1967; Vol. 1, p 514.
12. S. Brunauer, P. H. Emmett and E. Teller, *J. Am. Chem. Soc.*, 1938, **60**(2), 309-19.

13. S. Brunauer, L. S. Deming, W. S. Deming and E. Teller, On a Theory of the van der Waals Adsorption of Gases. *J. Am. Chem. Soc.*, 1940, **62**, 1723-32.
14. J. S. Gregg and K. S. W. Sing, *Adsorption, Surface Area and Porosity;*. 2nd ed.; Academic Press: London, 1982; p 303.
15. K. W. Sing, D. H. Everett, R. A. W. Haul, L. Moscou, R. A. Pierotti, J. Rouquerol and T. Siemieniewska, *Pure Appl. Chem.,* 1985, **57**(4), 603-19.
16. F. Rouquerol, J. Rouquerol and K. S. W. Sing, *Adsorption by Powders, Porous Solids*., Academic Press: London, 1999; p 467.
17. N. M. Hassan, T. K. Ghosh, A. L. Hines and S. K. Loyalka, *Gas Sep. Purif.*, 1992, 6, (4), 229-34.
18. A.V. J. Kiselev, *Colloid Interface Sci.*, 1968, **28**, 430.
19. G. D. J. Halsey, *Chem. Phys.*, 1948, **16**, 931.
20. I. Langmuir, *J. Am. Chem. Soc.*, 1918, **40**, 1361-1402.
21. F. Rouquerol, J. Rouquerol and K. Sing, *Adsorption by Powders and Porous Solids: Principles, Methodology and Applications*, Academic Press, San Diego **1999.**
22. S. Brunauer, P. H. Emmett and E. Teller, *J. Am. Chem. Soc.*, 1938, *60*, 309-319.
23. E. P. Barrett, L. G. Joyner and P. P. Halenda, *J. Am. Chem. Soc.*, **1951**, **73**, 373-380.
24. D. Dollimore and G. R. Heal, *J. Appl. Chem.*, 1964, **14**, 109-114.
25. G. J. Halsey, *Chem. Phys.*, 1948, **16**, 931-937.
26. J. H. de Boer, B. G. Linsen, Th. van der Plas and G. J. Zondervan, *J. Catal.*, 1965, **4**, 649-653.
27. M. M. Dubinin and L. V. Radushkevich, *Dokl. Akad. Nauk. SSSR*, 1947, **55**, 327-329.
28. M. M. Dubinin and V. A. Astakhov, *Adv. Chem. Ser.*, 1971, **102**, 69-85.
29. G. Horvath and K. Kawazoe, *J. Chem. Eng Jpn.*, 1983, **16**, 470-475.
30. A. Saito and H. C. Foley, *AIChE J.*, 1991, **37**, 429-436.
31. R. Evans, U. M. B. Marconi and P. J. Tarzona, *J. Chem. Soc., Faraday Trans. 2*, 1986, **82**, 1763.
32. P. I. Ravikovitch, A. Vishnyakov and A. Neimark, *Phys. rev. E*, 2001, **64**, 011602.
33. A. V. Neimark, P. I. Ravikovitch and A. Vishnyakov, *J. Phys.: Condens. Matter*, 2003, **15**, 347-365.
34. R. T. Yang, Gas Separation by Adsorption Process; Butterworth: Boston, 1997.

35. (*a*) J. L. R. Rowsell and O. M. Yaghi, *J. Am. Chem. Soc*., 2006, **128**, 1304; (*b*) M. Dincă, A. Dailly, Y. Liu, C. M. Brown, D. A. Neumann and J. R. Long, *J. Am. Chem. Soc*., 2006, **128**, 16876; (*c*) L. Czepirski and J. Jagiello, *Chem. Eng. Sci.*, 1989, **44**, 797.

36. R program http://www.R-project.org.

37. J. H. Cole, D. H. Everett, C. T. Marshall, A. R. Paniego, J. C Powl, F. J. Rodriguez-Reinoso, *J. Chem. Soc., Faraday Trans.*, 1974, **70**, 2154.

3. Hydrogen Storage in Metal-Organic Frameworks by Physisorption

3.1. Introduction

Storing of hydrogen for vehicular purpose is becoming increasingly important because of the steady decrease in fossil fuel resources and the CO_2 emission associated with the burning of carbon based fuels which are responsible for the rapid climate changes. In addition, hydrogen is an ideal candidate for clean energy carrier because it releases only water as by product after the oxidation in the fuel cell. However, despite having these unique sets of aforementioned attractive features which associate with the hydrogen economy, there are several hurdles that need to be overcome before realizing a safe, efficient and economical on-board hydrogen storage system.

Hydrogen has almost three time higher heat of combustion (123 MJ kg^{-1}) when compared to the gasoline (47 MJ kg^{-1}). This implies that if H_2 is applied in automobile as a fuel about 5 kg of H_2 would be required to achieve a driving range greater than 300 miles (480 km). Taking these facts into consideration, the US Department of Energy (DOE) has set up the targets for on-board H_2 storage systems in order to replace current carbon-based energy source in future vehicles. The H_2 storage targets for a complete system (including material, tank, regulators, valves, piping, mounting brackets, insulation, cooling capacity, etc.) by 2017 are 5.5 wt% in gravimetric capacity and 40 g L^{-1} in volumetric capacity at an operating temperature of -40 to -60 °C under a maximum delivery pressure of 100 atm.[1] Unfortunately, despite a great advancement with the hydrogen storage based research, none of materials developed could satisfy the DOE targets.

Several strategies have been pursued which involves the utilization of different kinds of materials to achieve these goals in conjunction to the use of compressed hydrogen gas and liquid hydrogen tanks. Among them, physisorption based storage system particularly MOFs seem to have the potential to overcome many issues related to various applications due to their facile tunability or the capability to vary the pore size and functionality in an amenable manner. In the following sections different parameters that influence the gas uptake in MOFs will be discussed.

3.2. Current Technologies and Sorption Based Methods

Technologies: The technologies which are currently being employed involve compressed hydrogen gas and liquid hydrogen tanks. In fact, compressed hydrogen gas tanks built from the

materials which can withstand the pressure up to 5000-1000 psi are already being utilized in some prototype hydrogen-powered vehicles. However, the major concerns associated with this technique are safety, volumetric capacity and costs. On the other hand liquid hydrogen provided the alternate way to store hydrogen with higher density (70.8 kg M^3) at normal pressure. However, in order to liquefy the gaseous hydrogen (liquefying temperature of 20.27 K), a large amount of energy needs to be spent; therefore, cost again remains one of the major issues.

Sorption Methods: Apart for the pure tank based storage, a wide variety of materials such as metal hydrides,[2] complex hydrides,[3-6] chemical hydrides,[7-9] carbohydrates,[10] clathrates,[11] inorganic nanotubes,[12] organic materials,[13] sorbents for example metal-organic frameworks (MOFs) and carbon materials,[14-16] etc. have been tested as hydrogen storage materials following either physisorption and chemisorption pathways.

In chemisorption based materials for instance, metal hydrides,[2] complex hydrides,[3-6] chemical hydrides[7-9], the hydrogen molecules are chemically bonded to the storage medium and therefore high gravimetric storage capacities are easily attained. However, high hydrogen desorption temperatures and non-reversibility, because the activation energy exists in the adsorption and desorption process is particularly high, remains as major problems.

Hydrogen physisorption, on the other hand, mainly involves weak van der Waals forces which permit the adsorption of hydrogen molecules on to the surface of the adsorbents and therefore preclude any significant change in the electronic orbital patterns of the species involved. Consequently, physisorption based system permits reversibility i.e. fast adsorption and desorption kinetics. Physisorption material encompasses porous carbons, zeolites, clathrates, organic polymers and porous metal-organic frameworks. As stated before, among physisorption based storage system, MOFs are extensively studied over the last decades. This is because these materials are synthesized from metal ions and organic building blocks, therefore provides the opportunity to readily tune the framework topology, pore size and shape, and most importantly the surface area by the selection of appropriate molecular building blocks. Furthermore, MOFs generally posses well defined structural motifs, permanent porosity after removal of the occluded guest molecules. Extensive studies have shown that the hydrogen storage capacities of these materials primarily depend on the available surface area and pore volume. However, the major problem associated with the use of physisorption based MOFs are their weak van der Waals

interaction (typically the interaction energy ranges between 4-8 kJ mol^{-1}) with the H_2 molecules.[17] Consequently, most of the physisorption based MOFs exhibited high storage capacities only at liquid nitrogen (cryogenic) temperature and relatively high pressures; however; these capacities drops dramatically (<1-2 wt%) at ambient temperature and pressure. Based on theoretical calculations, it was estimated that an average H_2-MOF interaction energy in the range of 15-20 kJ mol^{-1} would be required to deliver an adequate amount of hydrogen for on-board application purpose.[18]

3.3. Strategies for Improving Hydrogen Storage in MOFs

3.3.1. Increase in Surface Area and Pore Volume

The surface areas of MOFs are shown (Figure 1) to have a qualitative relationship with their hydrogen storage capacity at cryogenic temperature (77 K) and at high pressure. It is also generally observed that material with high surface area seems to posses high pore volumes and lower density. Certainly an optimum system should therefore comprise higher specific surface area and pore volume to maximize the storage capacity at 77 K and high pressure.

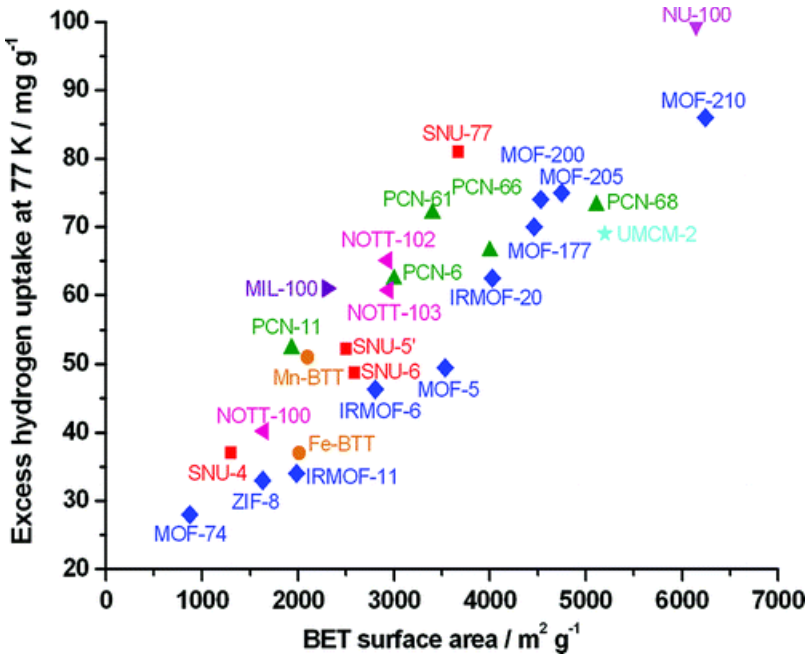

Figure 1. Excess high pressure H_2 uptake capacities at 77 K versus BET surface areas for some highly porous MOFs.[17]

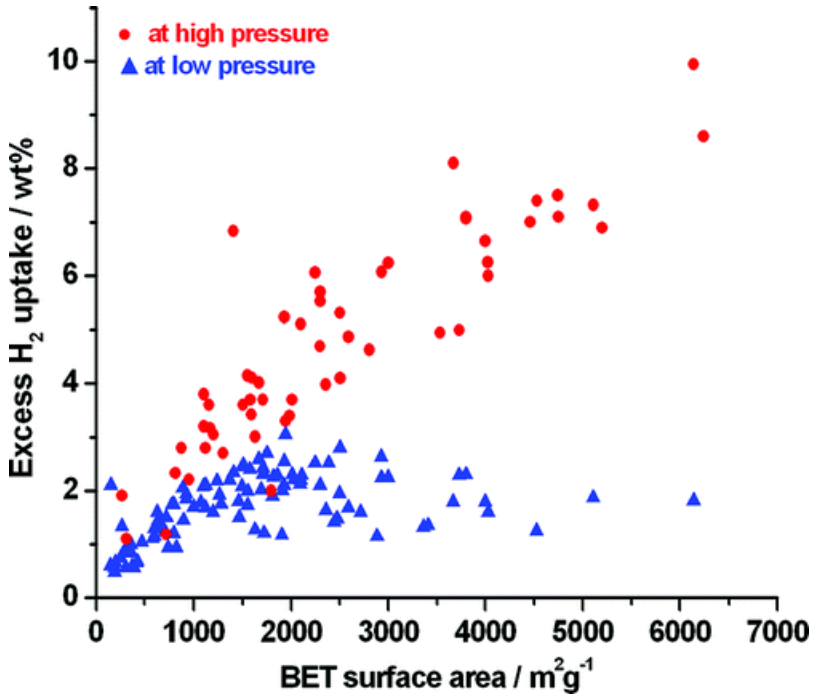

Figure 2. A plot showing the relationship between H_2 uptake capacities at 77 K and BET surface areas of various MOFs. Low pressure is 1 atm and high pressures are in the range of 10-90 bar.[17]

However, the situation may alter in a great extent when low pressure (i.e. adsorption at pressure below1atm) adsorption performances are taken into account. In fact, as can be seen from Figure 2, the hydrogen uptake at low pressure is superior for materials with surface areas less than 2000 m^2 g^{-1}. Nevertheless it should also be noted that the delivery amount of hydrogen by materials with lower surface area are largely limited to 2-3 wt%. It is evidences that, at low pressure the hydrogen molecules are preferentially adsorb at the most strongest site of the materials and are often influenced by several other factors such as small pore size, framework catenation, presence of coordinatively unsaturated metal centers etc. Some of these critical factors will be discussed in the later sections.

Table 1 presents some of the selected MOFs with unusual high surface area and pore volume and their corresponding cryogenic hydrogen adsorption data at high pressure.

Table1

Materials	A_{BET} (m^2g^{-1})	A_{Lang} (m^2g^{-1})	Vp (cm^3g^{-1})	Void volume (%)	Crystal density (g cm^{-3})	P (bar)	H_2@77 K (Excess uptake in wt%)	Q_{st}	Ref.
MOF-210	6240	10400	3.60	89	0.25	80	8.6		19
NU-100	6143		2.82			56	9.95	6.1	20
MOF-200	4530	10400	3.59	90	0.22	80	7.4		19
MOF-205	4460	6170	2.16	85	0.38	80	7		19
UMCM-2	5200	6060	2.32	83	0.40	46	6.9		21
PCN-68	5109	6033	2.13			50	7.32	6.09	22
MIL-101b		5500				80	6.1	10	23

A_{BET}: Apparent surface area calculated using BET model; A_{Lang}: Apparent surface area calculated using Langmuir modell; Vp: Pore volume; P: pressure in bar; Q_{st} is reported as the isosteric heat of adsorption calculated at the lowest coverage. Cells left blank when data was not reported.

The highest surface area recorded to date is for MOF-210 with 6240 m^2 g^{-1} (BET) and 10400 m^2 g^{-1} (Langmuir), which was reported by Furukawa et al. in 2010.[19] A comparable BET surface area (6143 m^2 g^{-1}) was later reported for NU-100 by Hupp group.[20] It should be noted that the estimated Langmuir surface area of MOF-200 is equivalent to MOF-210, although the former has relatively lower BET surface area (Table 1). The highest excess H_2 uptake reported for NU-100 is 99.5 mg g^{-1} at 56 bar and 77 K, which is higher when compared to the value (86 mg g^{-1}) reported for MOF-210 at 77 K and 80 bar. It could be presumed that the superior performance by NU-100, despite having comparable or little lower BET surface area over MOF-210, is due to the resultant nature i.e. high surface area coupled with the unsaturated open metal centers of NU-100. However, the performance alter when total uptake is considered i.e. total H_2 uptake by MOF-210 (17.6 wt%) is higher than NU-100 (16.4 wt%).

One of the chemical strategies to construct highly open framework material with higher surface is to use longer organic building bock. Although it is also observed that the utilization of longer linkers has the high tendency to yield catenated frameworks that could largely reduce the porosity of materials. Nevertheless, the approach is evidenced to be highly promising when the materials are constructed under a given framework topology and utilizes longer organic linkers. In fact, many of the MOFs with highest known surface areas for example MOF-210, MOF-205,

PCN-68 and UMCM-2 were synthesized under pre-designed framework topologies by replacing the shorter linkers with the elongated one.[19,20,22]

3.3.2. Framework Catenation

Physical entanglements of two or more identical frameworks are often defined as catenation.[24] It is shown that framework catenation can have influence to increase the hydrogen uptake capacity of MOFs by enhancing the MOF-H_2 interactions. An interesting study was performed by Zhao and coworkers which shows that the catenated PCN-6 have superior hydrogen uptake capacity than its non-catenated material PCN-6' over the entire pressure regimes (1-50 bar).[25] At higher pressure (50 bar) and at 77 K, the excess H_2 uptake of PCN-6 and PCN-6' was found to be 7.2 wt% and 4.2 wt% respectively. A similar trend was also observed when the measurement was performed at 298 K and 50 bar. Based on INS experiments it was supported that although the primary binding sites of both the materials are unsaturated Cu metal sites; however, at higher loading of hydrogen the interaction between H_2 molecules and the organic linkers becomes stronger in catenated PCN-6. Long and co-workers evidenced that the activated form of catenated $Mn_3[(Mn_4Cl)_3(TPT\text{-}3tz)_8]_2\cdot 25H_2O\cdot 15CH_3OH\cdot 95DMF$ have higher hydrogen storage capacity of 3.7 wt% at 77 K and 25 bar while comparing to non-catenated $Cu_3[(Cu_4Cl)_3(TPB\text{-}3tz)_8]_2\cdot 11CuCl_2\cdot 8H_2O\cdot 120DMF$, whose H_2 uptake capacity is 2.8 wt% at 77 K and 30 bar although both the materials were constructed from a similar kind of ligands.[26] Other reports also shows that materials with 4-fold catenation could deliver 1 wt% of H_2 at higher temperature (298 K) due to the increase in MOF-H_2 interaction triggered by the small pore size distribution of the catenated frameworks, although the estimated surface areas were only in the range of 200-300 m^2g^{-1}.[27]

Several reports have appeared in the literature which envisaged that the catenation of the frameworks could be controlled by rational designing of the organic building blocks. Indeed, Zhou et al. demonstrated a strategy to control the formation of catenated or non-catenated materials through addition of a template during the preparation of the materials under the solvothermal condition.[25*b*] It was shown that, if oxalic acid was used as a template during the synthesis of MOF, a non-catenated framework was formed; however, in the absence of oxalic acid a catenated framework should be formed. Other report by Farha et al. evidenced that catenation of MOF could be controlled through rational designing of the linker units.[28] Control

of catenation through adjustments of the reaction parameters such as temperature, and concentration was reported by Zaworotko and co-workers.[29] In their report they have shown that the two-fold catenated structure which was obtained from a reaction mixture containing Cd^{2+}, 4,4′-bpy and BDC linker at higher concentration and temperature could be isolated as a non-catenated framework while performing the reaction at room temperature and at lower concentration.

Despite the above mentioned benefits associated with the catenated frameworks to increased MOF-H_2 interactions, it should be emphasized that catenation reduces the porosity of the materials by decreasing the free volume and thus may have a detrimental effect on the high pressure H_2 storage.

3.3.3. Improving the Isosteric Heat of Adsorption

Many MOFs especially coupled with high specific surface area and pore volumes have been evaluated to deliver more than 10 wt% of hydrogen at cryogenic temperature and high pressure.[17] But unfortunately none of the MOFs could meet the targeted goals projected by the US DOE for H_2 storage materials that should be developed by 2017 mainly because of the weak interaction between the H_2 and the physisorption based MOF materials.[1] It is became clear that that the improved hydrogen storage performance could only be achieved by introducing strong adsorption sites in the MOFs and/or through optimization of the pore surface suitable for assisting H_2 molecules efficiently. Many approaches had been pursued including creating MOFs with unsaturated metal centers, doping MOFs with alkali metals, constructing MOFs with narrow pore size, through spillover technique to improve hydrogen uptake capacity as well as MOFs isosteric heat of adsorption towards H_2. Some of these approaches and their associative impact on hydrogen uptake will be discussed in the following sections.

3.3.3.1. Creating Unsaturated Metal Centers

Perhaps one of the very first MOF based on $M_2(O_2CR)_4$ paddlewheel building block which retained the structural integrity to offer vacant metal sites after thermal removal of axial ligands was structurally characterized by Yaghi and co-workers in 2000.[30] Currently several strategies has been adopted to successfully prepared MOFs with coordinatively unsaturated metal centers (UMCs).[17] Particularly, the generation of open metal sites through removal of the

coordinated solvent molecules attached to the SBUs are widely exploited. The SBUs which often bears coordinated solvent molecules at the axial sites are the bimetallic paddle-wheel units of $M_2(O_2CR)_4$ (M = Cu^{2+}, Zn^{2+} and Cd^{2+}). Apart from the above mentioned material reported by Yaghi group, another early investigated materials for this purpose is $[Cu_3(BTC)_2(H_2O)_3]_n$ (HKUST-1), which was built from benzene-1,3,5-tricarboxylate and Cu paddle-wheel SBUs (Figure 1).[31] Other interesting class of MOFs which offered potentially accessible metal cites after removal of the axial ligands from the paddle-wheel SBUs are discussed in the following paragraph.

It was evidenced that the removal of the axial DMF solvent of SNU-5′, $[\{Cu_2(abtc)(dmf)_2\}_3]$, leads to the formation of SNU-5, $[\{Cu_2(abtc)\}_3]$, which possesses open metal sites. The hydrogen sorption measurements showed that the uptake capacity of SNU-5 significantly improved from 1.83 wt% for SNU-5′ to 2.87 wt% for SNU-5 at 1 atm and 77 K. More importantly, the zero coverage interaction energy was reported to dramatically increase from 6.5 kJ mol^{-1} to 11.6 kJ mol^{-1} due to the presence of open metal cites in SNU-5.[32]

Zhou and co-workers have evidenced that the alignment of open metal sites in PCN-12, ($[Cu_6(C_s\text{-mdip})_2(C_{2v}\text{-mdip})(H_2O)_6]_3 \cdot DMA \cdot 6H_2O$), through removal of the axially coordinated aqua ligands of Cu paddlewheel SBUs resulted in the extraordinary gravimetric hydrogen storage capacity of 3.05 wt%, when compared to PCN-12′, ($[Cu_2(C_2v\text{-mdip})(H_2O)_2]$ 33DMSO), with an adsorption capacity of 2.40 wt%, where the open metal sites were out of alignment.[33]

Some other interesting materials with open metal sites generated from the Cu-paddle wheel SBUs include NOTT-10, -11 and NOTT-12, -16 comprising of tetra- and hexa-carboxylic acid ligands respectively, which was reported by Schröder and co-workers.[34,35]

Farah et al. reported NU-100, which proved to be one of the rare materials with exceptionally high porosity with BET surface area of 6143 m^2 g^{-1} and possessed potentially accessible open metal sites at the Cu-peddle wheel node and showed extraordinary high hydrogen uptake performance.[20]

Zhou group further reported a series of isostructural materials, incorporating open metal cites at the cu-paddle wheel node, for example PCN-61, PCN-66, PCN-68, and PCN-69 based on hexacarboxylic acid and Cu paddle wheel SBUs with exceptionally high hydrogen storage capacities.[36,37] Particularly, a record gravimetric hydrogen uptake capacity of PCN-68 was

reached to 130 mg g^{-1}. However, it should be mentioned that, despite having the open metal sites, the zero coverage interaction energy of PCN-68 was estimated to be 6.09 kJ mol^{-1}.

Perhaps the highest interaction energy was estimated for open metal site containing $[Co^{II}_4(\mu\text{-}OH_2)_4(MTB)_2]_n$ (SNU-15′).[38] It was suggested that the estimated high Q_{st} of SNU-15 might be attributed to the favorable metal-metal distance which makes it possible for a H_2 molecule to bind in a side-on fashion.

Other clusters for example oxo-centered trigonal $[M_3(\mu_3\text{-}O)(CO_2)_6]$ (where M can be Cr^{3+}, Al^{3+}, $Fe^{2+/3+}$, Ni^{2+} and In^{3+}) unit was utilized to construct wide variety of materials which displayed open metal cites in each of the metals trigonal unit. For example, open metal containing materials, MIL-53(Cr)/MIL-53(Al), reported by Férey and co-workers showed high uptake capacity of 3.1 wt%/3.8 wt% at 77 K and 1.6 MPa.[39] In addition it was also evidenced that these materials exhibits breathing phenomenon upon guest removal and re-adsorption.

Several other cluster units shown to produce open metal sites through removal of the coordinated ligands includes the trimeric chromium(III) octahedral clusters found in MIL-101,[40] $[InO_5(H_2O)]$ octahedra[41].

Bordiga et al. was the first to experimentally demonstrate the direct interaction between the H_2 and the exposed Cu^{2+} center of HKUST-1 by studying the IR stretching band at 4100 cm^{-1} for the adsorbed H_2 molecules.[42] Later investigation by other group using low-temperature powder neutron diffraction experiments showed that among six possible hydrogen adsorption sites in HKUST, the most favorable being at the close proximity to the copper site of the $M_2(O_2CR)_4$ paddlewheel building block, and in fact, the Cu^{2+}-D_2 was estimated to be 2.39 Å revealing a strong interaction phenomenon.[43] Long and co-workers investigated that framework materials $Mn_3[(Mn_4Cl)_3(BTT)_8(CH_3OH)_{10}]_2$ which possesses $M_4Cl(N_4CR)_8$ building blocks offers more stronger interactions between the Mn^{2+} and the D_2 as compared to the Cu^{2+}-D_2 interaction in HKUST-1 and distance estimated was reported to be only 2.27 Å based on powder neutron diffraction experiments.[44] A similar results was also obtained with other isostructural materials ($HCu[(Cu_4Cl)_3(BTT)_8]\cdot 3.5HCl$) where the Cu^{2+}-D_2 distance was estimated to be 2.47 Å.[45] More importantly, a zero coverage interaction energies were estimated for these materials in the range of 9-10 kJmol^{-1}.

3.3.3.2. Introduction of Metal Ions in the Pores

Recent finding suggests that the presence of counter-cations in the pores of MOFs may have beneficial effect to increase the interaction between the H_2 molecules and the metal ions. However, it should at the same time be noted that the added mass carried by the counter ions may associate with decrease in porosity of the material. One of the easiest ways to incorporate H_2 interacting metal ion entities is by constructing anionic framework which is charged balanced by the counter cations. Indeed, Eddaoudi and co-workers have reported synthesis of anionic zeolite-like frameworks, $[In_2(HImDC)_4 \cdot (HPP^{2+})]_{24} \cdot 36DMF \cdot 192H_2O$ (*rho*-ZMOF, HImDC = 4,5-imidazoledicarboxylic acid, HPP = 1,3,4,6,7,8-hexahydro-2H-pyrimido[1,2-a]pyrimidine), $[In(HImDC)_2 \cdot (HIM^+)] \cdot 4DMF \cdot CH_3CN \cdot 4H_2O$ (*sod*-ZMOF, HIM = protonated imidazole), and $[In(HImDC)_2 \cdot (DMA^+)]_{48}$ (DMA-*rho*-ZMOF, DMA = dimethylammonium).[46,47] The high H_2 interaction energy of DMA-*rho*-ZMOF was reported to be 8 kJ mol^{-1}. Further interesting study was performed taking these material, to exchange the cations HPP^{2+}, HIM^+ and DMA^+ with Na^+, Li^+ and Mg^{2+}. The hydrogen sorption amount and isosteric heat of H_2 adsorption were ascertained to be influenced positively by the exchange of the cations, although the extent was not very significant.

Another interesting investigation was carried out in the laboratory of Long where the Mn^{2+} ions in an anionic framework, $Mn_3[(Mn_4Cl)_3(BTT)_8]_2 \cdot 10CH_3OH$, was exchanged with a variety of metal ions such as Li^+, Cu^+, Fe^{2+}, Co^{2+}, Ni^{2+}, Cu^{2+}, and Zn^{2+}.[48] The influence of the exchanged metal ions on the hydrogen uptake performance and isosteric heat of H_2 adsorption were thoroughly investigated, although again the effects were found to be not significant.

Yang et al. reported that the substitution of H_2ppz^{2+} cation of $\{[H_2ppz][In_2(qptc)_2] \cdot 3.5DMF \cdot 5H_2O\}_\infty$ (qptc = 1,1′,4′,1″,4″,1‴-quaterphenyl-3,3‴,5,5‴-tetracarboxylate) (NOTT-200) with Li^+ resulted in the formation of $\{Li_{1.5}[H_3O]_{0.5}[In_2(qptc)_2] \cdot 11H_2O\}_\infty$ (NOTT-201) which was characterized with an enhanced H_2 adsorption capacity of 1.02 wt% at 78 K and 1 bar in compared to NOTT-200 having the H_2 adsorption capacity of 0.96 wt% under similar condition.[49] Furthermore the H_2 adsorption enthalpy was also reported to increased from 9.0 kJ mol^{-1} for NOTT-200 to 10.1 kJ mol^{-1} for NOTT-201.

Other strategies also include doping of alkali metal ions such as Li^+, Na^+, K^+, etc. into the MOFs through chemical reduction or by postsynthetic modification of the pendant functional groups for example –OH attached to the organic linkers to generate metal alkoxide entities, and

doping of metal ions into the frameworks without functional groups.[17] Hupp and co-workers have shown that the doping of $[Zn_2(NDC)_2(diPyNI)]$ with Li^+ cations could enhance the H_2 storage capacity form 0.93 wt% (the capacity of the original material) to 1.63 wt% at 77 K and 1 atm.[50] In addition the isosteric heat of hydrogen adsorption was also found to increase from 5.5 kJ mol^{-1} to 6.1 kJ mol^{-1} by the Li^+ ion doping. Thereafter, many theoretical investigations were undertaken using quantum mechanics (QM) calculation and GCMC simulations, which suggests that a significant enhancement of isosteric heat of hydrogen adsorption could be achieved by doping the alkali metal ions into the MOFs.[51]

Hupp's group further showed that the hydroxyl protons of the diol groups of the organic linker in the Zn(II) MOF (DO-MOF) could be exchanged with Li^+ and Mg^{2+} ions and can have positive impact on H_2 uptake (1.32 wt% at 1 atm) and isosteric heat of H_2 adsorption (6.3-6.6 kJ mol^{-1}) while comparing to the H_2 uptake capacity (1.23 wt% at 77 K and 1 atm) and the isosteric heat of H_2 adsorption (6.3-4.7 kJ mol^{-1}) of the original material DO-MOF.[52] Many other interesting investigations were also made in this direction.[53-55]

3.3.3.3. Spillover Effect of Metals

A hydrogen spillover could be defined as the dissociative chemisorptions or adsorption of hydrogen molecule on the metal and the subsequent migration of hydrogen in the atomic form to the surface of the supportive materials for instance alumina, carbon, etc.[56] By applying the concept of spillover in MOFs, Yang et al. reported a significantly enhanced room temperature hydrogen storage in IRMOF-1 and IRMOF-8 through mixing of Pt/AC (AC = active carbon) catalysts (contain upto 5 wt% Pt) with these MOFs.[57] Author evidenced in this report that the hydrogen storage capacity of IRMOF-1/IRMOF-8 could be improved from 0.4 wt%/0.5wt% to 1.56 wt%/1.8 wt% at room temperature. The author also reported that when a carbon bridge was introduced in the mixture containing Pt/AC and the MOFs, further increased H_2 uptake of both the modified materials were achieved.[58] Significantly, the hydrogen uptake capacities of the modified IRMOF-1 and IRMOF-8 combined with carbon bridged materials were reached to approx. 3 wt% and 4 wt%, respectively, at ambient temperature and 10 MPa, which are about 8 times higher than that of the original MOFs. Other report by Liu et al. also showed that when MIL-101 and MIL-53 were mixed with Pt/AC catalysts and carbon bridge, the H_2 storage

capacities were found to be 1.14 wt% and 0.63 wt% at 293 K and 5.0 MPa, which were significantly higher than their original materials.[59]

Despite a handful of reports which has appeared towards this approach, it is clear that the embedding of Pd or Pt nanoparticles should have beneficial effect on room temperature H_2 storage. However, the strategy may suffer from the reduced pore volume and surface area caused by blocking of the pores by the embedded nanoparticles. Furthermore, it is observed that the modified material may have high sensitivity toward air.[60] Nevertheless, doping MOFs with catalysts is still an effective approach to increase hydrogen storage capacities at higher temperature because the approach involves with a high adsorption enthalpy.

3.4. References

1. http://www1.eere.energy.gov/hydrogenandfuelcells/ storage/current_technology.html.
2. B. Sakintuna, F. Lamari-Darkrimb and M. Hirscher, *Int. J. Hydrogen Energy*, 2007, **32**, 1121.
3. F. Schuth, B. Bogdanovic and M. Felderhoff, *Chem. Commun.*, 2004, 2249.
4. S. Orimo, Y. Nakamori, J. R. Eliseo, A. Züttel and C. M. Jensen, *Chem. Rev.*, 2007, **107**, 4111.
5. W. Grochala and P. P. Edwards, *Chem. Rev.*, 2004, **104**, 1283.
6. C. H. Christensen, R. Z. Sørensen, T. Johannessen, U. J. Quaade, K. Honkala, T. D. Elmøe, R. Køhler and J. K. Nørskov, *J. Mater. Chem.*, 2005, **15**, 4106.
7. T. Hugle, M. Hartl and D. Lentz, *Chem.—Eur. J.,* 2011, **17**, 10184.
8. G. Alcaraz and S. Sabo-Etienne, *Angew. Chem., Int. Ed.*, 2010, **49**, 7170.
9. C. W. Hamilton, R. T. Baker, A. Staubitz, and I. Manners, *Chem. Soc. Rev.*, 2009, **38**, 279.
10. Y.-H. P. Zhang, *Int. J. Hydrogen Energy*, 2010, **35**, 10334.
11. V. V. Struzhkin, B. Militzer, W. L. Mao, H.-K. Mao and R. Hemley, *J. Chem. Rev.*, 2007, **107**, 4133.
12. J. Chen and F. Wu, *Appl. Phys.*, *A*: *Mater. Sci. Process*, 2004, **78**, 989.
13. N. B. McKeown and P. M. Budd, *Chem. Soc. Rev.*, 2006, **35**, 675.
14. H.-M. Cheng, Q.-H. Yang and C. Liu, *Carbon*, 2001, **39**, 1447.
15. R. H. Baughman, A. A. Zakhidov and W. A. de Heer, *Science*, 2002, **297**, 787.

16. R. Ströbel, J. Garche, P. T. Moseley, L. Jörissen and G. Wolf, *J. Power Sources*, 2006, **159**, 781.
17. M. P. Suh, H. J. Park, T. K. Prasad and D.-W. Lim, *Chem. Rev.*, 2012, **112**, 782–835.
18. S. K. Bhatia and A. L. Myers, *Langmuir*, 2006, **22**, 1688.
19. H. Furukawa, N. Ko, Y. B. Go, N. Aratani, S. Choi, A. O. Yazaydin, R. Q. Snurr, M. O'Keeffe, J. Kim and O. M. Yaghi, *Science*, 2010, **329**, 424.
20. O. K. Farha, A. O. Yazaydin, I. Eryazici, C. D. Malliakas, B. G. Hauser, M. G. Kanatzidis, S. T. Nguyen, R. Q. Snurr and J. T. Hupp, *Nat. Chem.*, 2010, **2**, 944.
21. K. Koh, A. G. Wong-Foy and A. J. Matzger, *J. Am. Chem. Soc.*, 2009, **131**, 4184-4185.
22. D. Yuan, D. Zhao, D. Sun and H.-C. Zhou, *Angew. Chem., Int. Ed.*, 2010, **49**, 5357.
23. M. Latroche, S. Surblé, C. Serre, C. Mellot-Draznieks, P. L. Llewellyn, J. H. Lee, J. S. Chang, S. H. Jhung and G. Férey, *Angew. Chem., Int. Ed.*, 2006, **45**, 8227-8231.
24. *Metal-Organic Frameworks: Design and Application*; L. R. MacGillivray (Ed.), Wiley: Hoboken, NJ, 2010.
25. (*a*) S. Ma, J. Eckert, P. M. Forster, J. W. Yoon,Y. K. Hwang, J.-S. Chang, C. D. Collier, J. B. Parise and H.-C. Zhou, *J. Am. Chem. Soc.*, 2008, **130**, 15896; (*b*) H.-C. Zhou, S. Q. Ma, D. F. Sun, M. Ambrogio, J. A. Fillinger and S. J. Parkin, *J. Am. Chem. Soc.*, 2007, **129**, 1858.
26. M. Dincă, A. Dailly, C. Tsay and J. R. Long, *Inorg. Chem.*, 2008, **47**, 11.
27. (*a*) B. Kesanli, Y. Cui, M. R. Smith, E. W. Bittner, B. C. Bockrath, and W. Lin, *Angew. Chem., Int. Ed.*, 2005, **44**, 72; (*b*) J. L. Rowsell and O. M. Yaghi, *Angew. Chem., Int. Ed.*, 2005, **44**, 4670.
28. O. K. Farha, C. D. Malliakas, M. G. Kanatzidis and J. T. Hupp, *J. Am. Chem. Soc.*, 2010, **132**, 950.
29. J. Zhang, L. Wojtas, R. W. Larsen, M. Eddaoudi and M. J. Zaworotko, *J. Am. Chem. Soc.*, 2009, **131**, 17040.
30. B. L. Chen, M. Eddaoudi, T. M. Reineke, J. W. Kampf, M. O'Keeffe and O. M. Yaghi, *J. Am. Chem. Soc.*, 2000, **122**, 11559-11560.
31. S. S. Y. Chui, S. M. F. Lo, J. P. H. Charmant, A. G. Orpen and I. D. Williams, *Science*, 1999, **283**, 1148.

32. Y.-G. Lee, H. R. Moon, Y. E. Cheon and M. P. Suh, *Angew. Chem., Int. Ed.*, 2008, **47**, 7741.

33. X.-S. Wang, S. Ma, P. M. Forster, D. Yuan, J. Eckert, J. L. Lopez, B. J. Murphy, J. B. Parise and H.-C. Zhou, *Angew. Chem., Int. Ed.*, 2008, **47**, 7263.

34. (*a*) X. Lin, J. Jia, X. Zhao, K. M. Thomas, A. J. Blake, G. S. Walker, N. R. Champness, P. Hubberstey and M. Schröder, *Angew. Chem., Int. Ed.*, 2006, **45**, 7358; (*b*) S. H. Yang, X. Lin, A. Dailly, A. J. Blake, P. Hubberstey, N. R. Champness and M. Schröder, *Chem.—Eur. J.*, 2009, **15**, 4829; (*c*) X. Lin, I. Telepeni, A. J. Blake, A. Dailly, C. M. Brown, J. M. Simmons, M. Zoppi, G. S. Walker, K. M. Thomas, T. J. Mays, P. Hubberstey, N. R. Champness and M. Schröder, *J. Am. Chem. Soc.*, 2009, **131**, 2159.

35. (*a*) Y. Yan, X. Lin, S. Yang, A. J. Blake, A. Dailly, N. R. Champness, P. Hubberstey and M. Schröder, *Chem. Commun.*, 2009, **45**, 1025; (*b*) Y. Yan, I. Telepeni, S. Yang, X. Lin, W. Kockelmann, A. Dailly, A. J. Blake, W. Lewis, G. S. Walker, D. R. Allan, S. A. Barnett, N. R. Champness and M. Schröder, *J. Am. Chem. Soc.*, 2010, **132**, 4092.

36. D. Yuan, D. Zhao, D. Sun and H.-C. Zhou, *Angew. Chem., Int. Ed.*, 2010, **49**, 5357

37. D. Yuan, D. Zhao and H.-C. Zhou, *Inorg. Chem.*, 2011, **50**, 10528–10530.

38. Y. E. Cheon and M. P. Suh, *Chem. Commun.*, 2009, **45**, 2296.

39. G. Férey, M. Latroche, C. Serre, F. Millange, T. Loiseau and A. Percheron-Guegan, *Chem. Commun.*, 2003, **24**, 2976.

40. M. Latroche, S. Sublé, C. Serre, C. Mellot-Draznieks,P. L. Llewellyn, J.-H. Lee, J.-S. Chang, S. H. Jhung and G. Férey, *Angew.Chem., Int. Ed.*, 2006, **45**, 8227.

41. Y. Liu, J. F. Eubank, A. J. Cairns, J. Eckert, V. C. Kravtsov, R. Luebke and M. Eddaoudi, *Angew. Chem., Int. Ed.*, 2007, **46**, 3278.

42. C. Prestipino, L. Regli, J. G. Vitillo, F. Bonino, A. Damin, C. Lamberti, A. Zecchina, P. L. Solari, K. O. Kongshaug and S. Bordiga, *Chem. Mater.,* 2006, **18**, 1337-1346.

43. V. K. Peterson, Y. Liu, C. M. Brown and C. J. Kepert, *J. Am. Chem. Soc.,* 2006, **128**, 15578-15579.

44. M. Dincă, A. Dailly, Y. Liu, C. M. Brown, D. A. Neumann and J. R. Long, *J. Am. Chem. Soc.,* 2006, **128**, 16876-16883.

45. M. Dincă, W. S. Han, Y. Liu, A. Dailly, C. M. Brown and J. R. Long, *Angew. Chem., Int. Ed.*, 2007, **46**, 1419-1422.

46. F. Nouar, J. Eckert, J. F. Eubank, P. Forster and M. Eddaoudi, *J. Am. Chem. Soc.*, 2009, **131**, 2864.
47. Y. Liu, V. C. Kravtsov, R. Larsen and M. Eddaoudi, *Chem. Commun.*, 2006, **42**, 1488.
48. M. Dincă and J. R. Long, *J. Am. Chem. Soc.*, 2007, **129**, 11172.
49. S. H. Yang, X. Lin, A. J. Blake, G. S. Walker, P. Hubberstey, N. R. Champness and M. Schröder, *Nat. Chem.*, 2009, 1, 487.
50. K. L. Mulfort and J. T. Hupp, *J. Am. Chem. Soc.*, 2007, **129**, 9604-9605.
51. (*a*) A. Blomqvist, C. M. Araffljo, P. Srepusharawoot and R. Ahuja, *Proc. Natl. Acad. Sci., U.S.A.*, 2007, **104**, 20173; (*b*) S. S. Han and W. A. Goddard, *J. Am. Chem. Soc.*, 2007, **129**, 8422; (*c*) S. S. Han and W. A. Goddard, *J. Phys. Chem.*, *C* 2008, **112**, 13431; (*d*) S. S. Han, S.-H. Choi and W. A. Goddard, *J. Phys. Chem.*, *C* 2011, **115**, 3507; (*d*) A. Mavrandonakis and W. Klopper, *J. Phys. Chem.*, *C* 2008, **112**, 11580; (*e*) P. Dalach, H. Frost, R. Q. Snurr and D. E. Ellis, *J. Phys. Chem.*, *C* 2008, **112**, 9278; (*f*) A. Mavrandonakis, E. Tylianakis, A. K. Stubos and G. E. Froudakis, *J. Phys. Chem.*, *C* 2008, **112**, 7290; (*g*) B. Huang, H. Lee, W. Duan, J. Ihm, *Appl. Phys. Lett.*, 2008, **93**, 63107; (*h*) Y. J. Choi, J. W. Lee, J. H. Choi and J. K. Kang, *Appl. Phys. Lett.*, 2008, **92**, 173102.
52. K. L. Mulfort, O. K. Farha, C. L. Stern, A. A. Sarjeant and J. T. Hupp, *J. Am. Chem. Soc.*, 2009, **131**, 3866.
53. D. Himsl, D. Wallacher and M. Hartmann, *Angew. Chem., Int. Ed.*, 2009, **48**, 4639
54. E. Klontzas, A. Mavrandonakis, E. Tylianakis and G. E. Froudakis, *Nano Lett.*, 2008, **8**, 1572.
55. J. A. Botas, G. Calleja, M. Sánchez-Sánchez and M. G. Orcajo, *Langmuir*, 2010, **26**, 5300.
56. S. T. Srinivas and P. K. Rao, *J. Catal.*, 1994, **148**, 470.
57. Y. Li and R. T. Yang, *J. Am. Chem. Soc.*, 2006, **128**, 726.
58. Y. Li and R. T. Yang, *J. Am. Chem. Soc.*, 2006, **128**, 8136.
59. Y.-Y. Liu, J.-L. Zeng, J. Zhang, F. Xu and L.-X. Sun, *Int. J. Hydrogen Energy.*, 2007, **32**, 4005.
60. Y. E. Cheon and M. P. Suh, *Angew. Chem., Int. Ed.*, 2009, **48**, 2899.

4. OBSECTIVES OF THE THESIS

Hydrogen Storage in MOMs:

Hydrogen is widely regarded as the solution to world's future energy supply owing to its extraordinary high gravimetric heat of combustion (120 MJ/kg) and clean burning (releases only water as byproduct) when compared to gasoline. In fact, this value is almost three times higher when compared to the gravimetric heat of combustion of gasoline (44.5 MJ/kg). However in contrary to gasoline, the density of hydrogen is extremely low (only 0.08 kg/m^3) at room temperature and at atmospheric pressure or even in its liquefied state under pressurized condition and at a very low temperature (20.3 K) the density can reach only up to one tenth than that of gasoline (700 kg/m^3), which presents the hurdle for the practical usage of hydrogen as a fuel.

As already discussed in chapter 3, current hydrogen storage based techniques deals with pressurized tank, cryogenic storage tank, chemisorption and physisorption. Pure tank based storage technology suffers from the safety concern and also from economic issues. Chemisorption based hydrogen storage systems on the other hand suffers from kinetic, reversibility and heat management issues due to the formation of strong chemical bonds between the hydrogen and the storage materials. In contrast to the aforementioned techniques, physisorption based storage technique primarily deals with weak interaction between the adsorbate and adsorbent, which permits fast kinetics, full reversibility and easily manageable heat during hydrogen fuelling.

Nano-porous materials are generally promising as carrier and storage media for gases by absorption. Much research has been initiated in this area, but the fields of amorphous carbon, silica and alumina as solid gas carriers, which are mainly based on relatively weak physical absorption forces, such as capillary physisorption and kinetic trapping effects, did not up until now show real breakthroughs towards practical applications with sufficient storage capacities at manageable temperatures. MOMs especially coupled with high degree of porosity and stability, on the other hand, have the advantage over the other porous materials for instance amorphous carbon or silica, that they possess chemical flexibility in chemical design allowing systematic design strategies that can be used for developing new materials. Indeed, inspired by the pioneering work of Yaghi and co-workers several hundreds of MOFs with different chemical entities has been evaluated based on their hydrogen storage capacity.[1,2] In fact, many of them exhibited extraordinary high volumetric and gravimetric hydrogen uptake at 77 K, which are

distinctly superior than that was achieved with any other porous materials. In addition, gravimetric storage capacity of some of the materials could easily meet the requirement to apply them in practical application purpose. However, the main concern remaining to be address with the hydrogen physisorption in MOFs is their insufficient interactions with H_2 at higher temperature, putting the barrier to realize significant delivery amount at near ambient temperatures. Indeed, the storage capacity by the best performed MOFs at temperature in the range of -30 to -40 °C could reach only up to 1-3 wt%, thereby leading to the obstacle to implement them for practical usage which required a minimum of 5.5 wt% including the full system. It has been shown that high interaction between the H_2 and MOFs could be achieved by constructing MOFs with coordinatively unsaturated metal centers, doping MOFs with alkali metals and constructing MOFs with narrow pore size distribution.[2] The impact of some of these critical parameters on hydrogen storage are already discussed in detailed in chapter 3

Along this direction of research, we believe that creation of MOFs with high charge density is another way to realize a high adsorption enthalpy with a wide loading amount of H_2. Therefore the major goal of the thesis will explore new strategies to introduce special chemical functionalities in the MOF surface either by incorporating molecular building blocks with unique chemical features in terms of polarity or through derivatization of the linkers of the performed MOFs with polar and polarizing groups and hydrogen bonding employing PSM approach. Furthermore new chemical strategies for introducing high concentration of unsaturated metal sites on the MOF surface will be investigated through unique chemical approaches.

Azulenes constitute dipolar aromatic systems and we anticipated that azulenes contained in a MOF could contribute to the buildup of coulombic fields required for the polarization and polarized binding of H_2. The polarized binding state of H_2 should provide considerable stabilization depending on the size of the electrical field.[3] It was calculated that the H_2 molecules over an azulene ring system would have higher interaction energy in comparison to simple benzene and isomeric naphthalene systems owing to its internal charge separation.[4] We believe that in MOFs the electrical field gradients of an appropriately arranged azulene unit should be cooperative and thus lead to an enhancement of polarized binding of H_2. In this context, two rigid molecular building block namely, 1,3- and 2,6-azulenedicarboxylic acid will be examined towards designing and construction of novel materials with unique structural features and to

introduce polarization effect of azulene on the MOF surface. The hydrogen storage performance by the new materials comprising of azulene back bone will be investigated.

The state of polarized H_2 binding in MOFs corresponds to recent findings in solution chemistry that the so-called "frustrated" Lewis pairs can squeeze a H_2 molecule between them. Indeed any small molecule even less polarizable ones for example H_2 can be "activated" in this fashion. The effect is believed to depend on the polarizing power of the polarizing groups:

$$LA\cdot\cdot\cdot H\text{-}H\cdot\cdot\cdot LB$$ where, LA = Lewis acid; LB = Lewis base

It was estimated that the binding forces of H_2 molecules can reach up to 6–8 kcal/mol in optimum cases.

Therefore, an interesting aspect of the research will attempt to take advantage of such polarized binding states through chemical modifications of the functionalized linkers of the performed MOFs. More specifically, attempts to functionalize the pendant amine group of MOFs with borane derivatives following postsynthetic modification approach will be under taken.

Chemosensing in MOMs:

High sensitive and selective detection of gas and vapor phase analytes for a range of potential applications including industrial process management, chemical threat detection, medical diagnostics, food quality control, occupational safety, and environmental monitoring are perceived to be of keen research interest over the last decades. In particular a significant research is being pursued towards the vapor phase detection of explosive analytes such as 2,4-dinitrotoluene, 2,4,6-trinitrotoluene and 2,4,6-trinitrophenol due to their importance in security screening, homeland security and environmental monitoring. Towards investigating more convenient and economically favorable alternatives to the well-trained canines[5] or sophisticated analytical instruments,[6] new molecular materials especially based on luminescent conjugated organic polymers that are capable of fast and reliable detection, *via* photoinduced electron transfer (PET) quenching mechanism, of the aforementioned analytes have recently been identified. More recently, it has been realized that metal-organic materials comprising suitable organic building block capable of forming π-complex with these electron deficient analytes,

could also serve as potentially high sensitive chemosensors. It is believed that the detection sensitivity of these chemosensors is primarily determined by transduction methods.[7,8] Therefore, design of new materials capable of enhancing the transduction signals, which result from the binding of analyte molecules are of great demand. Towards this direction of research, a part of the thesis work will also aim at the development of new metal-organic materials incorporating molecular building blocks based on triptycene receptors, which has been successfully evaluated in conjugated polymers for explosive detection purpose, for sensitive detection of explosive substances.

4.1. References

1. N. L. Rosi, J. Eckert, M. Eddaoudi, D. T. Vodak, J. Kim, M. O'Keeffe and O. M. Yaghi, *Science*, 2003, **300**, 1127-1129.
2. M. P. Suh, H. J. Park, T. K. Prasad and D.-W. Lim, *Chem. Rev.*, 2012, **112**, 782–835.
3. J.-Y. Hasegawa, M. Higuchi, Y. Hijikata and S. Kitagawa, *Chem. Mater.*, 2009, **21**, 1829.
4. (*a*) O. Hübner, A. Glöss, M. Fichtner and W. Klopper, *J. Phys. Chem. A*, 2004, **108**, 3019; (*b*) M. Wong, B. E. V. Kuiken, C. Buda and B. D. Dunietz, *J. Phys. Chem. C*, 2009, **113**, 12571.
5. K. G. Furton and L. J. Myers, *Talanta*, 2001, **54**, 487.
6. (*a*) P. Kolla, *Angew. Chem., Int. Ed. Engl.*, 1997, **36**, 800; (*b*) A. G. Davies, A. D. Burnett, W. H. Fan, E. H. Linfield and J. E. Cunningham, *Mater. Today*, 2008, **11**, 18.
7. (*a*) T. M. Swager, *Acc. Chem. Res.*, 1998, **31**, 201; (*b*) H. Sohn, M. J. Sailor, D. Magde and W. C. Trogler, *J. Am. Chem. Soc.*, 2003, **125**, 3821; (*c*) V. Williams and T. M. Swager, *Macromolecules*, 2000, **33**, 4069.
8. (*a*) J.-S. Yang and T. M. Swager, *J. Am. Chem. Soc.*, 1998, **120**, 5321; (*b*) J.-S. Yang and T. M. Swager, *J. Am. Chem. Soc.*, 1998, **120**, 11864; (*c*) D. Zhao and T. M. Swager, *Macromolecules*, 2005, **38**, 9377

5. AZULENE BASED METAL-ORGANIC FRAMEWORKS FOR STRONG ADSORPTION OF H_2

5.1. Publication 1

Azulene based metal-organic frameworks for strong adsorption of H_2

Samir Barman,[a] Hiroyasu Furukawa,[b] Olivier Blacque,[a] Koushik Venkatesan,[a] Omar M. Yaghi[b] and Heinz Berke*[a]*

[a] Department of Inorganic Chemistry, University of Zürich Winterthurerstrasse 190, CH-8057, Zürich (Switzerland).

[b] Center for Reticular Chemistry, Department of Chemistry and Biochemistry, University of California-Los Angeles, 607 Charles E. Young Drive East, Los Angeles, California 90095.

Chem. Commun., 2010, **46**, 7981-7983.

Azulene based metal–organic frameworks for strong adsorption of H_2†‡

Samir Barman,[a] Hiroyasu Furukawa,*[b] Olivier Blacque,[a] Koushik Venkatesan,[a] Omar M. Yaghi[b] and Heinz Berke*[a]

Received 15th July 2010, Accepted 3rd September 2010
DOI: 10.1039/c0cc02589e

Two Zn MOFs, MOF-645 and MOF-646, comprised of polarized 1,3-azulenedicarboxylate were synthesized. The guest free MOF-646 showed strong MOF-H_2 interactions (7.8–6.8 kJ mol^{-1}), which revealed the significant impact of internally polarized azulene backbone to stabilized H_2 molecules in the framework.

Due to the high fugacity coefficient of hydrogen, a dense storage form in a fuel cell vehicle has become important in the effort to achieve the DOE (US) targets.[1] In addition to the large storage space, implementation of the large adsorption enthalpy of H_2 (*ca.* 15 kJ mol^{-1}) is a key issue in building practical storage systems.[2] Because of the discovery of high surface area metal–organic frameworks (MOFs), it is possible to store more than 10 wt% of H_2 at 77 K,[3] but due to the very weak interactions between H_2 and the MOF framework, their storage capacity is not significant at 298 K.[1] Towards this end, creation of coordinatively unsaturated metal centers[4] and doping of MOFs with alkali metals[5] have been proposed. However, once these metal sites are blocked by H_2 molecules, the adsorption enthalpy should decrease drastically, which leads to another problem; *i.e.*, that the delivery amount of H_2 may not be large. Therefore, we believe that creation of MOFs with high charge density is another way to realize a high adsorption enthalpy with a wide loading amount of H_2.[6]

Azulenes constitute dipolar aromatic systems (Scheme 1) and we anticipated that azulenes contained in a MOF could contribute to the build up of coulombic fields required for the polarization and polarized binding of H_2.

The polarized binding state of H_2 provides considerable stabilization depending on the size of the electrical field.[7] It was calculated that the H_2 molecules over an azulene ring system would have higher interaction energy in comparison to simple benzene and isomeric naphthalene systems owing to its internal charge separation.[8] We believe that in MOFs the electrical field gradients of an appropriately arranged azulene unit should be cooperative and thus lead to an enhancement of polarized binding of H_2. Herein we report an alternate approach towards enhancing polarizability of the frameworks using internally polarized angular 1,3-azulenedicarboxylic acid (C_{2v} symmetry).[9] Specifically, we report the synthesis and characterization of two new MOFs,§ MOF-645 [$Zn_5(OH)_2(\mathbf{L})_4$] (**L** = 1,3-azulenedicarboxylate) and MOF-646 [$Zn_4O(\mathbf{L})_3$], and describe the H_2 uptake behaviors for guest free MOF-646.

Single crystals of MOF-645 were obtained by heating $H_2\mathbf{L}$ and zinc nitrate in a mixture of DMF/ EtOH/ H_2O (1.0 : 0.25 : 0.25 mL) at 90 °C (DMF = *N*,*N*-dimethylformamide).[10] The single crystal X-ray diffraction (SXRD) analysis¶ reveals that the structure of MOF-645 has a three-dimensional (3D) framework, which is constructed from unique pentanuclear zinc(II) clusters: $Zn_5(\mu_3\text{-}OH)_2(O_2C)_8(DMF)(H_2O)$ (Fig. 1a and b). Two Zn triangles, each with a central μ_3-OH group, share a central Zn corner. The central Zn atom is bridged to each of the other Zn atoms by a carboxylate.[11] The edges opposite the central Zn atom are each bridged by a carboxylate. Half of the edge Zn atoms have single chelating bidentate carboxylate,[11] respectively, while the other Zn atoms are coordinated to either DMF or a water molecule. In the overall crystal structure, these SBUs are linked to produce a **bcu** net (Fig. 1c).[12,13] If occluded and coordinated guests are removed, accessible void space is estimated to be 41%. However, in our attempt, the guest free form of MOF-645 did not take up N_2 at 77 K presumably due to structural decomposition as evidenced by the X-ray powder diffraction (PXRD) pattern.[13] Therefore, we strove to prepare another MOF with the same ligand **L**.

Synthesis of MOF-646 has been achieved by carrying out a solvothermal reaction between $H_2\mathbf{L}$ and zinc acetate in DMF.[10] From SXRD analysis (Fig. 1e), each Zn_4O unit is connected by ligand **L**. The Zn_4O unit is a slightly distorted tetrahedron and two DMF molecules are coordinated to one of the four Zn ions in the unit (Fig. 1d).[13,14] Although the chemical formula is the same as for other IRMOFs [$Zn_4O(link)_3$], the overall connectivity (**lcy**, Fig. 1f) is different from them (**pcu**) because of the bent ligand. The variation in the underlying topology from **pcu** to **lcy** could result in a

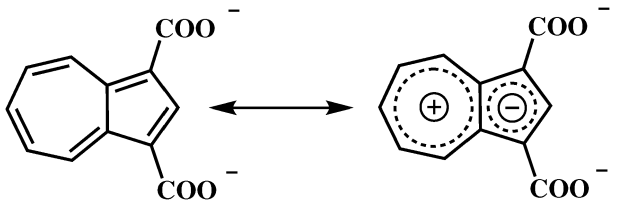

Scheme 1 Resonance form of 1,3-azulenedicarboxylate emphasizing its polar nature.

[a] *Department of Inorganic Chemistry, University of Zürich, Winterthurerstrasse 190, CH-8057, Zürich, Switzerland. E-mail: hberke@aci.uzh.ch; Fax: (+41) 44-635-6802*
[b] *Center for Reticular Chemistry, Department of Chemistry and Biochemistry, University of California-Los Angeles, 607 Charles E. Young Drive East, Los Angeles, California 90095, USA. E-mail: furukawa@chem.ucla.edu*

† This article is part of a ChemComm 'Hydrogen' web-based themed issue.

‡ Electronic supplementary information (ESI) available: Full synthetic procedures and characterization data including TGA, IR, PXRD. N_2 isotherms and single crystal X-ray diffraction data. CCDC 771570–771571. For ESI and crystallographic data in CIF or other electronic format see DOI: 10.1039/c0cc02589e

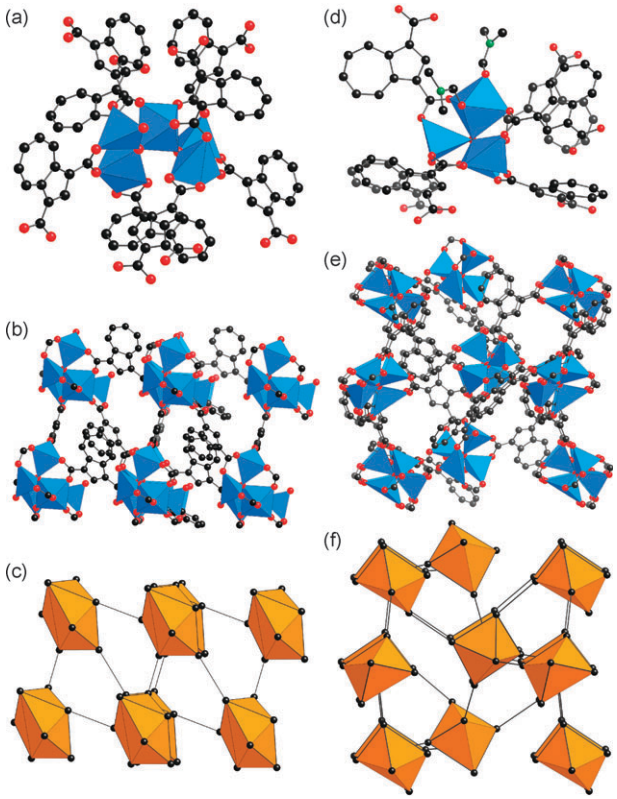

Fig. 1 $Zn_5(\mu_3\text{-}OH)_2(\mathbf{L})_8$ SBU with Zn shown as polyhedra (a) and view of crystalline framework of MOF-645 (b) in a **bcu** net (c). $Zn_4(\mu_4\text{-}O)(\mathbf{L})_6(DMF)_2$ SBU with Zn shown as polyhedra (d) and view of the single X-ray crystal structure of MOF-646 (e) in an **lcy** net (f). Atom colors: Zn, blue tetrahedra; O, red; C, black; N, green; all hydrogen atoms and terminal ligands on the SBUs except (d) are omitted for clarity.

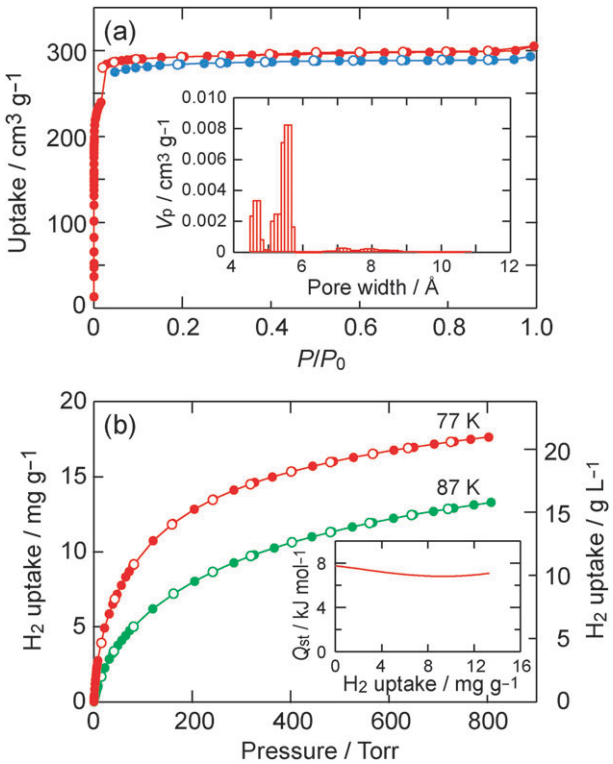

Fig. 2 (a) Ar isotherm for activated MOF-646 measured at 87 K. Inset: pore size distribution (histogram) for activated MOF-646, calculated from a NLDFT fit to the Ar adsorption data at 87 K.[13] (b) H_2 isotherms for activated MOF-646 measured at 77 (red) and 87 K (olive). Inset: the coverage dependencies of adsorption enthalpies of H_2 for activated MOF-646. Filled and open symbols for (a) and (b) represent adsorption and desorption branches respectively.

smaller pore size distribution (<7 Å) which should allow an extensive overlap of attractive potential of the pore wall and could mitigate the entropic gain at a higher temperature.[15]

Solvent guests in the as-synthesized form of MOF-646 were removed by first immersing the crystals in chloroform and then evacuating at 45 °C for 24 h.[13] The PXRD pattern of activated MOF-646 confirmed that it retained crystallinity.[13] Elemental microanalysis of the activated sample is consistent with the guest free material of $[Zn_4O(\mathbf{L})_3]$. The removal of coordinated DMF may affirm the nature of the open metal site in the Zn_4O unit.

The permanent porosity of the activated MOF-646 was demonstrated by measuring the Ar gas adsorption at 87 K (Fig. 2a). MOF-646 takes up Ar in the low pressure region which is indicative of the presence of microporosity. A small step at $P/P_0 = 0.02$ is probably due to either the pore blocking effect or reorientation of adsorbed Ar molecules. The Langmuir and BET surface areas of activated MOF-646 are estimated to be 1130 $m^2\ g^{-1}$ and 925 $m^2\ g^{-1}$, respectively.[16] To evaluate the pore size distribution of MOF-646, the Ar isotherm was analyzed using nonlocal density functional theory (NLDFT) based on a zeolite/silica model containing cylindrical pores.[17] The distribution calculated by fitting the MOF-646 adsorption data (<6 Å) revealed the pore width is within the realm of an ultramicropore.

In conjunction with the polarized pore wall and the small pore size distribution of MOF-646, we recorded the H_2 adsorption isotherms on the activated material. In spite of relatively high crystal density (1.19 g cm^{-3}), activated MOF-646 shows considerable H_2 uptake up to 17.5 mg g^{-1} at 77 K and 1 bar (Fig. 2b). This gravimetric uptake outperforms MOFs with Zn_4O SBUs except for IRMOF-11 whose nets are interwoven.[18] More importantly, the H_2 uptake in the volumetric unit (20.9 g L^{-1}) is approaching that of high performance MOFs having Cu open metal sites (22–24 g L^{-1} for HKUST-1, PCN-14, and SNU-5)[4c,h,j] measured under similar conditions.

To investigate the reason for the excellent H_2 uptake on activated MOF-646, coverage dependencies of the isosteric heat of adsorption (Q_{st}) were calculated from fits of its 77 and 87 K isotherms. As shown in Fig. 2b (inset), the Q_{st} curve is nearly flat throughout the loading range examined, which is in sharp contrast to many MOFs, especially those possessing open metal sites.[4a,d,h,j] The estimated Q_{st} (7.8–6.8 kJ mol^{-1}) is higher than representative MOFs, such as MOF-5, MOF-177 and HKUST-1,[3c,4c] although this is lower than MIL-101, $M_3[(M_4Cl)_3(BTT)_8]_2$ (M = Mn, Fe, Co, BTT^{3-} = 1,3,5-benzenetristetrazolate) analogues and other MOF materials.[19,4a,d–f,h,j] It is worth noting that, to our best knowledge, 7.1 kJ mol^{-1} of Q_{st} at 13 mg g^{-1} of adsorbed H_2 is one of the highest values among physisorption media.[20]

From the Q_{st} curve it is not possible to speculate the adsorption sites of H_2; however, if each Zn_4O unit confines 4 H_2 molecules as suggested by neutron diffraction studies,[21] the H_2 uptake corresponds to 8.5 mg g^{-1}. Considering that the Q_{st} value does not drop off after the occupation of the relatively strong binding sites, it is presumed that the internally polarized azulene backbone is advantageous to stabilize H_2 molecules in the framework, because smaller pore size distribution should not be effective to enhance the Q_{st} (but can improve Henry's constant).

Funding from the Swiss National Science Foundation (SNSF), University of Zurich and US DOE are gratefully acknowledged.

Notes and references

§ Synthesis of MOF-645: A mixture of *N*,*N*-dimethylformamide (DMF)/ethanol/H_2O (1.00/0.25/0.25 mL) containing 1,3-azulenedicarboxylic acid (0.005 g, 2.3×10^{-5} mol) and $Zn(NO_3)_2{\cdot}6H_2O$ (0.014 g, 4.62×10^{-5} mol) was sealed in a 20-mL glass vial. The vial was heated at a constant rate 0.5 °C min^{-1} to 90 °C for 48 h and then cooled at a constant rate 0.1 °C min^{-1} to room temperature. The dark red crystals were washed with a DMF/ ethanol mixture (3 × 3 mL) to give 0.007 g (Yield: 88% based on 1,3-azulenedicarboxylic acid).

MOF-646: 1,3-Azulenedicarboxylic acid (0.010 g, 4.6×10^{-5} mol) and $Zn(CH_3COO)_2{\cdot}2H_2O$ (0.010 g, 4.62×10^{-5} mol) were combined with 2 mL of DMF and sealed in a 20-mL glass vial and sonicated for several minutes. The vial was heated at a constant rate 2.0 °C min^{-1} to 120 °C for 20 h in a programmable oven. The vial was taken out from the oven while hot and the hexagonal plate-shaped crystals were washed with DMF (3 × 2 mL) to give 0.015 g (Yield: 80% based on 1,3-azulenedicarboxylic acid).

¶ Crystal data for MOF-645: $C_{51}H_{35}NO_{20}Zn_5{\cdot}C_3H_7NO$, M_r = 1381.85, monoclinic, space group *C*2, a = 15.7939(2), b = 16.3435(1), c = 12.2880(2) Å, β = 123.813(2)°, V = 2683.19(9) $Å^3$, Z = 2, d_{calcd} = 1.710 Mg m^{-3}, crystal size 0.33 × 0.21 × 0.06 mm^3, T = 153(2) K, λ = 0.71073 Å, R_1 = 0.0285 [$I > 2\sigma(I)$], wR_2 = 0.0770 (all data, 39 666 reflections), R_{int} = 0.0259, GOF = 1.022. Crystal data for MOF-646: $2(C_{84}H_{64}N_4O_{30}Zn_8){\cdot}5(C_3H_7NO){\cdot}4(H_2O)$, M_r = 4702.25, monoclinic, space group $P2_1$, a = 17.2344(6), b = 17.2237(6), c = 17.2923(7) Å, β = 90.548(4)°, V = 5132.8(3) $Å^3$, Z = 1, d_{calcd} = 1.521 Mg m^{-3}, crystal size 0.13 × 0.09 × 0.05 mm^3, T = 153(2) K, λ = 0.71073 Å, R_1 = 0.0468 [$I > 2\sigma(I)$], wR_2 = 0.0996 (all data, 30 148 reflections), R_{int} = 0.0520, GOF = 0.843.

1 (*a*) L. J. Murray, M. Dincă and J. R. Long, *Chem. Soc. Rev.*, 2009, **38**, 1294; (*b*) S. Ma and H.-C. Zhou, *Chem. Commun.*, 2010, **46**, 44.

2 S. K. Bhatia and A. L. Myers, *Langmuir*, 2006, **22**, 1688.

3 (*a*) S. S. Kaye, A. Dailly, O. M. Yaghi and J. R. Long, *J. Am. Chem. Soc.*, 2007, **129**, 14176; (*b*) Y. Yan, X. Lin, S. Yang, A. J. Blake, A. Dailly, N. R. Champness, P. Hubberstey and M. Schröder, *Chem. Commun.*, 2009, 1025; (*c*) H. Furukawa, M. A. Miller and O. M. Yaghi, *J. Mater. Chem.*, 2007, **17**, 3197; (*d*) H. Furukawa, N. Ko, Y. B. Go, N. Aratani, S. B. Choi, E. Choi, A. O. Yazaydin, R. Q. Snurr, M. O'Keeffe, J. Kim and O. M. Yaghi, *Science*, 2010, **329**, 424.

4 (*a*) M. Dincă and J. R. Long, *J. Am. Chem. Soc.*, 2005, **127**, 9376; (*b*) B. Chen, N. W. Ockwig, A. R. Millward, D. S. Contreras and O. M. Yaghi, *Angew. Chem., Int. Ed.*, 2005, **44**, 4745; (*c*) J. L. C. Rowsell and O. M. Yaghi, *J. Am. Chem. Soc.*, 2006, **128**, 1304; (*d*) M. Dincă, A. Dailly, Y. Liu, C. M. Brown, D. A. Neumann and J. R. Long, *J. Am. Chem. Soc.*, 2006, **128**, 16876; (*e*) M. Latroche, S. Surblé, C. Serre, C. Mellot-Draznieks, P. L. Llewellyn, J.-H. Lee, J.-S. Chang, S. H. Jhung and G. Férey, *Angew. Chem., Int. Ed.*, 2006, **45**, 8227; (*f*) M. Dincă, W. S. Han, Y. Liu, A. Dailly, C. M. Brown and J. R. Long, *Angew. Chem., Int. Ed.*, 2007, **46**, 1419; (*g*) X.-S. Wang, S. Ma, P. M. Forster, D. Yuan, J. Eckert, J. J. López, B. J. Murphy, J. B. Parise and H.-C. Zhou, *Angew. Chem., Int. Ed.*, 2008, **47**, 7263; (*h*) Y.-G. Lee, H. R. Moon and P. Suh, *Angew. Chem., Int. Ed.*, 2008, **47**, 7741; (*i*) W. Zhou, H. Wu and T. Yildirim, *J. Am. Chem. Soc.*, 2008, **130**, 15268; (*j*) S. Ma, J. M. Simmons, D. Sun, D. Yuan and H.-C. Zhou, *Inorg. Chem.*, 2009, **48**, 5263; (*k*) X. Lin, I. Telepeni, A. J. Blake, A. Dailly, C. M. Brown, J. M. Simmons, M. Zoppi, G. S. Walker, K. M. Thomas, T. J. Mays, P. Hubberstey, N. R. Champness and M. Schröder, *J. Am. Chem. Soc.*, 2009, **131**, 2159.

5 (*a*) S. S. Han and W. A. Goddard, *J. Am. Chem. Soc.*, 2007, **129**, 8422; (*b*) K. L. Mulfort and J. T. Hupp, *J. Am. Chem. Soc.*, 2007, **129**, 9604; (*c*) D. Himsl, D. Wallacher and M. Hartmann, *Angew. Chem., Int. Ed.*, 2009, **48**, 4639; (*d*) S. Yang, X. Lin, A. J. Blake, K. M. Thomas, P. Hubberstey, N. R. Champness and M. Schröder, *Chem. Commun.*, 2008, 6108.

6 (*a*) Y. Liu, J. F. Eubank, A. J. Cairns, J. Eckert, V. C. Kravtsov, R. Luebke and M. Eddaoudi, *Angew. Chem., Int. Ed.*, 2007, **46**, 3278; (*b*) D. F. Sava, V. C. Kravtsov, F. Nouar, L. Wojtas, J. F. Eubank and M. Eddaoudi, *J. Am. Chem. Soc.*, 2008, **130**, 3768.

7 J.-Y. Hasegawa, M. Higuchi, Y. Hijikata and S. Kitagawa, *Chem. Mater.*, 2009, **21**, 1829.

8 (*a*) O. Hübner, A. Glöss, M. Fichtner and W. Klopper, *J. Phys. Chem. A*, 2004, **108**, 3019; (*b*) M. Wong, B. E. V. Kuiken, C. Buda and B. D. Dunietz, *J. Phys. Chem. C*, 2009, **113**, 12571.

9 L. J. Mathias and C. G. Overberger, *J. Org. Chem.*, 1980, **45**, 1701.

10 Microanalysis for MOF-645, $[Zn_5(\mu_3\text{-}OH)_2(\mathbf{L})_4(DMF)(H_2O)]{\cdot}(DMF)$, calcd: C, 46.94; H, 3.06; N, 2.03%. Found: C, 46.1; H, 3.13; N, 2.02%. For MOF-646, $[Zn_4(\mu_4\text{-}O)(\mathbf{L})_3(DMF)_2]{\cdot}(DMF)_{1.25}{\cdot}(H_2O)$, calcd: C, 46.74; H, 3.67; N, 3.87%. Found: C, 46.54; H, 3.61; N, 4.26%.

11 Three oxygen atoms (O2, O3 and O5) of carboxylate linkers are disordered over two positions with fixed site occupancy factors of 0.5 : 0.5. Constraints on their displacement parameters were applied using EADP. See Fig. S1 in ESI for details.

12 M. O'Keeffe, M. A. Peskov, S. J. Ramsden and O. M. Yaghi, *Acc. Chem. Res.*, 2008, **41**, 1782.

13 See ESI for details.

14 (*a*) H. Chun and H. Jung, *Inorg. Chem.*, 2009, **48**, 417; (*b*) Y. Takashima, C. Bonneau, S. Furukawa, M. Kondo, R. Matsuda and S. Kitagawa, *Chem. Commun.*, 2010, **46**, 4142.

15 M. Rzepka, P. Lamp and M. A. de la Casa-Lillo, *J. Phys. Chem. B*, 1998, **102**, 10894.

16 The pore volume from the Ar isotherm is smaller than that from the N_2 isotherms. This indicates that the packing density of Ar in the pore should be lower than that of N_2. Indeed, estimated surface area based on the crystal structure (54% void space, 1260 m^2 g^{-1}) is almost the same as the Langmuir surface area from the N_2 isotherm (1250 m^2 g^{-1}).

17 P. I. Ravikovitch, D. Wei, W. T. Chueh, G. L. Haller and A. V. Neimark, *J. Phys. Chem. B*, 1997, **101**, 3671.

18 J. L. C. Rowsell, A. R. Millward, K. S. Park and O. M. Yaghi, *J. Am. Chem. Soc.*, 2004, **126**, 5666.

19 (*a*) M. Dincă and J. R. Long, *J. Am. Chem. Soc.*, 2007, **129**, 11172; (*b*) F. Nouar, J. F. Eubank, T. Bousquet, L. Wojtas, M. J. Zaworotko and M. Eddaoudi, *J. Am. Chem. Soc.*, 2008, **130**, 1833; (*c*) S. Ma and H.-C. Zhou, *J. Am. Chem. Soc.*, 2006, **128**, 11734; (*d*) B. Chen, X. Zhao, A. Putkham, K. Hong, E. B. Lobkovsky, E. J. Hurtado, A. J. Fletcher and K. M. Thomas, *J. Am. Chem. Soc.*, 2008, **130**, 6411.

20 O. K. Farha, K. L. Mulfort and J. T. Hupp, *Inorg. Chem.*, 2008, **47**, 10223.

21 E. C. Spencer, J. A. K. Howard, G. J. McIntyre, J. L. C. Rowsell and O. M. Yaghi, *Chem. Commun.*, 2006, 278.

ChemComm

Chemical Communications

Electronic Supplementary Information (19 pages)

Azulene Based Metal-Organic Frameworks for Strong Adsorption of H_2

Samir Barman[a], Hiroyasu Furukawa,*[b] Olivier Blacque,[a] Koushik Venkatesan, [a] Omar M. Yaghi[b] and Heinz Berke*[a]

[a] *Department of Inorganic Chemistry , University of Zürich Winterthurerstrasse 190, CH-8057, Zürich (Switzerland), E-mail: hberke@aci.uzh.ch, Fax: (+41) 44-635-6802*
[b] *Center for Reticular Chemistry, Department of Chemistry and Biochemistry, University of California-Los Angeles, 607 Charles E. Young Drive East, Los Angeles, California 90095.*
E-mail: furukawa@chem.ucla.edu

Table of Contents

Section S1 *Materials and general procedures*

All solvents and reagents were purchased commercially and, unless otherwise noted, were used without further purification. Microanalyses were carried out at the Anorganisch-Chemisches Institut of the University of Zurich. IR spectra were obtained by using ATR methods with a Bio-Rad FTS-45 FTIR spectrometer. The powder XRD patterns were obtained with a Bruker D8 Advance system equipped with Cu sealed tube (λ = 1.5406 Å). The following conditions were applied: 40 kV, 40 mA, increment = 0.007°, scan speed = 1.5 s / step. The simulated powder patterns were calculated from the single crystal X-ray diffraction data and generated with Mercury 2.2 software. All TGA experiments were performed under a N_2 atmosphere from 25 - 800 °C at a temperature ramp rate of 5 °C / min.

Section S2 *Synthesis*

1,3-Azulenedicarboxylic acid, was prepared according to the published procedure.[S1]

Synthesis of $[Zn_5(\mu_3\text{-}OH)_2(\mathbf{L})_4(DMF)(H_2O)]\cdot(DMF)$ **(**MOF-645**).** [**L** = 1,3-azulenedicarboxylate]

A mixture of *N*,*N*-dimethylformamide (DMF)/ C_2H_5OH/ H_2O (1.00/0.25/0.25 mL) containing 1,3-azulenedicarboxylic acid (0.005 g, 2.3×10^{-5} mol) and $Zn(NO_3)_2\cdot 6H_2O$ (0.014 g, 4.62×10^{-5} mol) was sealed in a glass vial. The vial was heated (0.5 °C min^{-1}) to 90 °C for 48 h and then cooled at 0.1 °C min^{-1} to room temperature. The dark red crystals were washed with a DMF/ ethanol mixture (3 × 3 mL) to give (yield: 0.007 g, 88% based on 1,3-azulenedicarboxylic acid). Elemental analysis calcd (%) for $C_{54}H_{42}N_2O_{21}Zn_5$ = $[Zn_5(\mu_3\text{-}OH)_2(\mathbf{L})_4(DMF)(H_2O)]\cdot(DMF)$: C 46.94, H 3.06, N 2.03; found C 46.1, H 3.13, N 2.02.

Synthesis of $[Zn_4(\mu_4\text{-}O)(\mathbf{L})_3(DMF)_2]\cdot(DMF)_{1.25}(H_2O)$ **(**MOF-646**).**

1,3-azulenedicarboxylic acid (0.010 g, 4.6×10^{-5} mol) and $Zn(CH_3COO)_2\cdot 2H_2O$ (0.010 g, 4.62×10^{-5} mol) were combined with 2 mL of DMF and sealed in a glass vial and sonicated for several minutes. The vial was heated to (2.0 °C min^{-1}) 120 °C for 20 h in a controllable oven. The vial was taken out from the oven while hot and the hexagonal plate-shaped crystals were washed with DMF (3 × 2 mL) (Yield: 0.015 g, 80% based on the ligand). Elemental analysis calcd (%) for

$C_{45.75}H_{42.75}N_{3.25}O_{17.25}Zn_4$ = $[Zn_4(\mu_4\text{-}O)(\mathbf{L})_3(DMF)_2]\cdot(DMF)_{1.25}(H_2O)$: C 46.74, H 3.67, N 3.87; found C 46.54, H 3.61, N 4.26.

Activation of $[Zn_4(\mu_4\text{-}O)(\mathbf{L})_3(DMF)_2]\cdot(DMF)_{1.25}(H_2O)$ **(**MOF-646**).**

The activated form of MOF-646 was prepared either by heating MOF-646 under vacuum ($< 10^{-3}$ torr) at 140 °C for 15 h or by evacuating at 45 °C following solvent exchange with chloroform. Elemental analysis calcd (%) for $C_{36}H_{18}O_{13}Zn_4$ = $[Zn_4O(\mathbf{L})_3]$: C 46.99, H 1.97, N 0.00; found C 46.35, H 1.98, N 0.00.

Section S3 *Crystallographic Data*

Single X-Ray Diffraction Studies on MOF-645 **and** MOF-646

Crystallographic data were collected at 153(2) K on an Oxford Xcalibur diffractometer (4-circle kappa platform, Ruby CCD detector and a single wavelength Enhance X-ray source with MoK_α radiation, λ = 0.71073 Å).[S2] The selected suitable single crystals were mounted using polybutene oil on the top of a glass fiber fixed on a goniometer head and immediately transferred to the diffractometer. Pre-experiment, data collection, analytical[S3] and multi-scan[S4] absorption corrections, and data reduction were performed with the Oxford program suite *CrysAlisPro*.[S4] The structures were solved with the Patterson (heavy atom) method and were refined by full-matrix least-squares methods on F^2 with SHELXL-97.[S5] All programs used during the crystal structure determination process are included in the WINGX software.[S6] The program PLATON[S7] was used to check the result of the X-ray analyses.

MOF-645 crystallizes in the non-centrosymmetric space group *C*2 with one solvent molecule of DMF per asymmetric unit. The solvent molecule is about a two-fold axis and positionally disordered over two positions with fixed site occupancy factors of 0.5:0.5. Soft restraints on its geometry and displacement parameters were used with the help of the DFIX, DELU and SIMU instructions of SHELXL-97.[S5] Three oxygen atoms (O2, O3 and O5) of carboxylate ligands are disordered over two positions with fixed site occupancy factors of 0.5:0.5. Constraints on their displacement parameters were applied using EADP. On the tetra-coordinate metal center Zn3, a substitutional disorder has been refined between coordinated DMF and water molecules with fixed site occupancy factors of 0.5:0.5. Only soft geometrical restraints (DFIX, DANG) were used to describe the positions of the hydrogen atoms of the water molecule. All other hydrogen positions were calculated after each cycle of refinement using a riding model, with C-H = 0.93 Å and $U_{iso}(H) = 1.2U_{eq}(C)$ for aromatic H atoms, with C-H = 0.98 Å and $U_{iso}(H) = 1.2U_{eq}(C)$ for the "methine" H atom on O1, and with C-H = 0.96 Å and $U_{iso}(H) = 1.5U_{eq}(C)$ for methyl H atoms.

MOF-646 crystallizes in the non-centrosymmetric space group $P2_1$ with two solvent molecules of DMF and eight molecules of water per asymmetric unit. In the crystal structure, the coordinated DMF molecule had to be partially refined over two positions with refined site occupancies of 0.435(14):0.565(14). Only soft restraints on displacement parameters (DELU,

SIMU) were used for selected carbon and oxygen atoms. All hydrogen positions were calculated after each cycle of refinement using a riding model, with C-H = 0.93 Å and $U_{iso}(H) = 1.2U_{eq}(C)$ for aromatic H atoms, and with C-H = 0.96 Å and $U_{iso}(H) = 1.5U_{eq}(C)$ for methyl H atoms.

Table S1. Summary of the X-ray diffraction studies of MOF-645 and MOF-646.

	MOF-645	MOF-646
empirical formula	$C_{51}H_{35}NO_{20}Zn_5$, C_3H_7NO	$(C_{84}H_{64}N_4O_{30}Zn_8)_2$, $5(C_3H_7NO)$, $4(H_2O)$
formula weight ($g \cdot mol^{-1}$)	1381.85	4702.25
temperature (K)	153(2)	153(2)
wavelength (Å)	0.71073	0.71073
crystal system, space group	monoclinic, *C* 2	monoclinic, *P* 2_1
a (Å)	15.7939(2)	17.2344(6)
b (Å)	16.6435(1)	17.2237(6)
c (Å)	12.2880(2)	17.2923(7)
α (°)	90	90
β (°)	123.831(2)	90.548(4)
γ (°)	90	90
volume ($Å^3$)	2683.19(9)	5132.8(3)
Z, density (calcd) ($Mg \cdot m^{-3}$)	2, 1.710	2, 1.521
abs coefficient (mm^{-1})	2.286	1.918
F(000)	1396	2392
crystal size (mm^3)	0.33 x 0.21 x 0.06	0.13 x 0.09 x 0.05
θ range (°)	2.6 to 32.6	2.4 to 25.7
reflections collected	39666	30148
reflections unique	9785 [R(int) = 0.0259]	17700 [R(int) = 0.0520]
completeness to θ (%)	99.9	99.9
absorption correction	semi-empirical from equivalents	analytical
max/min transmission	1.000 / 0.708	0.924 / 0.848
data / restraints / parameters	9785 / 76 / 416	17700 / 245 / 1302
goodness-of-fit on F^2	1.022	0.843
absolute structure parameter	0.007(7)	-0.003(11)
final R_1 and wR_2 indices [$I > 2\sigma(I)$]	0.0285, 0.0765	0.0468, 0.0931
R_1 and wR_2 indices (all data)	0.0307, 0.0770	0.0849, 0.0996

The unweighted R-factor is $R_1 = \sum(Fo - Fc)/\sum Fo$; $I > 2\sigma(I)$ *and the weighted R-factor is* $wR2 = \{\sum w(Fo^2 - Fc^2)^2/\sum w(Fo^2)^2\}^{1/2}$.

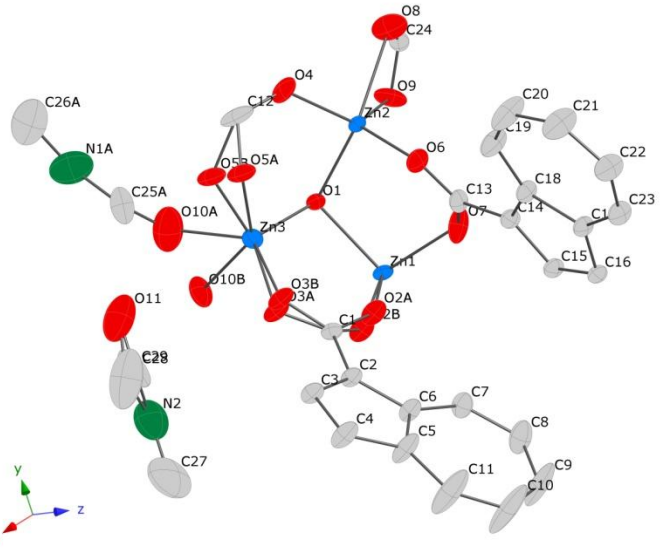

Fig. S1. ORTEP drawing (50% probability) of the asymmetric unit in MOF-645 is displayed with atomic labels. Three oxygen atoms (O2, O3 and O5) of carboxylate ligands are disordered over two positions with fixed site occupancy factors of 0.5:0.5. Color code: Zn, blue; N, dark green; O, red; C, gray. Hydrogen atoms have been omitted for simplicity.

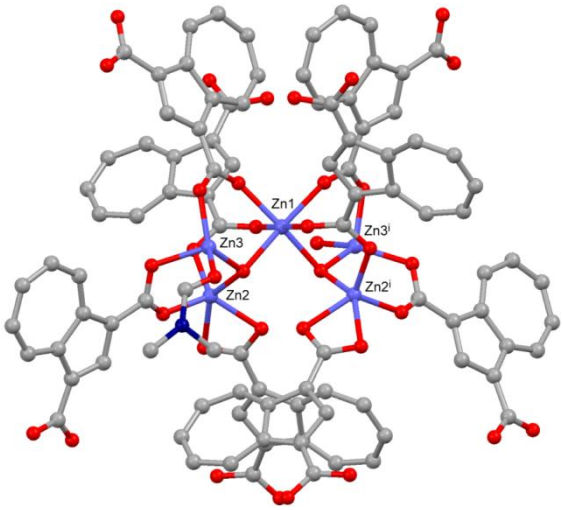

Fig. S2. A ball and stick presentation of the fundamental building unit of $[Zn_5(\mu_3\text{-}OH)_2(\mathbf{L})_4(DMF)(H_2O)]\cdot(DMF)$ (MOF-645). Color code: Zn, blue; N, dark blue; O, red; C, gray. Hydrogen atoms have been omitted for simplicity. Selected atom labels are shown.

a) b)

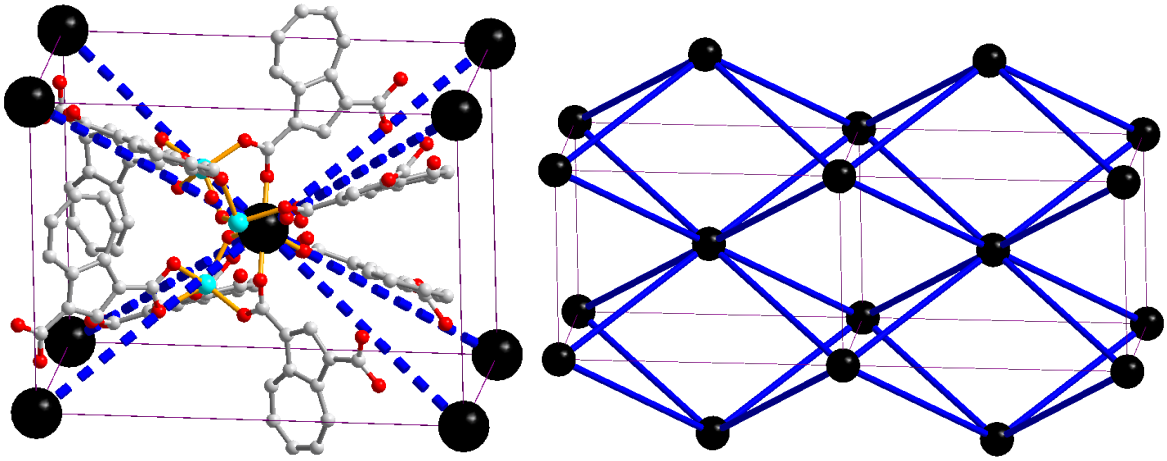

Fig. S3. X-ray structure of MOF-645: a) the topological view of MOF-645 in a cubic node; b) represents the fragment of the body-centered cubic lattice net (**bcu)** topology in MOF-645 stylized according to part a. (each of the vertices, black sphere, of a and b represents a [$Zn_5(\mu_3$-$OH)_2$] clustering unit).

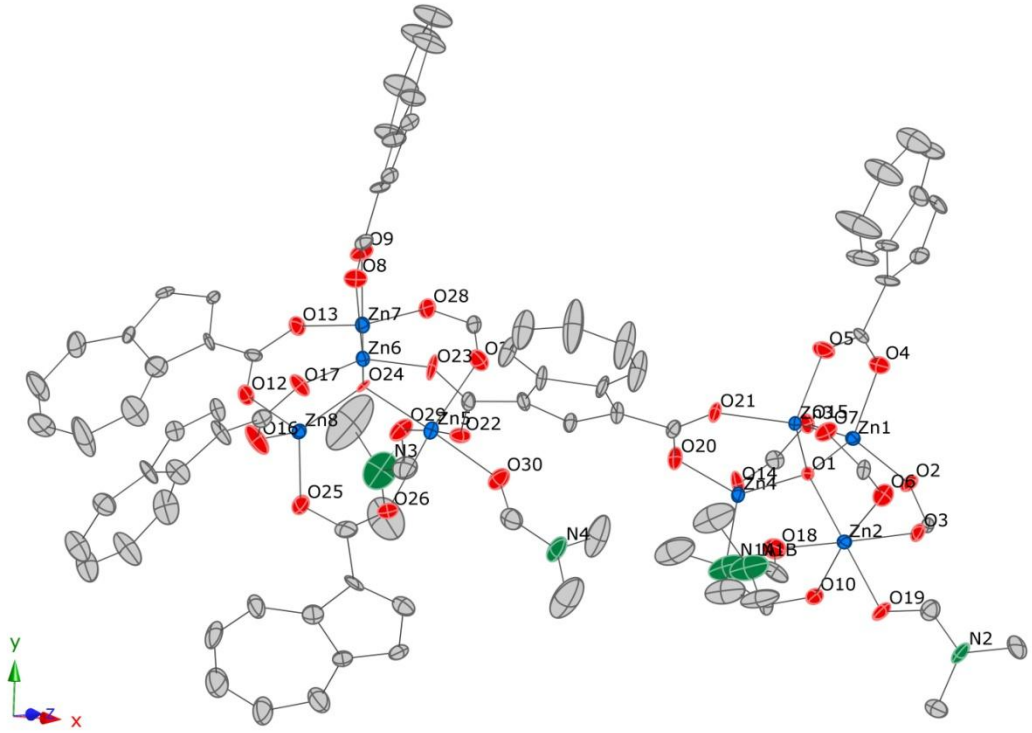

Fig. S4. ORTEP drawing (50% probability) of the asymmetric unit in MOF-646 is displayed with selected atomic labels. Color code: Zn, blue; N, dark green; O, red; C, gray. Hydrogen atoms have been omitted for simplicity.

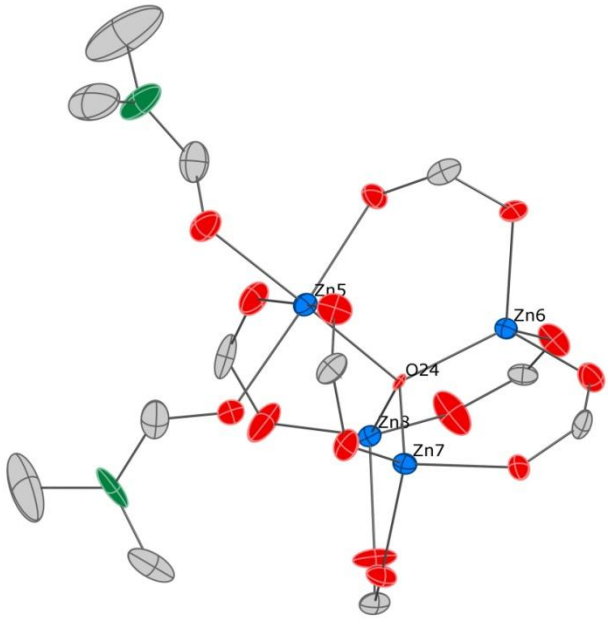

Fig. S5. ORTEP drawing (50% probability) of a $Zn_4(\mu_4\text{-O})$ unit in MOF-646 showing coordinated two DMF molecules.

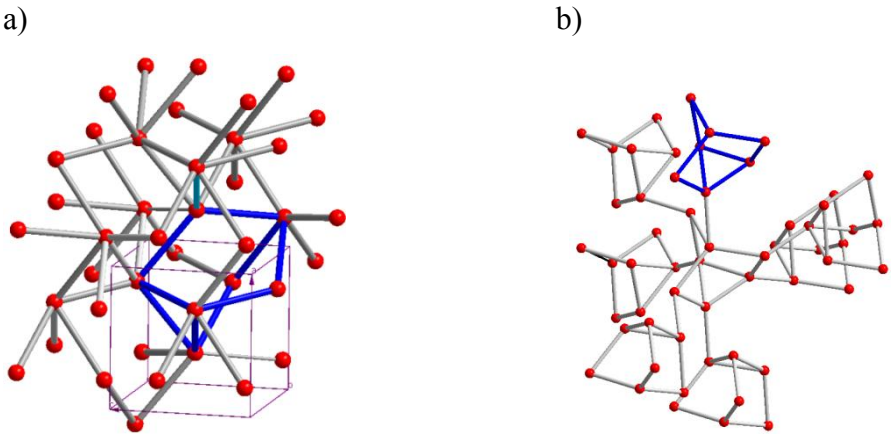

Fig. S6. a) and b) represent the fragment of the augmented **lcy** net and the extended 3D **lcy** net topology in MOF-646, respectively; the blue edges represent one kind of natural tiling [3.5^3] with one triangular and three pentagonal faces (each of the vertices, red sphere, represents the SBUs as shown in Fig. S5).

Section S4 *Powder X-Ray Diffraction Patterns*

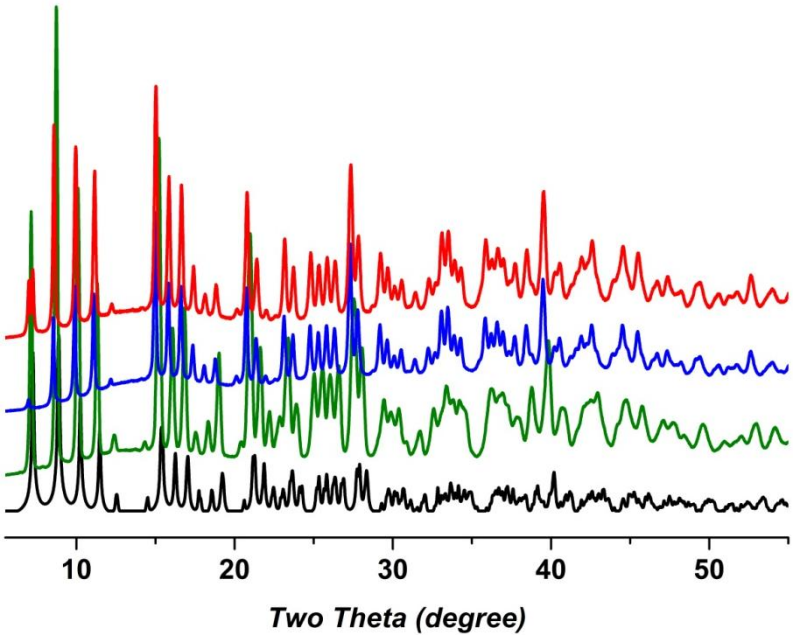

Fig. S7. Powder X-ray diffraction patterns: simulated from the single X-ray crystal structure of MOF-646 (black), as-prepared MOF-646 (olive), activated MOF-646 prepared by drying MOF-646 at 140 °C under vacuum for 15 h (blue) and sample prepared by evacuating at 45 °C for 36 h following solvent exchange with chloroform of MOF-646 (red).

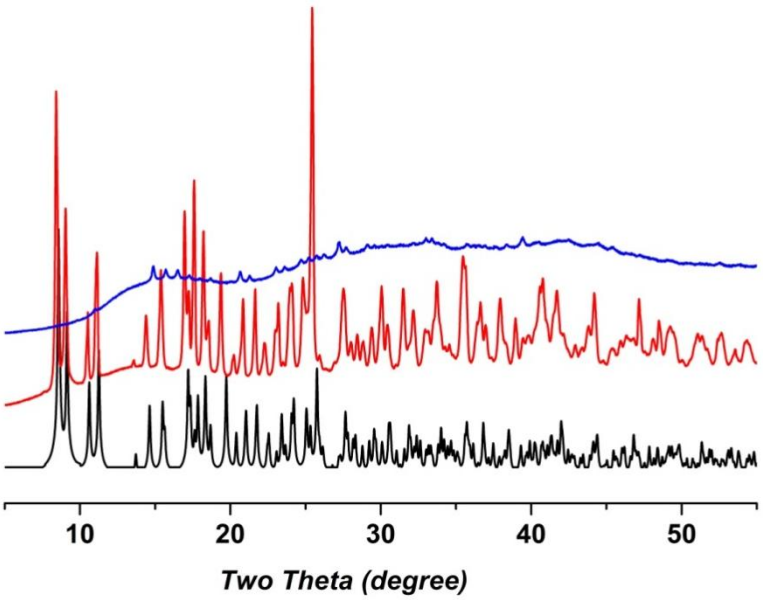

Fig. S8. Powder X-ray diffraction patterns for the simulation from the single crystal structure of MOF-645 (black), as-prepared MOF-645 (red) and MOF-645 drying at 200 °C for 18 h (blue).

Section S5 *IR Spectra*

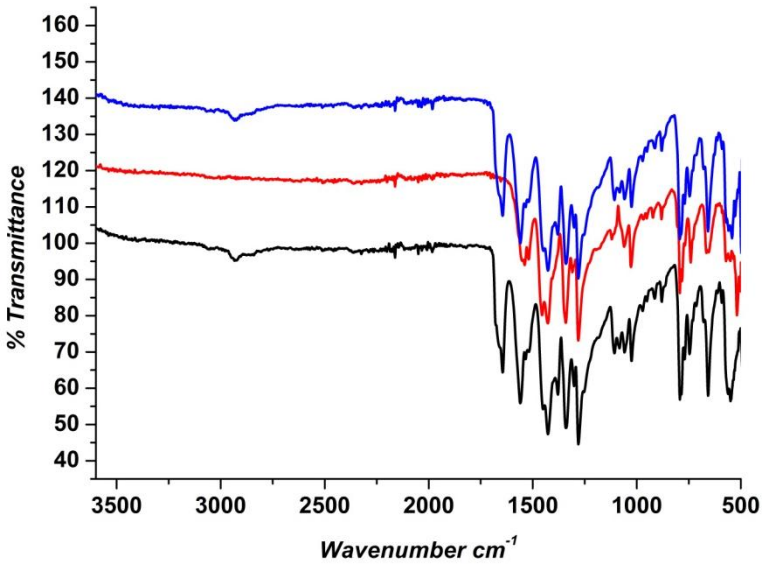

Fig. S9. ATR-IR spectra: as-synthesized MOF-646 (black), activated MOF-646 prepared by drying MOF-646 at 140 °C under vacuum for 15 h (red), sample obtained after immersing activated MOF-646 in DMF for 48 h at room temperature (blue)**.** Note that the C═O stretching frequency of DMF at 1645 cm^{-1} disappeared completely in activated MOF-646 and then reappeared upon soaking activated MOF-646 in DMF with almost the same intensity as was observed in the case of as-synthesized MOF-646.

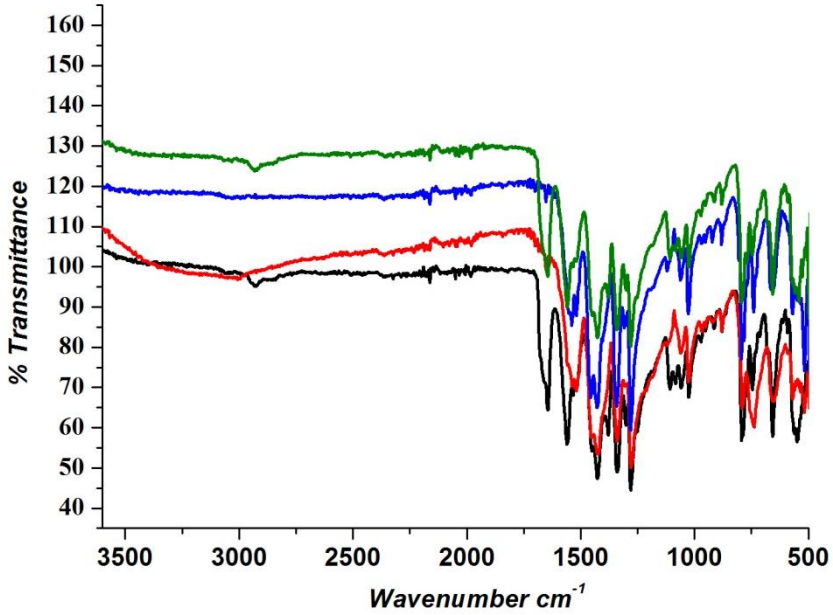

Fig. S10. ATR-IR spectra: as-synthesized MOF-646 (black), chloroform-exchanged sample of MOF-646 (red), sample prepared by evacuating at 45 °C for 36 h following solvent exchange with chloroform of MOF-646 (blue) and its re-solvated (immersion in DMF for 48 h at room temperature) form (olive).

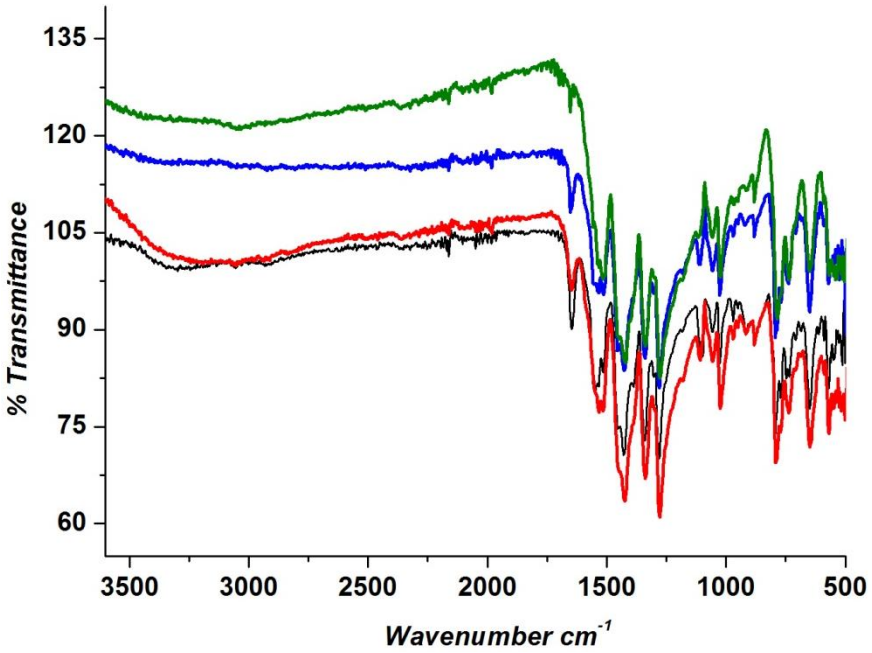

Fig. S11. ATR-IR spectra: as-synthesized MOF-645 (black), methanol-exchanged sample of MOF-645 (red), chloroform-exchanged sample of MOF-645 (blue), sample prepared by evacuating MOF-645 at 200 °C for 18 h (olive).

Section S6 *Thermal Gravimetric Analyses*

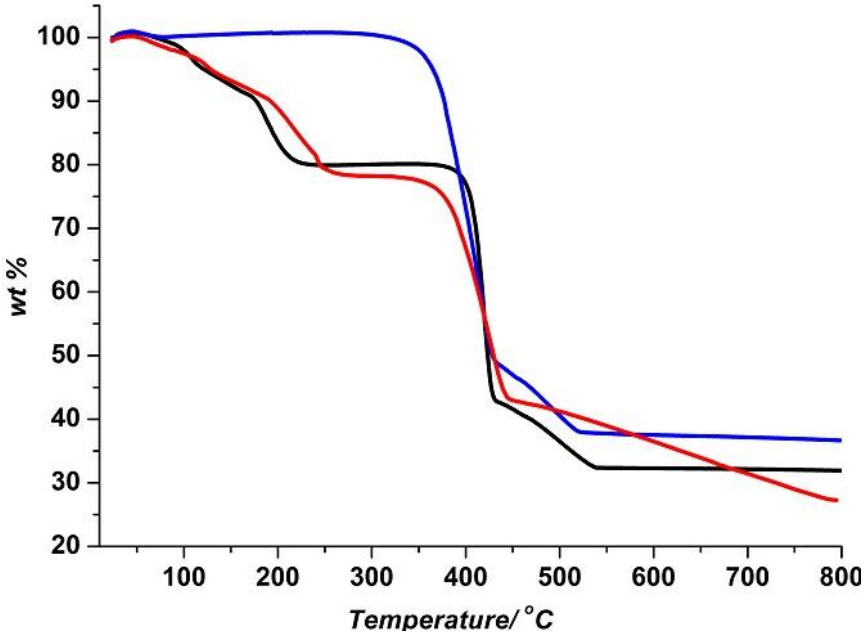

Fig. S12. TGA curves: as-synthesized MOF-646 (black), activated MOF-646 prepared by drying MOF-646 at 140 °C under vacuum for 15 h (blue) and sample obtained after immersing activated MOF-646 in DMF for 48 h at room temperature (red).

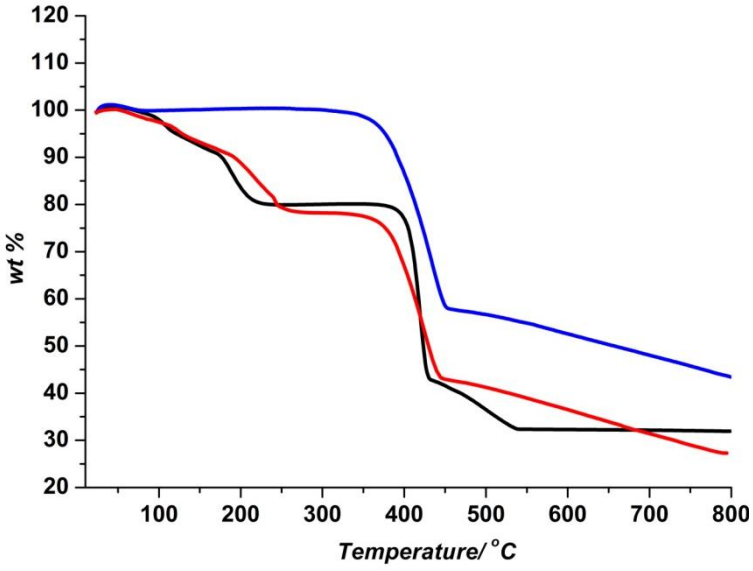

Fig. S13. TGA curves: as-synthesized MOF-646 (black), sample prepared by evacuating at 45 °C for 36 h following solvent exchange with chloroform of MOF-646 (blue) and its re-solvated (immersing in DMF for 48 h at room temperature) form (red).

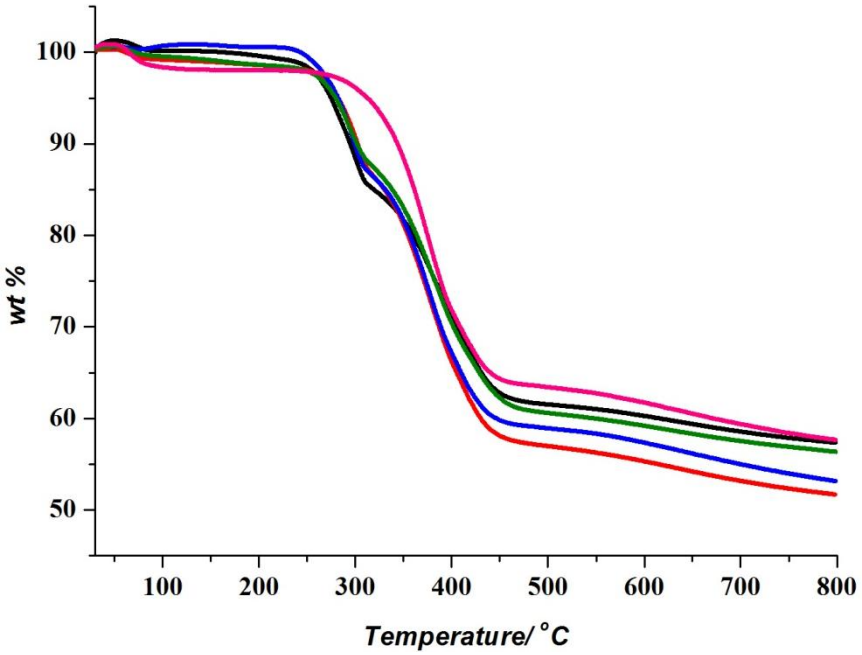

Fig. S14. TGA curves: as-synthesized MOF-645 (black), chloroform-exchanged sample of MOF-645 (red), methanol-exchanged sample of MOF-645 (blue), acetone-exchanged sample of MOF-645 (olive) and sample prepared by evacuating MOF-645 at 200 °C for 18 h (pink).

Section S7 *Gas Adsorption Measurements*

Low-pressure N_2, Ar, and H_2 adsorption measurements were performed on an Autosorb-1 (Quantachrome) volumetric analyzer.[S8] The samples were outgassed to 10^{-6} torr. Helium was used for the estimation of the dead volume, assuming that it is not adsorbed at any of the studied temperatures. Liquid N_2, and liquid Ar baths were used for adsorption measurements at 77 and 87 K, respectively. To provide high accuracy and precision in determining P/P_0, the saturation pressure P_0 was measured throughout the N_2 and Ar analyses by means of a dedicated saturation pressure transducer, which allowed us to monitor the vapor pressure for each data point. Ultra-high-purity grade Ar, N_2, H_2, and He (99.999% purity) were used throughout the adsorption experiments. Non-ideality of gases was obtained from the second virial coefficient at experimental temperature.[S9] Surface areas of the sample were determined from the N_2 as well as from the Ar adsorption isotherm for activated MOF-646, respectively. To estimate pore size distributions for activated MOF-646, Ar isotherms were analyzed using nonlocal density functional theory (NLDFT) implementing a hybrid kernel for Ar adsorption at 87 K based on a zeolite/silica model containing cylindrical pores.[S10] The cumulative pore volume for activated MOF-646 was calculated from a NLDFT fit to the Ar adsorption data for activated MOF-646.

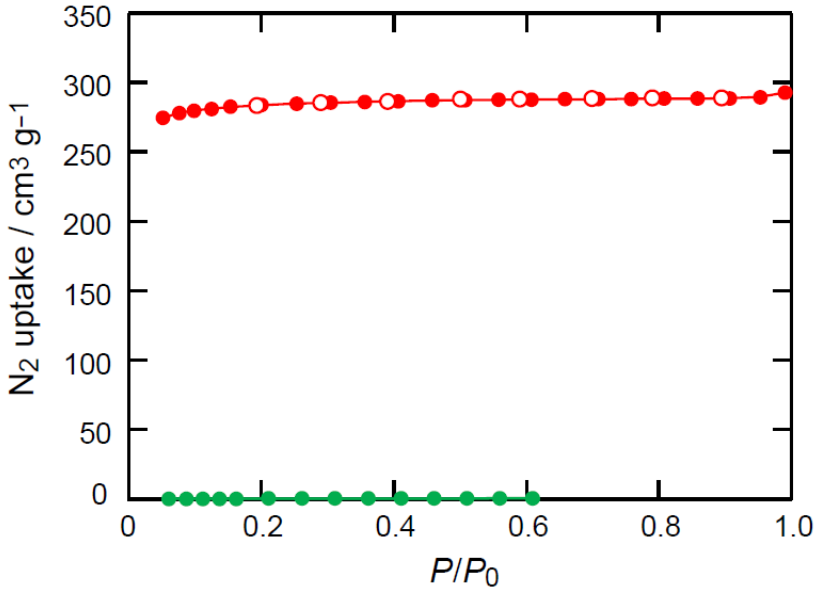

Fig. S15. N_2 isotherm at 77 K: activated MOF-646 (red), MOF-645 degassed at 200 °C for 14 h (olive). Filled and open circles represent adsorption and desorption branches, respectively. Connecting traces are guides for the eyes.

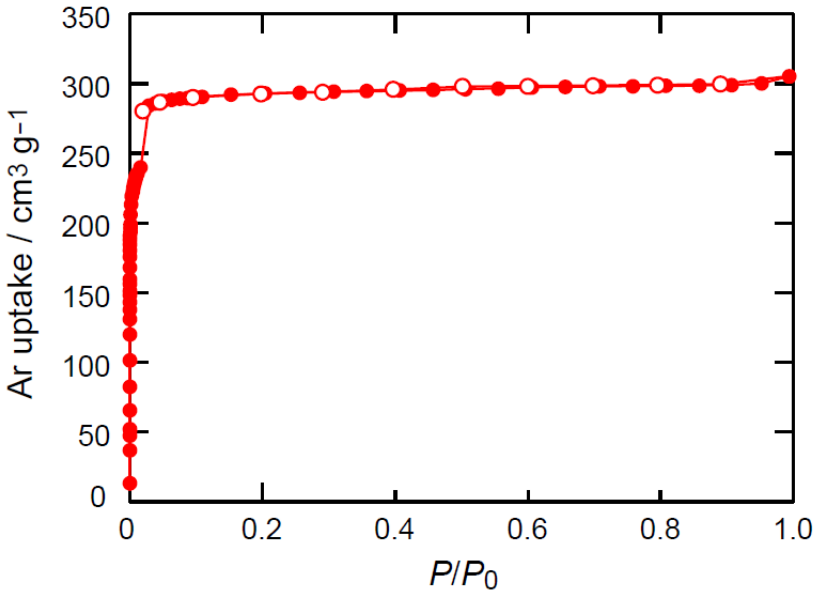

Fig. S16. Ar isotherm at 87 K for activated MOF-646. Filled and open circles represent adsorption and desorption branches, respectively. Connecting traces are guides for the eyes.

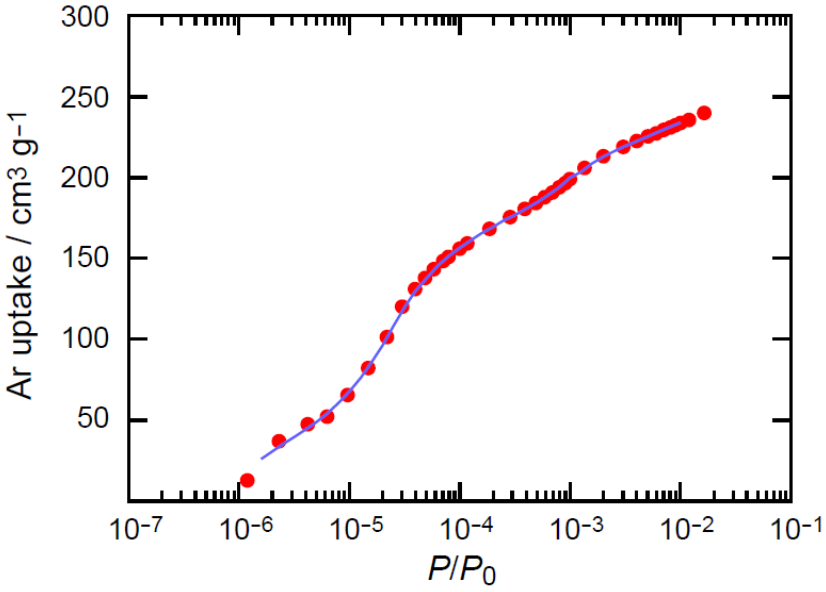

Fig. S17. Ar sorption isotherm at 87 K for activated MOF-646, comparison between experimental (red squares) and NLDFT isotherm (blue solid line).

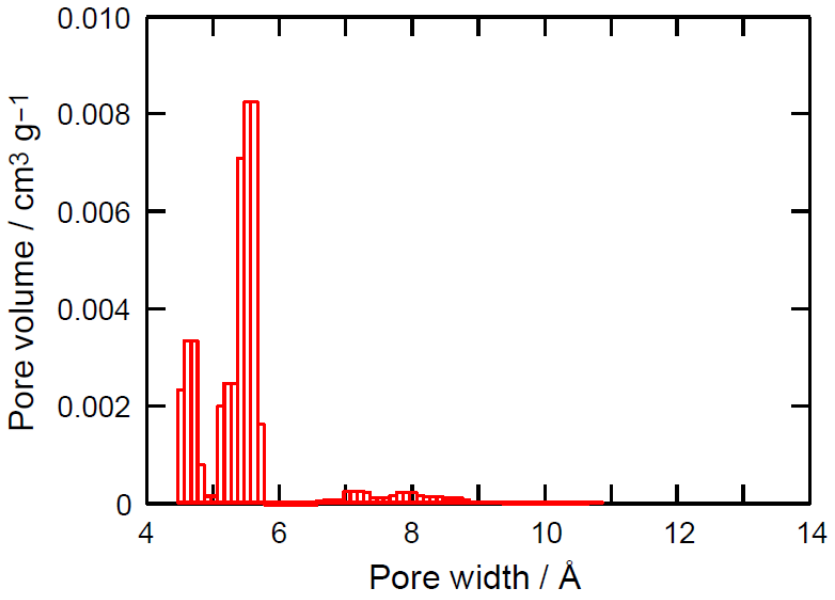

Fig. S18. Pore size distribution (histogram) for activated MOF-646, calculated from a NLDFT fit to the Ar adsorption data for activated MOF-646 in Fig. S17.

Table S2 Summary of N_2 and Ar adsorption measurements for activated MOF-646.

Guest	T / K	Gas uptake / mg g^{-1} [a]	Gas uptake / g L^{-1} [b]	Langmuir SA / m^2 g^{-1}	BET SA / m^2 g^{-1}	Calcd SA / m^2 g^{-1} [c]	PSD / Å [d]	V_p / cm^3 g^{-1}
N_2	77	366	436	1250	1060	1260	N.D.	0.45
Ar	87	545	649	1130	930	1260	4.5/5.5	0.38

[a]Amount of gas adsorbed at P/P_0 = 0.95 of gas pressure. [b]The values are calculated by multiplying the mass of adsorbed gas per gram by the density of the activated MOF-646 (1.19 g cm^{-3}), assuming that the cell volume of MOF-646 is retained in activated MOF-646. [c]The apparent surface area was estimated by using the Langmuir model on activated MOF-646. [d]The pore size distribution (PSD) was calculated from a NLDFT fit to the Ar adsorption data for activated MOF-646 as shown in Fig. S16. [e]The micropore volumes (V_p) were determined using the Dubinin-Raduskavich (DR) transformed N_2 and Ar isotherms across the linear region of the low pressure data.

Estimation of Isosteric Heat of H_2 Adsorption. The isosteric heat of H_2 adsorption was estimated for activated MOF-646 from the H_2 sorption data measured at 77 K and 87 K. A virial-type expression was used (eq 1), which is composed of parameters a_i and b_i that are independent of temperature.[S11] In eq 1, P is the pressure (torr), N is the amount of adsorbed H_2 gas (mg g^{-1}), T is the temperature (K), and m and n represent the number of coefficients required to adequately describe the isotherms.

$$\ln P = \ln N + \frac{1}{T}\sum_{i=0}^{m} a_i N^i + \sum_{i=0}^{n} b_i N^i \qquad (1)$$

To estimate the values of the isosteric heat of H_2 adsorption, eq 2 was applied, where R is the universal gas constant. The isotherms and fitted virial parameters are presented in Fig. S18.

$$Q_{st} = -R\sum_{i=0}^{m} a_i N^i \qquad (2)$$

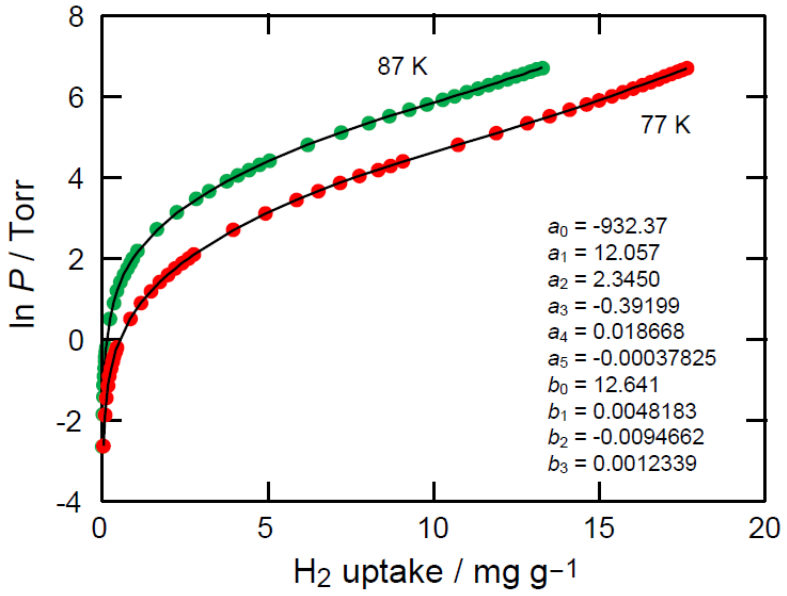

Fig. S19. H_2 isotherms for activated MOF-646 measured at 77 (red) and 87 K (olive). Fitted curves (black solid lines), obtained from the virial-type expansion, were used for the Q_{st} estimation.

Section S8 *References*

[S1] L. J. Mathias and C. G. Overberger, *J. Org. Chem.*, 1980, **45**, 1701.

[S2] Oxford Diffraction (2007). Xcalibur CCD system. Oxford Diffraction Ltd, Abingdon, Oxfordshire, England.

[S3] R. C. Clark and J. S. Reid, *Acta Cryst.*, 1995, **A51**, 887.

[S4] *CrysAlisPro* (Version 1.171.32.41), Oxford Diffraction Ltd, Abingdon, Oxfordshire, England.

[S5] G. M. Sheldrick, *Acta Cryst.*, 2008, **A64**, 112.

[S6] L. J. Farrugia, *J. Appl. Cryst.*, 1999, **32**, 837.

[S7] A. L. Spek, *J. Appl. Cryst.*, 2003, **36**, 7.

[S8] H. Furukawa, M. A. Miller and O. M. Yaghi, *J. Mater. Chem.*, 2007, **17**, 3197.

[S9] J. H. Dymond and E. B. Smith, *The Virial Coefficients of Pure Gases and Mixtures*; Clarendon Press: Oxford, 1980.

[S10] P. I. Ravikovitch, D. Wei, W. T. Chueh, G. L. Haller and A. V. Neimark, *J. Phys. Chem. B*, 1997, **101**, 3671.

[S11] (*a*) J. L. R. Rowsell and O. M. Yaghi, *J. Am. Chem. Soc*., 2006, **128**, 1304; (*b*) M. Dincă, A. Dailly, Y. Liu, C. M. Brown, D. A. Neumann and J. R. Long, *J. Am. Chem. Soc*., 2006, **128**, 16876; (*c*) L. Czepirski and J. Jagiello, *Chem. Eng. Sci.*, 1989, **44**, 797.

6. SYNTHEIS AND HYDROGEN ADSORPTION PROPERTIES OF INTERNALLY POLARIZED 2,6-AZULENEDICARBOXYLIC ACID BASED MOFs

6.1. Abstract

Two novel metal-organic frameworks (MOFs), namely MOF-649 and MOF-650, comprised of internally polarized 2,6-azulenedicarboxylate (2,6-azd) have been synthesized and characterized. Single-crystal X-ray diffraction study of MOF-649 [$Zn_2(2,6\text{-azd})_2(dabco)$] (where dabco = 1,4-diazabicyclo[2.2.2]octane) revealed a primitive cubic (**pcu**) structure constructed from $Zn_2(CO_2)_4$ paddle-wheel units. MOF-649 is isostructural to DUT-8(Zn) [$Zn_2(2,6\text{-ndc})_2(dabco)$] (where 2,6-ndc = 2,6-napthalenedicarboxylate). In overall 3D connectivity, the $Zn_2(CO_2)_4$ paddle-wheel units are bridged by 2,6-azd at the equatorial positions, while pillared by dabco at the axial position. On the other hand, MOF-650 [$Zn_4O(2,6\text{-azd})_3$] represents another 3D **pcu** network structure, which is isostructural to IRMOF-8 [$Zn_4O(2,6\text{-ndc})_3$] and is composed of $Zn_4O(CO_2)_6$ units joined via 2,6-azd. MOF-649/MOF-650 revealed a specific surface area (BET) of ~ 910/2630 $m^2\ g^{-1}$ and a specific micro pore volume of ~ 0.35/1.2 $cm^3\ g^{-1}$. The H_2 adsorption measurements showed that MOF-650 can take up 14.5 mg g^{-1} of hydrogen at 77 K and 1 bar with an estimated zero coverage isosteric heat of adsorption (Q_{st}) of 6.8 kJ mol^{-1}. The observed high Q_{st} at low coverage is believed to be due to the improved polarizability of $Zn_4O(CO_2)_4$ unit triggered by the azulene back bone. Furthermore, a computational analysis was carried out in order to investigate the structure and the electronic properties of MOF-650 and to subsequently understand its site specific interactions towards the dihydrogen molecule.

6.2. Introduction

Metal-organic frameworks (MOFs) are receiving immense research attention owing to their unique structural features, straightforwardly tunable functionality and potential applications in gas storage, separation and catalysis.[1] In particular, the discovery of extraordinarily high cryogenic (77 K) total hydrogen uptake (>10 wt%) by MOFs promotes them to be ideal storage media for clean energy.[1h-j,2] However, due to their insufficient interactions with H_2, the storage capacity appears to be insignificant at room temperature which hinders realization of practical usage.[3] Advancements was achieved by constructing MOFs with coordinatively unsaturated metal centers,[4] doping MOFs with alkali metals[5] and others[3] to improve their interaction energies

with dihydrogen. Furthermore it is believed that MOFs with high local charge densities would be accompanied by improved hydrogen adsorption enthalpy.[6] In this context we anticipated that incorporation of internally polarized azulene units of 2,6-azulenedicarboxylic acid (2,6-H_2azd) into the MOF backbone should lead to enhancement of the polarization potential *via* the coulombic field of the azulene, which is expected to improve the binding of dihydrogen locally and/or globally.[7,8] The asymmetric electrostatic feature of 2,6-azd (2,6-azulenedicarboxylate), for instance in comparison with isomeric naphthalene derivatives, provides opportunity to incorporate it into the MOF lattice in various orientations causing different overall electrostatics. We envisage that MOFs comprising azulene units in an appropriate arrangement can lead to a strongly polarizing environment by contributing individual dipole moments of the linkers, despite the fact that a random arrangement would presumably be favoured by entropy and has a great chance to occur under experimental reaction conditions. In order to justify our hypothesis and having the strut 2,6-H_2azd in hand, we embarked to synthesize prototype IRMOF-8 structure based on Zn_4O tetrahedron and frameworks possesses $Zn_2(CO_2)_4$ paddle-wheel units. This is merely due to the fact that the reticulated framework would be accompanied with uniform polarized pore walls, potentially high porosity and apparent high internal surface areas.[9,10] Particularly in this contribution, we report synthesis and gas sorption properties of two novel framework materials namely MOF-649 (isostructural to Zn_2(2,6-ndc)$_2$(dabco) [DUT-8(Zn)])[10h] and MOF-650 (isostructural to Zn_4O(2,6-ndc)$_3$ [IRMOF-8])[9] comprised of internally polarized 2,6-azd. We further complement the experimental results with a computational study using Density Functional Theory (DFT). In particular, we study the polarization within the MOF lattices, and investigate the site-specific adsorption properties of H_2 in MOF-650 and compare them with those in the isostructural, but unpolarized IRMOF-8.

6.3. Experimental Section

6.3.1. Materials and Methods

Synthesis of the 2,6-azulenedicarboxylic acid (2,6-H_2azd) was accomplished following a multi-step synthesis procedure as reported in the literature (See Scheme 1).[11,12] All commercially available reagents and solvents were purchased from Aldrich and were used as such without further purification. Diethylether (Et_2O) and tetrahydrofuran (THF) used in the reactions were dried by distillation under N_2 atmosphere using sodium benzophenone ketyl radical prior to use.

Anhydrous acetone and $CHCl_3$ (amylene stabilized) were purchased from Aldrich. Infrared (IR) spectra were recorded on a Perkin-Elmer 1600 Fourier transform spectrometer using KBr pellets with frequencies (ν_{max}) quoted in wavenumbers (cm^{-1}). Elemental microanalyses were carried out with a LECO CHNS-932 analyser. ^{1}H and ^{13}C NMR spectra were recorded on a Varian Mercury (200 MHz) spectrometer. Thermogravimetric analysis (TGA) data were obtained on a NETZSCH STA 449C instrument with a heating rate of 1 °C/min under a N_2 atmosphere. The powder X-ray diffraction (PXRD) patterns were obtained with a Bruker D8 Advance system equipped with Cu sealed tube (λ = 1.5406 Å). The following conditions were applied: 40 kV, 40 mA, increment = 0.007°, scan speed = 1.5 s/step. The guest free sample of MOF-649 was obtained on a Tousimis Samdri PVT-3D critical point dryer.

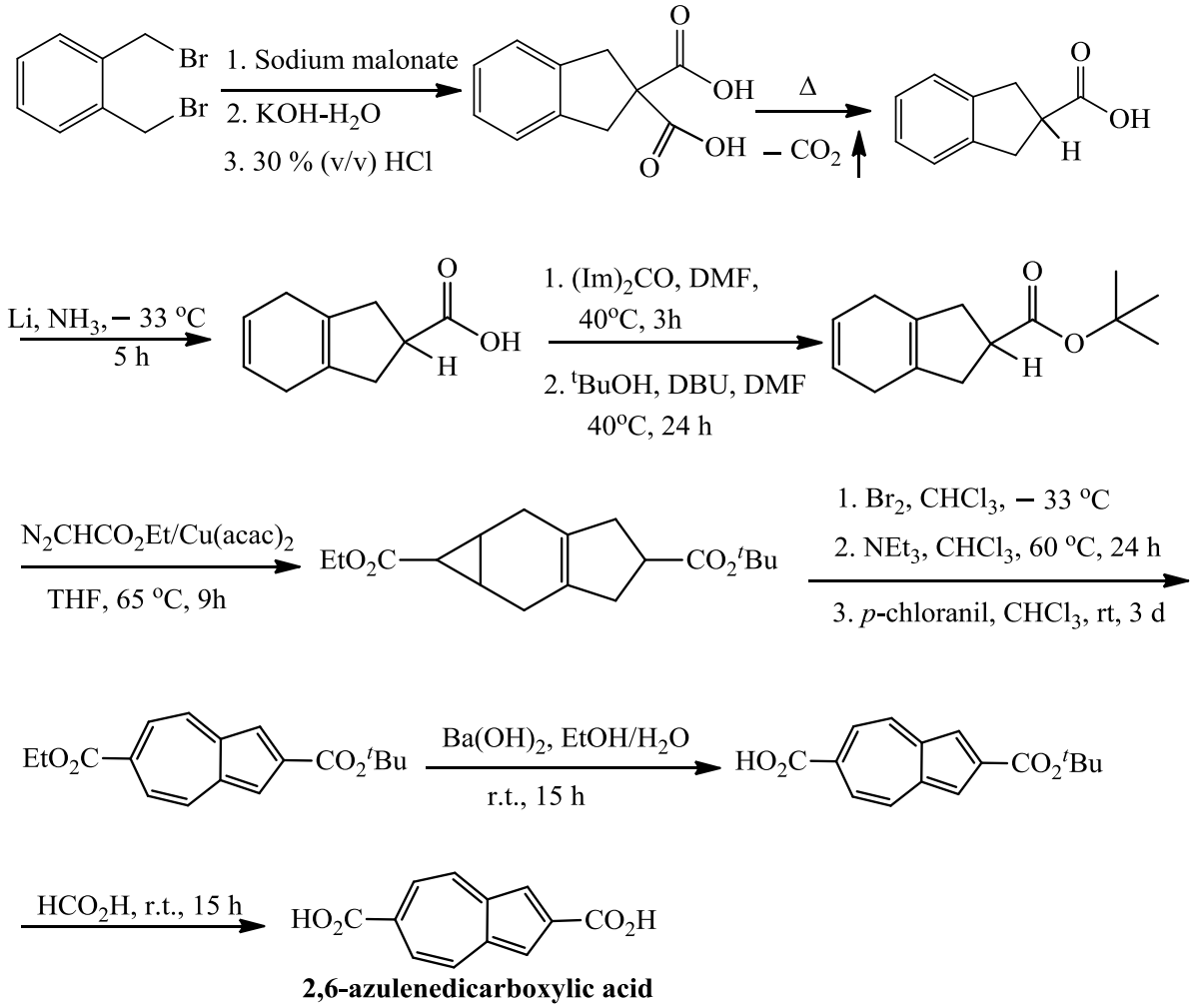

Scheme 1. Synthesis of 2,6-azulenedicarboxylic acid.

6.3.2. Synthesis

Synthesis of [Zn_2(2,6-azd)$_2$(dabco)]·(DMF)$_5$·(H_2O)$_2$ (MOF-649). 2,6-azulenedicarboxylic acid (0.027 g, 1.26×10^{-4} mol) and $Zn(NO_3)_2 \cdot 6H_2O$ (0.075 g, 2.52×10^{-4} mol) were dissolved in 1.8 mL of *N*,*N*-dimethylformamide (DMF). Dabco (0.0142 g, 1.26×10^{-4} mol) was then added to the solution, which immediately generated a large amount of dark blue precipitate. The mixture was filtered using a 60 mL PYREX glass funnel of fine porosity. The filtrate was collected, and the solution was sealed in a 20 mL glass vial. The vial was heated to 85 °C (1.0 °C min^{-1}) for 60 h in a controllable oven and then cooled down at room temperature. The dark blue-green needle shaped crystals were collected by filtration and washed with DMF (3 × 2 mL). Elemental microanalysis for MOF-649, $[Zn_2(2,6\text{-azd})_2(dabco)]\cdot(DMF)_5\cdot(H_2O)_2 \equiv C_{45}H_{63}O_{15}N_7Zn_2$, calculated (%): C 50.38, H 5.92, N 9.14; found C 50.19, H 6.12, N 8.99. FT-IR (KBr, 4000–400 cm^{-1}): 3468 (m, br), 2930 (m, br), 1658 (vs), 1590 (m), 1501 (w), 1350 (vs), 1297 (w), 1251 (w), 1205 (m), 1087 (s), 1048 (m), 1015 (w), 923 (w), 877 (w), 811 (m), 786 (s), 654 (m), 609 (w), 576 (m). To obtain the guest free material the DMF washed crystals were washed with (3 × 2 mL) of $CHCl_3$ followed by soaking the crystals in 10 mL of $CHCl_3$ for 3 days with fresh $CHCl_3$ added every 24 h. The final $CHCl_3$ exchanged material was then thoroughly washed with anhydrous acetone prior to trying to activate the material under supercritical CO_2 drier.

Synthesis of [Zn_4O(2,6-azd)$_3$]·(DMF)$_6$·(H_2O)$_4$ (MOF-650). 2,6-H_2azd (0.068 g, 3.12×10^{-4} mol) and $Zn(NO_3)_2 \cdot 6H_2O$ (0.139 g, 4.67×10^{-4} mol) were dissolved in 8.5 mL mixture of DMF/1-methyl-2-pyrrolidone (NMP) (1.5:1, v/v). The clear dark blue solution was transferred into a 20 mL glass vial and 0.57 mL of EtOH was added. After the vial was tightly capped it was heated to 90 °C at a rate of 1.5 °C/min for 60 h in an isothermal oven. Cubic shaped dark blue crystals were removed from the mother liquor contained in the vial and washed with DMF/NMP (1:1) (3 × 5 mL). Elemental microanalysis for the air dried MOF-650, $[Zn_4O(2,6\text{-azd})_3]\cdot(DMF)_6\cdot(H_2O)_4 \equiv C_{54}H_{68}O_{23}N_6Zn_4$, calculated (%): C 45.33, H 4.79, N 5.87; found C 44.57, H 4.01, N 5.73. To obtain the guest-free materials the final washed crystals were soaked in 10 mL of $CHCl_3$ for 3 days with fresh $CHCl_3$ added every 24 h. The $CHCl_3$ exchanged material was activated at 50 °C for 12 h under dynamic pump. FT-IR (KBr, 4000–400 cm^{-1}): 3420 (s, br), 2929 (m, br), 1660 (vs), 1612 (s), 1575 (w), 1489 (w), 1410 (vs), 1360 (w), 1256 (w), 1199 (w), 1100 (w), 925 (w), 790 (s), 660 (w), 584(w).

6.3.3. Single-Crystal X-Ray Diffraction

Single-crystal X-ray diffraction (SXRD) data for MOF-649 and MOF-650 were collected at 293(2) K on a Xcalibur diffractometer (Agilent Technologies, Ruby CCD detector) using a single wavelength Enhance X-ray source with MoKα radiation, λ = 0.71073 Å.[13] The selected single crystals were mounted using polybutene oil on the top of a glass fiber fixed on a goniometer head and immediately transferred to the diffractometer. Pre-experiment, data collection, analytical absorption correction,[14] and data reduction were performed with the Oxford program suite CrysAlisPro.[13] The crystal structures were solved with SHELXS97[15] using direct methods and was refined by full-matrix least-squares methods on F2 with SHELXL97.[15] All programs used during the crystal structure determination process are included in the WINGX software.[16] The program PLATON[17] was used to check the results of the X-ray analyses. The electron densities corresponding to the disordered guest molecules of MOF-649 and MOF-650 were flattened using 'SQUEEZE'[18] option of PLATON. The chemical formula of MOF-649 and MOF-650 were determined using a combination of thermogravimetric analysis (TGA), elemental analysis, and single-crystal X-ray diffraction (SXRD) studies. The crystallographic details of both the MOFs are summarized in Table 1.

Table 1. Crystallographic Data and Structural Refinement Summary for MOF-649 and MOF-650[a]

	MOF-649	MOF-650
empirical formula	$C_{15}H_{12}O_4NZn$	$C_{36}H_{12}O_{13}Zn_4$
formula weight ($g \cdot mol^{-1}$)	671.28	920.04
wavelength (Å)	0.71073	0.71073
crystal system,	orthorhombic,	cubic,
space group	*Cmmm*	*Fm-3m*
a (Å)	16.052 (5)	30.5557 (17)
b (Å)	21.172 (5)	30.5557 (17)
c (Å)	9.625 (5)	30.5557 (17)
$\alpha = \beta = \gamma$ (°)	90	90
volume ($Å^3$)	3271.08(213)	28528.4(3)
Z	4	8

[a]Data based on the *PLATON/SQUEEZE*[18] model.

6.3.4. Gas Sorption Measurements

Low-pressure N_2, and H_2 adsorption measurements for MOF-649 and MOF-650 were performed on an Autosorb-1 (Quantachrome) volumetric analyzer[19] and Micromeritics ASAP 2020 respectively. The samples were outgassed to 10^{-6} Torr. Helium was used for the estimation of the dead volume, assuming that it is not adsorbed at any of the studied temperatures. Liquid N_2, and liquid Ar baths were used for adsorption measurements at 77 and 87 K, respectively. Ultra-high-purity grade N_2, H_2, and He (99.999% purity) were used throughout the adsorption experiments.

6.3.5. Computational Details

All density-functional theory (DFT) calculations were performed with the Quickstep module[20] of the cp2k program package[21]. The exchange-correlation energy was treated with the revised PBE functional[22] and van der Waals-contributions were accounted for using the Grimme D3 formalism[23]. Double-zeta valence polarized basis sets of the MOLOPT type[24] and Goedecker-Teter-Hutter pseudopotentials[25] were used for all elements. The electronic density was expanded in plane waves up to a cut-off energy of 500 Ry.

MOFs were modeled as infinite cubic crystals based on a supercell containing eight Zn_4O clusters. The cell size of MOF-650 was fixed at the minimum-energy value of a_0 = 31.0 Å (1.45% larger than the experimental structure) and that of IRMOF-8 at a_0 = 30.5 Å. Hydrogen molecules were adsorbed at the various binding sites (See Figure 8) and the structure was fully relaxed.

6.4. Results and Discussion

6.4.1. Synthesis and Characterization of MOF-649 and 650

[Zn_2(2,6-azd)$_2$(dabco)] (MOF-649). Heating a mixture of $Zn(NO_3)_2 \cdot 6H_2O$, 2,6-H_2azd and dabco in DMF at 85 °C gives dark blue-green needle shaped crystals. Single X-ray crystal diffraction (SXRD) analysis (Table 1) reveals that the basic structure of MOF-649 is composed of two-dimensional rhombic grids based on $Zn_2(RCO_2)_4$ paddle-wheel SBUs (Figure. 1a), which are bridged by the linear ditopic azulene linker at the equatorial positions and pillared by dabco at the axial positions to lead to an overall 3D structure with primitive cubic (**pcu**) net topology

(Figure 1b). The Zn–O distances in the paddle wheel are 2.035(2) Å and the Zn–Zn distance is 2.947(5) Å. Although the overall topology of the framework could be described in a primitive cubic net, the Zn_2 paddle wheel and 2,6-azd linkers form a rhombic grid (Figure 1b). A similar structural feature was also observed in the case of benzene included $[Zn_2(1,4\text{-bdc})_2(dabco)]$.[10d] Both dabco pillars and the azulene rings of MOF-649 are disordered. The wide open channels of approximately 15.7 × 9.0 Å running along the *c* axis are interlinked by relative smaller windows (5.2 × 4.3 Å). A large total solvent accessible void was calculated to be 68%.[17]

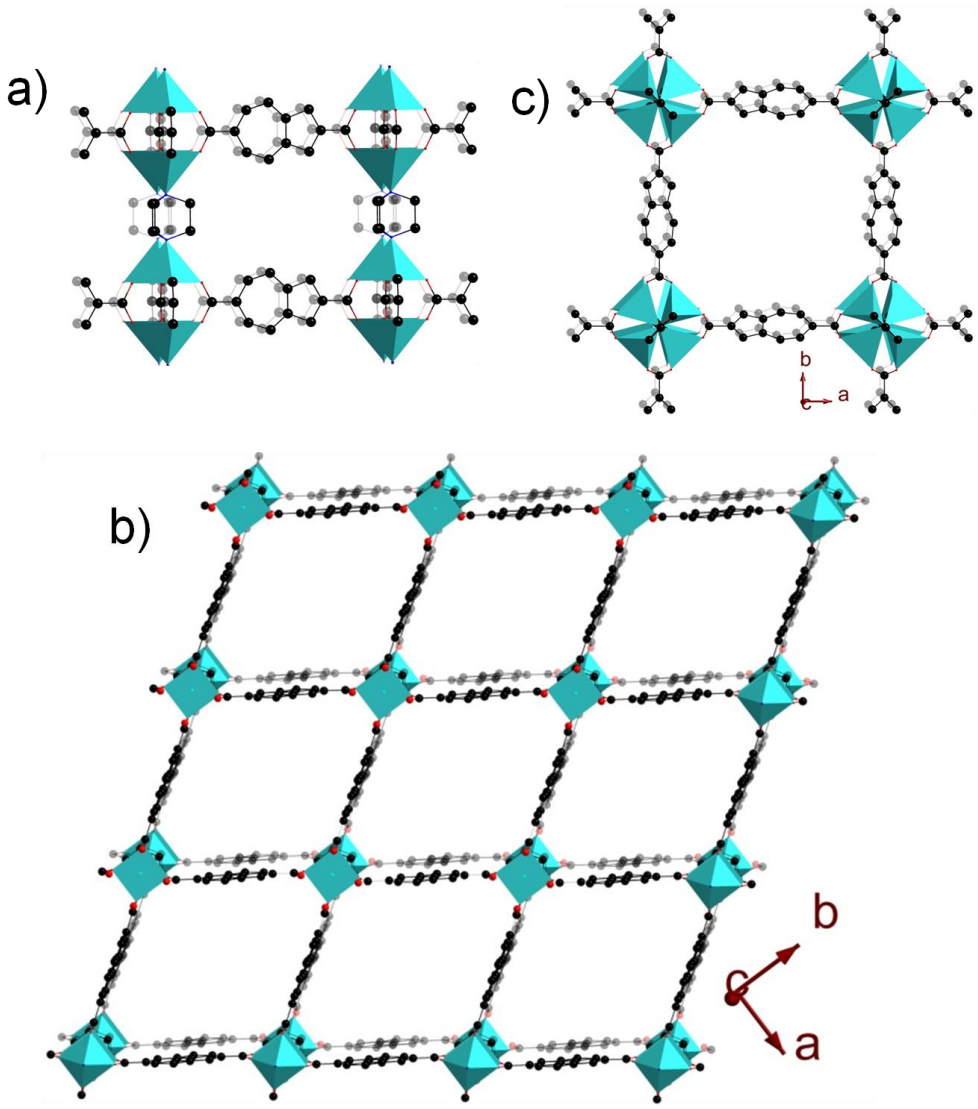

Figure 1. Partial view of the single crystal X-ray structure of MOF-649 exhibiting its 3D framework constructed *via* pillaring the 2D rhombic grids through dabco (a); the primitive cubic net (**pcu**) in MOF-649 showing its wide open channels of approximately 15.7 × 9.0 Å running

along the crystallographic *c* axis (b) and the partial view of the single crystal X-ray structure of MOF-650 exhibiting its **pcu** net topology constructed via connection through octahedral shaped $Zn_4O(COO)_6$ SBUs (c). In case of a, b and c, the orientational disordered of the azulene units were neglected for clarity. Atom colors: Zn, aqua (polyhedra); O, red; C, black and N, blue (for a and b). Hydrogen atoms of the azulene linkers and the dabco pillar units (for a and b) are also omitted for clarity.

[$Zn_4O(2,6\text{-azd})_3$] (MOF-650). The structure of MOF-650 can be described as an augmented 3D **pcu** framework composed of octahedral shaped $Zn_4O(CO_2)_6$ cluster units (Figure 1c) and is isostructural to IRMOF-8.[9] The SXRD analysis of a suitable single crystals revealed the center-to-center distance between two octahedral SBUs to be 15.278 Å, which is slightly greater than isoreticular IRMOF-8 (15.046 Å).[9] Simulations of these crystals are in good agreement, giving average values of 15.50 and 15.25 Å for these distances, respectively. The 2,6-azd linkers are disordered. The structure has a larger cavity and pore aperture of 18.2 and 9.8 Å in diameters, respectively.

Structural features of MOF-650 and IRMOF-8 from simulations. The 2,6-azd linker (Figure 2a, top) is asymmetric and can thus be incorporated into the cage of MOF-650 in two different orientations. While in the experiment this presumably occurs randomly, we chose to model two extreme cases, where all linkers are either antiparallel ('*nonpolar*') or parallel ('*polar*'). We

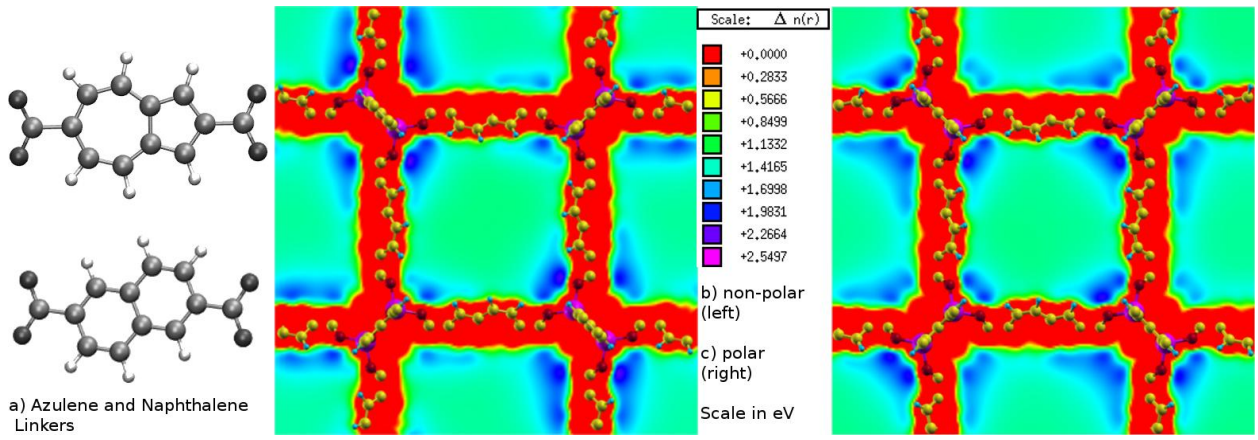

Figure 2. Structures of the linkers (a) and electrostatic potential along cube face of MOF-650 in the *nonpolar* (b) and *polar* configurations (c).

Table 2. Vectorial components of the dipolemoment (Debyes) in the *nonpolar*, *polar* MOF-650 and IRMOF-8.

	μ_X	μ_Y	μ_Z	$\|\mu\|$
650 *nonpolar*	-0.022	0.055	-0.055	0.081
650 *polar*	21.02	20.94	20.82	36.25
IRMOF-8	0.394	0.048	0.129	0.417

expect that the former configuration results in an overall cancellation of the total dipole moment, while in the latter all dipole moments should add up to give a strongly polarized system. Indeed, our calculations confirm this assumption (see Table 2 for the dipole moments of MOF-650 in the two configurations and IRMOF-8), indicating that the '*polar*' MOF-650 has a 450 and 90 times greater dipole moment than the '*nonpolar*' MOF-650 and the isoreticular IRMOF-8, respectively. In addition, the effect of the alignment of the linkers is also reflected in the electrostatic potential of the system. Figure 2b and c show the electrostatic potential of a cut through the face of the cubic cage of MOF-650 in the '*polar*' and '*nonpolar*' configurations. In particular, one notes the varying shape of the blue region depending on whether a corner is bordered by the 5 membered or 7-membered ring side of azulene. Compare for instance the top-right corner of the cage in Figure 2c to the bottom left corner. The former is adjacent to three 5-membered ring ends, and has three 7-membered ring ends on the far side of the Zn_4O cluster. The situation is reversed for the opposite corner. Furthermore, it should be noted that the tilted orientation of the linkers results in two different cages, one bordered by the faces of the linkers and another by their edges. As the primary cell in our set-up is of the former type we refer to this as '*inside*' and to the latter as '*outside*'. This distinction was also found to change the electrostatic potential in the middle of the cell by about 0.5 eV.

6.4.2. Low Pressure Gas Adsorption Study

In order to obtain activated materials, as-prepared MOF-649 and MOF-650 were immersed in chloroform (amylene stabilized) for 3 d. During the exchange the chloroform was refreshed three times. TGA studies on the as-synthesized, $CHCl_3$ exchanged and the activated samples are depicted in Figure 3.

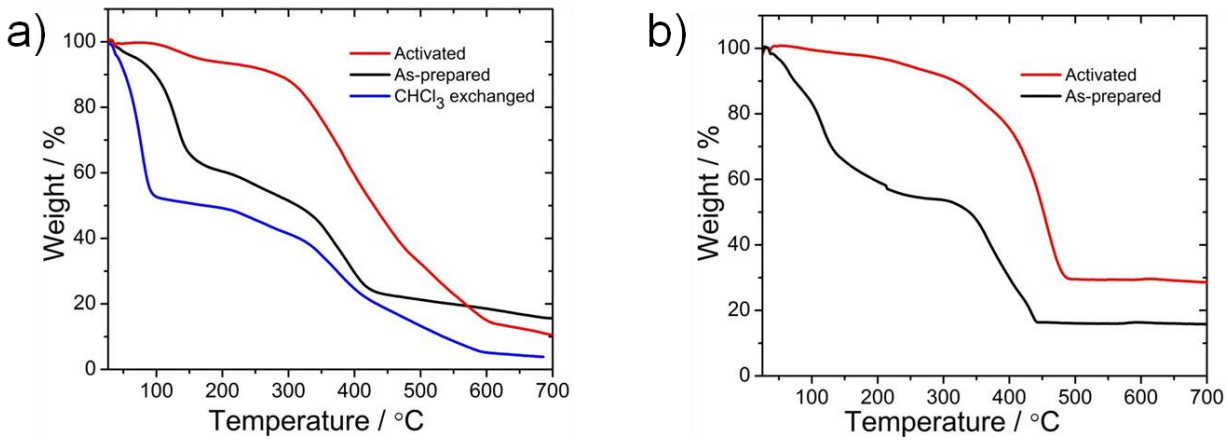

Figure 3. a), TGA traces of MOF-649: as-prepared (black), $CHCl_3$ exchanged (blue) and the activated material obtained after degassing the $CHCl_3$ exchanged MOF-649 at room temperature for 20 h (red). b), TGA traces of MOF-650: as-prepared (black) and the activated material obtained after degassing the $CHCl_3$ exchanged MOF-650 at 50 °C for 12 h (red).

Our attempts to measure the N_2 isotherm of the activated MOF-649 obtained after degassing the $CHCl_3$ exchanged sample at room temperature showed no significant uptake (Figure 4). This might be due to the partial collapse of the framework integrity under guest free condition as evidenced by the PXRD. However, performing the supercritical drying (SCD) using an acetone washed sample followed by degassing at 80 °C allowed to improve the accessible surface area up to 990 $m^2\ g^{-1}$, but unfortunately this is still far below the values reported with other isoreticular pillared MOFs.[10d,e,h] The PXRD analysis of the crystalline material obtained either from SCD or from degassing MOF-649 following SCD indicated some structural change upon guest exclusion (Figure 5a). In this context, it is worth noting that an irreversible structural change during activation was also reported with the isostructural framework material of $Zn_2(2,6\text{-ndc})_2(dabco)$ [DUT-8(Zn)].[10h] The N_2 adsorption measurement of the activated MOF-649 obtained after SCD followed by degassing at 80 °C showed typical Type I sorption behavior (Figure 6a), exhibiting its micro-porous nature. The Langmuir/BET surface areas and the pore volume of the activated MOF-649 were estimated to be 990/910 $m^2\ g^{-1}$ and 0.35 $cm^3\ g^{-1}$, respectively, which is comparable or slightly higher than the value reported for the isostructural material of DUT-8(Zn).[10h]

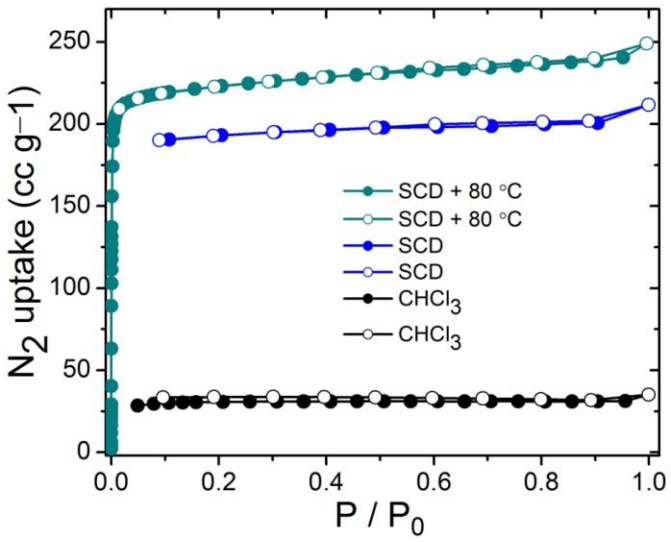

Figure 4. N_2 isotherm at 77 K: activated MOF-649 obtained after degassing chloroform exchanged materials at room temperature (black), activated MOF-649 obtained after SCD (blue) and activated MOF-649 obtained after SCD followed by degassing at 80 °C (cyan). Filled and open circles represent adsorption and desorption branches, respectively. Connecting traces are guides for the eyes.

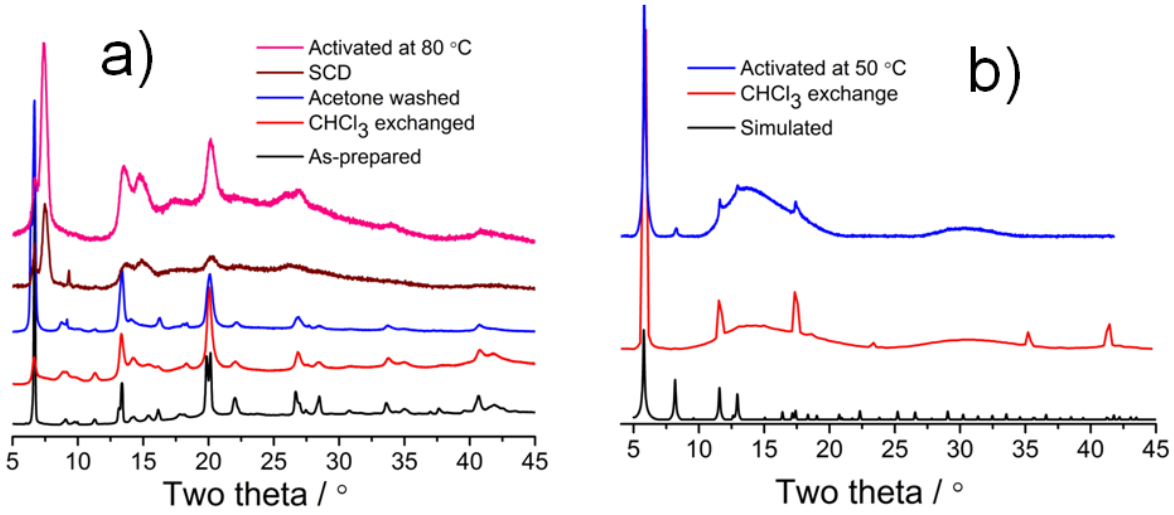

Figure 5. Powder X-ray diffraction patterns for MOF-649 (a): as-prepared (black), $CHCl_3$ exchanged (red), $CHCl_3$ exchanged material washed with anhydrous acetone for 2 h (blue), material prepared after SCD following acetone exchange for 2 h (wine), the material prepared after degassing the SCD material at 80 °C for 3 h (pink). PXRD patterns for MOF-650 (b):

Simulated (black), after $CHCl_3$ exchange of as-prepared materials (red) and the activated material obtained after degassing the $CHCl_3$ exchanged material at 50 °C for 12 h.

In contrast to MOF-649, the PXRD analysis of the activated MOF-650 (Figure 5b) shows no significant change in the pattern indicating the robust nature of the guest free material. The permanent porosity of the activated MOF-650 was further corroborated from a N_2 adsorption measurement depicted in Figure 6a. The typical Type-I isotherm also provided evidence the micro-porous nature of MOF-650. From the adsorption branch of N_2 isotherm we estimated the Langmuir/BET surface area of 3230/2630 $m^2\ g^{-1}$ for the activated MOF-650.

The low-pressure H_2 uptake measurement shows that the activated MOF-649 and MOF-650 can take up 7 and 14.5 mg g^{-1} of H_2 at 77 K and 1 bar (Figure 6b), respectively. The H_2 uptake by MOF-649 is relatively low in comparison to our previously reported value for MOF-646 having comparable or marginally higher BET surface area; but having a smaller pore size distribution.[7] Incidentally, the H_2 uptake is found to be higher (i.e. 4.12 and 6.97 mg g^{-1} for DUT-8(Zn) and MOF-649, respectively) when compared to the isostructural $Zn_2(2,6\text{-ndc})_2(dabco)$ despite their comparable pore volumes.[10h] On the other hand the H_2 uptake by activated MOF-650 is similar to the values reported for IRMOF-8,[26] although it has a relatively high apparent surface area except for the data reported by Feldblyum et al.[26]

To investigate the influence of polarization triggered by the coulombic field of azulene on stabilizing H_2 in the activated MOFs, the coverage dependencies of adsorption enthalpies (Q_{st}) of

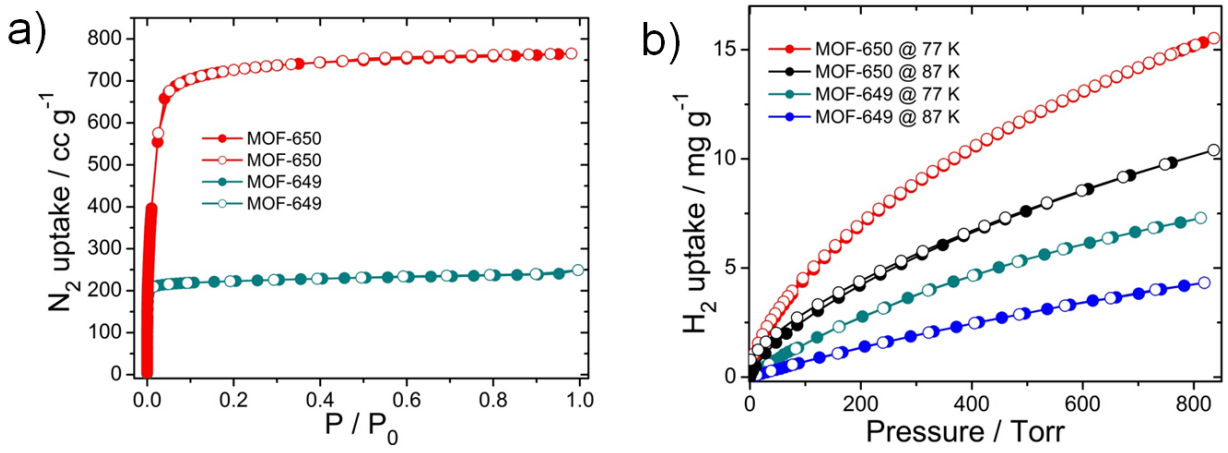

Figure 6. N_2 (a) and H_2 (b) isotherms of the activated MOFs. Filled and open circles represent adsorption and desorption branches, respectively. Connecting traces are guides for the eye.

H_2 were calculated from fits of their corresponding 77 and 87K isotherms. As presented in Figure 7, the Q_{st} at zero coverage for MOF-649 was estimated to be 5.3 kJ mol^{-1}, which is in line with the value reported for the isoreticular pillared MOFs and no significant effect of azulene to stabilize hydrogen was obseved.[27] In contrast, a low coverage Q_{st} of 6.8 kJ mol^{-1} was obtained for MOF-650, which is clearly higher when compared to the value estimated for representative MOF-5 and other non-interpenetrated MOFs having a **pcu** net topology and Zn_4O SBUs.[4c,26,28] From the Q_{st} plot it is also apparent that the interaction energy drops considerably with the amount adsorbed to 4.2 kJ mol^{-1} at the limit of the interpolation. Such a phenomenon indicates the presence of strong binding sites in the material, which become occupied at ~4.3 mg g^{-1} (corresponds to 2 H_2 molecules per $[Zn_4O(2,6\text{-azd})_3]$ formula unit) of H_2 loading. Considering the $Zn_4O(CO)_6$ (SBUs) moiety exhibits as the strongest binding location as demonstrated

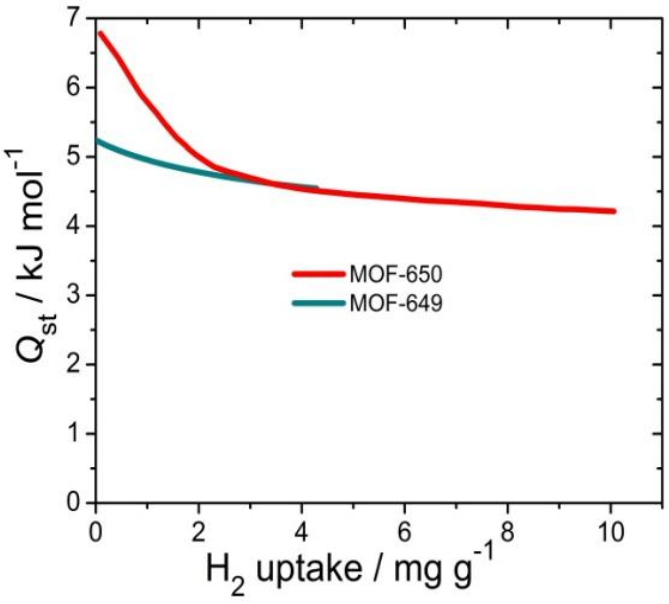

Fig 7. The coverage dependencies of adsorption enthalpies of H_2 in activated MOFs.

by neutron diffraction studies,[29] we surmise that the observed high Q_{st} at low coverage is presumably due to the improved polarizability of the SBUs, triggered by the associated azulene functionality, if not determined by the direct confinement of hydrogen on the linkers. To further rationalise our hypothesis we performed a computational analysis using an optimized unit cell (based on SXRD data) of MOF-650 to investigate its site specific interaction with H_2. The results are described in the following section.

Calculation of Site-specific Hydrogen adsorption in MOF-650 and IRMOF-8. We selected five possible adsorption sites for hydrogen in the MOFs. Three of them are located near the SBUs and two on the linker, as depicted in Figure 8. We placed hydrogen molecules at each site, in both parallel and perpendicular arrangements relative to the plane of the linker. For adsorption in the corners "perpendicular" refers to the hydrogen molecule being in line with the diagonal of the cube and "parallel" is rotated by 90 degrees from this. The structures were then fully optimized and the corresponding adsorption energies at various sites were calculated. Table 3 and 4 summarizes the calculated adsorption energies for the *polar*, *nonpolar* MOF-650 and IRMOF-8 respectively. It should be noted that a major contribution to the adsorption energy is due to van der Waals interactions, which we treat in an approximate way with the Grimme D3 formalism.[23] This substantially improves adsorption energies compared to a DFT-only treatment[30], but can exhibit some overbinding. Furthermore, as the calculations are carried out at zero Kelvin, adsorption energies may be higher than what is accessible in finite- temperature experiments. From this data depicted in Table 3 it is apparent that the most stable adsorption occurs at sites 1 and 2 in the vicinity of the SBUs. While a significantly less favourable adsorption (about 6-7 kJ mol^{-1} lower in energy) was observed at the sites 3 and 4 close to the linker. Furthermore, the

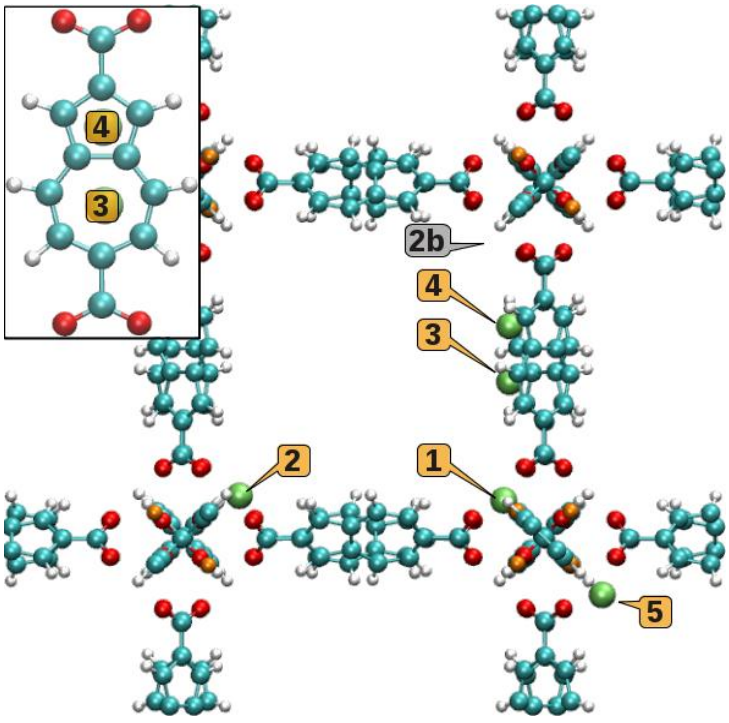

Figure 8. The coverage dependencies of adsorption enthalpies of H_2 in activated MOFs.

Table 3. Binding energy of a single H_2 molecule at various sites in IRMOF-8. Energies given in kJ mol^{-1}

Site	*nonpolar*	*polar*
	perpendicular / parallel	perpendicular / parallel
1	-13.76[a] / -13.44	-13.23[a] / -13.7 1
2	-13.17[a] / -13.72	-10.23[b] / -13.44[b]
3	-5.20 / -4.61	—[c] / —[c]
4	-6.01 / -5.29	—[c] / —[c]
5	-7.08 / -8.22	-7.27 / -7.06

[a]The hydrogen molecule does not remain in the *perpendicular* configuration, but moves to a *parallel* one

[b]This refers to a different adsorption position, 2b

[c]Not determined, as the energy is equivalent to the *nonpolar* case

Table 4. Binding energy of a single H_2 molecule at various sites in IRMOF-8. Energies given in kJ mol^{-1}

Site	perpendicular	parallel
1	-12.43[a]	-12.14
2	—[b]	—[b]
3	-4.75	-4.81[a]
4	—[b]	—[b]
5	-7.88	-7.34

[a]The hydrogen molecule does not remain in the indicated configuration, but moves to the other one

[b]Not determined, as it is equal to another site

preferred orientation of the H_2 molecule in MOF-650 seems to be the parallel one, in which orientation it spontaneously moves into during the optimization process. In the case when this rearrangement did not happen the adsorption is 3 kJ mol^{-1} weaker in site 2 of the '*polar*' MOF. While site 5 is also located rather near to the Zn_4O center, it lies in the '*outside*' region, i.e. surrounded by only the edges of the linkers and not their faces. Consequently a lower adsorption energy was obtained due to the reduced contact between hydrogen and the linkers. When H_2 is perpendicular to the linker the adsorption energy is lowered further, presumably also because of

the reduced contact between linker and MOF. Note also that the 7-membered ring site is less favorable than the 5-membered ring site.[8]

The absorption energies of H_2 in the naphthalene-based IRMOF-8 were also calculated (Table 4). Interestingly, the adsorption at site 1 was found to be less stable by about 1.3 kJ mol^{-1} when compared to the equivalent position in MOF-650. Adsorption at the linker is also slightly worse, although the difference is smaller. Moreover, in this case the H_2 molecule seems to prefer a perpendicular arrangement.

The calculations do not predict a significant improvement of H_2 uptake in the strongly polarized MOF-650. The effect of the modified electrostatic potential in the lattice may not be sufficient to create an electrostatic trap for the H_2 molecule, which itself lacks the polarity to interact strongly with an electric field. On the other hand, the influence of the linker and its polarity cannot be fully disregarded, as the two isomers naphthalene and azulene do indeed influence the interaction strength as evidenced by the comparison of MOF-650 and IRMOF-8.

6.4.3. Conclusions

Two novel framework materials, namely MOF-649 and MOF-650, comprised of internally polarized linear 2,6-azulenedicarboxylic acid were prepared and structurally characterized. Permanent porosity and hydrogen sorption properties of the guest free materials were evaluated. Interestingly, MOF-650 showed relatively high gravimetric hydrogen storage capacity of 14.5 mg g^{-1} and exhibited a high enthalpy of H_2 adsorption (6.8 kJ mol^{-1}) at low coverage. A detailed theoretical analysis of the H_2 adsorbed MOFs showed that the H_2 binding energies are significantly larger in the vicinity to the SBU's than on the top of the azulene units. Apparently due to the orientation of the azulene units from the unpolar dipole moment compensated framework arrangement to the polar dipole moment enhanced framework arrangement does has too low influence on the overall electrostatics or on the cooperativity of the H_2 binding energies at the SBUs or on the top of the azulene units.

6.5. References

1. (*a*) M. Eddaoudi, D. B. Moler, H. Li, B. Chen, T. M. Reineke, M. O'Keeffe and O. M. Yaghi, *Acc. Chem. Res.*, 2001, **34**, 319; (*b*) O. M. Yaghi, M. O'Keeffe, N. W. Ockwig, H. K. Chae, M. Eddaoudi and J. Kim, *Nature*, 2003, **423**, 705; (*c*) S. Kitagawa, R. Kitaura

and S. Noro, *Angew. Chem., Int. Ed.*, 2004, **43**, 2334; (*d*) G. Ferey, *Chem. Soc. Rev.*, 2008, **37**, 191; (*e*) R. E. Morris and P. S. Wheatley, *Angew. Chem., Int. Ed.*, 2008, **47**, 4966; (*f*) B. Chen, M. Eddaoudi, T. M. Reineke, J. W. Kampf, M. O'Keeffe and O. M. Yaghi, *J. Am. Chem. Soc.*, 2000, **122**, 11559; (*g*) S. Ma, D. Sun, J. M. Simmons, C. D. Collier, D. Yuan and H.-C. Zhou, *J. Am. Chem. Soc.*, 2008, **130**, 1012; (*h*) Y. Yan, X. Lin, S. Yang, A. J. Blake, A. Dailly, N. R. Champness, P. Hubberstey and M. Schröder, *Chem. Commun.*, 2009, 1025; (*i*) H. Furukawa, N. Ko, Y. B. Go, N. Aratani, S. B. Choi, E. Choi, A. O. Yazaydin, R. Q. Snurr, M. O'Keeffe, J. Kim and O. M. Yaghi, *Science*, 2010, **329**, 424; (*j*) O. K. Farha, O. Yazaydın, I. Eryazici, C. Malliakas, B. Hauser, M. G. Kanatzidis, S. T. Nguyen, R. Q. Snurr and J. T. Hupp, *Nature Chem.*, 2010, **2**, 2010, 944; (*k*) S. Horike, M. Dincă, K. Tamaki and J. R. Long, *J. Am. Chem. Soc.*, 2008, **130**, 5854; (*l*) J. Lee, O. K. Farha, J. Roberts, K. A. Scheidt, S. T. Nguyen and J. T. Hupp, *Chem. Soc. Rev.*, 2009, **38**, 1450; (*m*) J. R. Li, R. J. Kuppler and H.-C. Zhou, *Chem. Soc. Rev.*, 2009, **38**, 1477.

2. (*a*) S. S. Kaye, A. Dailly, O. M. Yaghi and J. R. Long, *J. Am. Chem. Soc.*, 2007, **129**, 14176; (*b*) H. J. Park, M. P. Suh, *Chem. Eur. J.*, 2008, **14**, 8812; (*c*) Sumida, K.; Hill, M. R.; Horike, S.; Dailly, A.; Long, J. R. *J. Am. Chem. Soc.* **2009**, *131*, 15120; (*d*) Han, D.; Jiang, F.-L.; Wu, M.-Y.; Chen, L.; Chen, Q.-X.; Hong, M.-C. *Chem. Commun.* **2011**, *47*, 9861. (*e*) Yan, Y.; Yang, S.; Blake, A. J.; Lewis, W.; Poirier, E.; Barnett, S. A.; Champness, N. R.; Schröder, M. *Chem. Commun.* **2011**, *47*, 9995; (*f*) Park, H. J.; Lim, D.-W.; Yang, W. S.; Oh, T.-R.; Suh, M. P. *Chem. Eur. J.* **2011**, *17*, 7251.

3. (*a*) L. J. Murray; M. Dincă, J. R. Long, *Chem. Soc. Rev.*, 2009, **38**, 1294; (*b*) S. Ma, H.-C. Zhou, *Chem. Commun.*, 2010, **46**, 44; (*c*) M. P. Suh, H. J. Park, T. K. Prasad, D.-W. Lim, *Chem. Rev.*, 2012, **112**, 782.

4. (4) (*a*) M. Dincă and J. R. Long, *J. Am. Chem. Soc.*, 2005, **127**, 9376; (*b*) B. Chen, N. W. Ockwig, A. R. Millward, D. S. Contreras and O. M. Yaghi, *Angew. Chem., Int. Ed.*, 2005, **44**, 4745; (*c*) J. L. C. Rowsell and O. M. Yaghi, *J. Am. Chem. Soc.*, 2006, **128**, 1304; (*d*) M. Dincă, A. Dailly, Y. Liu, C. M. Brown, D. A. Neumann and J. R. Long, *J. Am. Chem. Soc.*, 2006, **128**, 16876; (*e*) M. Latroche, S. Surblé, C. Serre, C. Mellot-Draznieks, P. L. Llewellyn, J.-H. Lee, J.-S. Chang, S. H. Jhung and G. Férey, *Angew. Chem., Int. Ed.*, 2006, **45**, 8227; (*f*) M. Dincă, W. S. Han, Y. Liu, A. Dailly, C. M. Brown and J. R. Long,

Angew. Chem., Int. Ed., 2007, **46**, 1419; (*g*) X.-S. Wang, S. Ma, P. M. Forster, D. Yuan, J. Eckert, J. J. López, B. J. Murphy, J. B. Parise and H.-C Zhou, *Angew. Chem. Int. Ed.*, 2008, **47**, 7263; (*h*) Y.-G. Lee, H. R. Moon and P. Suh, *Angew. Chem., Int. Ed.*, 2008, **47**, 7741; (*i*) W. Zhou, H. Wu and T. Yildirim, *J. Am. Chem. Soc.*, 2008, **130**, 15268; (*j*) S. Ma, J. M. Simmons, D. Sun, D. Yuan and H.-C. Zhou, *Inorg. Chem.*, 2009, **48**, 5263; (*k*) X. Lin, I. Telepeni, A. J. Blake, A. Dailly, C. M. Brown, J. M. Simmons, M. Zoppi, G. S. Walker, K. M. Thomas, T. J. Mays, P. Hubberstey, N. R. Champness and M. Schröder, *J. Am. Chem. Soc.*, 2009, **131**, 2159.

5. (*a*) S. S. Han and W. A. Goddard, *J. Am. Chem. Soc.*, 2007, **129**, 8422; (*b*) K. L. Mulfort and J. T. Hupp, *J. Am. Chem. Soc.*, 2007, **129**, 9604; (*c*) D. Himsl, D. Wallacher and M. Hartmann, *Angew. Chem., Int. Ed.*, 2009, **48**, 4639; (*d*) S. Yang, X. Lin; A. J. Blake; K. M. Thomas, P. Hubberstey, N. R. Champness, and M. Schröder, *Chem. Commun.*, 2008, 6108.

6. (*a*) Y. Liu, J. F. Eubank, A. J. Cairns, J. Eckert, V. C. Kravtsov, R. Luebke and M. Eddaoudi, *Angew. Chem., Int. Ed.*, 2007, **46**, 3278; (*b*) D. F. Sava, V. C. Kravtsov, F. Nouar, L. Wojtas, J. F. Eubank and M. Eddaoudi, *J. Am. Chem. Soc.*, 2008, **130**, 3768.

7. S. Barman, H. Furukawa, O. Blacque, K. Venkatesan, O. M. Yaghi and H. Berke, *Chem. Commun.*, 2010, **46**, 7981.

8. (*a*) O. Hübner, A. Glöss, M. Fichtner and W. Klopper, *J. Phys. Chem. A*, 2004, **108**, 3019; (*b*) M. Wong, B. E. V. Kuiken, C. Buda and B. D. Dunietz, *J. Phys. Chem. C*, 2009, **113**, 12571.

9. M. Eddaoudi, J. Kim, N. Rosi, D. Vodak, J. Wachter, M. O'Keeffe and O. M. Yaghi, *Science*, 2002, **295**, 469.

10. (*a*) K. Seki and W. Mori, *J. Phys. Chem. B*, 2002, **106**, 1380; (*b*) K. Seki, S. Takamizawa and W. Mori, *Chem. Lett.*, 2001, 332; (*c*) K. Seki, *Chem. Commun.*, 2001, 1496; (*d*) D. N. Dybtsev, H. Chun and K. Kim, *Angew. Chem. Int. Ed.*, 2004, **43**, 5033; (*e*) H. Chun, D. N. Dybtsev, H. Kim and K. Kim, *Chem.–Eur. J.*, 2005, **11**, 3521; (*f*) T. Takei, T. Ii, J. Kawashima, T. Ohmura, M. Ichikawa, M. Hosoe, Y. Shinya, I. Kanoya and W. Mori, *Chem. Lett.*, 2007, **36**, 1136; (*g*) H. C. Hoffmann, B. Assfour, F. Epperlein, N. Klein, S. Paasch, I. Senkovska, S. Kaskel, G. Seifert and E. Brunner, *J. Am. Chem. Soc.*, 2011, **133**, 8681; (*h*) N. Klein, H. C. Hoffmann, A. Cadiau, J. Getzschmann, M. R. Lohe, S.

Paasch, T. Heydenreich, K. Adil, I. Senkovska, E. Brunner and S. Kaskel, *J. Mater. Chem.*, 2012, **22**, 10303.

11. G. L. B. Carlson, F. H. Quina, B. M. Zarnegar and D. G. Whitten, *J. Am. Chem. Soc.*, 1975, **97**, 347.
12. M. V. Barybin, M. H. Chisholm, N. S. Dalal, T. H. Holovics, N. J. Patmore, R. E. Robinson and D. J. Zipse, *J. Am. Chem. Soc.*, 2005, **127**, 15182.
13. Agilent Technologies (formerly Oxford Diffraction), Yarnton, England, 2011.
14. R. C. Clark and J. S. Reid, *Acta Cryst.*, 1995, **A51**, 887.
15. G. M. Sheldrick, *Acta Cryst.*, 2008, **A64**, 112.
16. L. J. Farrugia, *J. Appl. Cryst.*, 1999, **32**, 837.
17. A. L. Spek, *J. Appl. Cryst.*, 2003, **36**, 7.
18. A. L. Spek, PLATON99 A Multipurpose Crystallographic Tool, Utrecht University: Utrecht, 1999.
19. H. Furukawa, M. A. Miller and O. M. Yaghi, *J. Mater. Chem.*, 2007, **17**, 3197.
20. J. Vandevondele, M. Krack, F. Mohamed, M. Parrinello, T. Chassaing and J. Hutter, *Comput. Phys. Commun.*, 2005, **167**, 103.
21. CP2K version 2.3 (Development Version), CP2K developers group (2012), CP2K is freely available from http://www.cp2k.org/.
22. Y. K. Zhang and W. T. Yang, *Phys. Rev. Lett.*, 1998, **80**, 890.
23. S. Grimme, J. Antony, S. Ehrlich and H. J. Krieg, *Chem. Phys.*, 2010, **132**, 154104.
24. J. Vandevondele and J. Hutter, *J. Chem. Phys.*, 2007, **127**, 114105.
25. S. Goedecker, M. Teter and J. Hutter, *Phys. Rev. B*, 1996, **54**, 1703.
26. J. I. Feldblyum, A. G. Wong-Foy and A. J. Matzger, *Chem. Commun.* 2012, **48**, 9828.
27. (*a*) J. Y. Lee, D. H. Olson, L. Pan, T. J. Emge and J. Li, *Adv. Funct. Mater.*, 2007, **17**, 1255; (*b*) Z. Wang, K. K. Tanabe and S. M. Cohen, *Chem.–Eur. J.*, 2010, **16**, 212.
28. A. Dailly, J. J. Vajo, C. C. Ahn, *J. Phys. Chem. B*, 2006, **110**, 1099.
29. E. C. Spencer, J. A. K. Howard, G. J. McIntyre, J. L. C. Rowsell and O. M. Yaghi, *Chem. Commun.*, 2006, 278.
30. K. Sillar, A. Hofmann and J. Sauer, *J. Am. Chem. Soc.*, 2009, **131**, 4143.

7. POSTSYNTHESIS AMINO BORANE FUNCTIONALIZATION OF IRMOF-3 AND DMOF-1-NH_2

7.1. Materials and General Procedures

All solvents and reagents were purchased commercially and, unless otherwise noted, were used without further purification. Microanalyses were carried out at the Anorganisch-Chemisches Institut of the University of Zurich. Elemental analyses (for boron) were performed by Mikroanalytisches Labor Pascher, Remagen, Germany. Fourier transform infrared (FT-IR) spectra were recorded on a Perkin-Elmer BXII spectrometer with KBr pellets. The solid state UV/vis spectra were recorded on a Perkin-Elmer Lambda 650S spectrometer. The powder XRD patterns were obtained with a Bruker D8 Advance system equipped with Cu sealed tube (λ = 1.5406 Å). All solid state $^{11}B\{^1H\}$, ^{15}N, ^{13}C and $^{2}H\{^1H\}$ NMR were recorded on Bruker AV-500 spectrometers. Solid samples were spun at 5 kHz, using 4 mm ZrO_2 rotors filled up in a glovebox under dried nitrogen atmosphere. The ^{15}N and ^{11}B chemical shifts were referenced to CH_3NO_2 (δ = 0 ppm) and liquid BF_3OEt_2 (δ = 0 ppm) respectively. All the ^{2}H and ^{13}C chemical shifts were referenced to TMS-d_{12} (δ = 0 ppm).

7.2. Synthesis of Amino Borane Functionalized MOFs

The activated material of DMOF-1-NH_2 and IRMOF-3 was prepared according to the literature procedure.[1,2] Whereas the ^{15}N-labeled activated DMOF-1-NH_2 (DMOF-1-$^{15}NH_2$) and IRMOF-3 (IRMOF-3 with ^{15}N-labeled amine functionality) was synthesized by an analogous preparation,[1,2] replacing the natural abundance 2-aminoterephthalic acid (^{14}N natural abundance of 99.6%)[3] with the analogous 2-aminoterephthalic acid-^{15}N.[4] The source for B_2H_6 and B_2D_6 was prepared by the metathesis reaction of $LiBH_4$ and $LiBD_4$, respectively, with $ZnCl_2$ in a Spex 8000 M mixer mill for 90 min according to the following reactions.[5]

$$5LiBH_4 + 2ZnCl_2 \rightarrow LiZn_2(BH_4)_5 + 4LiCl$$

$$5LiBD_4 + 2ZnCl_2 \rightarrow LiZn_2(BD_4)_5 + 4LiCl$$

In a typical reaction procedure the activated MOFs and the diborane source were placed in two different heatable vessels connected by gas-permeable stainless steel tubing (Figure 1). The

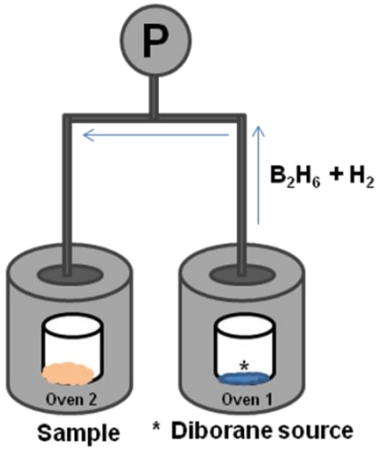

Figure 1. Schematic representation of the basic experimental set-up for borane reaction with activated DMOF-1-NH_2 and IRMOF-3. The scheme shows the diborane source that is connected with the activated sample in a closed system. The pressure is monitored by pressure gauge P.

overall system during the experiment is closed and the pressure could be monitored throughout the experiment. The experiment is carried out by initially heating the diborane source to 140 °C to facilitate the diborane release while the activated MOFs were allowed to react under ambient condition. Typically, 150-200 mg of the diborane source was filled in the temperature controlled container, which is connected with the vessel containing the activated MOFs, to generate an approximately 1.8-2 bar of hydrogen/diborane pressure in the system.

***Synthesis of DMOF-1-NH_2BH_3*:** Activated DMOF-1-NH_2 (0.180 mg, 2.99×10^{-4} mmol) was allowed to react with H_2/B_2H_6 (1.8-2 bar) at room temperature for 20 minutes following the procedure mentioned above to yield 188.27 mg of DMOF-1-NH_2BH_3 (Yield: 100% with respect to DMOF-1-NH_2). Microanalysis for DMOF-1-NH_2BH_3, $C_{22}H_{28}B_2N_4O_8Zn_2$, Calcd: C, 42.08; H, 4.49, N, 8.91%. Found: C, 41.00; H, 4.34, N, 9.11%. ICP-AES for DMOF-1-NH_2BH_3, Calcd: B, 3.44, Zn, 20.79%. Found: B, 3.55, Zn, 20.02%.

***Synthesis of DMOF-1-NH_2BD_3*:** Activated DMOF-1-NH_2 (0.165 mg, 2.66×10^{-4} mmol) was allowed to react with H_2/B_2D_6 (1.95 bar) at room temperature for 20 minutes to yield 168.72 mg of DMOF-1-NH_2BD_3 (Yield: 100% with respect to DMOF-1-NH_2).

***Synthesis of DMOF-1-$^{15}NH_2BD_3$*:** Activated DMOF-1-$^{15}NH_2$ (0.177 mg, 2.93×10^{-4} mmol) was allowed to react with H_2/B_2D_6 (2 bar) at room temperature for 20 minutes to yield 186.0 mg of DMOF-1-$^{15}NH_2BD_3$ (Yield: 100% with respect to DMOF-1-$^{15}NH_2$).

***Synthesis of IRMOF-3-BH_3*:** Activated IRMOF-3 (0.186 mg, 2.20×10^{-4} mmol) was allowed to react with H_2/B_2H_6 (1.6 bar) at room temperature for 25 minutes following the procedure mentioned above to yield 195.4 mg of IRMOF-3-BH_3 (Yield: 100% with respect to IRMOF-3). Microanalysis for IRMOF-3-BH_3, $C_{24}H_{24}B_3N_3O_{13}Zn_4$, Calcd: C, 33.66; H, 2.82, N, 4.91%. Found: C, 33.39; H, 2.64, N, 5.05%.

***Synthesis of IRMOF-3-BD_3*:** Activated IRMOF-3 (0.180 mg, 2.20×10^{-4} mmol) was allowed to react with H_2/B_2D_6 (2 bar) at room temperature for 20 minutes following the procedure mentioned above to yield 185.7 mg of IRMOF-3-BD_3 (Yield: 97.2% with respect to IRMOF-3).

***Synthesis of IRMOF-3-BH_3 (with ^{15}N-labeled amine functionality)*:** Activated IRMOF-3, with ^{15}N-labeled amine functionality, (0.175 mg, 2.12×10^{-4} mmol) was allowed to react with H_2/B_2H_6 (2 bar) at room temperature for 20 minutes to yield 179.0 mg of IRMOF-3-BH_3 (Yield: 97.3% with respect to IRMOF-3).

7.3. Single Crystal X-Ray Diffraction Studies on Guest Free DMOF-1-NH_2

Single-crystal X-ray diffraction data were collected at 183(2) K on a Xcalibur diffractometer (Agilent Technologies, Ruby CCD detector) using a single wavelength Enhance X-ray source with MoK_α radiation, λ = 0.71073 Å.[6] The selected suitable single crystal was mounted using polybutene oil on the top of a glass fiber fixed on a goniometer head and immediately transferred to the diffractometer. Pre-experiment, data collection, analytical absorption corrections,[7] and data reduction were performed with the Oxford program suite *CrysAlisPro*.[6] The crystal structure was solved with SHELXS97[8] using direct methods and was refined by full-matrix least-squares methods on F^2 with SHELXL97.[8] All programs used during the crystal structure determination process are included in the WINGX software.[9] The program PLATON[10] was used to check the result of the X-ray analysis.

Due to the highly symmetrical space group and framework, most of the non-H atoms are disordered over two (O1, C3), three (C4) or four sites (N2). Nevertheless, only 22 restraints were used for the entire model to correct the anisotropic thermal parameters of the disordered N1, N2, C2, C3 and C4 atoms (before DELU and SIMU instructions of SHELXL97[S8]). All H positions were calculated after each cycle of refinement using a riding model, with C-H = 0.93 Å and U_{iso}(H) = 1.2U_{eq}(C) for aromatic H atoms, with C—H = 0.97 Å and U_{iso}(H) = 1.2U_{eq}(C) for methylene H atoms, and with N—H = 0.86 Å and U_{iso}(H) = 1.2U_{eq}(C) for amino H atoms. No classic hydrogen bonds were found in the crystal structure. Attempts to solve the structure in *P*4/m or even *P*4, all three space groups having no reflection conditions, did not result in the disappearance of the heavy disorders. On the contrary, the disorders were much more tedious to deal with for worse results. For *P*4/mmm: R_1 = 0.0275 [I > 2σ(I)], wR_2 = 0.0729 (all data, 1073 reflections); for *P*4/m: R_1 = 0.0307 [I > 2σ(I)], wR_2 = 0.0813 (all data, 1853 reflections); for *P*4: R_1 > 0.05 [I > 2σ(I)], wR_2 > 0.12 (all data, 3518 reflections).

Table 1. Summary of the X-ray diffraction studies of guest free DMOF-1-NH_2.

	DMOF-1-NH_2
empirical formula	$C_{22}H_{22}N_4O_8Zn_2$
formula weight ($g \cdot mol^{-1}$)	601.18
temperature (K)	183(2)
wavelength (Å)	0.71073
crystal system, space group	tetragonal, *P*4/*mmm*
a (Å)	10.9487(2)
b (Å)	10.9487(2)
c (Å)	9.5950(2)
α (°)	90
β (°)	90
γ (°)	90
volume ($Å^3$)	1150.19(4)
Z, density (calcd) ($Mg \cdot m^{-3}$)	1, 0.868
abs coefficient (mm^{-1})	1.072
F(000)	306
crystal size (mm^3)	0.38 x 0.24 x 0.20
θ range (°)	2.63 to 30.50
reflections collected	14032
reflections unique	1073 [*R*(int) = 0.0246]
completeness to θ (%)	99.5
absorption correction	analytical
max/min transmission	0.675 / 0.575
data / restraints / parameters	1038 / 22 / 51
goodness-of-fit on F^2	1.131
final R_1 and wR_2 indices [$I > 2\sigma(I)$]	0.0275, 0.0722
R_1 and wR_2 indices (all data)	0.0287, 0.0729
largest diff. peak and hole ($e.Å^{-3}$)	0.471, -0.290

The unweighted R-factor is $R_1 = \sum(Fo - Fc)/\sum Fo$; $I > 2\sigma(I)$ *and the weighted R-factor is* $wR_2 = \{\sum w(Fo^2 - Fc^2)^2/\sum w(Fo^2)^2\}^{1/2}$.

7.4. Result and Discussion

To accomplish the desired amino borane derivatives, we strived to carry out gas-solid phase reactions between the activated IRMOF-3 and DMOF-1-NH_2 and diborane (B_2H_6). However, our initial attempts to derivatize the free amine functionality with -BH_3 unit using excess of diborane and at elevated temperatures (form 45-150 °C) resulted in the loss of structural coherence, as evidenced by powder X-ray diffraction (PXRD) analysis. Therefore, to investigate the structural response of both of the activated MOFs to B_2H_6 exposure in detail, we carried out room temperature *in situ* powder X-ray diffraction experiments. The results obtained are depicted in Figure 2 and 3. In case of DMOF-1-NH_2 increasing diborane exposure time induced a shift of the indicated PXRD reflections to higher angles along with a gradual decrease in intensity (Figure 2). This indicates shrinking of the lattice parameters before collapse of the framework occurs at about 30-35 min of diborane exposure. On the other hand for IRMOF-3, the position of the peaks was unaltered before the collapse of the framework(s) integrity occurred, indicative of a stiffer framework (Figure 3).

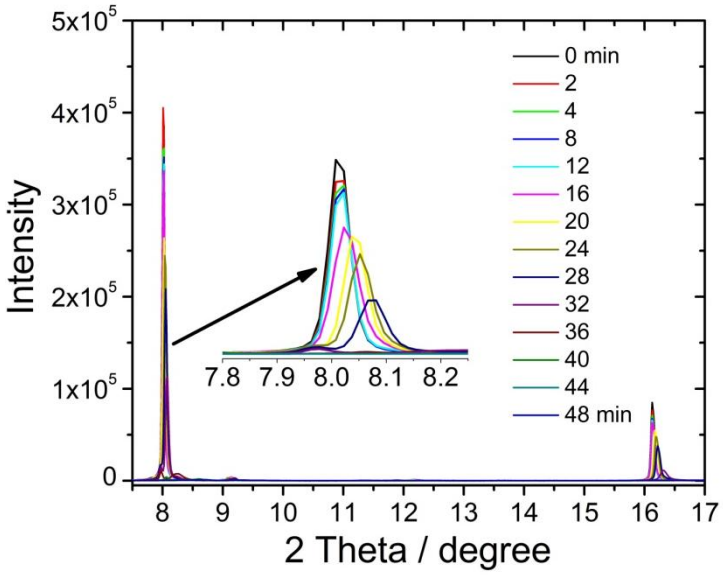

Figure 2. Time dependent *in situ* PXRD investigation of the stability of DMOF-1-NH_2 under gaseous H_2/B_2H_6 (2 bar) at room temperature. The inset magnified portion of the figure emphasizes the change in the peak position with diborane exposure time.

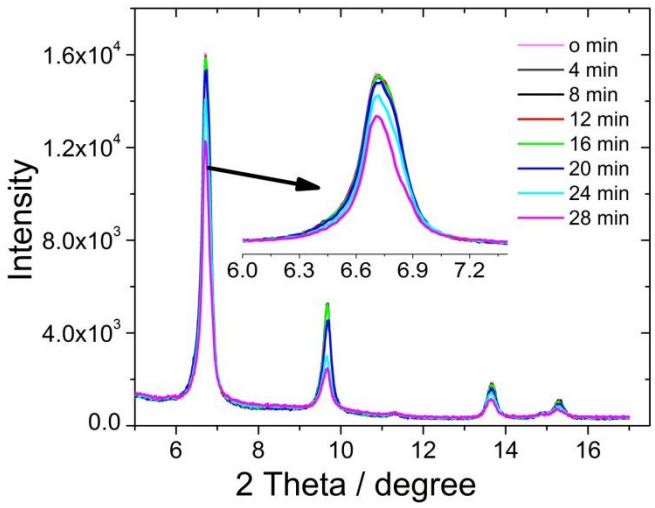

Figure 3. Time dependent *in situ* PXRD investigation of the reactivity of IRMOF-3 with gaseous H_2/B_2H_6 (2 bar) at room temperature.

A first indication of the successful modification is a distinct colour change. When the activated MOFs were exposed to diborane atmosphere (2 bar) for 15-20 min at room temperature, an intense colour change of the materials became recognizable (shifted UV-vis absorptions, see spectra in Figure 4). Thus, yellowish crystals of activated DMOF-1-NH_2 changed to bright

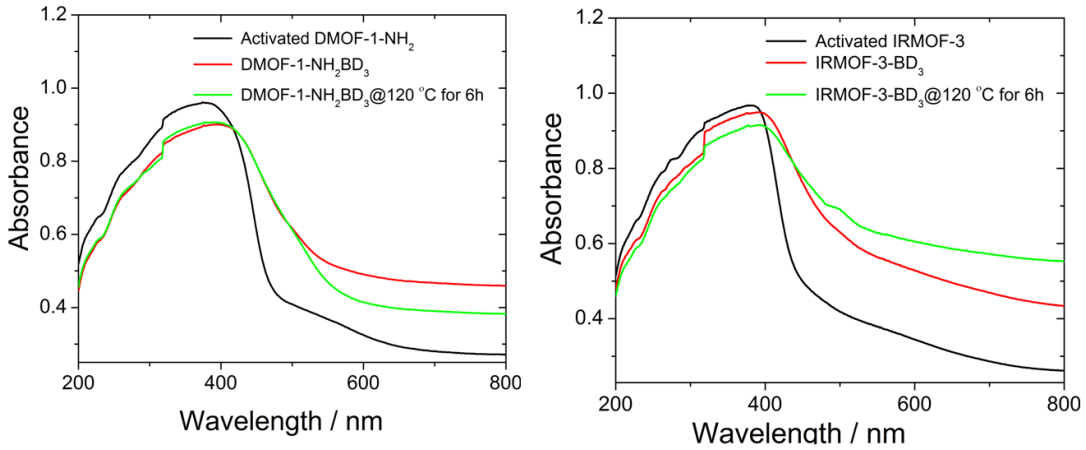

Figure 4. Solid-state UV/vis spectra of DMOF-1-NH_2 and its amino borane substituted products (left) and IRMOF-3 its amino borane substituted products (right) respectively measured in the 200 - 800 nm range.

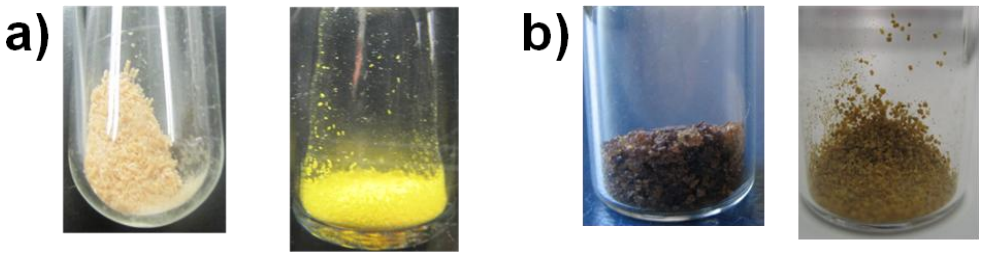

Figure 5. (a), Photo of activated DMOF-1-NH_2 (left); freshly prepared DMOF-1-NH_2BH_3 (middle) obtained after 20 min of diborane (2 bar) exposure and the material obtained after storing freshly prepared DMOF-1-NH_2BH_3 at room temperature for 1 week (right). (b), Photo of activated IRMOF-3 (left) and freshly prepared IRMOF-3-BH_3 (right).

yellow after modification which is designated as DMOF-1-NH_2BH_3 (Figure 5a) and brown crystals of activated IRMOF-3 to yellowish-brown for the BH_3 modified IRMOF-3 (designated IRMOF-3-BH_3) (Figure 5b).

When the modified materials were analysed with solid state $^{11}B\{^1H\}$ NMR (Figure 6) under static condition, a broad resonance centered at around 10 ppm was observed, which indicates the incorporation of boron moiety. Although, the chemical environment abound the boron centres could not be interpreted due to the extremely broad nature of the peak. The FTIR spectroscopic analysis of freshly prepared amino borane substituted DMOF-1-NH_2BH_3 clearly indicated covalent binding of the incorporated –BH_3 group by the appearance of several new and strong bands (Figure 7). The characteristic band at 2377 cm^{-1} with two shoulders at 2325 cm^{-1} and 2273 cm^{-1} could be identified as the B-H antisymmetric and symmetric stretching frequencies, respectively.

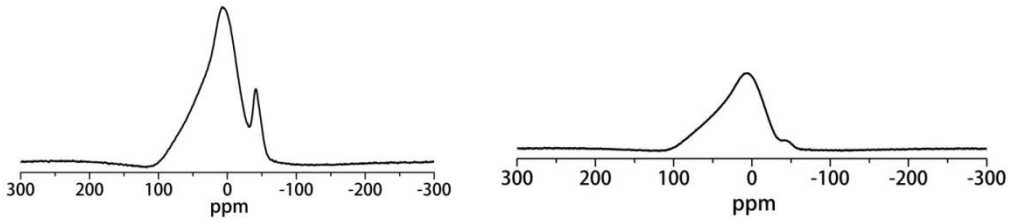

Figure 6. Room temperature solid state static $^{11}B\{^1H\}$ NMR spectra of freshly prepared DMOF-1-NH_2BH_3 (left) and IRMOF-3-BH_3 (right).

It was further observed that, when the freshly prepared amino borane functionalized MOFs were stored at room temperature, a second color change of the materials were observed (Figure S2, SI)

and a simultaneous loss of frameworks integrity was ascertained from the PXRD analysis. Furthermore, based on PXRD analysis we recently inferred that the modified materials tent to degrade at room temperature and are found to be only stable at low temperatures (below 0 to -10 °C). Therefore, further investigations would be needed to understand the chemical nature and the properties of the amino borane substituted MOFs before realizing their utilities towards hydrogen storage.

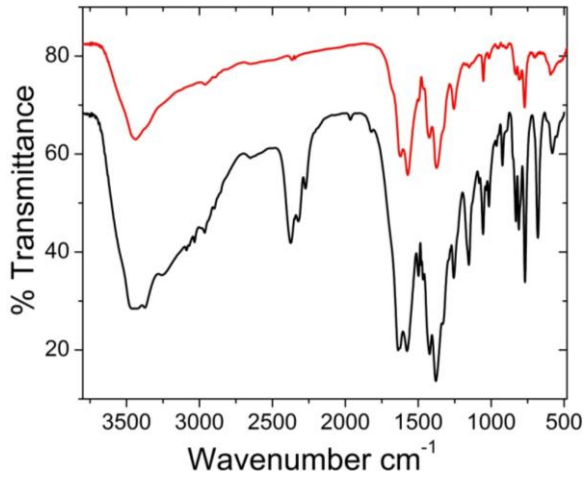

Figure 7. a), The FTIR spectra of activated DMOF-1-NH_2 (red) and as-prepared DMOF-1-NH_2BH_3 (black).

7.5. References

1. Z. Wang, K. K. Tanabe and Seth M. Cohen, *Inorg. Chem.*, 2009, **48**, 296.
2. J. L. C. Rowsell and O. M. Yaghi, *J. Am. Chem. Soc.*, 2006, **128**, 1304.
3. R. K. Harris and E. D. Becker, Pulse and Fourier Transform NMR, Introduction to Theory and Methods, Academic Press, New York, 1971.
4. W. Morris, R. E. Taylor, C. Dybowski, O. M. Yaghi and M. A. Garcia-Garibay, *J. Mol. Struct.*, 2011, **1004**, 94.
5. (*a*) Ravnsbæk, D; Filinchuk, Y; Cerenius, Y; Jakobsen, H. J; Besenbacher, F; Skibsted, J; Jensen, T. R. *Angew. Chem., Int. Ed.*, 2009, **48**, 6659; (*b*) Friedrichs, O.; Remhof, A.; Borgschulte, A.; Buchter, F.; Orimo, S. I.; Züttel, A. *Phys. Chem. Chem., Phys.* 2010, **12**, 10919.
6. Agilent Technologies (formerly Oxford Diffraction), Yarnton, England, 2011.

7. Clark, R.C.; Reid, J. S. *Acta Cryst.*, **1995**, *A51*, 887.
8. Sheldrick, G. M. *Acta Crystallographica Section A* **2008**, *64*, 112.
9. Farrugia, L. J. *J. Appl. Cryst.*, **1999**, *32*, 837.
10. Spek, A. L. *J. Appl. Cryst.*, **2003**, *36*, 7.

8. INCORPORATION OF ACTIVE METAL SITES IN MOFs *VIA IN SITU* GENERATED LIGAND DEFICIENT METAL-LINKER COMPLEXES

8.1. Publication 2

Incorporation of active metal sites in MOFs *via in situ* generated ligand deficient metal-linker complexes

Samir Barman,[a] Hiroyasu Furukawa,[b] Oliver Blacque,[a] Koushik Venkatesan,[a] Omar M. Yaghi,[b] Guo-Xin Jin,[c] and Heinz Berke*[a]*

[a] Department of Inorganic Chemistry, University of Zürich Winterthurerstrasse 190, CH-8057, Zürich (Switzerland).

[b] Center for Reticular Chemistry, Department of Chemistry and Biochemistry, University of California-Los Angeles, 607 Charles E. Young Drive East, Los Angeles, California 90095.

[c] Shanghai Key Laboratory of Molecular Catalysis and Innovative Material, Department of Chemistry, Fudan University, 200433, Shanghai, P. R. China

Chem. Commun., 2011, **47**, 11882-11884.

View Online / Journal Homepage / Table of Contents for this issue
Dynamic Article Links

ChemComm

Cite this: *Chem. Commun.*, 2011, **47**, 11882–11884

www.rsc.org/chemcomm

COMMUNICATION

Incorporation of active metal sites in MOFs *via in situ* generated ligand deficient metal–linker complexes†

Samir Barman,[a] Hiroyasu Furukawa,*[b] Olivier Blacque,[a] Koushik Venkatesan,[a] Omar M. Yaghi,[b] Guo-Xin Jin[c] and Heinz Berke*[a]

Received 20th July 2011, Accepted 27th September 2011
DOI: 10.1039/c1cc14387e

Two novel 3D MOFs, namely MOF-647A and MOF-648 (previously unknown trinodal 4-connected net), comprised of Cu ions and pyrazole-3,5-dicarboxylate were synthesized and characterized. A strategy for incorporating open metal sites in MOFs was investigated by utilizing an *in situ* generated metal–linker complex as a precursor to construct MOF-648.

Metal–organic frameworks (MOFs) were discovered to be among the most intriguing candidates for diversification of their inherent properties. Due to their fascinating topologies and pore size tunability,[1] the resultant nature of the MOFs such as high surface area and large pore volume is expected to be utilized in gas storage, separation and catalysis.[2] Since the properties of the pores could be varied by functionalization of the organic struts, it is believed that the incorporation of active sites in the framework could additionally open up promising avenues to enhance the storage and catalytic performance.[2] To this end, several procedures have been proposed: (i) creation of open metal sites by removing coordinated solvents[3] and (ii) postsynthetic metalation of MOFs having metal binding sites.[4] Although these are powerful techniques, there is still a limitation to such kinds of available species as well as difficulty in the preparation of organic linkers with metal binding sites. If one can prepare small metal–linker complexes as precursors and can connect them to build an extended structure (Scheme 1), the proposed frameworks would be replete with potential accessible metal sites (after removal of leaving groups). Keeping this in mind, we chose 1*H*-pyrazole-3,5-dicarboxylic acid as an organic linker with the ability to generate two types of binding moieties (*i.e.* carboxylate and pyrazole functionalities).

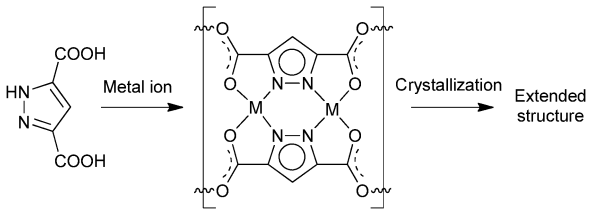

Scheme 1 The square unit (middle) can be utilized to form a MOF structure.

Indeed, there are many examples of pyrazole-bridged cyclic dinuclear complexes where two identical metals (like Cu^{2+}, Ni^{2+}, Pd^{2+}, Pt^{2+}, and V^{4+} ions) are bridged by this bifunctional unit.[5] These dinuclear complexes could act as squared bridging units enabling further extension of structural motifs. In general, utilization of square bridging ligands is expected to lead to the formation of a framework with numerous topologies such as **sql**, **cag**, **nbo**, and **cds** nets,[6] although the connectivity with the MOFs should be influenced by the coordinating capabilities of the central metal ions and the metal oxide cluster units.[7]

It is interesting to note that despite the multifunctional coordination ability of pyrazole-3,5-dicarboxylate, reports about transition metal based, non-hydrogen bonded, 3D structures are rare; furthermore, in some cases the framework was achieved by the use of pillar ligands.[5c–e,8] In this study we used Cu^{2+} as the metal source for the following reasons: (i) it can easily form dinuclear metallacycles and (ii) it has versatile coordination ability which might facilitate the formation of 3D structures. Here we describe the synthesis and structural characterization of MOF-647A ($[Cu_3(\mathbf{L})_2{\cdot}(DMF)_2(H_2O)_3]$), MOF-647B ($[Cu_3(\mathbf{L})_2{\cdot}(THF)_2\ (H_2O)_2]$) and MOF-648 ($[Cu_{12}(\mathbf{L})_8{\cdot}(DMF)_9]{\cdot}(DMF)_2(H_2O)_2$) (where **L** = pyrazole-3,5-dicarboxylate)‡ §[9] and the attempted activation of MOF-648, which has been constructed from the pyrazole-bridged cyclic dinuclear unit.

The preparation of the MOFs was conducted using $Cu(NO_3)_2{\cdot}2.5H_2O$ and 1*H*-pyrazole-3,5-dicarboxylic acid in *N*,*N*-dimethylformamide (DMF). The solvent mixture of the two reagents was heated to 100 °C for 20 h, whereupon a mixture of MOF-647A and MOF-648 was obtained (ESI†, Section S2).[10] Single-crystal X-ray diffraction (SXRD) analysis revealed that MOF-647A is comprised of the basic trinuclear repeat unit $[Cu_3(\mathbf{L})_2{\cdot}(DMF)_2(H_2O)_3]$[9] (Fig. 1a) to form a doubly interpenetrated **dia** framework (Fig. 1b; Fig. S2 (ESI†)). All the

[a] *Department of Inorganic Chemistry, University of Zürich, Winterthurerstrasse 190, CH-8057, Zürich, Switzerland. E-mail: berke@aci.uzh.ch; Fax: +41 44-635-6802*
[b] *Center for Reticular Chemistry, Department of Chemistry and Biochemistry, University of California-Los Angeles, 607 Charles E. Young Drive East, Los Angeles, California 90095, USA. E-mail: furukawa@chem.ucla.edu*
[c] *Shanghai Key Laboratory of Molecular Catalysis and Innovative Material, Department of Chemistry, Fudan University, 200433, Shanghai, P. R. China*

† Electronic supplementary information (ESI) available: Full synthetic procedures and characterization data including TGA, IR, PXRD, N_2, H_2 and CO_2 isotherms and single crystal X-ray diffraction data. CCDC 829034–829036. For ESI and crystallographic data in CIF or other electronic format, see DOI: 10.1039/c1cc14387e

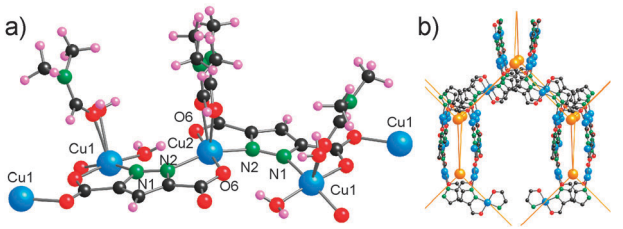

Fig. 1 (a) Part of the single crystal X-ray structure of MOF-647A, exhibiting the trinuclear repeating unit with selected atoms numbered. To simplify the 3D network (**dia** net) in MOF-647A, orange balls can be displaced (b) (Fig. S2, ESI†). Atom colors: Cu, aqua; O, red; C, black; N, green; H, pink.

five-coordinated distorted square pyramidal Cu^{2+} ions of a trinuclear subunit are chelated by trianionic pyrazolate ligands. The central five-coordinated copper ion, Cu(2), lies on a crystallographic two-fold axis. Axial–equatorial carboxylate bridges between Cu(1) atoms of adjacent trimer units lead to formation of the extended 3D structure (Fig. S3, ESI†). The DMF guest of the as-prepared MOF-647A was exchanged with anhydrous THF to give $[Cu_3(\mathbf{L})_2{\cdot}(THF)_2(H_2O)_2]$ (MOF-647B). The formula was established based on SXRD, TGA and powder X-ray diffraction (PXRD) experiments (ESI†, Sections S2, S4 and S5).§ The analysis of the SXRD structure of MOF-647B provided evidence that the overall structural integrity was retained as MOF-647A with the exception of minor changes in the crystallographic parameters (Fig. S4 and Table S1, ESI†).

In our efforts to obtain single phase crystalline material of MOF-648 we inferred that the solvent to substrate ratio, as well as the metal to ligand stoichiometry, play an important role in the control of the self-assembly. Indeed, performing the solvothermal reaction using the metal to ligand ratio of 2 : 1 under dilute conditions yielded phase pure crystals of MOF-648 (ESI†, Section S2).[10] The SXRD analysis revealed formation of the bimetallacyclic Cu_2N_4 ring (Fig. 2a) where the center-to-center distance between the two Cu^{2+} ions (*i.e.* Cu(1) and Cu(3)) is 3.99 Å. Both Cu ions are doubly chelated by two pyrazole ligands to form distorted squares (Scheme 1), and in addition one or two DMF molecules are coordinated to Cu(1) and Cu(3), respectively (Fig. S5, ESI†). In the overall 3D structural connectivity, the bimetallic square unit ($Cu_2\mathbf{L}_2$) (essentially acting as 4-connected square planar nodes) is connected to the adjacent squares *via* coordination to Cu(2) (which also acted as 4-connected square planar nodes (Fig. 2b)) and Cu(4) (acts as a tetrahedral node (Fig. 2c)) to establish the trinodal 4-connected network structure. To comprehend the network connectivity of MOF-648 requires more than routine attention and can be described as a novel trinodal 4-connected net (**sbr**) having the minimum number of kinds of edge (2) for the trinodal net (Fig. 2d; Fig. S6, ESI†).

MOF-648 possesses two nearly rhombic channels along the crystallographic *b* axis, whose diameters without contacting the interior van der Waals surface are approximately 6.4 Å (Fig. 2e). The free channels are occluded by guest coordinated and non-coordinated DMF and H_2O molecules. If the occluded and coordinated guests are removed, the accessible void space is estimated to be 66%. To access the porous structure with evenly distributed open metal sites, as-prepared crystals of MOF-648 were soaked in anhydrous acetone for 3 days, during which the

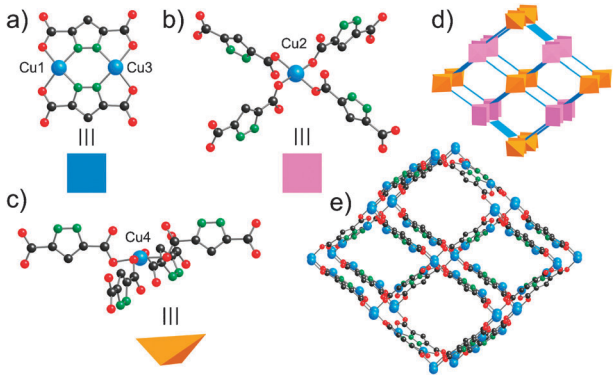

Fig. 2 The square planar nodes generated from a six membered bimetallacycle (a) are connected *via* Cu(2), which also act as square planar nodes (b), and Cu(4) (the tetrahedral nodes (c)) to compose a non-interpenetrated trinodal 4-connected net (d) in MOF-648. (e) Part of the X-ray single crystal structure of MOF-648 viewed down the crystallographic *b* axis. Atom colors: Cu, aqua; O, red; C, black; N, green. Coordinated and free guests and hydrogen atoms are omitted for clarity.

activation solvent was decanted and freshly replenished three times. Unfortunately, the PXRD data indicate that our attempts to evacuate the pore, followed by a heat treatment (up to 80 °C) of the acetone exchanged sample, lead to structural decomposition (Fig. S10, ESI†). Indeed, N_2 and H_2 isotherms did not show meaningful uptake in the low-pressure range, probably due to the loss of microporosity. To mitigate the structural collapse, supercritical CO_2 activation (SCD) was performed using the acetone-exchanged material.[2d] The activation of the acetone exchanged MOF-648 at 45 °C for 24 h following SCD allowed us to remove the free guests.

The N_2 uptake in the low-pressure region at 77 K was still low, and the BET surface area was determined to be 26 $m^2\ g^{-1}$. Surprisingly, the uptake started to increase at around P/P_0 = 0.05 and a large hysteresis loop was observed (Fig. S17, ESI†). If we use a desorption branch for the estimation, the Langmuir surface area can be calculated to be 690 $m^2\ g^{-1}$. The reason for the hysteresis is not well understood; however, it can probably be attributable to structural transformation as confirmed by the PXRD measurements (Fig. S11, ESI†). Although we were unable to determine the cell parameters of the activated MOF-648 owing to the low resolution of the PXRD pattern, it is likely that the framework was compressed along the crystallographic *c*-axis (Fig. S12, ESI†). In such a scenario, the expected pore diameter should be smaller than 5 Å, even if all guests are removed from the pore, which can be responsible for the significant hysteresis in the N_2 isotherm. However, it is unlikely that the pore shape was fully re-expanded by the adsorption of N_2, because the N_2 uptake is only half the expected value if the pore is fully evacuated. In addition, the PXRD pattern of the resolvated sample deviates significantly from either the original or the activated MOF-648 structures (Fig. S13, ESI†), which may indicate that the framework is not flexible enough to allow a reversible structural transformation as demonstrated with MIL-53.[11]

We also recorded the H_2 and CO_2 isotherms because the kinetic diameter of these gases is smaller than that of N_2;[2h] however, the H_2 uptake (12 $cm^3\ g^{-1}$, Fig. S18, ESI†) by the

activated MOF-648 at 77 K and 800 torr was close to that of N_2 at $P/P_0 = 0.05$, which is even smaller than that of another MOF with a similar pore volume.[12] This indicates that only a limited number of H_2 molecules can diffuse into the pores. Interestingly, the activated MOF-648 can take up an appreciable amount of CO_2 at 298 K (Fig. S19, ESI†) and the value is comparable to another MOF having a similar pore volume.[12] Considering that CO_2 generally has a larger adsorption enthalpy than H_2 and N_2, the released heat can be compensated to obtain the energy to diffuse into the pores.

In conclusion, the given conceptually new approach for incorporation of active metal sites in MOFs could be investigated *via* the formation of $[Cu_{12}(\mathbf{L})_8{\cdot}(DMF)_9]{\cdot}(DMF)_2(H_2O)_2$ (MOF-648). The highly open framework of MOF-648 might become a prototype, from which numerous new MOFs having potentially accessible metal sites can be derived.

Funding from the Swiss National Science Foundation (SNSF), University of Zurich and US DOE is gratefully acknowledged. The authors would like to thank Prof. Michael O'Keeffe (Arizona State University) and Dr. Carolyn B. Knobler (University of California-Los Angeles) for valuable insights and discussions.

Notes and references

‡ MOF-647A: $Cu(NO_3)_2{\cdot}2.5H_2O$ (0.276 g, 1.15 mmol) and 1*H*-pyrazole-3,5-dicarboxylic acid (0.072 g, 0.415 mmol) were dissolved in 8 mL of DMF in a 20 mL glass vial. After capping tightly, the vials were heated to 75 °C at a rate of 2 °C min^{-1} for 48 h in an isothermal oven. The vials, containing thin plate blue crystals, were removed from the mother liquor and washed with DMF (3 × 5 mL).

MOF-648: $Cu(NO_3)_2{\cdot}2.5H_2O$ (0.11 g, 0.57 mmol) and 1*H*-pyrazole-3,5-dicarboxylic acid (0.050 g, 0.28 mmol) were dissolved in 20 mL of DMF in a 50 mL glass vial. After capping tightly, the vials were heated to 100 °C at a rate of 1 °C min^{-1} for 12 h in an isothermal oven. The vials, containing dark blue-green block crystals, were removed from the mother liquor and washed with DMF (3 × 5 mL).

§ Crystal data for MOF-647A: $C_{15.71}H_{21.51}Cu_3N_{5.9}O_{13}$, tetragonal, space group $I4_1/acd$, $a = 17.6342(6)$, $b = 17.6342(6)$, $c = 33.4999(11)$ Å, $\alpha = \beta = \gamma = 90°$, $V = 10417.3(6)$ $Å^3$, $Z = 16$, $d_{calcd} = 1.762$ Mg m^{-3}, crystal size 0.13 × 0.09 × 0.05 mm^3, $T = 153(2)$ K, $\lambda = 0.71073$ Å, $R_1 = 0.0399$ [$I > 2\sigma(I)$], $wR_2 = 0.0930$ (all data, 24 570 reflections), $R_{int} = 0.1413$, GOF = 0.738. Crystal data for MOF-647B: $C_{73}H_{85}Cu_{12}N_{27}O_{45}$, orthorhombic, space group *Pbcm*, $a = 15.3345(1)$, $b = 14.5465(1)$, $c = 26.2229(3)$ Å, $\alpha = \beta = \gamma = 90°$, $V = 5849.37(9)$ $Å^3$, $Z = 2$, $d_{calcd} = 1.603$ Mg m^{-3}, crystal size 0.34 × 0.23 × 0.17 mm^3, $T = 153(2)$ K, $\lambda = 0.71073$ Å, $R_1 = 0.0535$ [$I > 2\sigma(I)$], $wR_2 = 0.1820$ (all data, 87 527 reflections), $R_{int} = 0.0721$, GOF = 1.037. MOF-648: $C_{18}H_{22}Cu_3N_4O_{12}$, tetragonal, space group $I4_1/acd$, $a = 17.1637(5)$, $b = 17.1637(5)$, $c = 34.0665(6)$ Å, $\alpha = \beta = \gamma = 90°$, $V = 10\,035.7(5)$ $Å^3$, $Z = 16$, $d_{calcd} = 1.792$ Mg m^{-3}, crystal size 0.19 × 0.10 × 0.04 mm^3, $T = 183(2)$ K, $\lambda = 0.71073$ Å, $R_1 = 0.0731$ [$I > 2\sigma(I)$], $wR_2 = 0.2363$ (all data, 11 076 reflections), $R_{int} = 0.0433$, GOF = 0.921.

1 (*a*) M. Eddaoudi, D. B. Moler, H. Li, B. Chen, T. M. Reineke, M. O'Keeffe and O. M. Yaghi, *Acc. Chem. Res.*, 2001, **34**, 319; (*b*) O. M. Yaghi, M. O'Keeffe, N. W. Ockwig, H. K. Chae, M. Eddaoudi and J. Kim, *Nature*, 2003, **423**, 705; (*c*) S. Kitagawa, R. Kitaura and S. Noro, *Angew. Chem., Int. Ed.*, 2004, **43**, 2334; (*d*) G. Ferey, *Chem. Soc. Rev.*, 2008, **37**, 191; (*e*) R. E. Morris and P. S. Wheatley, *Angew. Chem., Int. Ed.*, 2008, **47**, 4966.

2 (*a*) B. Chen, M. Eddaoudi, T. M. Reineke, J. W. Kampf, M. O'Keeffe and O. M. Yaghi, *J. Am. Chem. Soc.*, 2000, **122**, 11559; (*b*) S. Ma, D. Sun, J. M. Simmons, C. D. Collier, D. Yuan and H.-C. Zhou, *J. Am. Chem. Soc.*, 2008, **130**, 1012; (*c*) Y. Yan, X. Lin, S. Yang, A. J. Blake, A. Dailly, N. R. Champness, P. Hubberstey and M. Schröder, *Chem. Commun.*, 2009, 1025; (*d*) H. Furukawa, N. Ko, Y. B. Go, N. Aratani, S. B. Choi, E. Choi, A. O. Yazaydin, R. Q. Snurr, M. O'Keeffe, J. Kim and O. M. Yaghi, *Science*, 2010, **329**, 424; (*e*) O. K. Farha, O. Yazaydın, I. Eryazici, C. Malliakas, B. Hauser, M. G. Kanatzidis, S. T. Nguyen, R. Q. Snurr and J. T. Hupp, *Nat. Chem.*, 2010, **2**, 944; (*f*) S. Horike, M. Dincă, K. Tamaki and J. R. Long, *J. Am. Chem. Soc.*, 2008, **130**, 5854; (*g*) J. Lee, O. K. Farha, J. Roberts, K. A. Scheidt, S. T. Nguyen and J. T. Hupp, *Chem. Soc. Rev.*, 2009, **38**, 1450; (*h*) J. R. Li, R. J. Kuppler and H.-C. Zhou, *Chem. Soc. Rev.*, 2009, **38**, 1477.

3 (*a*) B. Chen, N. W. Ockwig, A. R. Millward, D. S. Contreras and O. M. Yaghi, *Angew. Chem., Int. Ed.*, 2005, **44**, 4745; (*b*) M. Dincă, A. Dailly, Y. Liu, C. M. Brown, D. A. Neumann and J. R. Long, *J. Am. Chem. Soc.*, 2006, **128**, 16876; (*c*) M. Dincă and J. R. Long, *Angew. Chem., Int. Ed.*, 2008, **47**, 6766; (*d*) M. Latroche, S. Surblé, C. Serre, C. Mellot-Draznieks, P. L. Llewellyn, J.-H. Lee, J.-S. Chang, S. H. Jhung and G. Ferey, *Angew. Chem., Int. Ed.*, 2006, **45**, 8227; (*e*) J. L. C. Rowsell and O. M. Yaghi, *J. Am. Chem. Soc.*, 2006, **128**, 1304; (*f*) Y.-G. Lee, H. R. Moon, Y. E. Cheon and M. P. Suh, *Angew. Chem., Int. Ed.*, 2008, **47**, 7741; (*g*) X.-S. Wang, S. Ma, P. M. Forster, D. Yuan, J. Eckert, J. J. López, B. J. Murphy, J. B. Parise and H.-C. Zhou, *Angew. Chem., Int. Ed.*, 2008, **47**, 7263; (*h*) W. Zhou, H. Wu and T. Yildirim, *J. Am. Chem. Soc.*, 2008, **130**, 15268; (*i*) L. J. Murray, M. Dincă, J. Yano, S. Chavan, S. Bordiga, C. M. Brown and J. R. Long, *J. Am. Chem. Soc.*, 2010, **132**, 7856; (*j*) V. Colombo, S. Galli, H. J. Choi, G. D. Han, A. Maspero, G. Palmisano, N. Masciocchi and J. R. Long, *Chem. Sci.*, 2011, **2**, 1311.

4 (*a*) C. J. Doonan, W. Morris, H. Furukawa and O. M. Yaghi, *J. Am. Chem. Soc.*, 2009, **131**, 9492; (*b*) S. Chavan, J. G. Vitillo, M. J. Uddin, F. Bonino, C. Lamberti, E. Groppo, K. P. Lillerud and S. Bordiga, *Chem. Mater.*, 2010, **22**, 4602; (*c*) E. D. Bloch, D. Britt, C. Lee, C. J. Doonan, F. J. Uribe-Romo, H. Furukawa, J. R. Long and O. M. Yaghi, *J. Am. Chem. Soc.*, 2010, **132**, 14382; (*d*) Z. Q. Wang and S. M. Cohen, *Chem. Soc. Rev.*, 2009, **38**, 1315.

5 (*a*) J. C. Bayon, P. Esteban, G. Net, P. G. Rasmussen, K. N. Baker, C. W. Hahn and M. M. Gumz, *Inorg. Chem.*, 1991, **30**, 2572; (*b*) C. W. Hahn, P. G. Rasmussen and J. C. Bayon, *Inorg. Chem.*, 1992, **31**, 1963; (*c*) P. King, R. Clerac, C. E. Anson, C. Coulon and A. K. Powell, *Inorg. Chem.*, 2003, **42**, 3492; (*d*) P. King, R. Clerac, C. E. Anson and A. K. Powell, *Dalton Trans.*, 2004, 852; (*e*) L. Pan, N. Ching, X. Y. Huang and J. Li, *Chem.–Eur. J.*, 2001, **7**, 4431; (*f*) J. L. Tian, S. P. Yan, D. Z. Liao, Z. H. Jiang and P. Cheng, *Inorg. Chem. Commun.*, 2003, **6**, 1025.

6 (*a*) M. Eddaoudi, J. Kim, D. Vodak, A. Sudik, J. Wachter, M. O'Keeffe and O. M. Yaghi, *Proc. Natl. Acad. Sci. U. S. A.*, 2002, **99**, 4900; (*b*) H. Furukawa, J. Kim, N. W. Ockwig, M. O'Keeffe and O. M. Yaghi, *J. Am. Chem. Soc.*, 2008, **130**, 11650; (*c*) M. O'Keeffe, M. A. Peskov, S. J. Ramsden and O. M. Yaghi, *Acc. Chem. Res.*, 2008, **41**, 1782.

7 (*a*) C. Janiak, *Dalton Trans.*, 2003, 2781; (*b*) R. Robson, *Dalton Trans.*, 2008, 5113.

8 (*a*) L. Pan, X. Y. Huang and J. Li, *J. Solid State Chem.*, 2000, **152**, 236; (*b*) X.-H. Zhou, X.-D. Du, G.-N. Li, J.-L. Zuo and X.-Z. You, *Cryst. Growth Des.*, 2009, **9**, 4487.

9 For simplicity the crystallographic formula of MOF-647A, $[Cu_3(\mathbf{L})_2{\cdot}(DMF)_{1.9}(H_2O)_{3.1}]$, is represented as $[Cu_3(\mathbf{L})_2{\cdot}(DMF)_2(H_2O)_3]$.

10 Microanalysis for MOF-647A, $[Cu_3(\mathbf{L})_2{\cdot}(DMF)_{1.9}(H_2O)_{3.1}]$, calcd: C, 27.28; H, 3.13; N, 11.95%. Found: C, 26.8; H, 3.28; N, 11.5%. For MOF-648,$[Cu_{12}(\mathbf{L})_8{\cdot}(DMF)_9]{\cdot}(DMF)_2(H_2O)_2$, calcd: C, 31.04; H, 3.03; N, 13.40%. Found: C, 30.1; H, 3.9; N, 13.36%.

11 (*a*) C. Serre, F. Millange, C. Thouvenot, M. Noguès, G. Marsolier, D. Louër and G. Ferey, *J. Am. Chem. Soc.*, 2002, **124**, 13519; (*b*) T. Loiseau, C. Serre, C. Huguenard, G. Fink, F. Taulelle, M. Henry, T. Bataille and G. Ferey, *Chem.–Eur. J.*, 2004, **10**, 1373; (*c*) G. Ferey and C. Serre, *Chem. Soc. Rev.*, 2009, **38**, 1380.

12 J. A. R. Navarro, E. Barea, J. M. Salas, N. Masciocchi, S. Galli, A. Sironi, C. O. Ania and J. B. Parra, *Inorg. Chem.*, 2006, **45**, 2397.

Supplementary Material (ESI) for Chemical Communications
This journal is (c) The Royal Society of Chemistry 2011

Electronic Supplementary Information (20 pages)

Incorporation of active metal sites in MOFs *via in situ* generated ligand deficient metal-linker complexes

Samir Barman,[a] Hiroyasu Furukawa,*[b] Olivier Blacque,[a] Koushik Venkatesan,[a] Omar M. Yaghi,[b] Guo-Xin Jin[c] and Heinz Berke*[a]

[a] *Department of Inorganic Chemistry, University of Zürich Winterthurerstrasse 190, CH-8057, Zürich (Switzerland) Fax: (+41) 44-635-6802, E-mail: hberke@aci.uzh.ch*
[b] *Center for Reticular Chemistry, Department of Chemistry and Biochemistry, University of California-Los Angeles, 607 Charles E. Young Drive East, Los Angeles, California 90095, E-mail: furukawa@chem.ucla.edu*
[c] *Shanghai Key Laboratory of Molecular Catalysis and Innovative Material, Department of Chemistry, Fudan University, 200433, Shanghai, P. R. China.*

Table of Contents

Section S1 *Materials and General Procedures*

All solvents and reagents were purchased commercially and, unless otherwise noted, were used without further purification. Microanalyses were carried out at the Anorganisch-Chemisches Institut of the University of Zurich. FTIR spectra were obtained by using a Bio-Rad FTS-45 FTIR spectrometer. The powder XRD patterns were obtained with a Bruker D8 Advance system equipped with a Cu sealed tube (λ = 1.5406 Å). The following conditions were applied: 40 kV, 40 mA, increment = 0.007°, scan speed = 1.5 s / step. The simulated powder patterns were calculated from the single crystal X-ray diffraction data and generated with Mercury 2.3 software. All TGA experiments were performed under a N_2 atmosphere from 25 - 800 °C at a temperature ramp rate of 5 °C / min.

Section S2 *Synthesis*

Synthesis of MOF-647A **and** MOF-648**:**

$Cu(NO_3)_2 \cdot 2.5H_2O$ (2.76 g, 11.45 mmol) and 1*H*-pyrazole-3,5-dicarboxylic acid (0.72 g, 4.15 mmol) were dissolved in 100 mL of *N*,*N*-dimethylformamide (DMF) and the clear solution was divided in ten 20 mL vials. After they were tightly capped the vials were heated to 100 °C at a rate of 2 °C/min for 20 h in an isothermal oven. A mixture of light green thin-plate and dark blue-green block crystals was removed from the vial containing the mother liquor and washed with DMF (3 × 5 mL). The mixture of crystalline compounds was purified and separated by (a) sonicating, (b) filtering, (c) washing with DMF, and (d) depositing in a separation funnel, followed by the addition of 17.3:11 (v:v) CH_2Br_2:DMF.[S1] Because of the density difference of the two type of crystals, the light green thin-plate crystals of MOF-647A (450 mg) float to the top of the solution, while the dark blue-green block crystals of MOF-648 (480 mg) stay at the bottom. Elemental analysis calcd (%) for $C_{15.71}H_{21.51}Cu_3N_{5.90}O_{13}$ (MOF-647A) = $[Cu_3(\mathbf{L})_2 \cdot (DMF)_{1.9}(H_2O)_{3.1}]$ (**L** = pyrazole-3,5-dicarboxylate): C 27.28, H 3.13, N 11.95; found: C 26.80, H, 3.28, N 11.5. IR (KBr, cm^{-1}): for MOF-647A: 3117 (br), 1636 (m), 1582 (s), 1451 (s), 1384 (s), 1335 (s), 1281 (s), 1102 (m), 1057 (s), 1017 (s), 849 (s), 775 (s), 671 (m), 628 (w).

Elemental analysis calcd (%) for $C_{73}H_{85}Cu_{12}N_{27}O_{45}$ (MOF-648) = $[Cu_{12}(\mathbf{L})_8(DMF)_9] \cdot (DMF)_2(H_2O)_2$: C 31.06, H 3.03, N 13.4; found: C 28.60, H 3.25, N 12.70. IR (KBr, cm^{-1}): for MOF-648: 3167 (br), 1636 (w), 1583 (m), 1514 (w), 1384 (s), 1335 (m), 1282

(m), 1102 (m), 1058 (s), 1017 (m), 847 (m), 775 (s), 671 (w), 626 (m). The volatility of the co-crystallized solvents in the samples contributes to the discrepancy in the elemental analyses.

Single phase preparation of MOF-647A**.**

$Cu(NO_3)_2 \cdot 2.5H_2O$ (0.276 g, 1.145 mmol) and 1*H*-pyrazole-3,5-dicarboxylic acid (0.072 g, 0.415 mmol) were dissolved in 8 ml of DMF in a 20 mL glass vial. After the vials were tightly capped they were heated to 75 °C at a rate of 2 °C/min for 48 h in an isothermal oven. Thin plate blue crystals were removed from the mother liquor contained in the vial and washed with DMF (3 × 5 mL). Elemental analysis calcd (%) for $C_{15.71}H_{21.51}Cu_3N_{5.90}O_{13}$ (MOF-647A) = C 27.28, H 3.13, N 11.95; found: C 26.80, H, 3.28, N 11.5.

Single phase preparation of MOF-648**.**

$Cu(NO_3)_2 \cdot 2.5H_2O$ (0.13 g, 0.57 mmol) and 1*H*-pyrazole-3,5-dicarboxylic acid (0.05 g, 0.28 mmol) were dissolved in 20 mL of DMF in a 50 mL glass vial. After they were tightly capped the vials were heated to 100 °C at a rate of 1 °C/min for 12 h in an isothermal oven. Dark blue-green block crystals were removed from the mother liquor contained in a vial and washed with DMF (3 × 5 mL). Elemental analysis calcd (%) for $C_{73}H_{85}Cu_{12}N_{27}O_{45}$ (MOF-648) = C 31.06, H 3.03, N 13.40; found: C 29.5, H 3.94, N 13.36. The volatility of the co-crystallized solvents in the samples contributes to the discrepancy in the elemental analyses. IR (KBr, cm^{-1}): for MOF-648: 3167 (br), 1636 (w), 1583 (m), 1514 (w), 1384 (s), 1335 (m), 1282 (m), 1102 (m), 1058 (s), 1017 (m), 847 (m), 775 (s), 671 (w), 626 (m).

Preparation of MOF-647B**.**

About 50 mg of the as-prepared form of MOF-647A was thoroughly washed with fresh DMF followed by washing with anhydrous THF (5 × 5 mL). The THF washed material was then soaked in fresh anhydrous THF for 3 days with fresh THF added every 24 h.

Section S3 *Crystallographic Data*

Single X-Ray Diffraction Studies on MOF-647A**,** MOF-647B **and** MOF-648

Crystallographic data for all the MOFs were collected on an Oxford Xcalibur diffractometer (4-circle kappa platform, Ruby CCD detector and a single wavelength Enhance X-ray source with MoK_α radiation, λ = 0.71073 Å)[S2] at 183(2) K. The selected suitable single crystals were mounted using polybutene oil on the top of a glass fiber fixed on a goniometer head and immediately transferred to the diffractometer. Pre-experiment, data collection, analytical absorption corrections,[S3] and data reduction were performed with the Oxford program suite *CrysAlisPro*.[S4] The structures were solved with the Patterson (heavy atom) method and were refined by full-matrix least-squares methods on F^2 with SHELXL-97.[S5] All programs used during the crystal structure determination process are included in the WINGX software.[S5] The program PLATON[S6] was used to check the results of the X-ray analyses. Crystallographic data for the structural analyses have been deposited with the Cambridge Crystallographic Data Centre, CCDC-829034 for MOF-647A, CCDC-829035 for MOF-647B and CCDC-829036 for MOF-648. These data can be obtained free of charge from The Cambridge Crystallographic Data Centre via www.ccdc.cam.ac.uk/data_request/cif.

In MOF-647A one Cu atom is five-coordinated by three O atoms and two N atoms while the second Cu atom is five-coordinated by four O atoms and one N atom. The latter Cu atom is either coordinated by a DMF molecule or a water molecule with site-occupancy factors of 0.451(6) and 0.549(6), respectively. The central Cu(2) atom lies on a crystallographic two-fold axis. Some restraints and constraints were used to correct the thermal parameters of the disordered Cu-coordinated DMF molecule and the positions of the water H atoms (EADP, DFIX and DANG commands in *SHELXL97*). All other H positions were calculated after each cycle of refinement using a riding model, with C-H = 0.93 Å and $U_{iso}(H) = 1.2U_{eq}(C)$ for aromatic H atoms, and with C-H = 0.96 Å and $U_{iso}(H) = 1.5U_{eq}(C)$ for methyl H atoms.

In MOF-647B one Cu atom is five-coordinate by two N atoms, two carboxylate O atoms and one O atom from a THF molecule. The other Cu atom is either four-coordinated or five-coordinated depending on the orientation of the disordered THF (site-occupancy factor *sof* of 0.5). The water H atoms were located in a difference Fourier map but they were refined with fixed coordinates and $U_{iso}(H) = 1.5U_{eq}(O)$. All other H positions were calculated after each cycle

of refinement using a riding model, with C-H = 0.93 Å and U_{iso}(H) = 1.2U_{eq}(C) for aromatic H atoms, and with C-H = 0.97 Å and U_{iso}(H) = 1.2U_{eq}(C) for methylene H atoms.

In MOF-648 two Cu atoms exhibit a square-planar geometry (coordinated by four O atoms), one Cu atom is five-coordinated by three O atoms and two N atoms, and one Cu atom is either fix-coordinated by three O atoms and two N atoms or six-coordinated by four O atoms and two N atoms depending on the orientation of the disordered DMF (site-occupancy factor *sof* of 0.25). The three-dimensional framework contains three Cu-coordinated DMF molecules while cavities are occupied by solvent molecules of DMF (*sof* = 1) and water (disordered molecules with *sof* = 0.5). Some restraints and constraints were used to correct the geometry and thermal parameters of the isolated and disordered DMF molecules (EADP and SAME commands in *SHELXL97*). All H positions were calculated after each cycle of refinement using a riding model, with C-H = 0.93 Å and U_{iso}(H) = 1.2U_{eq}(C) for aromatic H atoms, and with C-H = 0.96 Å and U_{iso}(H) = 1.5U_{eq}(C) for methyl H atoms. The water H atoms could not be located and were not introduced in the model.

Table S1. Summary of the X-ray diffraction studies of MOF-647A, MOF-647B and MOF-648.

	MOF-647A	MOF-647B	MOF-648
empirical formula	$C_{15.71}H_{21.51}Cu_3N_{5.90}O_{13}$	$C_{18}H_{22}Cu_3N_4O_{12}$	$C_{73}H_{85}Cu_{12}N_{27}O_{45}$
formula weight ($g \cdot mol^{-1}$)	691.65	677.05	2823.28
temperature (K)	183(2)	183(2)	183(2)
wavelength (Å)	0.71073	0.71073	0.71073
crystal system, space group	tetragonal, $I\,4_1/acd$	tetragonal, $I\,4_1/acd$	orthorhombic, *Pbcm*
a (Å)	17.6342(6)	17.1637(5)	15.3345(1)
b (Å)	17.6342(6)	17.1637(5)	14.5465(1)
c (Å)	33.4999(11)	34.0665(6)	26.2229(3)
α (deg)	90	90	90
β (deg)	90	90	90
γ (deg)	90	90	90
volume ($Å^3$)	10417.3(6)	10035.7(5)	5849.37(9)
Z, density (calcd) ($Mg \cdot m^{-3}$)	16, 1.762	16, 1.792	2, 1.603
abs coefficient (mm^{-1})	2.499	2.587	2.224 mm
F(000)	5568.8	5456	2840
crystal size (mm^3)	0.13 × 0.09 × 0.05	0.19 × 0.10 × 0.04	0.34 × 0.23 × 0.17
θ range (deg)	2.43 to 25.68	2.66 to 25.68	2.48 to 30.51
reflections collected	24570	11076	87527
reflections unique	2480 / R_{int} = 0.141	2325 / R_{int} = 0.043	9101 / R_{int} = 0.072
completeness to θ (%)	99.9	97.2	99.9
absorption correction	analytical	analytical	analytical
max/min transmission	0.788 and 0.604	0.917 and 0.746	0.741 and 0.591
data / restraints / parameters	978 / 7 / 181	1155 / 0 / 158	6196 / 16 / 363
goodness-of-fit on F^2	0.738	0.921	1.037
final R_1 and wR_2 indices [$I > 2\sigma(I)$]	0.0399, 0.0800	0.0731, 0.2122	0.0535, 0.1738
R_1 and wR_2 indices (all data)	0.1357, 0.0930	0.1319, 0.2363	0.0773, 0.1820
largest diff. peak and hole ($e.A^{-3}$)	0.382, -0.466	2.318, -0.906	2.375, -2.413

The unweighted R-factor is $R_1 = \sum(Fo - Fc)/\sum Fo$; $I > 2\sigma(I)$ and the weighted R-factor is $wR2 = \{\sum w(Fo^2 - Fc^2)^2/\sum w(Fo^2)^2\}^{1/2}$.

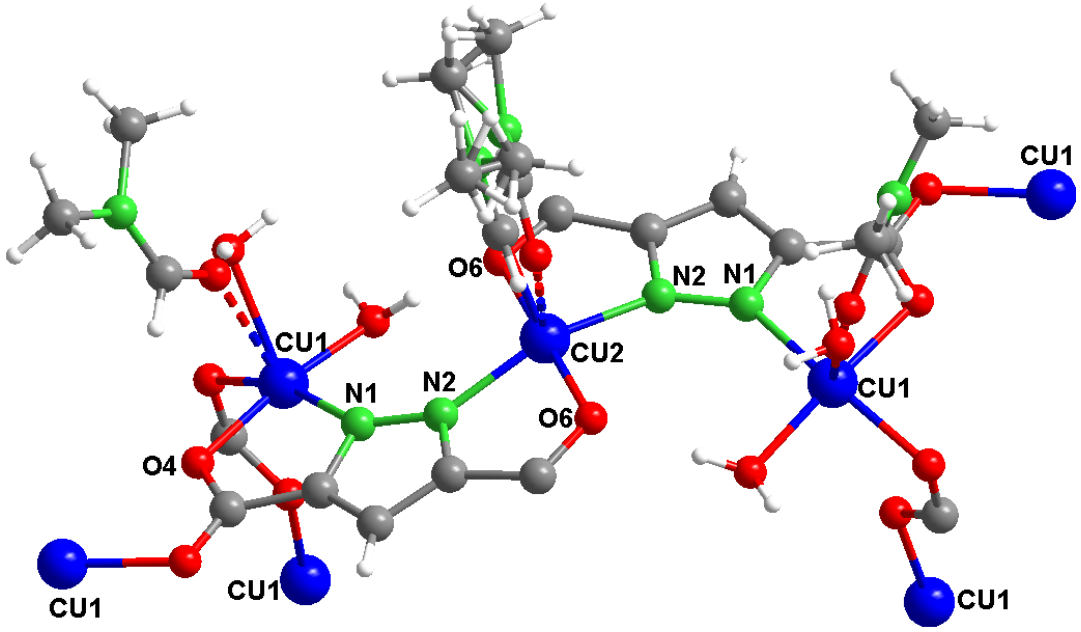

Fig. S1. A ball and stick presentation of the coordination environment of the trinuclear building unit in MOF-647A ($[Cu_3(\mathbf{L})_2 \cdot (DMF)_{1.9}(H_2O)_{3.1}]$). The coordination of the disordered DMF and water solvents at Cu(1) with site-occupancy factor of 0.451(6) and 0.549(6) are shown in dashed and solid bonds respectively. In Cu(2), one of the disordered coordinated DMF with a site-occupancy factor of 0.5 is shown with a dashed bond. Color code: Cu, blue; N, green; O, red; C, gray; H, white. Selected atom labels are shown.

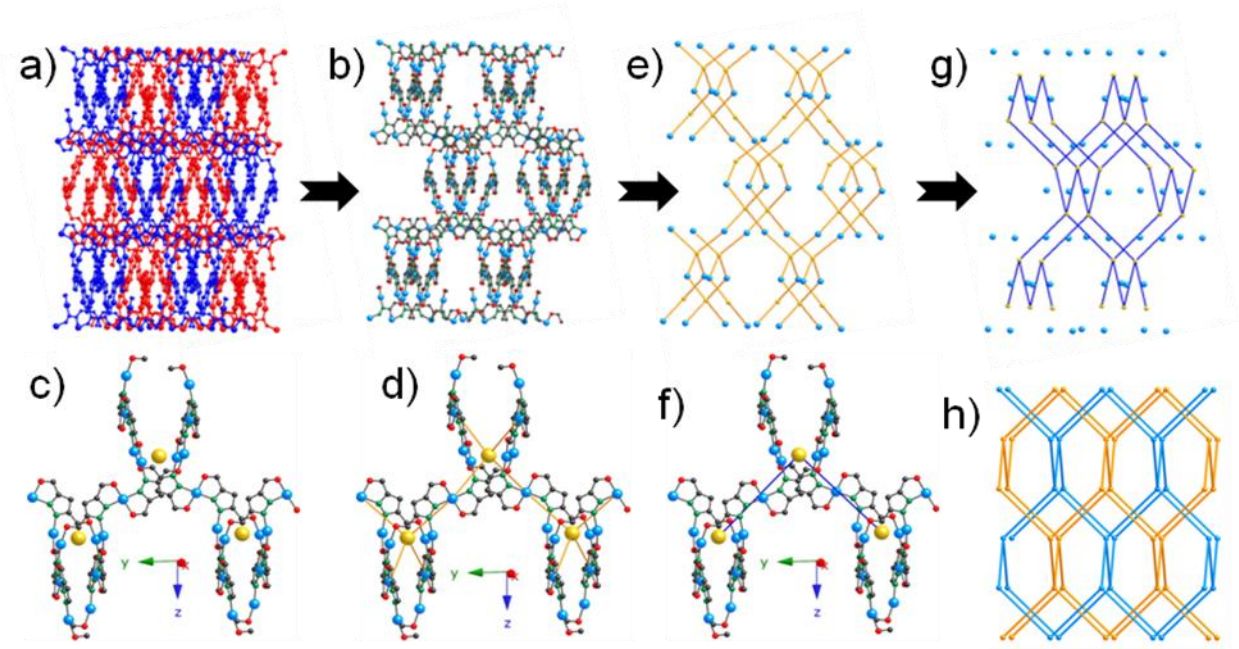

Fig. S2. Topological analysis of MOF-647A: Part of the doubly interpenetrated frameworks presented in a ball and stick model, where one of the frameworks is shown in blue and the other in red color (a); after removing the single blue net (b); to simplify the connectivity in (b), yellow spheres (near 4 Cu(1) atoms) could be displaced (c); after connecting the yellow spheres via Cu(2) (d), the simplified net (e) could be generated; to further simplify the overall 3D net (**dia**) connectivity (g), the connection through Cu(2) (since they do not take part in 3D connectivity) was ignored (f); schematic of the real doubly interpenetrated **dia** net (h). Coordinated guests and hydrogen atoms are omitted for clarity. Color code: Cu, blue; N, green; O, red; C, gray.

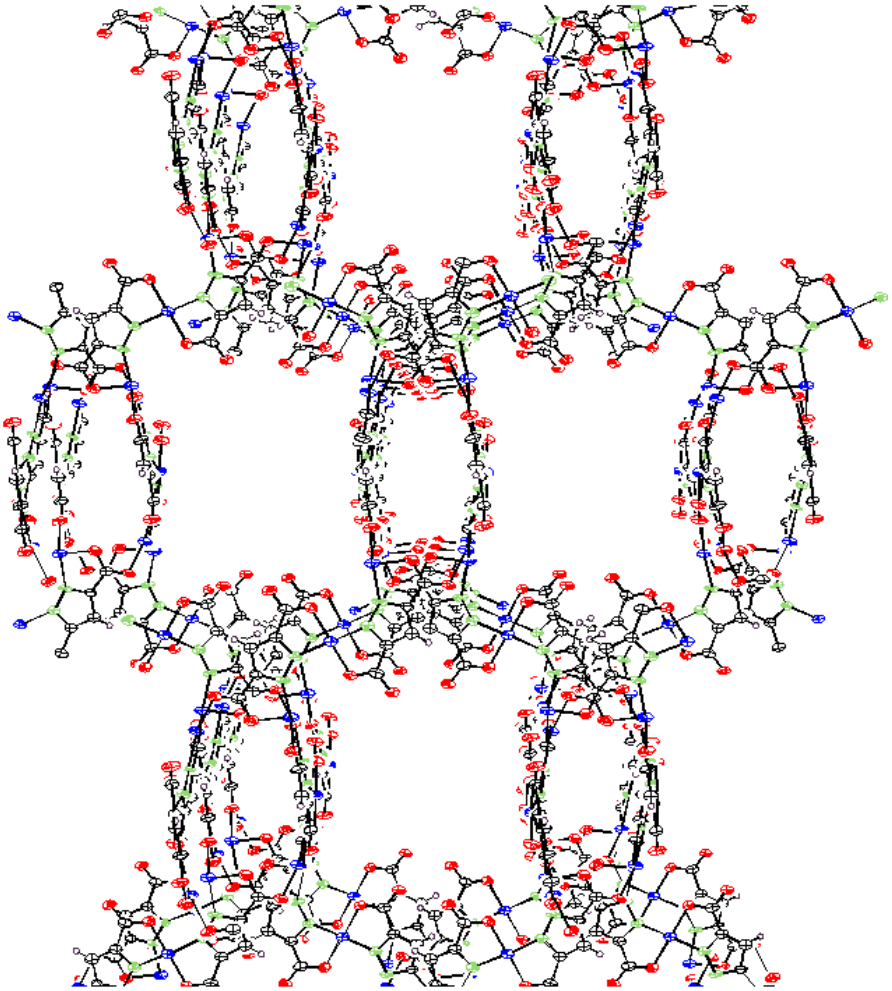

Fig. S3. ORTEP drawing (50% probability) of the part of the extended 3D structure of MOF-647A ($[Cu_3(\mathbf{L})_2 \cdot (DMF)_{1.9}(H_2O)_{3.1}]$) viewed down along the crystallographic *a* axis. Color code: Cu, blue; N, yellow-green; O, red; C, black; H, violet. Coordinated solvent molecules of DMF and H_2O are omitted for clarity.

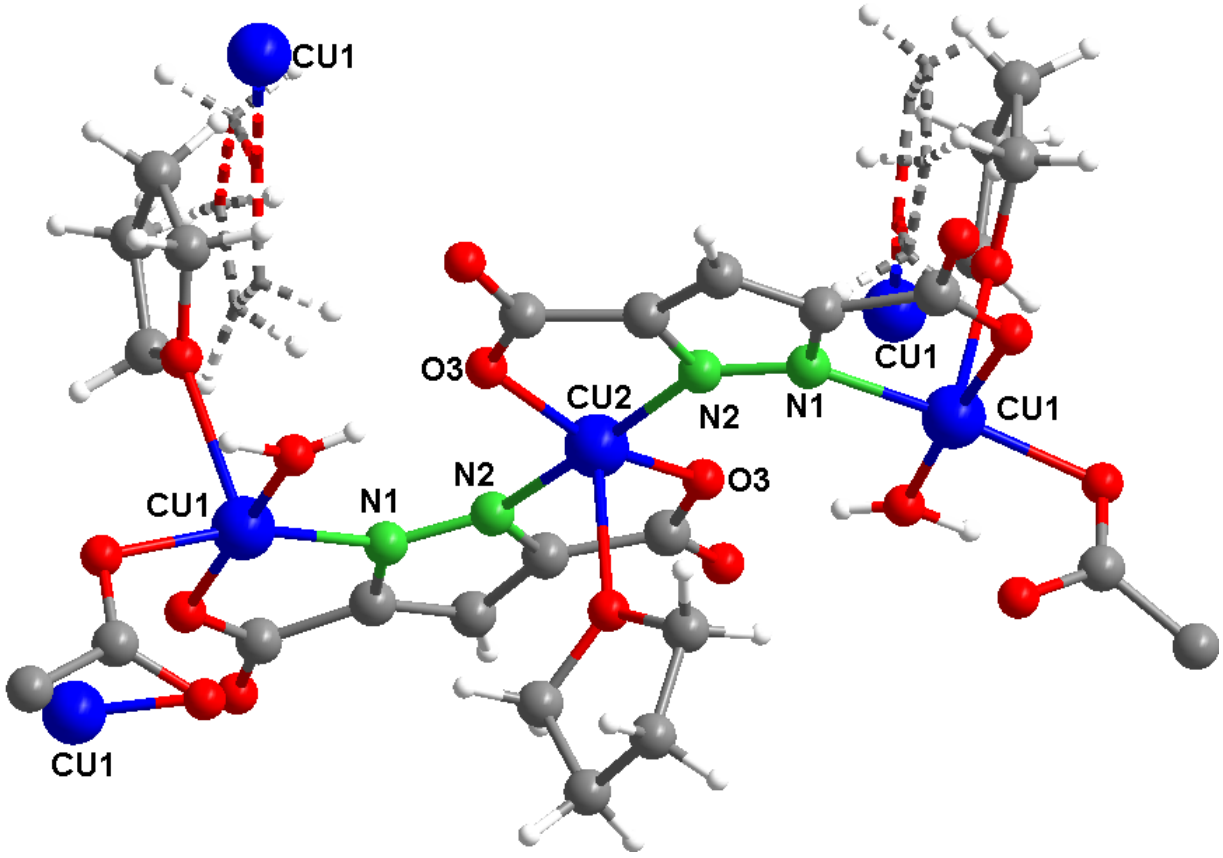

Fig. S4. A ball and stick presentation of the coordination environment of the trinuclear building unit in MOF-647B ($[Cu_3(\mathbf{L})_2 \cdot (THF)_2(H_2O)_2]$). The central Cu(2) ion is doubly chelated by two pyrazolate ligands and the fifth coordination site is occupied by the THF molecule to fulfil the distorted square pyramidal geometry. Meanwhile each of the Cu(1) can either be considered as tetra or penta coordinated depending upon the orientation of the THF molecules. One of the orientations of the THF molecule is represented with dotted lines. Color code: Cu, blue; N, green; O, red; C, gray; H, white. Selected atom labels are shown.

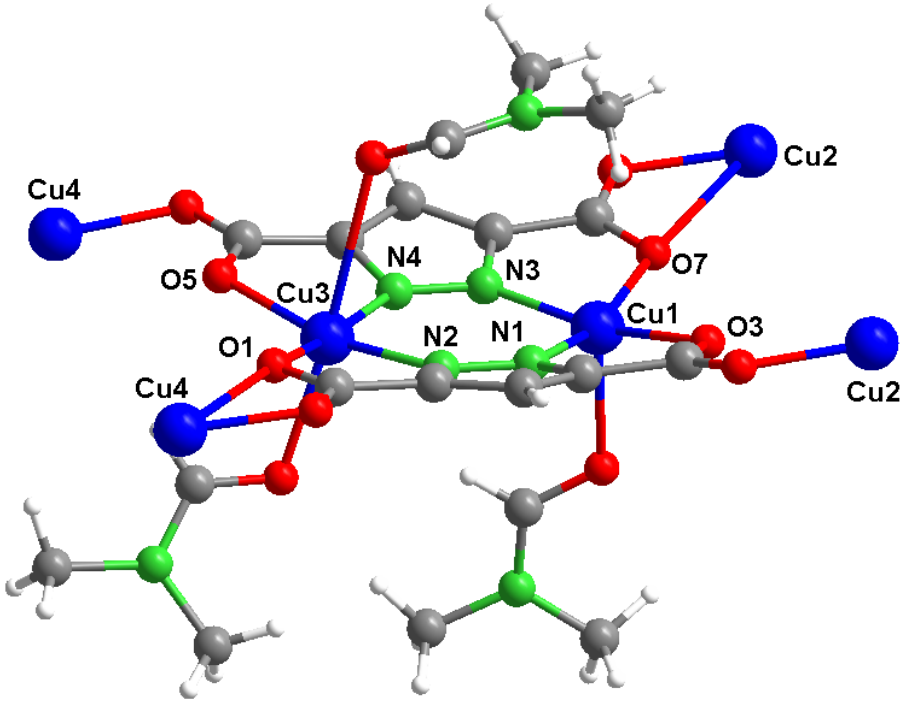

Fig. S5. A ball and stick presentation of the coordination environment of the six-membered bimetallacyclic ring in MOF-648 (**[**Cu_{12}(**L**)$_8$·$(DMF)_9$]·$(DMF)_2(H_2O)_2$). Color code: Cu, blue; N, green; O, red; C, gray; H, white. Selected atom labels are shown.

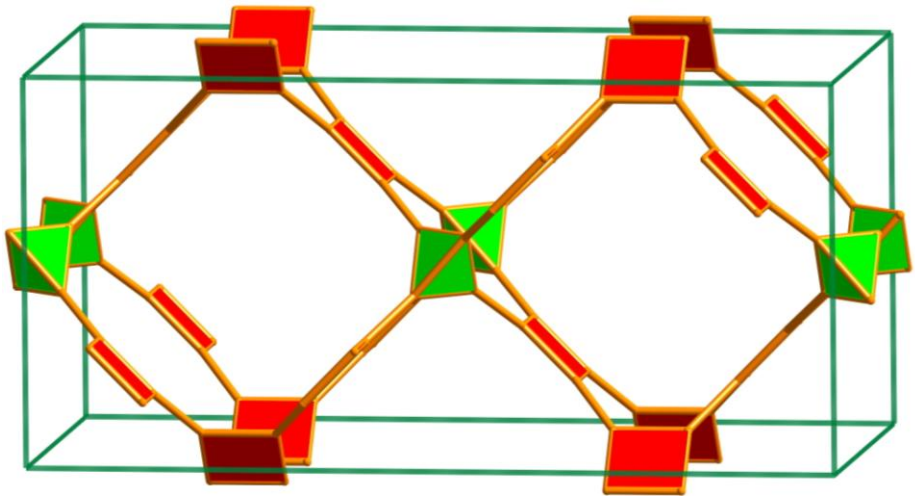

Fig. S6. Schematic presentation of an augmented trinodal 4-connected net (**sbr**) having the minimum number of kinds of edge (2) for the trinodal net as observed in MOF-648.

Systre[S7] **file for sbr in** MOF-648:

CRYSTAL
NAME sbr
GROUP Cmma
CELL 4.61883 2.30925 2.30954 90.0000 90.0000 90.0000
NODE 1 4 0.37500 0.25000 0.25000
NODE 2 4 0.00000 0.00000 0.50000
NODE 3 4 0.25000 0.00000 0.00000
EDGE 2 0.12500 -0.25000 0.25000
EDGE 3 0.12500 0.25000 -0.25000
END

Section S4 *Powder X-Ray Diffraction Patterns*

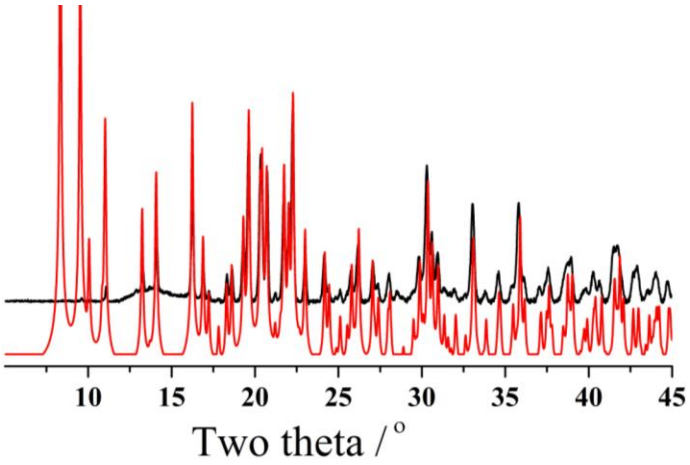

Fig. S7. Powder X-ray diffraction patterns: simulated from the single X-ray crystal structure of MOF-647A (red) and as-prepared MOF-647A (black).

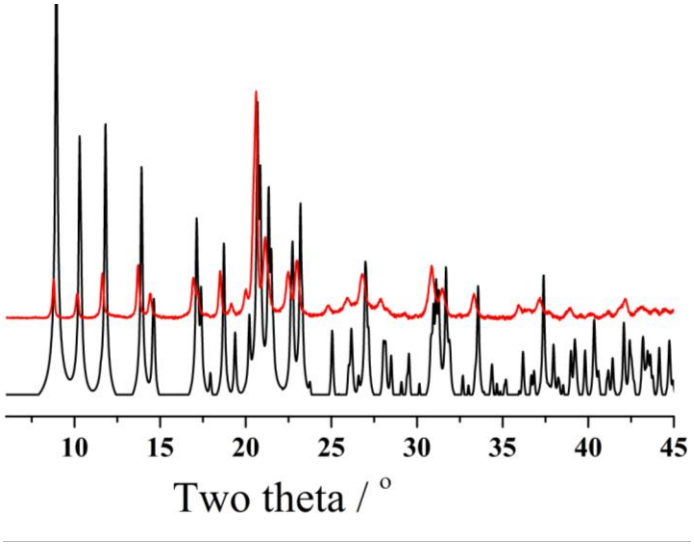

Fig. S8. Powder X-ray diffraction patterns: simulated from the X-ray single crystal structure of MOF-647B (black) and as-prepared MOF-647B (red).

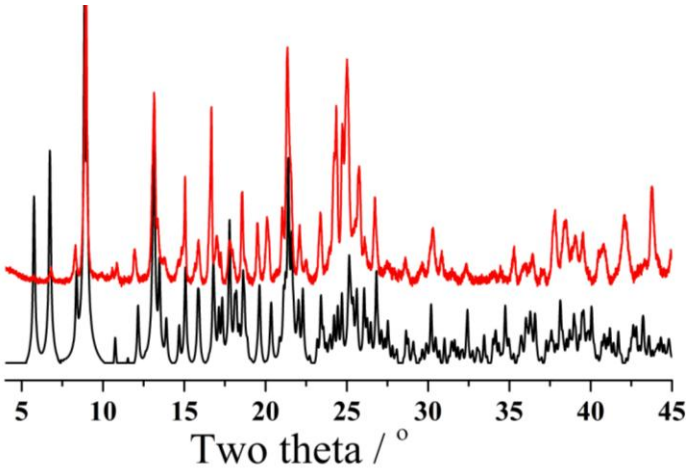

Fig. S9. Powder X-ray diffraction patterns for the simulation from the single crystal structure of MOF-648 (black), as-prepared MOF-648 (red).

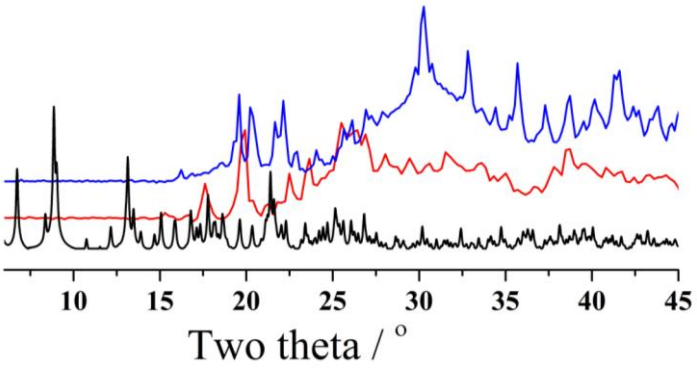

Fig. S10. Powder X-ray diffraction patterns for the simulation from the single crystal structure of MOF-648 (black), activated material prepared after degassing the acetone exchanged (for 3 d) material at 80 °C for 4 h (red) and the material obtained after resolvation of the activated sample with DMF for 24 h and at room temperature (blue).

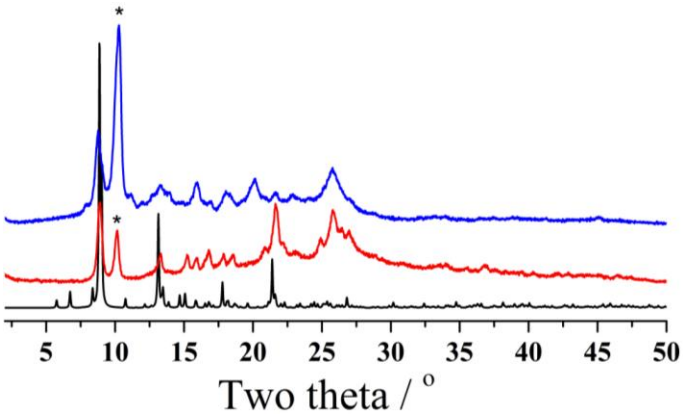

Fig. S11. Powder X-ray diffraction patterns for the simulation from the single crystal structure of MOF-648 (black), material prepared after SCD following acetone exchange for 3 d (red), the material prepared after degassing the SCD material at 50 °C for 3 h (blue). Note that the new and relatively low intensity peak at $2\theta = 10.2°$ (marked with an asterisk) which appears after SCD activation becomes more intense after heating at 50 °C whereas simultaneously the intense peak around $2\theta = 8.9°$ (for [102] and [111] reflections) goes down.

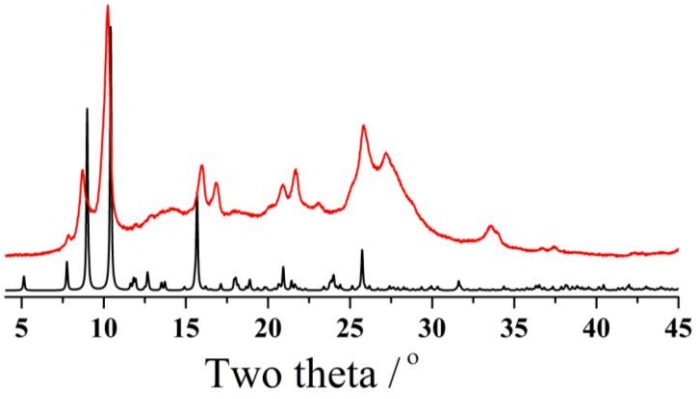

Fig. S12. Powder X-ray diffraction patterns for the simulation from the single crystal structure of MOF-648 (black) with modified cell parameters (a = 17.2 Å, b = 15.2 Å and c = 19.5 Å) assuming that the space group (orthorhombic, *Pbcm*) was unaltered while the crystal lattice was compressed along the c-axis throughout the activation process and the material was prepared after degassing the SCD material at 50 °C for 3 h (red).

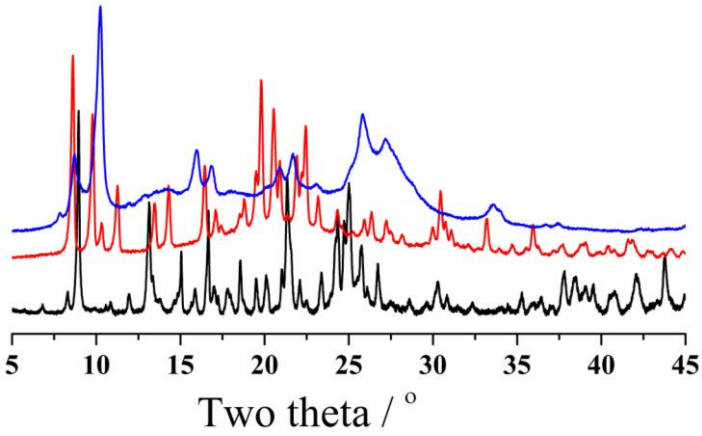

Fig. S13. Powder X-ray diffraction patterns for the as-prepared MOF-648 (black), the material prepared after degassing the SCD material at 50 °C for 3 h (blue) and the material obtained after resolvation of the activated sample with DMF (red).

Section S5 *Thermal Gravimetric Analysis*

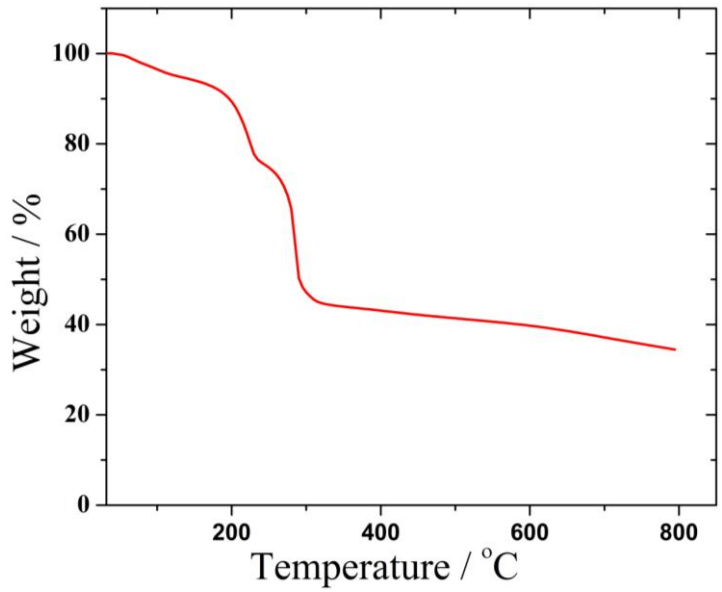

Fig. S14. TGA trace of as-synthesized MOF-647A.

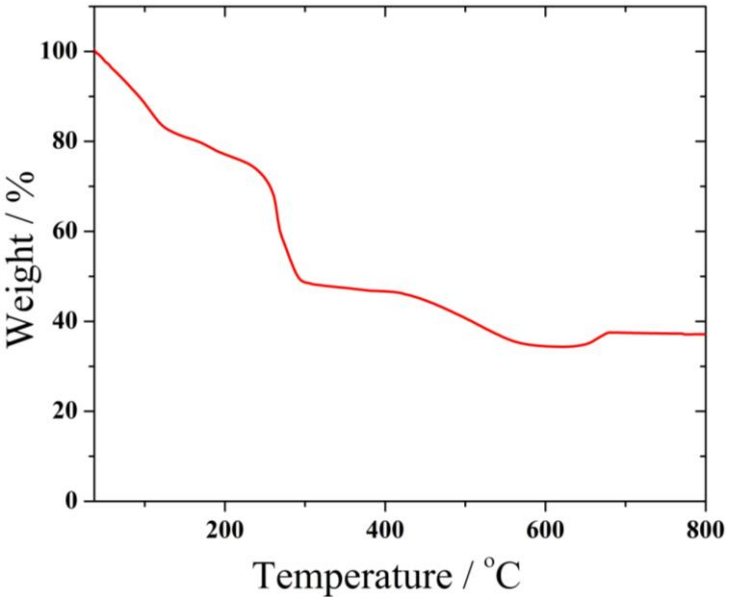

Fig. S15. TGA trace of as-synthesized MOF-647B.

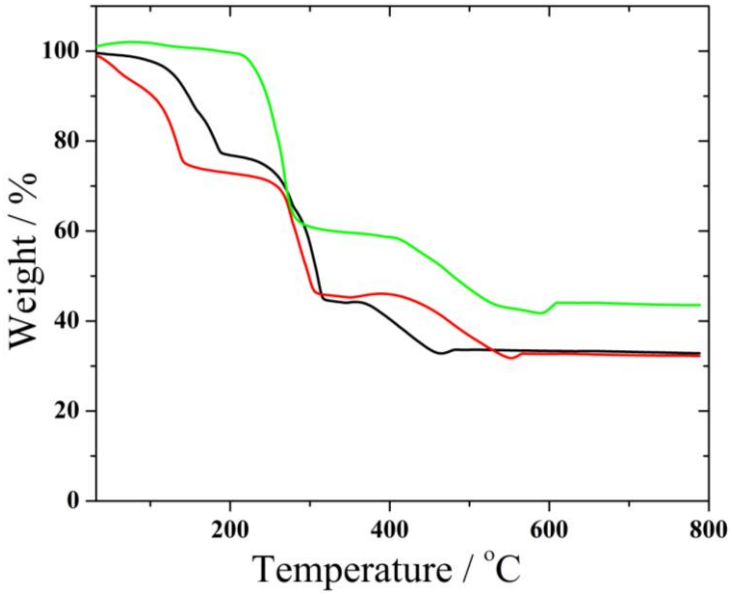

Fig. S16. TGA traces of as-synthesized MOF-648 (black), acetone exchanged for 3 d (red) and the activated material obtained after degassing the acetone exchanged material at 50-70 °C for 4 h.

Section S6 *Gas Adsorption Measurements*

Low-pressure N_2, H_2 and CO_2 adsorption measurements were performed on an Autosorb-1 (Quantachrome) volumetric analyzer.[S8] The samples were outgassed to 10^{-6} torr. Helium was used for the estimation of the dead volume, assuming that it is not adsorbed at any of the studied temperatures. Liquid N_2 bath was used for adsorption measurements at 77 K. Ultra-high-purity grade He, N_2, H_2 and CO_2 were used throughout the adsorption experiments.

For porosity measurements, as-synthesized MOF-648 was immersed in acetone for 24 h, during which the activation solvent was replenished three times. The sample was evacuated with supercritical CO_2 in a Tousimis Samdri PVT-3D critical point dryer.[S9,S10] Briefly, the acetone-containing sample was placed in the chamber and acetone was exchanged with liquid CO_2. After that the chamber containing the sample and liquid CO_2 was heated up around 40 ºC and kept under the supercritical condition (typically 1300 psi) for 1 h. The CO_2 was slowly vented (ca. 1 h) from the chamber at around 40 ºC. After the bleeding, the sample was degassing at 45 °C for 24 h to yield porous material.

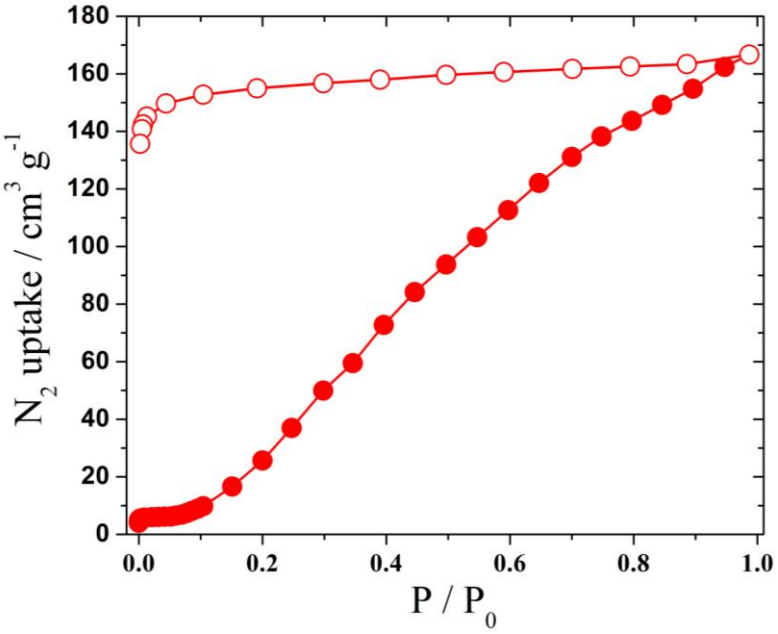

Fig. S17. N_2 isotherm of MOF-648 measured at 77 K. Filled and open circles represent adsorption and desorption branches, respectively. Connecting traces are guides for the eye.

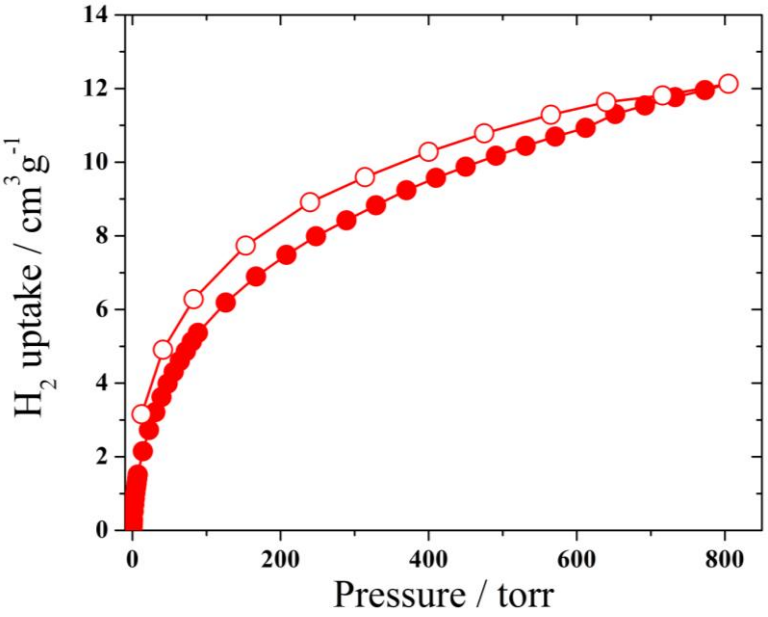

Fig. S18. H_2 isotherm of the activated MOF-648 measured at 77 K. Filled and open circles represent adsorption and desorption branches, respectively. Connecting traces are guides for the eye.

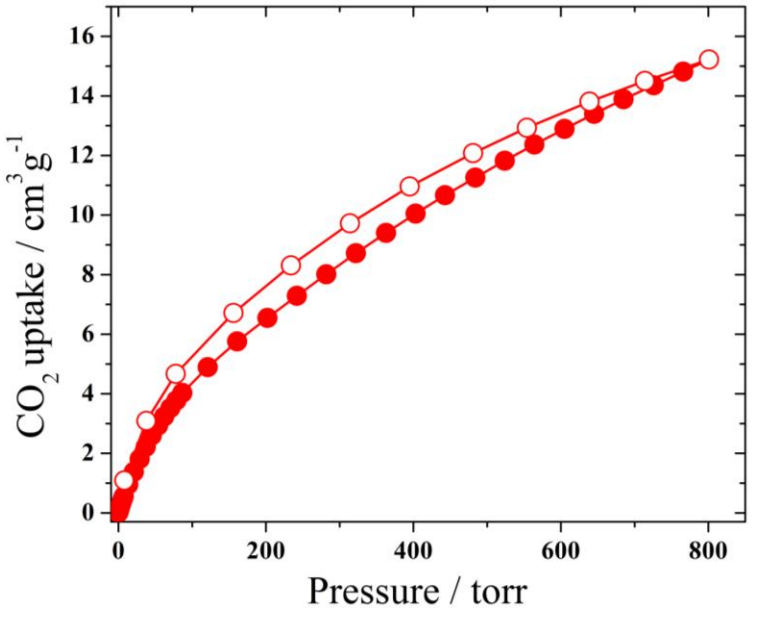

Fig. S19. CO_2 isotherm of the activated MOF-648 measured at 298 K. Filled and open circles represent adsorption and desorption branches, respectively. Connecting traces are guides for the eye.

Section S7 *References*

[S1] O. K. Farha, K. L. Mulfort, A. M. Thorsness and J. T. Hupp, *J. Am. Chem. Soc.*, 2008, **130**, 8598.

[S2] Oxford Diffraction (2007). Xcalibur CCD system. Oxford Diffraction Ltd, Abingdon, Oxfordshire, England.

[S3] R. C. Clark, and J. S. Reid, *Acta Cryst.*, 1995, **A51**, 887.

[S4] G. M. Sheldrick, *Acta Cryst.*, 2008, **A64**, 112.

[S5] L. J. Farrugia, *J. Appl. Cryst.*, 1999, **32**, 837.

[S6] A. L. Spek, *J. Appl. Cryst.*, 2003, **36**, 7.

[S7] More information can be found at http://gavrog.sourceforge.net/

[S8] H. Furukawa, M. A. Miller and O. M. Yaghi, *J. Mater. Chem.*, 2007, **17**, 3197.

[S9] A. P. Nelson, O. K. Farha, K. L. Mulfort and J. T. Hupp, *J. Am. Chem. Soc.*, 2009, **131**, 458.

[S10] H. Furukawa, N. Ko, Y. B. Go, N. Aratani, S. B. Choi, E. Choi, A. O. Yazaydin, R. Q. Snurr, M. O'Keeffe, J. Kim and O. M. Yaghi, *Science*, 2010, **329**, 424.

9. TRIPTYCENE BASED LUMINESCENT METAL-ORGANIC GELS FOR CHEMOSENSING

9.1. Publication 3

Triptycene based luminescent metal-organic gels for chemosensing

Samir Barman, Jai Anand Garg, Olivier Blacque, Koushik Venkatesan, and Heinz Berke**

Department of Inorganic Chemistry, University of Zürich Winterthurerstrasse 190, CH-8057, Zürich (Switzerland).

Chem. Commun., 2012, **48**, 11127-11129.

View Online / Journal Homepage / Table of Contents for this issue
Dynamic Article Links

ChemComm

Cite this: *Chem. Commun.*, 2012, **48**, 11127–11129

www.rsc.org/chemcomm

COMMUNICATION

Triptycene based luminescent metal–organic gels for chemosensing†

Samir Barman, Jai Anand Garg, Olivier Blacque, Koushik Venkatesan* and Heinz Berke*

Received 20th June 2012, Accepted 10th August 2012
DOI: 10.1039/c2cc34430k

We report a novel luminescent Al-based metal–organic gel G1 comprising 1,4,5,8-triptycenetetracarboxylic acid, which exhibits highly sensitive detection towards nitro aromatic compounds particularly picric acid. Furthermore, under identical reaction conditions, using a Co(II) salt instead, a novel 3D framework material, *trip*-MOF-1, was isolated and its sensitivity towards picric acid was also evaluated.

Design and development of chemosensors for rapid and selective detection of ultra-trace nitroaromatic analytes (explosives), particularly 2,4,6-trinitrotoluene (2,4,6-TNT), 2,4-dinitrotoluene (2,4-DNT), and picric acid (PA), are perceived to be of great importance due to their potential utility in national security screening and also for the environmental concerns.[1] Electron deficient nature of the aforementioned analytes makes them amenable for detection by electron rich fluorescence sensors *via* a photoinduced electron transfer (PET) quenching mechanism.[2] Because the detection sensitivity of the chemosensors is primarily determined by transduction methods,[3,4a–c] design of new materials capable of enhancing the transduction signals, which result from the binding of analyte molecules, is in great demand. Particularly, over the last two decades, Swager and co-workers have pioneered the detection of TNT among other explosives and toxic pollutants using conjugated polymeric (capable of facile long range exciton migration) materials *via* a fluorescence quenching mechanism. Receptors especially based on triptycene derivatives have been successfully employed in the polymer backbone.[1b,4] It has been suggested that incorporation of such rigid 3-D moieties mitigates π-stacking and excimer formation owing to its unique structural motifs while allowing diffusion or hosting of analyte molecules in its geometric void space.[4a,5] Although organic conjugated polymers comprising triptycene have been successfully demonstrated to detect explosives with high sensitivity, to our knowledge, there is no report of triptycene containing metal–organic material used for this purpose. In this contribution, we have sought to investigate the sensing efficiency of the triptycene based coordination polymeric gels,[6] anticipating that the shape-persistent properties of the rigid triptycene unit will remain unaltered. Particularly, we report here a novel synthetic method for the preparation of triptycene based metal–organic gel and its utility as a chemical sensor.

Heating a clear mixture of $Al(NO_3)_3{\cdot}9H_2O$ and 1,4,5,8-triptycenetetracarboxylic acid (H_4ttc)[7] in *N*,*N*-dimethylformamide (DMF) readily yielded an opaque Al-gel material **G1** (Fig. 1a, concluded based on the tube inversion test) within a few hours (see ESI† for details). The FT-IR spectra of the xerogel (Fig. S4, ESI†) clearly showed that the bands due to the carboxylates are shifted to lower frequencies (for example 1693 to 1626 cm^{-1}) with respect to the free ligand. This unambiguously suggests the presence of carboxylate in the metal coordination sphere. Further the gel is not thermoreversible indicating the coordination polymeric nature of the gel network. It is also apparently stable under sealed conditions. However, when open to the air it shrinks markedly over a period of several days. The Al-gel **G1** is also stable when subsequently immersed in various organic solvents such as alcohols, DMSO, DMF and acetone. Microscopic examination of the air-dried gels under a scanning electron microscope (SEM) (Fig. 1c) revealed a sponge-like structure with a disordered arrangement of interconnected macropores in the size range of 50–90 nm.

Dynamic rheology was performed using Al-gel **G1** (overall ~8% DMF gel)[8] to further evaluate its gel-like character. In a typical frequency sweep experiment, the elastic modulus G′ and the viscous modulus G″ were plotted as a function of the angular frequency 'ω' at a constant strain of 0.1%.

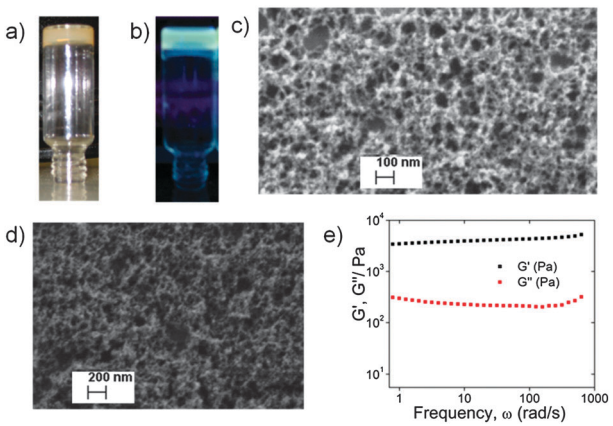

Fig. 1 The photo of as-prepared Al-gel **G1** (a) and Al-gel **G1** under UV lamp (b); the SEM image of the xerogels (air-dried form of as-prepared Al-gel **G1**) (c) and the xerogel prepared from the ethanol dispersed form of as-prepared Al-gel **G1** (d); rheological response of the Al-gel **G1** (e).

Department of Inorganic Chemistry, University of Zürich, Winterthurerstrasse 190, CH-8057, Zürich, Switzerland. E-mail: hberke@aci.uzh.ch, venkatesan.koushik@aci.uzh.ch; Fax: +41 44-635-6802

† Electronic supplementary information (ESI) available: Full synthetic procedures and characterization data including TGA, IR, PXRD, and single crystal X-ray diffraction data. CCDC 872964. For ESI and crystallographic data in CIF or other electronic format see DOI: 10.1039/c2cc34430k

Fig. 1e shows that the G′ values (~4.1 kPa) remained invariant with frequency over a considerable period of the time scale and were significantly higher in magnitude than the corresponding G″ supporting its remarkable gel-like response.

In order to evaluate the scope of the synthetic procedure, other metal precursor salts containing Co(II) and Cr(III) were examined under optimized conditions.[9] Unlike $Al(NO_3)_3 \cdot 9H_2O$, the reaction between $Co(NO_3) \cdot 6H_2O$ and H_4ttc did not result in the formation of gel material, instead allowed the isolation of a crystalline product (designated *trip*-MOF-**1**) of the formula $[Co_2(ttc)(DMF)(H_2O)]$ (*ttc* = 1,4,5,8-triptycene-tetracarboxylate) as established based on single crystal X-ray diffraction (SXRD) and elemental microanalysis.[10] The *trip*-MOF-**1** was further characterized by TGA, FT-IR and powder X-ray diffraction (PXRD) analysis (see ESI† for details). The SXRD analysis revealed that the structure of *trip*-MOF-**1** (Fig. 2a and b) is built up from two Co(II) cations, one *ttc* anion, one metal-coordinated water and DMF solvent molecules. The Co(II) centers are located at special positions with a site-occupancy factor of 0.5. The Co1 atoms lie on two-fold axes while the Co2 atoms lie on centers of inversion. Co1 is tetrahedrally coordinated by four carboxylate oxygen atoms from four different *ttc* ligands and Co2 is octahedrally coordinated by four carboxylate oxygen atoms from two different *ttc* ligands, one oxygen atom from a water molecule and one oxygen atom from a DMF molecule. The *trans* water and DMF ligands are disordered over two sets of sites with an occupancy of 0.5 while the *ttc* ligand is extensively disordered about a crystallographic center of inversion. The Co cations are linked by the *ttc* anions into a three-dimensional framework. Structural analysis of *trip*-MOF-**1** using TOPOS software[11] reveals a 2-nodal 4,6-c net (Fig. 2c) with stoichiometry (4-c)(6-c) and the Schläfli symbol for the net is $\{3^2.8^4\}\{3^4.4^2.8^4.9^4.10\}$.

The tempting light emission from the Al-gel **G1** either in its as-prepared (Fig. 1b) or in the dispersed form in ethanol prompted us to explore its potential application as a chemosensor. Interestingly, no change in the network skeleton was observed when as-prepared Al-gel **G1** was suspended in ethanol (Fig. 1d). The photoluminescence spectra of the ethanol dispersed Al-gel **G1** exhibits strong fluorescence maxima at 385 nm upon excitation at 318 nm,[12] which is red shifted by 10 nm in comparison to the peak at 375 nm (excitation at 315 nm) for the H_4ttc ligand (Fig. S8, ESI†). The fluorescence attenuation of the Al-gel **G1** dispersed in ethanol was investigated using different analytes (quenchers),[13] and the percent (%) quenching is depicted in Fig. 3a. It clearly reveals the varied fluorescence quenching response upon addition of analytes with various degrees of electron deficiency. While an insignificant quenching was observed for nitromethane (NM), chlorobenzene (CB), nitrobenzene (NB) and 1,3-dinitrobenzene (1,3-DNB), a highly efficient quenching was observed for hydroxy substituted nitroarenes *p*-nitrophenol (*p*-NP), 2,4-dinitrophenol (2,4-DNP), 2,6-dinitrophenol (2,6-DNP) and PA. In contrast to the general trend exhibited by the phenolic arenes, *m*-nitrophenol (*m*-NP) however showed low quenching efficiency. This reveals the potentiality for selective detection of 2,4-DNP, 2,6-DNP and *p*-NP over its *m*-substituted analogues. Explaining the trend in selectivity among the hydroxy substituted nitroarenes (*p*-NP, 2,4-DNP, 2,6-DNP and PA); the polarizability and also the π–π interacting ability of the analytes seem to be the most influential. Accordingly, *m*-NP shows lower quenching efficiency as compared to *p*-NP which has greater polarizability.[14] Non-aromatic analytes such as nitromethane also showed a lower quenching response due to the lack of π–π interactions. It is worth mentioning here that, *p*-NP derivatives are also amongst the most toxic pollutants evaluated by US Environmental Protection Agency (EPA).[15] Significantly, Al-gel **G1** showed highest sensitivity towards PA (Fig. 3a) and the limit of detection (LOD) was observed in the range of 5–10 ppb. The fluorescence attenuation of PA and 2,4-DNT (which shows a moderate quenching response) was further evaluated based on the Stern–Volmer plot depicted in Fig. 3b. As expected the Stern–Volmer binding constant, $K_{sv} = 5.3 \times 10^5\ M^{-1}$, obtained for PA was higher than $2.19 \times 10^4\ M^{-1}$ estimated for 2,4-DNT, which evidences a more facile PET from the excited state of the receptor (Al-gel **G1**) to the relatively low lying LUMO orbital of PA (Section S8, ESI†).[1e,3b,16] Incidentally, the K_{sv} ($5.3 \times 10^5\ M^{-1}$) obtained for PA is found to be superior when compared to the other literature known values for fluorescence based chemosensors.[1e,17] Furthermore, when a discrete ligand (H_4ttc) was used as a PA sensor, a significantly low K_{sv} value of $1.2 \times 10^5\ M^{-1}$ was obtained *versus* $5.3 \times 10^5\ M^{-1}$ for the Al-gel **G1**. The improved attenuation response in the case of Al-gel **G1** evidences the impact of the self-assembly of the triptycene receptors into macroporous structures to facilitate long range exciton migration.[18b,e]

In conjunction to the Al-gel **G1** we further evaluated *trip*-MOF-**1**[18] and Cr-gel **G2**[9] as PA sensors (Fig. S24, ESI†). The K_{sv} values obtained for *trip*-MOF-**1** ($5.2 \times 10^4\ M^{-1}$) and Cr-gel **G2** ($4.8 \times 10^4\ M^{-1}$) were however found to be lower

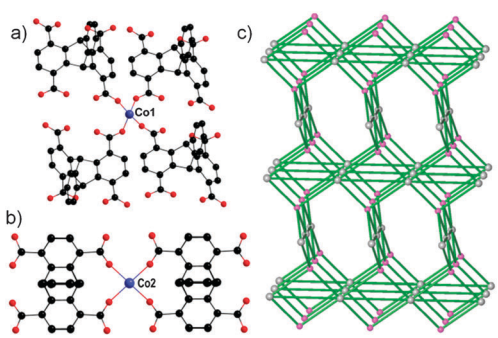

Fig. 2 Partial view of the single X-ray crystal structure of *trip*-MOF-**1**, showing the coordination environment around the metal centers Co1 (a) and Co2 (b) with selected atoms numbered. Atom colors: Co, blue; O, red; C, black. All coordinated solvents and hydrogen atoms are omitted for clarity. (c) Partial view of the 2-nodal 4,6-c net in *trip*-MOF-**1**.

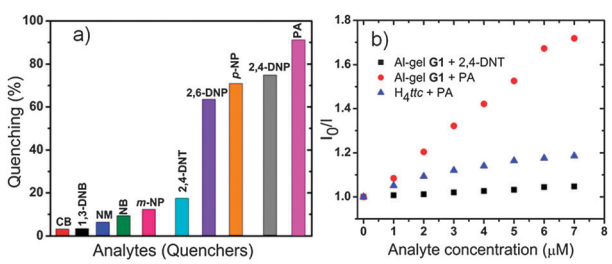

Fig. 3 (a) The percent (%) quenching of the fluorescence of as-prepared Al-gel **G1** dispersed in ethanol by the addition of different analytes (quenchers) at room temperature. (b) The Stern–Volmer plots for the titration of Al-gel **G1** (with DNT, black square and PA, red circle) and H_4ttc (with PA, blue triangle).

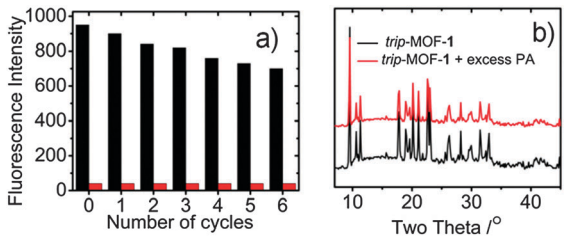

Fig. 4 (a) Reproducibility of the quenching ability of Al-gel **G1** dispersed in ethanol to PA solution. The black bars represent the initial fluorescence intensity and the red bars represent the intensity upon addition of 100 μL (1 mM) of a solution of PA. (b) PXRD pattern of pristine *trip*-MOF-**1** (black) and its ethanol washed material obtained after the treatment with an excess of PA (2 mM) solution in ethanol (red).

than that obtained for Al-gel **G1**. This indicates that the metal–organic material incorporating Al(III) ions has pronounced sensitivity towards PA when compared to Co(II) and Cr(III). The degradation of the coordination network upon addition of acidic analytes such as PA in ethanol could be ruled out by establishing an identical PXRD pattern of pristine *trip*-MOF-**1** and its PA treated material (Fig. 4b).

The sensing ability of the Al-gel **G1** in the solid state when exposed to saturated vapour of various analytes was evaluated (Fig. S26, ESI†). Upon exposure to NB vapour for 6 min, a significant quenching (55%) of the initial intensity was observed. On the other hand, a relatively low quenching (13%) effect was seen in the case of 2,4-DNT and a further diminished response was noted for PA (9%). This is in stark contrast to what was observed in the solution medium. The overall quenching response in the solid state seems to be limited by the relative vapour pressure of the analytes following the order NB > > 2,4-DNT > PA.

The ethanol dispersed Al-gel **G1** could be regenerated and reused for a significant number of cycles by centrifuging the dispersed solution after use and washing several times with ethanol (Fig. 4a and Fig. S25, ESI†). The recovery of the initial emission intensity to a significant extent (~75% after 6 cycles) implies high photostability of the material.

In summary, we have developed luminescent metal–organic materials based on the triptycene receptor for the sensitive detection of nitro aromatic compounds. Particularly, Al-gel **G1** exhibits superior response towards PA. The observed sensitivity could be attributed to the self-assembly of the triptycene receptors into coordination polymeric gel. Such luminescent metal–organic materials can be used as an alternative platform for chemo- and biosensing.

Funding from the Swiss National Science Foundation (SNSF) and University of Zürich is gratefully acknowledged.

Notes and references

1 (*a*) J. I. Steinfeld and J. Wormhoudt, *Annu. Rev. Phys. Chem.*, 1998, **49**, 203; (*b*) D. T. McQuade, A. E. Pullen and T. M. Swager, *Chem. Rev.*, 2000, **100**, 2537; (*c*) K. J. Albert, N. S. Lewis, C. L. Schauer, G. A. Sotzing, S. E. Stitzel, T. P. Vaid and D. R. Walt, *Chem. Rev.*, 2000, **100**, 2595; (*d*) K. J. Albert, M. L. Myrick, S. B. Brown, D. J. James, F. P. Milanovich and D. R. Walt, *Environ. Sci. Technol.*, 2001, **35**, 3193; (*e*) H. Sohn, R. M. Calhoun, M. J. Sailor and W. C. Trogler, *Angew. Chem., Int. Ed.*, 2001, **40**, 2104; (*f*) S. J. Toal and W. C. Trogler, *J. Mater. Chem.*, 2006, **16**, 2871; (*g*) S. Singh, *J. Hazard. Mater.*, 2007, **144**, 15; (*h*) M. E. Germain and M. J. Knapp, *Chem. Soc. Rev.*, 2009, **38**, 2543.

2 (*a*) S. W. Thomas III, J. P. Amara, R. E. Bjork and T. M. Swager, *Chem. Commun.*, 2005, 4572; (*b*) S. Zhang, F. Lü, L. Gao, L. Ding and Y. Fang, *Langmuir*, 2007, **23**, 1584; (*c*) M. S. Meaney and V. L. McGuffin, *Anal. Bioanal. Chem.*, 2008, **391**, 2557; (*d*) H. Cavaye, P. E. Shaw, X. Wang, P. L. Burn, S.-C. Lu and P. Meredith, *Macromolecules*, 2010, **43**, 10253; (*e*) D. A. Olley, E. J. Wren, G. Vamvounis, M. J. Fernee, X. Wang, P. L. Burn, P. Meredith and P. E. Shaw, *Chem. Mater.*, 2011, **23**, 789.

3 (*a*) T. M. Swager, *Acc. Chem. Res.*, 1998, **31**, 201; (*b*) H. Sohn, M. J. Sailor, D. Magde and W. C. Trogler, *J. Am. Chem. Soc.*, 2003, **125**, 3821; (*c*) V. E. Williams and T. M. Swager, *Macromolecules*, 2000, **33**, 4069.

4 (*a*) J.-S. Yang and T. M. Swager, *J. Am. Chem. Soc.*, 1998, **120**, 5321; (*b*) J.-S. Yang and T. M. Swager, *J. Am. Chem. Soc.*, 1998, **120**, 11864; (*c*) D. Zhao and T. M. Swager, *Macromolecules*, 2005, **38**, 9377; (*d*) S. W. Thomas III, G. D. Joly and T. M. Swager, *Chem. Rev.*, 2007, **107**, 1339.

5 (*a*) P. D. Bartlett, M. J. Ryan and S. G. Cohen, *J. Am. Chem. Soc.*, 1942, **64**, 2649; (*b*) H. Hart, S. Shamouilian and Y. Takehira, *J. Org. Chem.*, 1981, **46**, 4427; (*c*) H. Hart, A. Bashir-Hashemi, J. Luo and M. A. Meador, *Tetrahedron*, 1986, **42**, 1641; (*d*) T. M. Long and T. M. Swager, *J. Am. Chem. Soc.*, 2002, **124**, 3826; (*e*) T. M. Swager, *Acc. Chem. Res.*, 2008, **41**, 1181.

6 (*a*) B. Xing, M.-F. Choi and B. Xu, *Chem.–Eur. J.*, 2002, **8**, 5028; (*b*) B. Xing, M.-F. Choi and B. Xu, *Chem. Commun.*, 2002, 362; (*c*) B. Xing, M.-F. Choi, Z. Zhou and B. Xu, *Langmuir*, 2002, **18**, 9654; (*d*) J. B. Beck and S. J. Rowan, *J. Am. Chem. Soc.*, 2003, **125**, 13922; (*e*) Q. Wei and S. L. James, *Chem. Commun.*, 2005, 1555; (*f*) F. Fages, *Angew. Chem., Int. Ed.*, 2006, **45**, 1680; (*g*) G. O. Lloyd and J. W. Steed, *Nat. Chem.*, 2009, **1**, 437; (*h*) M.-O. M. Piepenbrock, G. O. Lloyd, N. Clarke and J. W. Steed, *Chem. Rev.*, 2010, **110**, 1960.

7 (*a*) M. Rybáčková, M. Bělohradský, P. Holý, R. Pohl, V. Dekoj and J. Závada, *Synthesis*, 2007, **10**, 1554; (*b*) T.-L. Chan, T. C. W. Mak, C.-D. Poon, H. N. C. Wong, J. H. Jia and L. L. Wang, *Tetrahedron*, 1986, **42**, 655.

8 The minimum gelator concentration (MGC) was found to be as low as 1.5 wt% (See Fig. S1, ESI†), however, for better rheological response we chose to use ~8.0 wt% DMF gel.

9 Under optimized reaction conditions Cr(III) yielded a dark-green gel material **G2** confirmed by the tube inversion test (Section S2, ESI†).

10 Microanalysis for *trip*-MOF-**1**, $[Co_2(ttc)(DMF)(H_2O)]$, calcd: C, 51.04; H, 3.01; N, 2.20%. Found: C, 51.52; H, 3.12; N, 2.61%.

11 (*a*) V. A. Blatov, L. Carlucci, G. Ciani and D. M. Proserpio, *CrystEngComm*, 2004, **6**, 377; (*b*) V. A. Blatov, A. P. Shevchenko and V. N. Serezhkin, *J. Appl. Crystallogr.*, 2000, **33**, 1193.

12 In addition to the intense fluorescence maxima at 385 nm, relatively less intense peaks were observed in the region of 450–550 nm.

13 No significant difference in the quenching behavior was observed when either the as-prepared Al-gel **G1** or its xerogel was suspended in ethanol.

14 R. Bursi, M. Lankhorst and D. Feil, *J. Comput. Chem.*, 1995, **16**, 545.

15 4-Nitrophenol, Health and Environmental Effects Profile, No. 135, US Environmental Protection Agency, Washington, DC 1980.

16 (*a*) J. C. Sanchez, A. G. DiPasquale, A. L. Rheingold and W. C. Trogler, *Chem. Mater.*, 2007, **19**, 6459; (*b*) J. C. Sanchez and W. C. Trogler, *J. Mater. Chem.*, 2008, **18**, 3143.

17 (*a*) G. He, H. Peng, T. Liu, M. Yang, Y. Zhang and Y. Fang, *J. Mater. Chem.*, 2009, **19**, 7347; (*b*) S. Shanmugaraju, D. Samanta, B. Gole and P. S. Mukherjee, *Dalton Trans.*, 2011, **40**, 12333; (*c*) N. Venkatramaiah, S. Kumar and S. Patil, *Chem. Commun.*, 2012, **48**, 5007.

18 (*a*) A. Lan, K. Li, H. Wu, D. H. Olson, T. J. Emge, W. Ki, M. Hong and J. Li, *Angew. Chem., Int. Ed.*, 2009, **48**, 2334; (*b*) C. Zhang, Y. Che, Z. Zhang, X. Yang and L. Zang, *Chem. Commun.*, 2011, **47**, 2336; (*c*) Z. Zhang, S. Xiang, X. Rao, Q. Zheng, F. R. Fronczek, G. Qian and B. Chen, *Chem. Commun.*, 2010, **46**, 7205; (*d*) S. Pramanik, C. Zheng, X. Zhang, T. J. Emge and J. Li, *J. Am. Chem. Soc.*, 2011, **133**, 4153; (*e*) B. Gole, A. K. Bar and P. S. Mukherjee, *Chem. Commun.*, 2011, **47**, 12137.

Electronic Supplementary Information (22 pages)

Triptycene based luminescent metal-organic gels for chemosensing

Samir Barman, Jai Anand Garg, Olivier Blacque, Koushik Venkatesan,* and Heinz Berke*

Department of Inorganic Chemistry, University of Zürich, Winterthurerstrasse 190, CH-8057, Zürich (Switzerland)
E-mail: venkatesan.koushik@aci.uzh.ch (K. V.), hberke@aci.uzh.ch (H. B.), Fax: (+41) 44-635-6802

Table of Contents

Section S1 *Materials and General Procedures*

All solvents and reagents were purchased commercially and, unless otherwise noted, were used without further purification. Microanalyses were carried out at the Anorganisch-Chemisches Institut of the University of Zurich. FTIR spectra were obtained by using a Bio-Rad FTS-45 FTIR spectrometer. The powder XRD patterns were obtained with a Bruker D8 Advance system equipped with a Cu sealed tube (λ = 1.5406 Å). The following conditions were applied: 40 kV, 40 mA, increment = 0.007°, scan speed = 1.5 s/step. The simulated powder pattern was calculated from the single crystal X-ray diffraction data and generated with Mercury 2.3 software. All TGA experiments were performed under a N_2 atmosphere from 25 - 800 °C at a temperature ramp rate of 1 °C/min. Scanning Electron Microscopy (SEM) was recorded in a JEOL, JMS-6700F, field emission scanning electron microscope. Rheology experiments were performed in an SDT Q series advanced rheometer AR 2000.

Section S2 *Synthesis*

Synthesis of 1,4,5,8-triptycenetetracarboxylic acid was accomplished according to the Scheme S1 following multi-step synthetic procedure reported in the literature.[S1,S2]

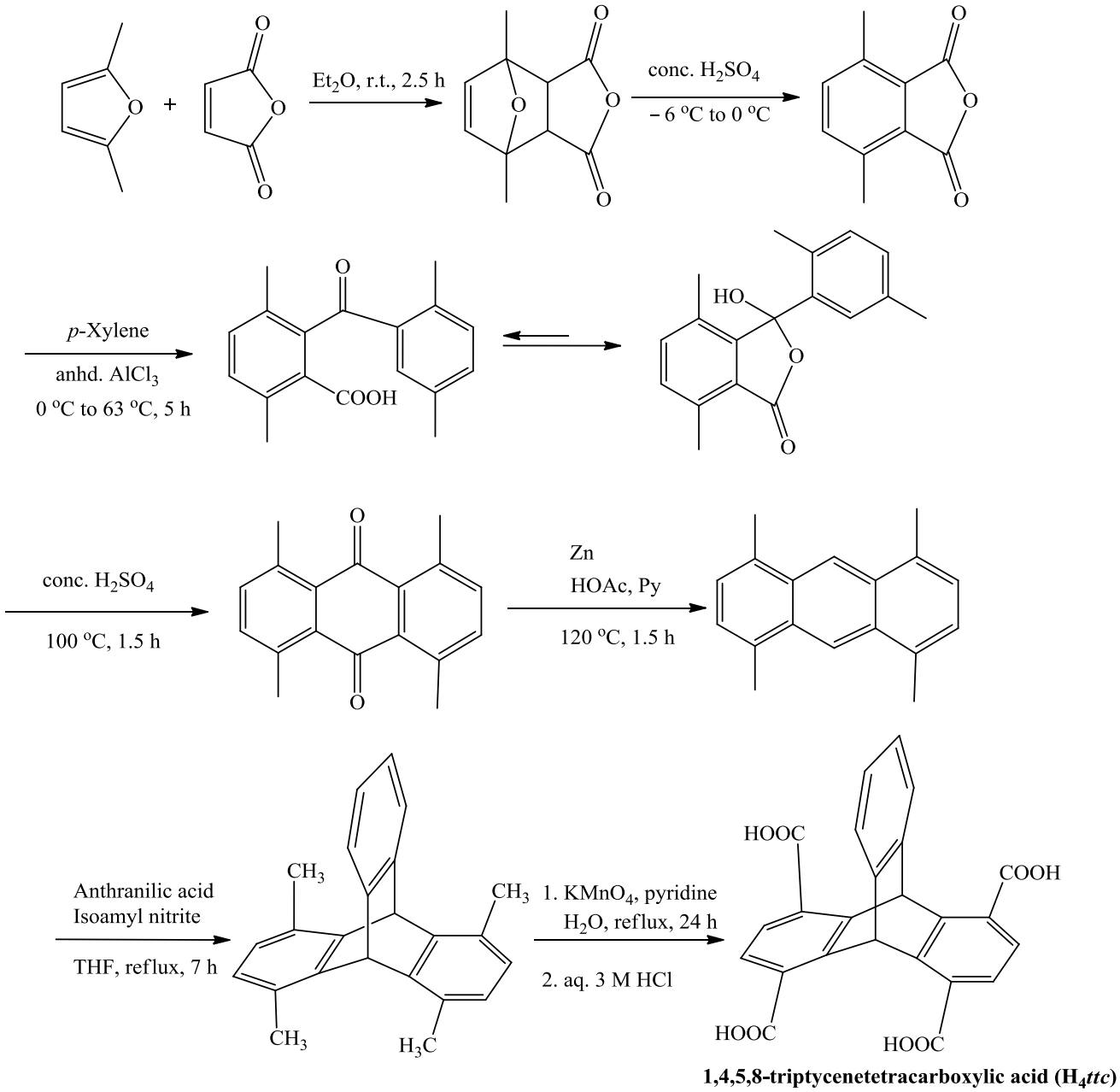

Scheme S1. Synthesis of 1,4,5,8-triptycenetetracarboxylic acid (H_4ttc).

Synthesis of Al-Gel G1.

$Al(NO_3)_3 \cdot 9H_2O$ (0.054 g, 0.144 mmol) and 1,4,5,8-triptycenetetracarboxylic acid (0.03 g, 0.069 mmol) were dissolved in 1 mL of DMF in a 2 mL glass vial. After capping tightly, the vial was heated to 125 °C at a rate of 2 °C/min for 5-20 h in an isothermal oven to yield the opaque Al-gel **G1** (Fig. S2).

Microanalysis of the xerogel (air dried gel), Found: C, 33.24; H, 5.68; N, 11.9%.

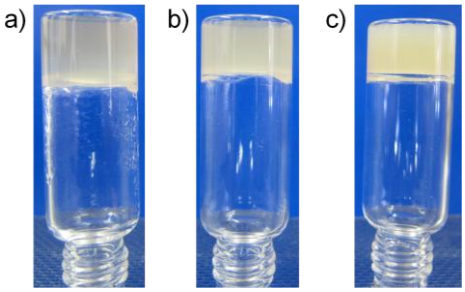

Fig. S1. The photo of as-prepared Al-gel obtained when the overall concetration (w/v) of 1.5 wt% (a), 2.5 wt% (b) and 5 wt% (c) (considering all the reactants) was employed.

Synthesis of Cr-Gel G2.

$Cr(NO_3)_3 \cdot 9H_2O$ (0.057 g, 0.135 mmol) and 1,4,5,8-triptycenetetracarboxylic acid (0.03 g, 0.069 mmol) were dissolved in 2 mL of DMF in a 4 mL glass vial. After capping tightly, the vial was heated to 125 °C at a rate of 2 °C/min for 5-20 h in an isothermal oven to yield the dark-green Cr-gel material **G2** (Fig. S2).

Microanalysis of the Cr-xerogel (air dried gel), Found: C, 33.48; H, 5.51; N, 11.55%.

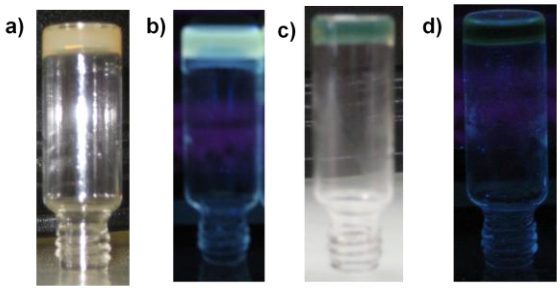

Fig. S2. The photo of as-prepared Al-gel **G1** (a), Al-gel **G1** under uv lamp (b) and as-prepared Cr-gel **G2** (c) and Cr-gel **G2** under uv lamp (d).

Synthesis of *trip*-MOF-1 [Co_2(*ttc*)(DMF)(H_2O)] (*ttc* = 1,4,5,8-triptycenetetracarboxylate).

$Co(NO_3)_2 \cdot 6H_2O$ (0.020 g, 0.069 mmol) and 1,4,5,8-triptycenetetracarboxylic acid (0.020 g, 0.046 mmol) were dissolved in 0.6 mL of DMF in a 2 mL glass vial. After capping tightly, the vial was heated to 125 °C at a rate of 2 °C/min for 20 h in an isothermal oven. The vial containing dark purple crystals were removed from the mother liquor and washed with DMF (3 × 5 mL) [yield: 0.015 g, 51% based on 1,4,5,8-triptycenetetracarboxylic acid]. Elemental analysis calcd (%) for $C_{27}H_{19}Co_2NO_{10}$ = [Co_2(*ttc*)(DMF)(H_2O)]: C 51.04, H 3.01, N 2.20; found C, 51.52; H, 3.12; N, 2.61.

Section S3 *Crystallographic Data*

Single X-Ray Crystal Diffraction Studies on *trip*-MOF-1

Single-crystal X-ray diffraction data was collected at 183(2) K on a Xcalibur diffractometer (Agilent Technologies, Ruby CCD detector) using a single wavelength Enhance X-ray source with MoKα radiation, λ = 0.71073 Å.[S3] The selected suitable single crystal was mounted using polybutene oil on the top of a glass fiber fixed on a goniometer head and immediately transferred to the diffractometer. Pre-experiment, data collection, analytical absorption correction,[S4] and data reduction were performed with the Oxford program suite CrysAlisPro.[S3] The crystal structure was solved with SHELXS97[S5] using direct methods and was refined by full-matrix least-squares methods on F2 with SHELXL97.[S5] All programs used during the crystal structure determination process are included in the WINGX software.[S6] The program PLATON[S7] was used to check the result of the X-ray analysis.

CCDC 872964 contain the supplementary crystallographic data for this paper. These data can be obtained free of charge from The Cambridge Crystallographic Data Centre via www.ccdc.cam.ac.uk/data_request/cif

Table S1. Summary of the X-ray diffraction studies of *trip*-MOF-**1**.

	trip-MOF-**1**
empirical formula	$C_{27}H_{19}Co_2NO_{10}$
formula weight ($g \cdot mol^{-1}$)	635.29
temperature (K)	183(2)
wavelength (Å)	0.71073
crystal system, space group	Monoclinic, C 2/ *c*
a (Å)	17.1691(5)
b (Å)	11.0334(5)
c (Å)	16.3274(6)
α (°)	90
β (°)	98.302(3)
γ (°)	90
volume ($Å^3$)	3060.5(2)
Z, density (calcd) ($Mg \cdot m^{-3}$)	4, 1.379
abs coefficient (mm^{-1})	1.135
F(000)	1288
crystal size (mm^3)	0.23 x 0.08 x 0.02
θ range (°)	2.45 to 25.00
reflections collected	9118
reflections unique	2691 [*R*(int) = 0.0246]
completeness to θ (%)	99.9
absorption correction	analytical
max/min transmission	0.975 / 0.864
data / restraints / parameters	1970 / 12 / 254
goodness-of-fit on F^2	1.107
final R_1 and wR_2 indices [$I > 2\sigma(I)$]	0.0756, 0.2135
R_1 and wR_2 indices (all data)	0.1048, 0.2256
largest diff. peak and hole ($e.Å^{-3}$)	0.796, -0.728

The unweighted R-factor is $R_1 = \sum(Fo - Fc)/\sum Fo$; $I > 2\sigma(I)$ *and the weighted R-factor is* $wR_2 = \{\sum w(Fo^2 - Fc^2)^2/\sum w(Fo^2)^2\}^{1/2}$.

Section S4 *Powder X-Ray Diffraction Patterns*

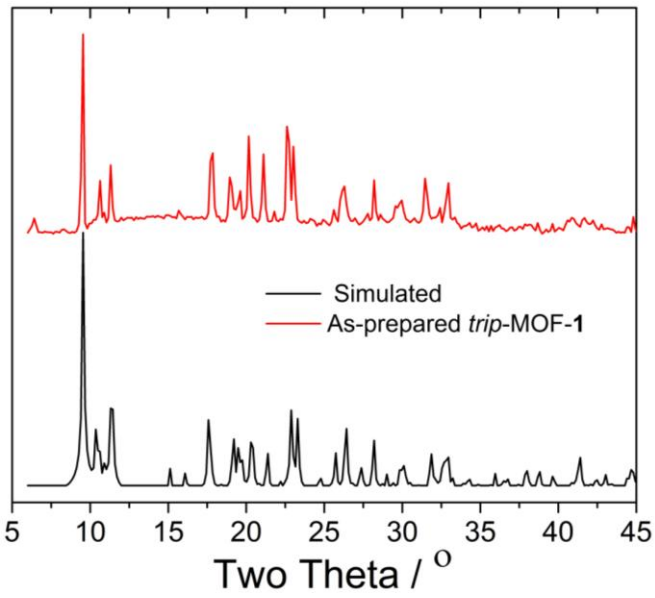

Fig. S3. Powder X-ray diffraction patterns: simulated from the single crystal X-ray structure of *trip*-MOF-**1** (black) and as-prepared *trip*-MOF-**1** (red).

Section S5 *IR Spectra*

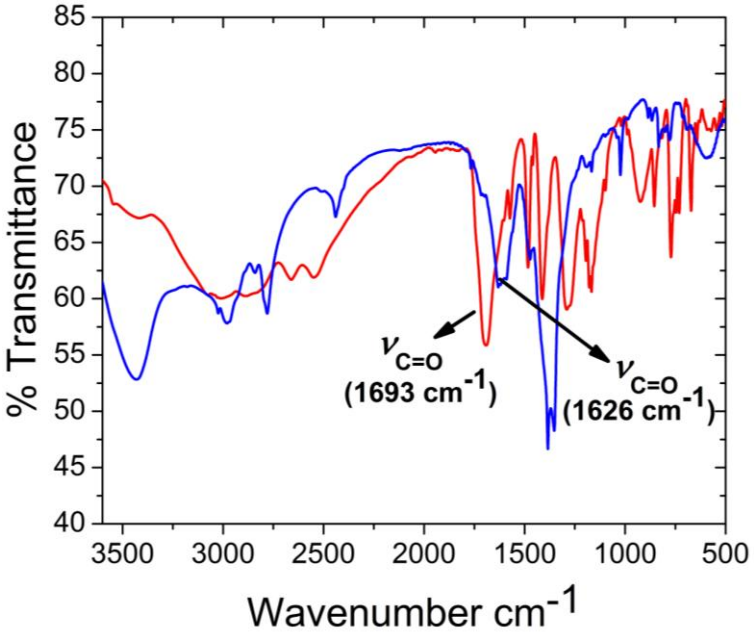

Fig. S4. FT-IR spectra of the xerogel of Al-gel **G1** (blue) and the ligand H_4*ttc* (red).

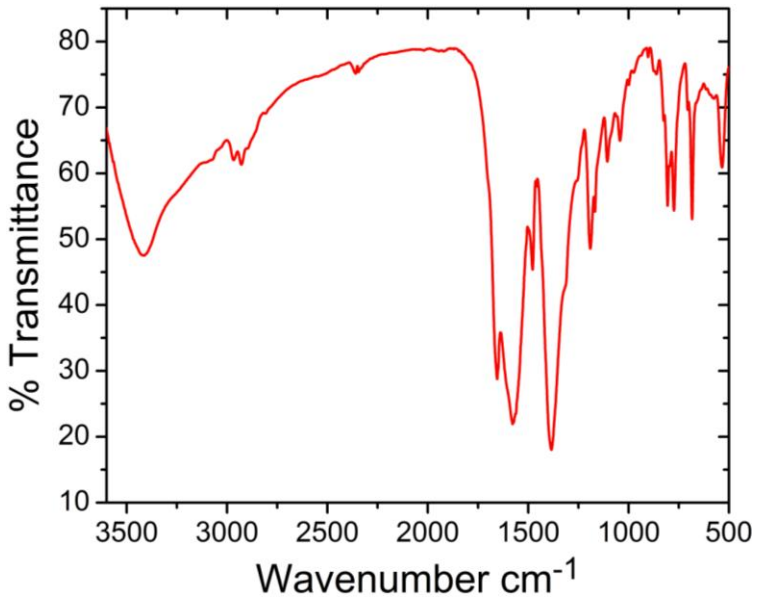

Fig. S5. FT-IR spectrum of as-prepared *trip*-MOF-**1**.

Section S6 *Thermal Gravimetric Analysis*

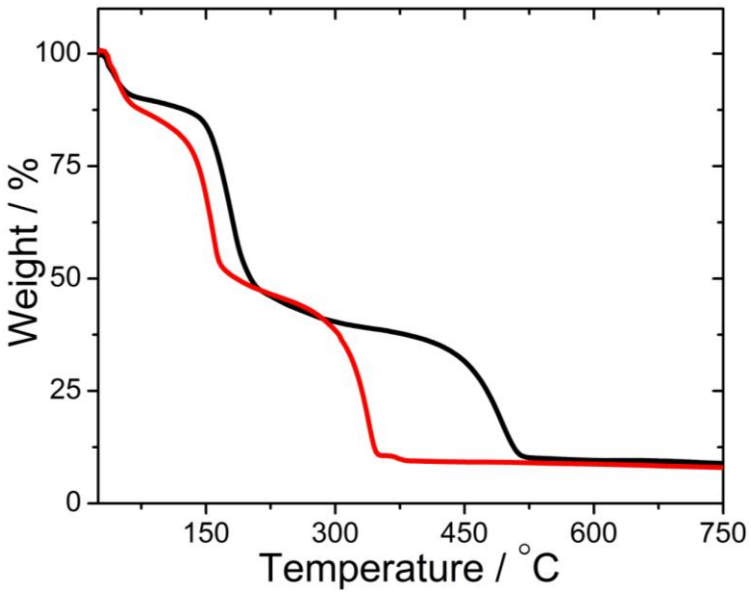

Fig. S6. TGA trace of xerogels (air dried) of as-prepared Al-gel **G1** (black) and as-prepared Cr-gel **G2** (red).

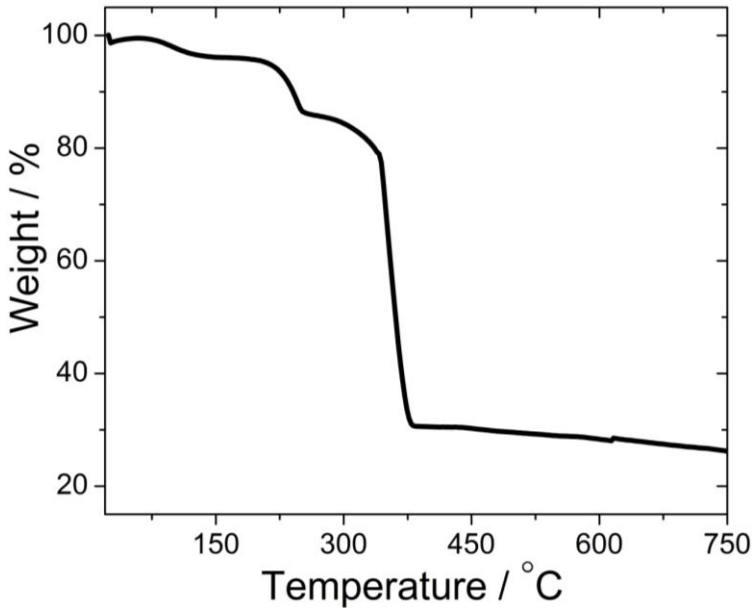

Fig. S7. TGA trace of as-prepared *trip*-MOF-**1**.

Section S7 *Photophysical Study*

Preparation of stock solutions: In a typical preparation of stock solution for the Al-gel **G1** and Cr-gel **G2**, approximately 5 mg of as-prepared gel materials (or 0.20 mg of their corresponding xerogels) were suspended in 2 mL of ethanol and allowed to stir at room temperature for at least 20 hrs to give cloudy white and light green suspensions respectively. In the case of *trip*-MOF-**1**, the as-prepared MOF crystals (1 mg) were thoroughly washed with ethanol and solvent decanted. The crystals were then placed in an empty vial containing 5 mL of fresh ethanol which was then allowed to crush mechanically by vigorous stirring with a stir bar at room temperature for 20 hrs to generate a purple cloudy suspension of *trip*-MOF-**1**. The resulting suspension of gels/crystals were then carefully stored under sealed conditions.

The steady-state fluorescence spectra as well as the quenching experiments with different analytes were carried out by subsequently placing 2 mL of individual stock solutions in quartz cell of 1 cm width while stirring. All the titrations were carried out by gradually adding quenchers (analytes) (1 mM) solution in an incremental fashion. Their corresponding fluorescence emission spectra were recorded at 298 K. Each titration was repeated at least three times to get concordant value. For all measurements, dispersed solution of the receptors were

excited at λ_{ex} = 318 nm and their corresponding emission wavelength was monitored from λ_{em} = 340 nm to 580 nm.

For estimating the Stern-Volmer binding constant, exactly 2 mL of the above mentioned stock solution of the individual receptors were used for the titration. The emission intensity was recorded 10 minutes after the addition of the analytes under stirring conditions in order to ensure sufficient time for the diffusion of quenchers to the receptors.

The Stern-Volmer equation $I_o/I = 1+ K_{sv}[Q]$, where I_o, I are the fluorescence intensity before and after addition of the quencher, K_{sv} is the Stern-Volmer quenching rate constant and [Q] is the concentration of the quenchers, was used for the determination of the binding constant.

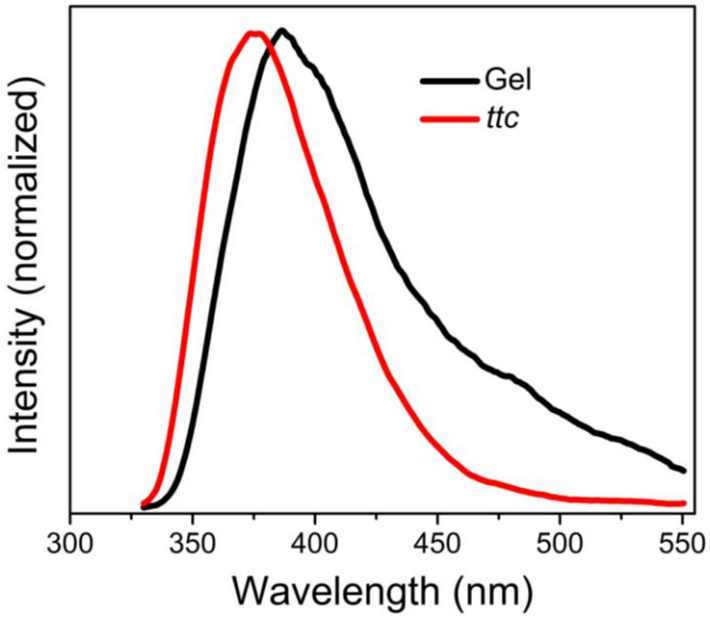

Fig. S8. Emission spectra of H_4*ttc* (red) dispersed in ethanol followed by addition of few drops of DMF (excited at 315 nm) and of ethanol dispersed Al-gel **G1** (black) (excited at 318 nm).

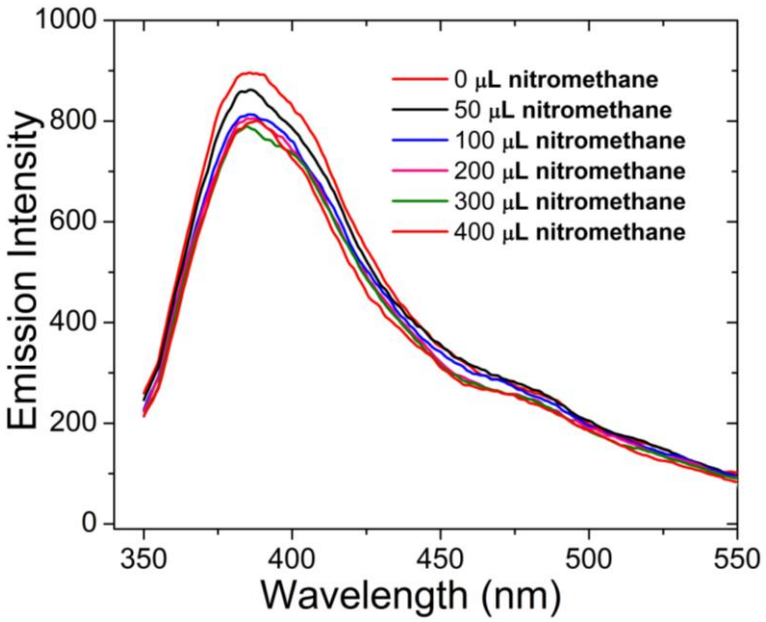

Fig. S9. Fluorescence titration of Al-gel **G1** dispersed in ethanol with the addition of different volume of 1 mM solution of nitromethane in ethanol.

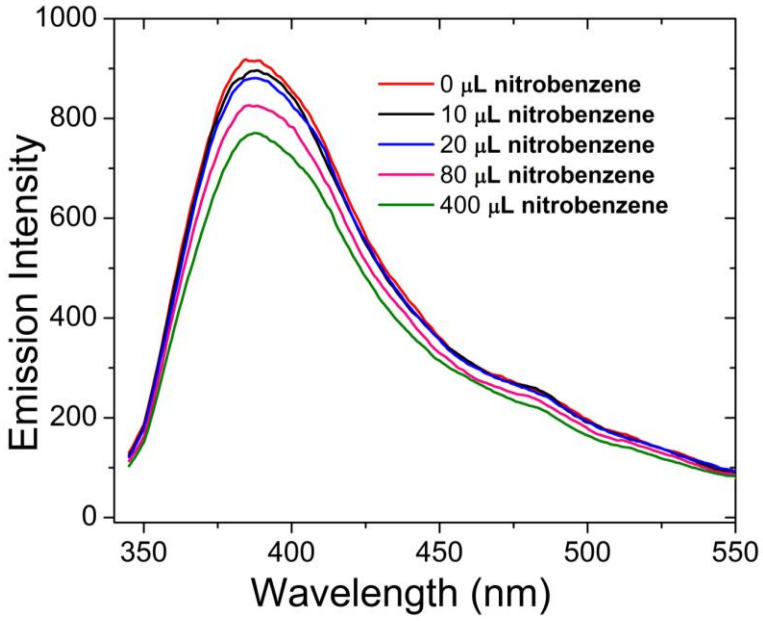

Fig. S10. Fluorescence titration of Al-gel **G1** dispersed in ethanol with the addition of different volume of 1 mM solution of nitrobenzene in ethanol.

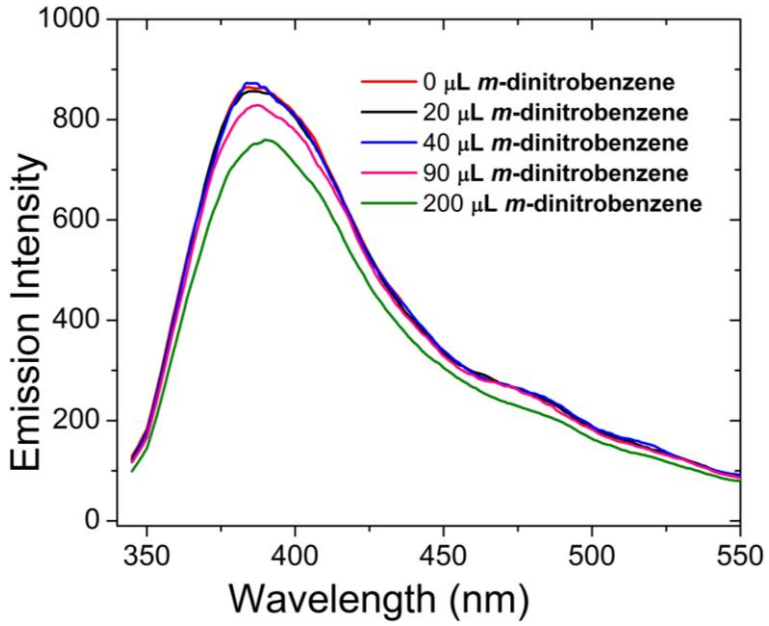

Fig. S11. Fluorescence titration of Al-gel **G1** dispersed in ethanol with the addition of different volume of 1 mM solution of *m*-dinitrobenzene in ethanol.

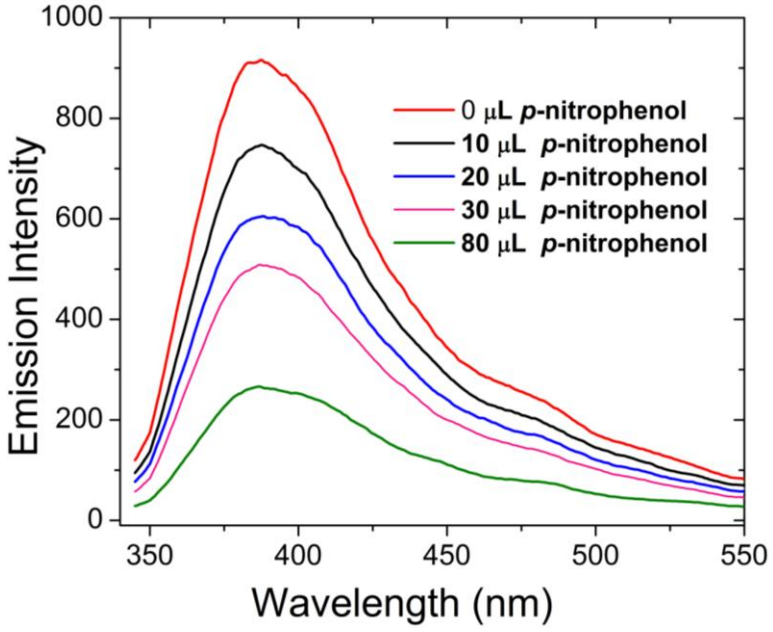

Fig. S12. Fluorescence titration of Al-gel **G1** dispersed in ethanol with the addition of different volume of 1 mM solution of *p*-nitrophenol in ethanol.

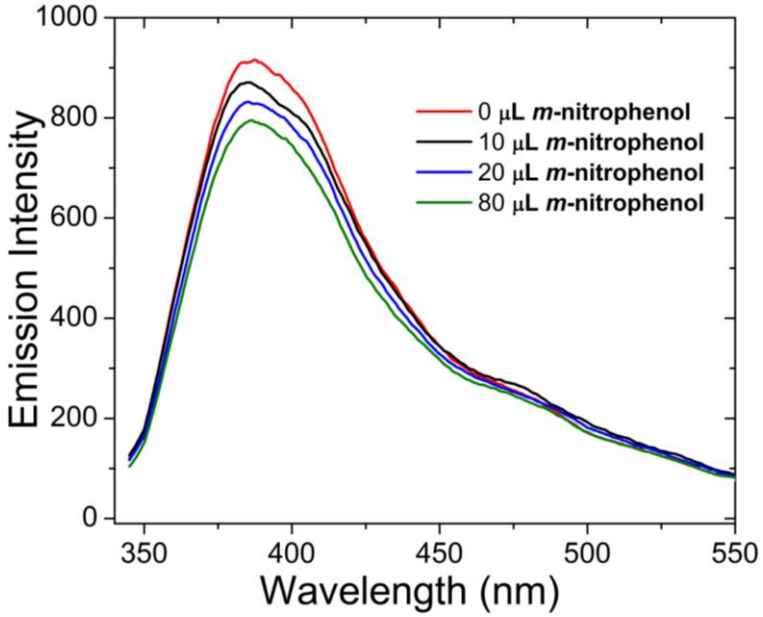

Fig. S13. Fluorescence titration of Al-gel **G1** dispersed in ethanol with the addition of different volume of 1 mM solution of *m*-nitrophenol in ethanol.

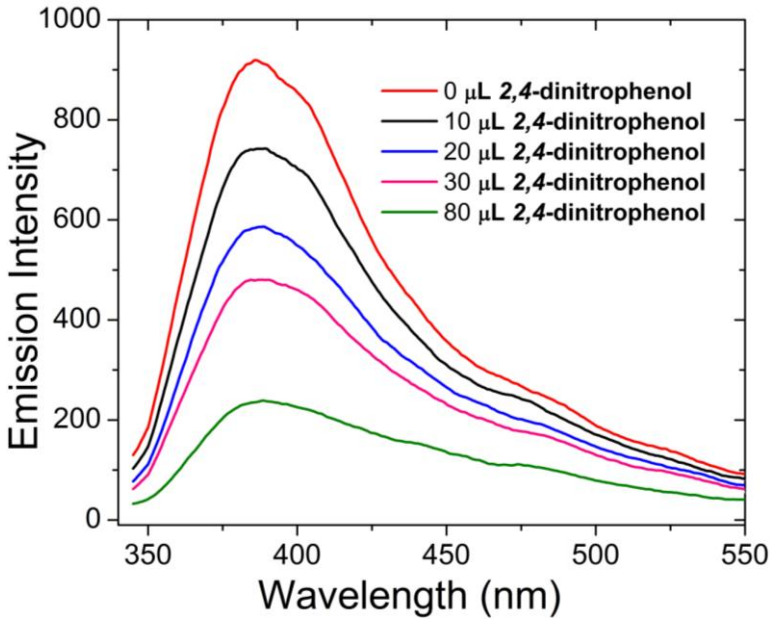

Fig. S14. Fluorescence titration of Al-gel **G1** dispersed in ethanol with the addition of different volume of 1 mM solution of 2,4-dinitrophenol in ethanol.

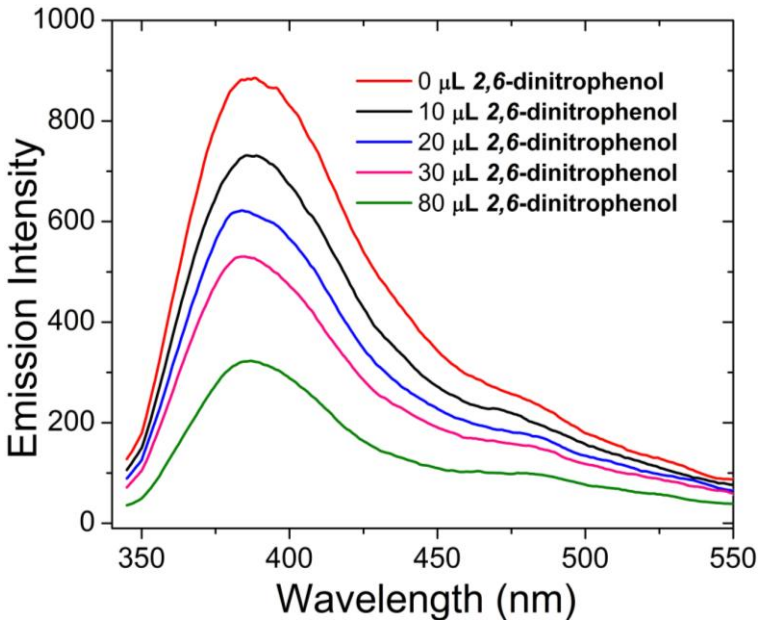

Fig. S15. Fluorescence titration of Al-gel **G1** dispersed in ethanol with the addition of different volume of 1 mM solution of 2,6-dinitrophenol in ethanol.

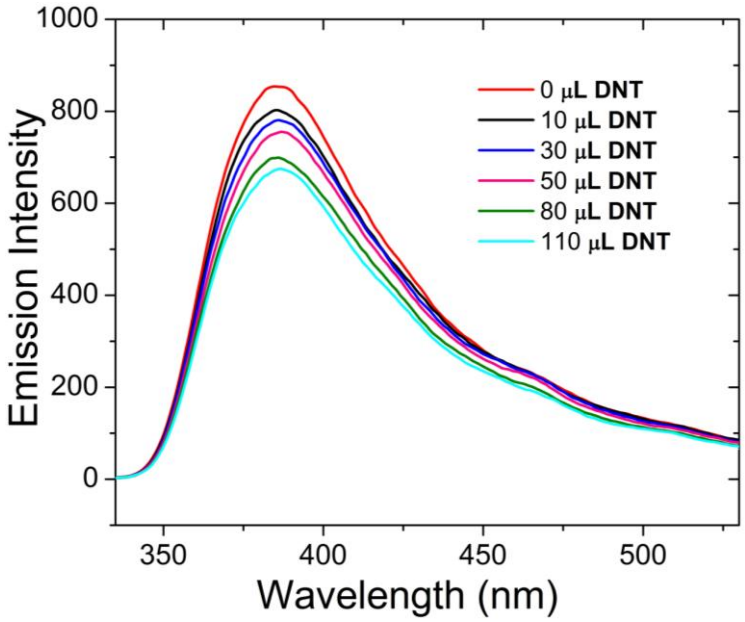

Fig. S16. Fluorescence titration of Al-gel **G1** dispersed in ethanol with the addition of different volume of 1 mM solution of 2,4-dinitrotoluene (2,4-DNT) in ethanol.

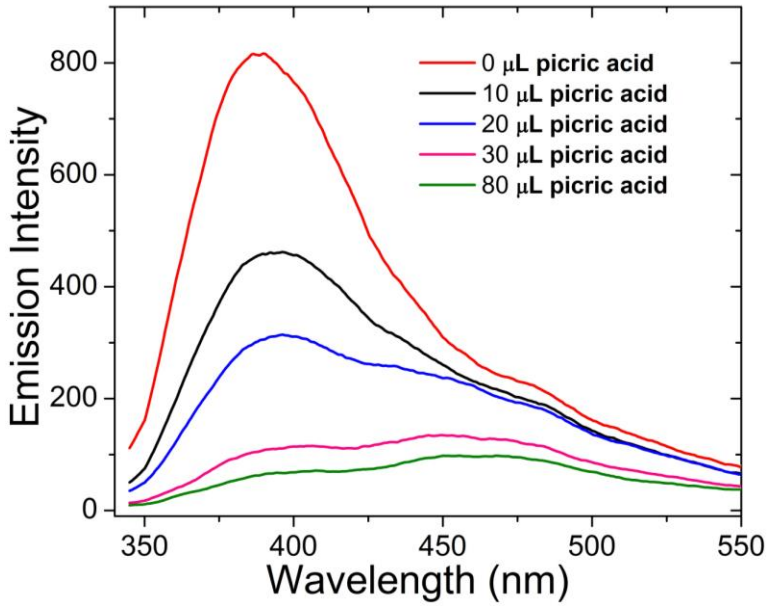

Fig. S17. Fluorescence titration of Al-gel **G1** dispersed in ethanol with the addition of different volume of 1 mM solution of picric acid in ethanol.

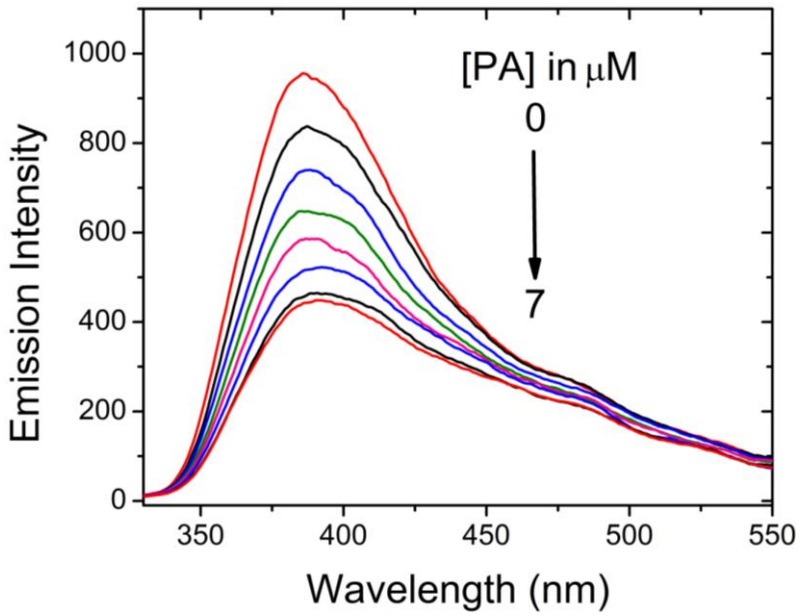

Fig. S18. Fluorescence titration of Al-gel **G1** dispersed in ethanol with the addition of various concentration of PA.

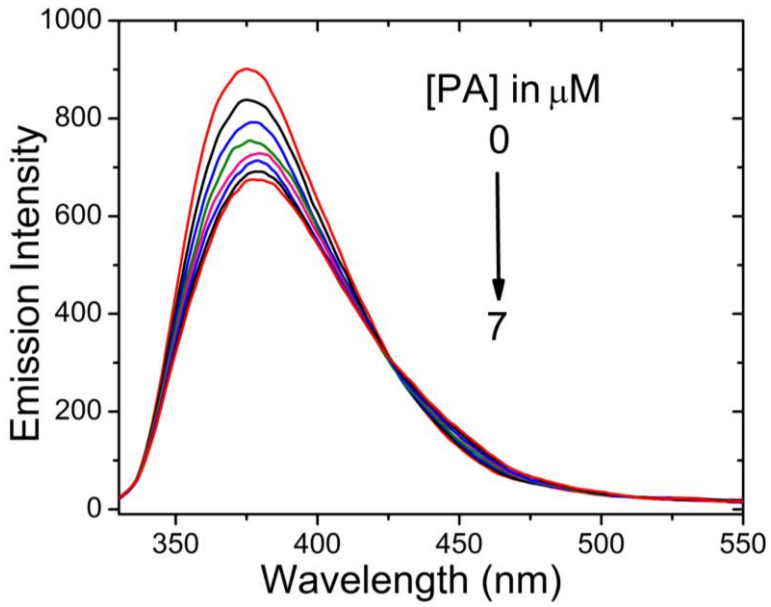

Fig. S19. Fluorescence titration of H_4*ttc* suspended in ethanol with the addition of various concentration of PA (excited at 315 nm).

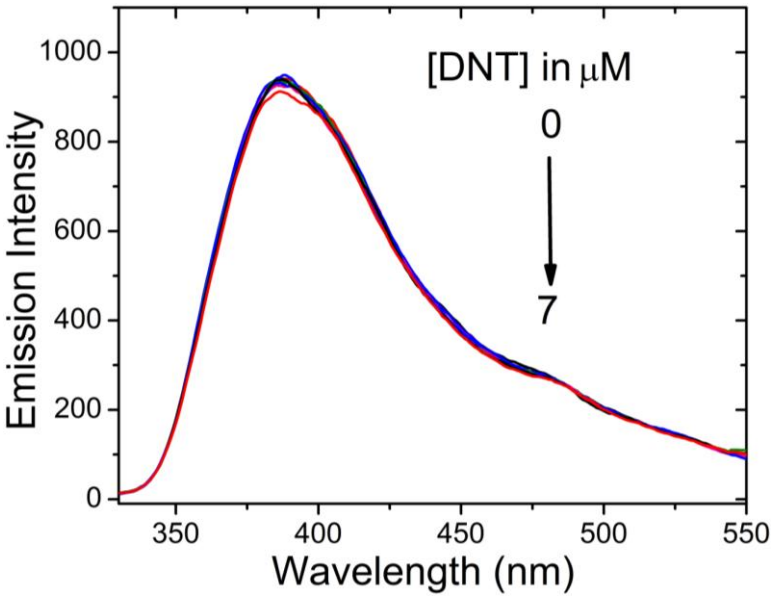

Fig. S20. Fluorescence titration of Al-gel **G1** dispersed in ethanol with the addition of various concentration of 2,4-DNT.

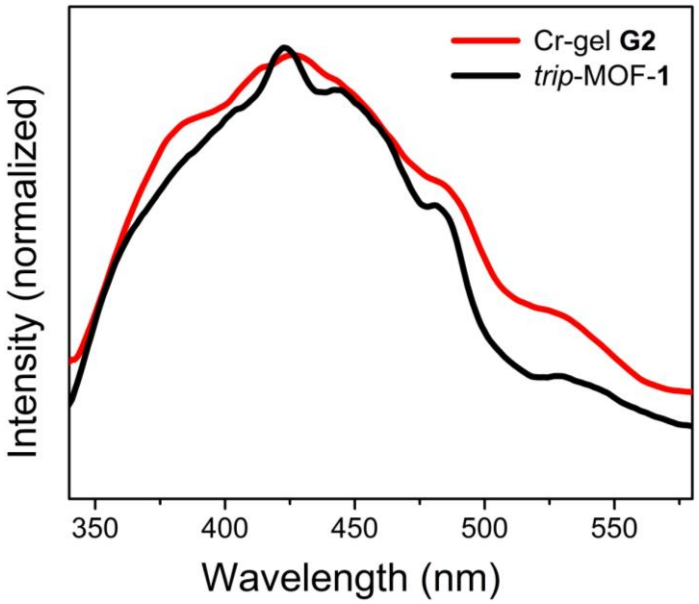

Fig. S21. Emission spectra of ethanol dispersed Cr-gel **G2** (red) and *trip*-MOF-**1** (black) (excited at 318 nm).

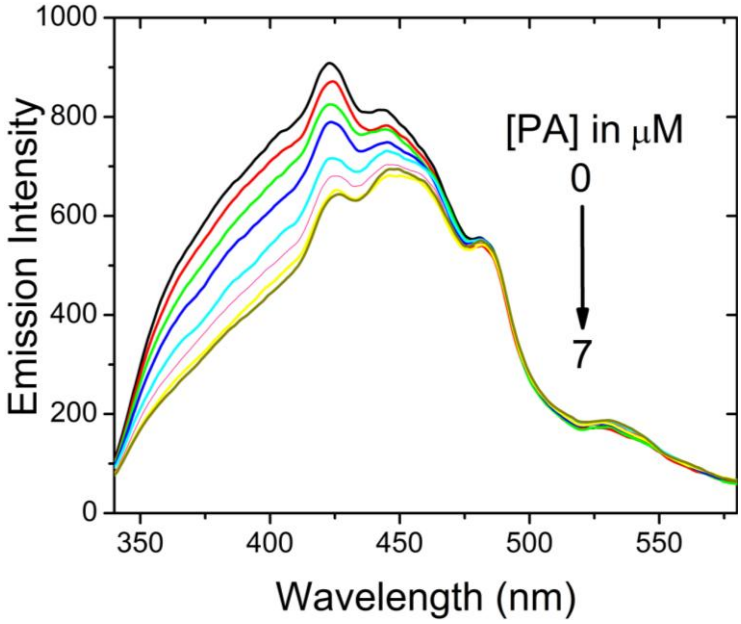

Fig. S22. Fluorescence titration of *trip*-MOF-**1** dispersed in ethanol with the addition of various concentration of PA.

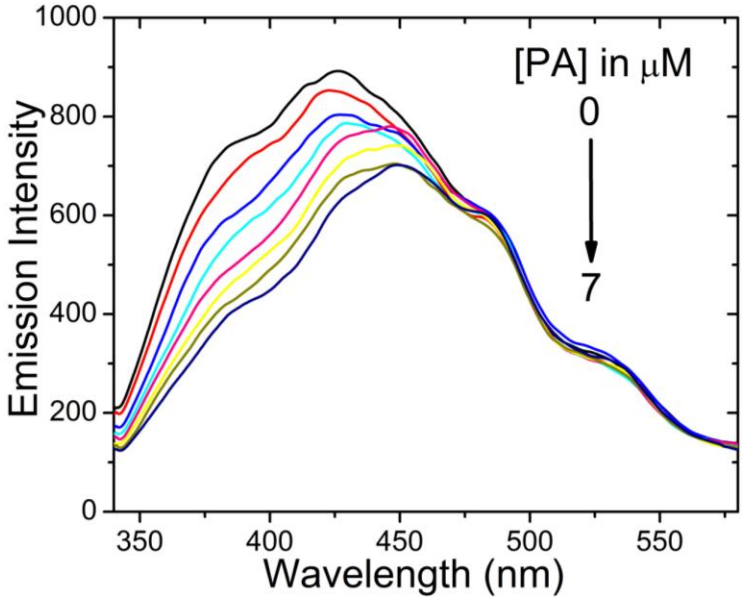

Fig. S23. Fluorescence titration of Cr-gel **G2** dispersed in ethanol with the addition of various concentration of PA.

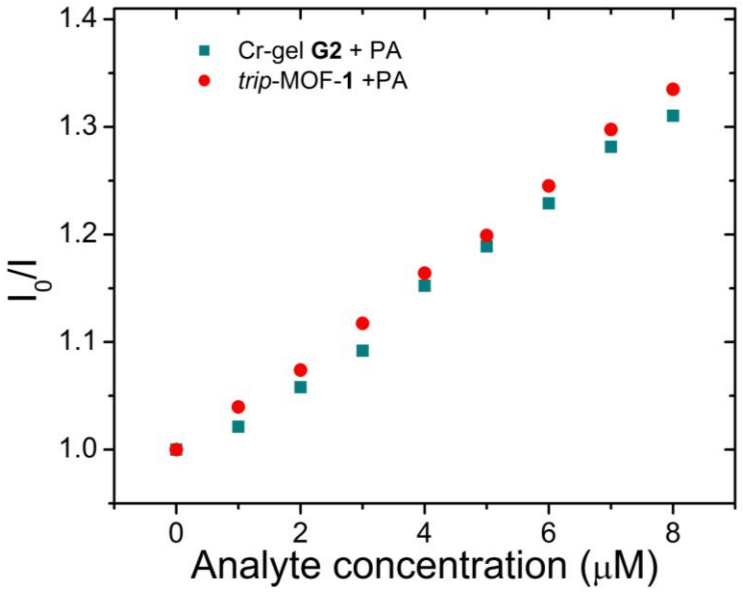

Fig. S24. The Stern-Volmer plots for the titration of Cr-gel **G2** (dark cyan square) and *trip*-MOF-**1** (red circle) with PA.

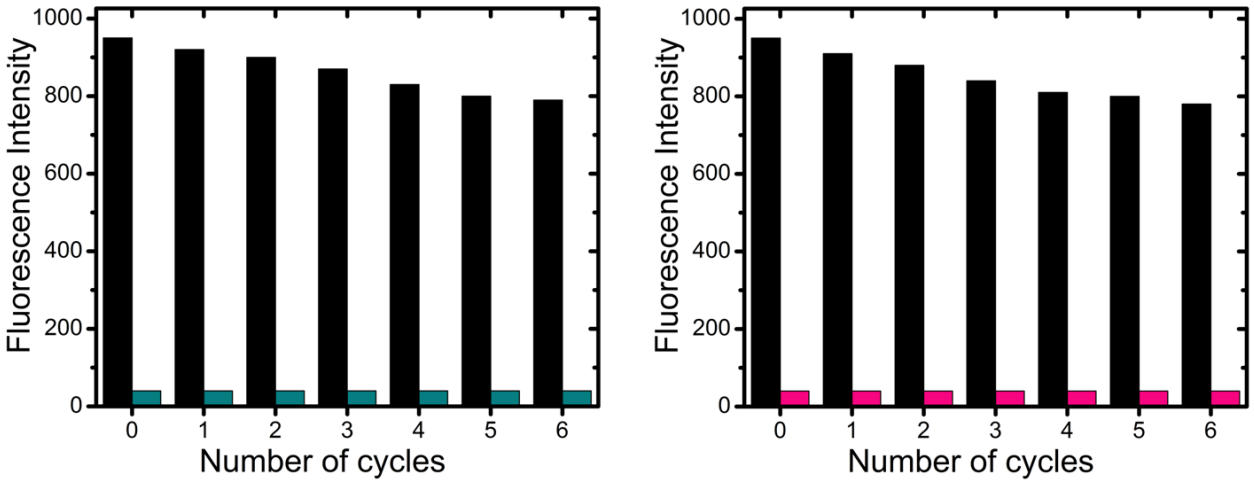

Fig. S25. Reproducibility of the quenching ability of *trip*-MOF-**1** (left) and Cr-gel **G2** (right) dispersed in ethanol to picric acid (PA) solution. The materials were recovered by centrifuging after each experiment and washed several times (4-5) with ethanol. The black bars (for both the materials) represent the initial fluorescence intensities where as the corresponding dark cyan and pink bars represent the intensities of *trip*-MOF-**1** and Cr-gel **G2 a**fter the addition of 100 μL (1 mM) of a solution of PA, respectively.

Solid state fluorescence study

Saturated vapour of nitrobenzene (NB), 2,4-dinitrotoluene (2,4-DNT), and picric acid (PA) were generated by keeping the analyte compounds in a sealed tube for three days to ensure that the equilibrated vapour pressure is reached. The solid state fluorescence quenching study was carried out by keeping the quartz plate coated with a thin film of Al-xerogel (prepared by smearing the as-prepared Al-gel **G1** in quartz plate followed by drying in air for 24 h at room temperature) in sealed tubes containing analytes for specific time. The fluorescence spectra of the exposed films (Fig. S26) were recorded immediately after taking out from the sealed tube without any delay.

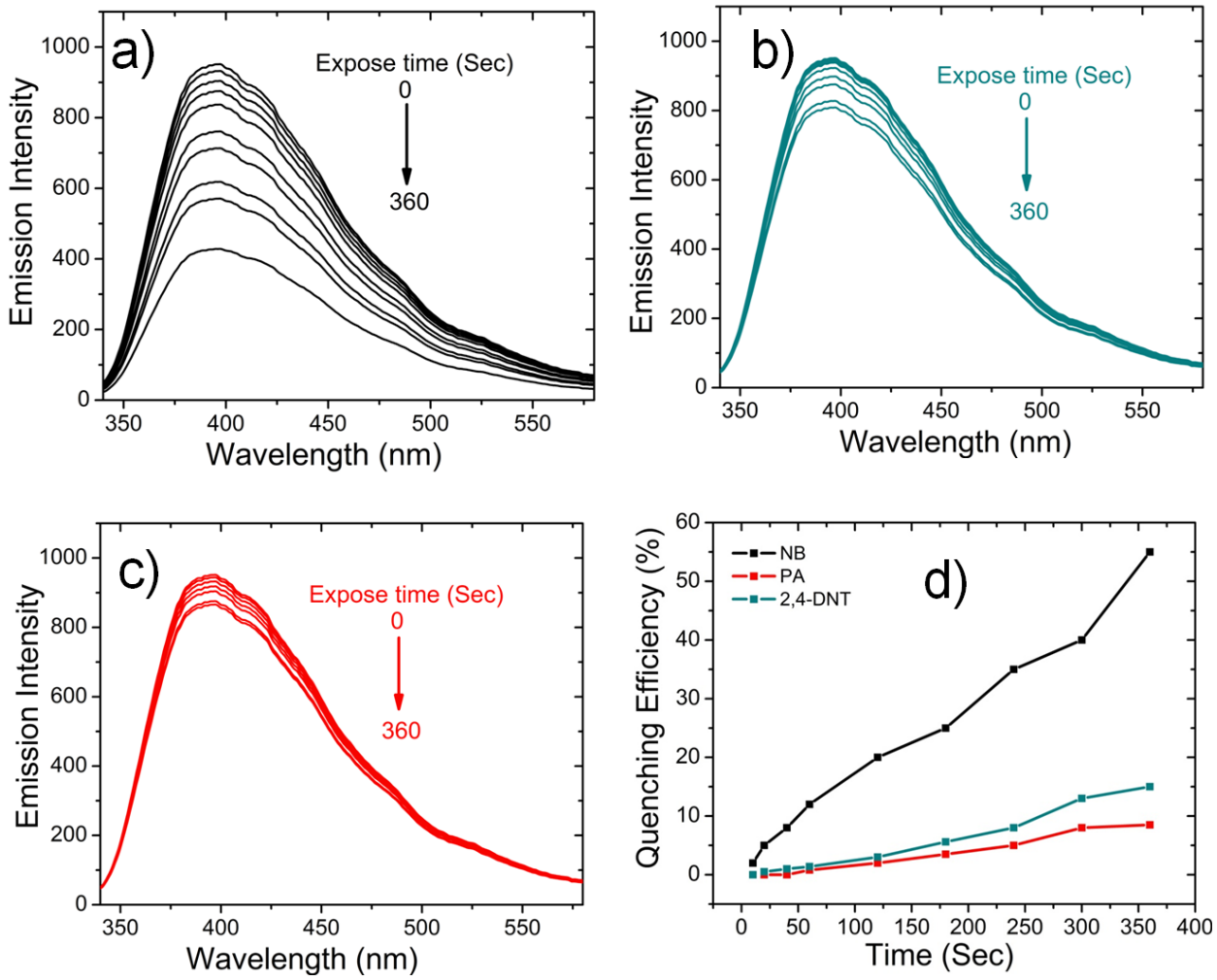

Fig. S26. The time dependent emission spectra of Al-gel **G1** thin film upon exposure to saturated vapors of nitro benzene (a), 2,4-DNT (b) and PA (c). Plot of the solid state fluorescence quenching efficiency of NB (d, black), 2,4-DNT (d, dark cyan) and PA (d, red) at different time (sec) interval.

Section S8 *Computational Data*

To gain deeper understanding for the superior quenching of the luminescence intensity of Al-gel **G1** by PA over 2,4-DNT (reflected by the relatively high Stern-Volmer binding constant determined for PA), we resorted to perform density functional theory (DFT) calculations at the B3LYP/6-31G(d) level (Fig. S27). For simplicity we used discrete ligand (H_4*ttc*) as model compound. The calculation indeed revealed that the LUMO energy of PA (-3.89 eV) is much lower than that of 2,4-DNT (-2.97 eV) with respect to the LUMO energy of H_4*ttc* (-1.85 eV) favouring strong electron transfer in the case of PA.

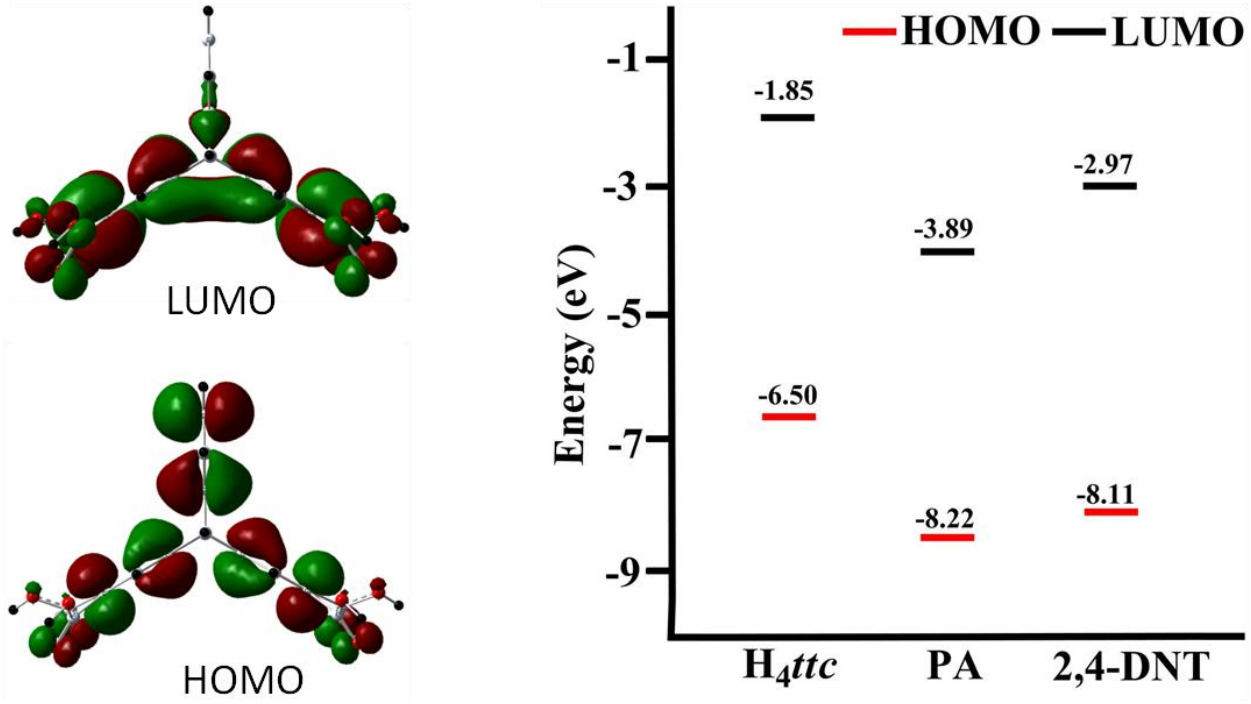

Fig. S27. HOMO (left, bottom) and LUMO (left, top) of H_4*ttc* and the energy levels (right) calculated for H_4*ttc*, PA and DNT at the B3LYP/6–31G(d) level of theory with Gaussian09[S8].

Section S9 *References*

[S1] M. Rybáčková, M. Bělohradský, P. Holý, R. Pohl, V. Dekoj and J. Závada, *Synthesis* 2007, **10**, 1554.

[S2] T.-L. Chan, T. C. W. Mak, C.-D. Poon, H. N. C. Wong, J. H. Jia and L. L. Wang, *Tetrahedron*, 1986, **42**, 655.

[S3] Agilent Technologies (formerly Oxford Diffraction), Yarnton, England, 2011.

[S4] R. C. Clark and J. S. Reid, *Acta Crystallogr.*, 1995, **A51**, 887.

[S5] G. M. Sheldrick, *Acta Crystallogr. Sect. A*, 2008, **64**, 112.

[S6] L. J. Farrugia, *J. Appl. Crystallogr.*, 1999, **32**, 837.

[S7] A. L. Spek, *J. Appl. Crystallogr.*, 2003, **36**, 7.

[S8] Gaussian 09, Revision B.01, M. J. Frisch, G. W. Trucks, H. B. Schlegel, G. E. Scuseria, M. A. Robb, J. R. Cheeseman, G. Scalmani, V. Barone, B. Mennucci, G. A. Petersson, H. Nakatsuji, M. Caricato, X. Li, H. P. Hratchian, A. F. Izmaylov, J. Bloino, . Zheng, J. L. Sonnenberg, M. Hada, M. Ehara, K. Toyota, R. Fukuda, J. Hasegawa, M. Ishida, T. Nakajima, Y. Honda, O. Kitao, H. Nakai, T. Vreven, J. A. Montgomery, Jr., J. E. Peralta, F. Ogliaro, M. Bearpark, J. J. Heyd, E. Brothers, K. N. Kudin, V. N. Staroverov, T. Keith, R. Kobayashi, J. Normand, K. Raghavachari, A. Rendell, J. C. Burant, S. S. Iyengar, J. Tomasi, M. Cossi, N. Rega, J. M. Millam, M. Klene, J. E. Knox, J. B. Cross, V. Bakken, C. Adamo, J. Jaramillo, R. Gomperts, R. E. Stratmann, O. Yazyev, A. J. Austin, R. Cammi, C. Pomelli, J. W. Ochterski, R. L. Martin, K. Morokuma, V. G. Zakrzewski, G. A. Voth, P. Salvador, J. J. Dannenberg, S. Dapprich, A. D. Daniels, O. Farkas, J. B. Foresman, J. V. Ortiz, J. Cioslowski, and D. J. Fox, Gaussian, Inc., Wallingford CT, 2010.

10. SUMMARY

The research presented in this dissertation explores new chemical strategies to construct chemically tuned metal-organic materials (MOMs) in terms of increase in polarization to achieve improved hydrogen storage capacities and enthalpy of hydrogen adsorption. In addition, we have developed a novel method for postsynthetic modification of amine functionalized materials to introduce polarizing groups under gas-solid phase reactions. Furthermore, a new approach of incorporating high concentration of vacant metal binding sites has been investigated.

In another part of the thesis, we have employed 3D shape-persistent organic receptor comprising of triptycene tetracarboxylate for the highly selective and sensitive detection of explosives *via* photo induced electron transfer quenching mechanism.

As could be seen from the motivations of the thesis, one of the primary goal of our research focused on careful selection of rigid organic building blocks to construct open framework materials, which were thought to create the potential for kinetic trapping of hydrogen molecules through additionally by secondary binding forces, such as advanced polar binding by dipole-dipole or dipole-induced dipole interactions. In this context, two internally polarized ditopic organic linkers namely 1,3- and 2,6-azulenedicarboxylate possessing azulene back bone were employed to construct the open frameworks with different structural motifs.

Indeed, the utilization of angular ditopic linker, 1,3-azulenedicarboxylic acid, permitted the assembly of two unique metal-organic materials namely, MOF-645 and MOF-646 with polarized pore walls. The MOF-645 represents a 3D framework with **bcu** net topology which is constructed from unique pentanuclear zinc(II) clusters: $Zn_5(\mu_3\text{-}OH)_2(O_2C)_8(DMF)(H_2O)$. Although MOF-645 possesses potentially moderate accessible void space of about 40% as could be calculated after removal of the coordinated and non coordinated solvent molecules. Our attempts to activate MOF-645 failed due to the loss of structural integrity as evidenced from PXRD experiments. On the other hand, MOF-646 showed a rarely observed **lcy** net topology, which is different from the topology (**pcu)** observed for IRMOFs with Zn_4O unit despite their identical chemical formula. This could be presumed to be due to the bent nature of the ditopic linker. The variation in the underlying net topology from **pcu** (the topology of IRMOFs) to **lcy** resulted in smaller pore size distribution of MOF-646 with interconnected polarized pores. Unlike MOF-645, permanent porosity of guest free MOF-546 was established and the Langmuir

surface areas of 1130 and 1250 m^2g^{-1} were estimated based on Ar and N_2 isotherms respectively. The resultant nature of MOF-646 i.e. small pore size distribution and the polarized pore walls were reflected by its unique hydrogen adsorption behavior. In spite of relatively high crystal density of MOF-646, it showed relatively high hydrogen uptake up to 17.5 mg g^{-1} at 77 K and 1 bar, which is superior when compared to other framework materials with Zn_4O SBUs except for IRMOF-11, whose nets are interwoven.. The H_2 uptake in volumetric unit (20.9 g L^{-1}) was also found to be higher when compared to other MOFs and comparable to MOFs with Cu open metal sites. MOF-646 also showed a unique interaction behavior towards H_2, where the Q_{st} curve was observed to be nearly flat throughout the H_2 loading range examined, which is in sharp contrast to many other MOFs, especially those possessing open metal sites. A zero coverage value was estimated to be 7.8 kJ mol^{-1}. These results revealed that the MOFs with internally polarized azulene backbone might be beneficial to stabilize H_2 molecules in the frameworks.

Reticular design provides a unique platform to link symmetrical building unit into extended porous structures with strong bonds. Indeed, this discipline has been successfully exploited to prepare several families of isoreticular MOFs with potentially high porosity and rigidity. Particularly, frameworks with **nbo** net topology which possesses linear ditopic organic linkers and $Zn_4O(CO_2)_6$ or paddle wheel $M_2(CO_2)_4$ [M = Zn, Cu, Co etc.] SBUs as molecular building blocks have been easily synthesized. Keeping this recent development in mind we examined this approach to construct chemically tuned isoreticular MOFs comprising of internally polarized rigid linear building block, 2,6-azulenedicarboxylate, and $Zn_4O(CO_2)_6$ or $Zn_2(CO_2)_4$ paddle wheel SBUs. Indeed, performing solvothermal reaction between $Zn(NO_3)_2.6H_2O$ and 2,6-azulenedicarboxylic acid under optimized reaction conditions resulted in the formation of a highly open 3D MOF, namely MOF-650, with **nbo** net topology. MOF-650 was found to be isostructural to prototype IRMOF-8. On the other hand, addition of organic pillar unit 1,4-diazabicyclo[2.2.2]octane (dabco) into the reaction mixture containing Zn(II) metal ions and 2,6-azulenedicarboxylic acid allowed us to construct a pillared MOF, MOF-649, based on $Zn_2(CO_2)_4$ SBUs and is isostructural to $Zn_2(2,6\text{-ndc})_2(dabco)$ [DUT-8(Zn)].

Attempts were made to obtain the guest free materials of MOF-649 under supercritical CO_2 activation. However, the nitrogen adsorption measurement showed that a maximum Langmuir surface area of 990 m^2g^{-1} could only be attained. Based on PXRD analysis it could be emphasized that the observed low porosity of activated MOF-649 is due to the structural

changes, which occur upon guest removal. In contrast to MOF-649, the activated MOF-650 showed high porosity and stability in absence of guest solvent molecules. The Langmuir/BET surface area and pore volume was estimated to be 3230/2630 $m^2 g^{-1}$ and 1.2 $cm^3 g^{-1}$ respectively as determined based on N_2 adsorption measurement.

Low-pressure H_2 uptake measurements reveals that the activated MOF-649 and MOF-650 can take up 7 and 14.5 mg g^{-1} of H_2 at 77 K and 1 bar, respectively. The H_2 uptake by MOF-649 is relatively low compared to the data obtained for MOF-646 despite their comparable porosity.
In addition, the hydrogen uptake data obtained for MOF-650 was found to be comparable to its isostructural IRMOF-8, although it has a relatively high apparent surface area.

The coverage dependencies of adsorption enthalpies (Q_{st}) of H_2 for activated MOF-649 and MOF-650 were calculated from fits of their corresponding 77 and 87 K isotherms. The Q_{st} at zero coverage for MOF-649 was estimated to be 5.3 kJ mol^{-1}, which is in line with the value reported for isoreticular pillared MOFs. Therefore, no significant effect of azulene to stabilize hydrogen molecules in MOF-649 was ascertained. On the other hand, MOF-650 exhibited high interaction towards H_2 with a low coverage Q_{st} was estimated to be 6.8 kJ mol^{-1}, which is higher when compared to the value reported for MOF-5 and isostrcutural IRMOF-8. In addition, the Q_{st} plot also exhibited that the interaction energy drops considerably with the amount adsorbed to 4.2 kJ mol^{-1} at the limit of the interpolation. Such phenomenon indicates the presence of strong binding sites in the material, which become occupied at ~4.3 mg g^{-1} (corresponds to 2 H_2 molecules per $[Zn_4O(2,6\text{-azd})_3]$ formula unit) of H_2 loading. Considering the $Zn_4O(CO)_6$ (SBUs) moiety exhibits as the strongest binding location as was suggested by neutron diffraction studies, it could be surmised that the observed high Q_{st} at low coverage is presumably due to the improved polarizability of the SBUs, triggered by the associated azulene functionality, if not determined by the direct confinement of hydrogen on the linkers.

Postsynthetic modification approach provides an attractive pathway to manipulate the chemical and electronic properties of the host materials by modifying the existing functional groups of the pre-synthesized MOFs or to introduce a range of functional groups which are potentially important. We investigated this approach to functionalize the pendant amine groups of IRMOF-3 and DMOF-1-NH_2 with amino borane derivatives by undertaking gas-solid phase reactions between the activated MOFs and diborane (B_2H_6). In order to optimize the reaction conditions for accomplishing the desired amino borane functionalized MOFs, *in situ* PXRD

experiments were performed. The amino borane functionalized MOFs i.e. DMOF-1-NH_2BH_3 and IRMOF-3-BH_3 were observed to adopt a distinct color when compared to their unmodified materials. The presence of covalently bonded $–BH_3$ functionality in the modified MOFs was supported by FTIR spectroscopic analysis. The characteristic band found at 2377 cm^{-1} with two shoulders at 2325 cm^{-1} and 2273 cm^{-1} could be identified as the B-H antisymmetric and symmetric stretching frequencies, respectively. Further support of the successful formation of DMOF-1-NH_2BH_3 and IRMOF-3-BH_3 was ascertained from the ^{11}B NMR and ICPAES analysis.

As part of the goal of the thesis towards the preparation of MOMs with high concentration of unsaturated metal centers, we exploited a novel chemical strategy to build extended structure which in principle could replete with potentially accessible metal sites using the concept of utilization of *in situ* prepared small metal–linker complex based on 1*H*-pyrazole-3,5-dicarboxylic acid as precursors building block. Indeed, our conceptual approach of utilizing the small square bridging unit of pyrazole-bridged cyclic dicopper complex was investigated via the formation of highly open framework, MOF-648 $[Cu_{12}(L)_8(DMF)_9]\cdot(DMF)_2(H_2O)_2$, with potentially accessible metal sites in its compact spaces. The initial attempts were found to result in the formation of a mixture of MOFs i.e. MOF-647 and MOF-648. However, careful adjustment of solvent to substrate ratio, as well as the metal to ligand stoichiometry allowed us to synthesize MOF-648 in a pure phase. Single crystal X-ray diffraction analysis reveals that the structure of MOF-647A comprises basic trinuclear repeat unit $[Cu_3(L)_2\cdot(DMF)_2(H_2O)_3]$ (where L = pyrazole-3,5-dicarboxylate) to form a doubly interpenetrated **dia** framework. The coordinated DMF solvents of the as-prepared MOF-647A was demonstrated to be exchanged with anhydrous THF to give MOF-647B, $[Cu_3(L)_2\cdot(THF)_2(H_2O)_2]$, and the structure of MOF-647B was also evaluated based on single crystal X-ray diffraction study.

In search of suitable metal-organic materials which could potentially act as chemosensors for the detection of nitroaromatic explosives for example picric acid and 2,4-dinitrotoluene, we prepared a series of materials by linking triptycene based organic linkers, 1,4,5,8-triptycenetetracarboxylate, with various metal ions. Use of Al^{3+} and Cr^{3+} as metal ions resulted in the formation of luminescent gel materials Al-gel **G1** and Cr-gel **G2**. The coordination polymeric nature of the Al-gel **G1** gels could be supported by microscopic examination of the air dried materials under scanning electron microscope (SEM). In contrary, the reaction between the 1,4,5,8-triptycenetetracarboxylate and Co^{2+} allowed us to prepare a crystalline product, *trip*-

MOF-**1** [Co_2(*ttc*)(DMF)(H_2O)] (where *ttc* = 1,4,5,8-teriptycenetetracarboxylate), the structure of which was evaluated by the single crystal X-ray diffraction studies. In fact, highly luminescent Al-gel **G1** exhibited a unique sensing behavior towards the detection of picric acid and other electron deficient nitroarenes. The observed sensitivity was primarily attributed to the self-assembly of the triptycene receptors into coordination polymeric gel. A relatively diminished response of Cr-gel **G2** and *trip*-MOF-**1** towards picric acid was observed.

I. APPENDIX

I.I. Abstract

Porous metal-organic frameworks are extensively studied in last decades as one of the promising hydrogen storage materials due to their extraordinary high specific surface areas, tunable pore sizes, functionalizable pore walls and well-defined hydrogen binding sites. Recent finding evidenced that metal-organic frameworks (MOFs) coupled with high surface areas and porosity could deliver as high as 10-15 wt% hydrogen at liquid nitrogen temperature and at 40-80 bar of hydrogen pressure. The storage capacity however, in sharp contrast, drop dramatically to below one tenth of the cryogenic delivery amount at near ambient temperatures, which perhaps would be more compatible for practical application. This is mainly because the H_2 adsorption in MOFs occurs *via* physisorption process and therefore involves only a weak van der Waals interaction as primary binding force. Various approaches have been recently demonstrated to increase the binding forces between the host MOFs and the hydrogen to realize significant delivery amount at relative higher temperatures. Guided with the knowledge from the recent exploration, we have developed chemically tuned porous MOFs by means of rational designing of organic counterpart of the materials or through grafting of appropriate chemical entities on the surface of the functional group containing MOFs. Such chemical tuning are deemed critical to furnish advanced polar binding by dipole-dipole or dipole-induced dipole interactions or hydrogen bonding in conjunction to the kinetic trapping of H_2 molecules.

In particular, the research presented here has exploited systematic designing, synthesis and postsynthetic modification of MOFs for hydrogen storage and sensitive detection of nitroaromatic explosives. In order to investigate the impact of polarization effect on stabilizing the H_2 molecules in MOFs, a series of novel metal-organic frameworks comprising of internally polarized azulene ligands were developed and their hydrogen storage performance were thoroughly studied. In addition, a novel method for postsynthetic modification of amine functionalized MOFs to introduce polarizing groups under gas-solid phase reactions was demonstrated.

Besides, an innovative strategy for incorporating high concentration of vacant metal binding sites in the MOFs has been investigated. The presence of such metal binding sites had been proven to be beneficial to assist the hydrogen molecules.

In a yet another study we have employed 3D shape-persistent organic receptor comprising of triptycene tetracarboxylate for the highly selective and sensitive detection of explosives *via* photo induced electron transfer quenching mechanism.

In brief, the thesis work has contributed to the fields of hydrogen storage and chemosensing utilizing MOMs.

I.II. Zusammenfassung

Poröse metallorganische Gerüste (engl. **m**etal-**o**rganic **f**rameworks, MOFs) wurden in den letzten Dekaden, auf Grund ihrer hohen spezifischen Oberfläche, abstimmbarer Porengrösse, funktionalisierbarer Porenwände und definierter Wasserstoffbindungstellen, intensiv als vielversprechendes Wasserstoffspeichermaterial untersucht. Neuere Ergebnisse belegen, dass MOFs mit grosser Oberfläche und hoher Porosität bis zu 10-15 Gew.-% Wasserstoff bei Flüssig-Stickstoff-Temperatur und 40-80 bar Wasserstoffdruck liefern können. Die Speicherkapazität bei Raumtemperatur, die wahrscheinlich bedeutend für praktische Anwendung wäre, sinkt dazu im Gegensatz dramatisch unter ein Zehntel der Kapazität bei tiefem Temperaturen. Der Hauptgrund hierfür ist, dass die Wasserstoffadsorption in MOFs durch Physisorptionsprozesse geschieht und daher nur schwache van-der-Waals-Kräfte die primäre Bindungskraft bilden. Verschiedene Ansätze haben kürzlich gezeigt wie Bindungskräfte zwischen MOFs und Wasserstoff verstärkt werden können, um so signifikante Mengen Wasserstoff bei relativ höheren Temperaturen zu liefern. Basierend auf neueren bekannten Ergebnissen, entwickelten wir chemisch abstimmbare, poröse MOFs durch rationelles Design der organischen Bausteine der Materialien oder durch Anbringung geeigneter chemischer Bausteine an die Oberflächer der funktionelle Gruppen tragenden MOFs. Die chemische Abstimmung scheint bedeutend, um fortgeschrittene polare Bindungen durch Dipol-Dipol- oder Dipol-induzierter Dipol-Wechselwirkungen oder Wasserstoffbindungen in Verbindung mit kinetischem Einfangen der Wasserstoffmoleküle zu sein.

Im Besonderen hat die hier präsentierte Forschungsarbeit das systematische Design, Synthese und postsynthetische Modifikation von MOFs für Wasserstoffspeicherung und den sensitiven Nachweis von nitroaromatischen Sprengstoffen untersucht. Um den Effekt der Polarisierung auf die Stabilisierung von Wasserstoff in MOFs zu untersuchen, wurde eine Reihe neuer MOFs, basierend auf polarisierten Azulenliganden, entwickelt und ihre

Wasserstoffspeichereigenschaften wurden intensiv untersucht. Zusätzlich konnte eine neue Methode für die postsynthetische Modifikation amin-funktionalisierter MOFs zur Einführung polarisierter Gruppen durch Gasphasen-Festphasen-Reaktionen aufgezeigt werden.

Des Weiteren wurde eine innovative Strategie zu Einführung hoher Konzentrationen von vakanten Metallbindungstellen untersucht. Die Anwesenheit die Metallbindungsstellen wurde als förderlich für die Unterstützung von Wasserstoffmolekülen nachgewiesen.

In einer weiteren Studie haben wir 3D-formbeständige organische Rezeptoren basierend auf Triptycentetracarboxylat für den hochselektiven und hochsensitiven Nachweis von Sprengstoffen duch lichtinduzierten Elektronentransfer-Quenching-Mechanismus angewendet.

Zusammenfassend betrachtet, hat diese Doktorarbeit zum Feld der Wasserstoffspeicherung und der Nutzung von MOFs als Chemosensoren beigetragen.

I.III. List of Prepared Compounds

MOF-645: $[Zn_5(\mu_3\text{-}OH)_2(\mathbf{L})_4(DMF)(H_2O)]\cdot(DMF)$, **L** = 1,3-azulenedicarboxylate

MOF-646: $[Zn_4(\mu_4\text{-}O)(\mathbf{L})_3(DMF)_2]\cdot(DMF)_{1.25}(H_2O)$, **L** = 1,3-azulenedicarboxylate

MOF-647A: $[Cu_3(\mathbf{L})_2(DMF)_{1.9}(H_2O)_{3.1}]$, **L** = pyrazole-3,5-dicarboxylate

MOF-647B: $[Cu_3(\mathbf{L})_2(THF)_2(H_2O)_2]$, **L** = pyrazole-3,5-dicarboxylate

MOF-648: $[Cu_{12}(\mathbf{L})_8(DMF)_9]\cdot(DMF)_2(H_2O)_2$, **L** = pyrazole-3,5-dicarboxylate

MOF-649: $[Zn_2(2,6\text{-azd})_2(dabco)]\cdot(DMF)_5(H_2O)_2$

MOF-650: $[Zn_4O(2,6\text{-azd})_3]\cdot(DMF)_6(H_2O)_4$

IRMOF-3-BH_3: $Zn_4O[(BH_3NH_2\text{-}BDC)_3]$

DMOF-1-NH_2BH_3: $[Zn_2(BH_3NH_2\text{-}BDC)_2(DABCO)]$

Tript-MOF-**1**: $[Co_2(ttc)(DMF)(H_2O)]$ (*ttc* = 1,4,5,8-triptycenetetracarboxylate)

Gel materials: Al-gel-**G1** and Cr-gel-**G2**

II. CURRICULUM VITAE

Name: Samir BARMAN

Date of birth: 24.02.1983

Place of Birth: Dubrajpur, West Bengal, India

Nationality: Indian

ACADEMIC QUALIFICATIONS:

July 2008-present University of Zurich, Switzerland
Ph.D. thesis work
Thesis title: Design, Synthesis and Postsynthetic Modification of Metal-Organic Frameworks for Hydrogen Storage and Chemosensing
Advisor: Prof. Dr. Heinz. Berke

2005-2007 Indian Institute of Technology Bombay, India
Major in Chemistry, Master of Science
Project title: "Pd, Au and Ag complexes of O/N-functionalized and Non-functionalized N-heterocyclic carbene ligands."
Advisor: Prof. Dr. Prasenjit Ghosh

2001-2005 B.Sc. Chemistry (Honors), Vidyasagar University, India

1999-2001 West Bengal Council of Higher Secondary Education, India

1999 West Bengal Board of Secondary Education, India

RESEARCH INTEREST:

Organometallic Chemistry, Coordination Chemistry, Supramolecular Chemistry, Porous Materials, Organic Synthesis, Functional Materials, Polymer Chemistry

PUBLICATIONS:

[1] L. Ray, V. Katiyar, **S. Barman**, M. J. Raihan, H. Nanavati, M. M. Shaikh and P. Ghosh, "Gold(I) N-heterocyclic Carbene Based Initiator for Bulk Ring-Opening Polymerization of L-lactide", *J. Organomet. Chem.* 2007, **692**, 4259-4269.

[2] L. Ray, **S. Barman**, M. M. Shaikh and P. Ghosh, "Highly Convenient Amine-free Sonogashira Coupling in Air in a Polar Mixed Aqueous

Medium by trans- and cis-$(NHC)_2PdX_2$ (X = Cl, Br) Complexes of N/O-functionalized N-heterocyclic Carbenes", *Chem. Eur. J.*, 2008, **14**, 6646-6655.

[3] **S. Barman**, H. Furukawa, O. Blacque, K. Venkatesan, O. M. Yaghi and H. Berke, "Azulene based metal-organic frameworks for strong adsorption of H_2", *Chem. Commun.*, 2010, 46, 7981-7983.

[4] **S. Barman**, H. Furukawa, O. Blacque, K. Venkatesan, O. M. Yaghi, Guo-Xin Jin and H. Berke, "Incorporation of active metal sites in MOFs *via in situ* generated ligand deficient metal-linker complexes", *Chem. Commun.*, 2011, 47, 11882-11884.

[5] **S. Barman**, J. Garg, O. Blacque, K. Venkatesan and H. Berke, "Triptycene based luminescent metal-organic gels for chemosensing", *Chem. Commun.*, 2012, **48**, 11127-11129.